A Ph.D. Dissertation on

Multi-level Dimension Decomposition Approach For Structural Reliability Analysis

submitted by

Amit Kumar Rathi

(11610409)

under the supervision of

Dr. Arunasis Chakraborty

DEPARTMENT OF CIVIL ENGINEERING

INDIAN INSTITUTE OF TECHNOLOGY GUWAHATI

May, 2019

Certificate

It is certified that the work contained in the dissertation entitled **"Multi-level Dimension Decomposition Approach for Structural Reliability Analysis"**, by **Amit Kumar Rathi (11610409)** for the partial fulfillment of the requirements for the award of the *Doctor of Philosophy* (*Ph.D.*) in *Civil Engineering* with the specialization in *Structural Engineering* at the *Indian Institute of Technology Guwahati, India* is an authentic work. This work has been carried out under my sole supervision and it has not been submitted elsewhere for the award of a degree.

Dr. Arunasis Chakraborty
Associate Professor
Department of Civil Engineering
Indian Institute of Technology Guwahati
Guwahati - 781039, India

Date: 27 May, 2019

Acknowledgements

The quest for learning more and more has always been a motive of my life and thus, certainly, the destiny has always showered the fortune of making appointments with the persons who are truly dedicated to the work. One such person is, *Dr. Arunasis Chakraborty*, who acted as my supervisor, mentor and guru. First of all, I bow for a wholehearted gratitude that he accepted me as his disciple, in spite of knowing my past that I pursued a Master's degree in a different field, and my knowledge and understanding regarding Structural Engineering were average. It's been my greatest pleasure and experience to work and learn under him. I owe him a great tribute for improving my understanding of structural reliability based design, structural dynamics and other academic as well as non-academic fields. He taught me the fundamentals and built my knowledge base in a logical sequence. He also helped me to improve my writing skills, which are very essential at every level. His constant earnest support and encouragement helped me to develop a profound interest and a vivid understanding of the subject. His judicious feedback and vital motivating interactions from time to time inspired me to lay effective hard work which indeed helped me to put together this work.

Sincere thanks to the members of the Doctoral Committee, *Prof. Sudip Talukdar*, *Prof. Anjan Dutta*, *Prof. Sajal K. Deb* and my supervisor for their critical reviews, suggestions and encouragement which directed me in making this work a worthy effort. I have also received vital support, encouragement and understanding from course instructors, especially *Prof. Rajib Kumar Bhattacharjya*, *Dr. Kaustubh Dasgupta* and *Dr. Sandip Das*. I wish to convey my special thanks to the Civil Engineering faculty and staff fraternity for a memorable stay in this institute. Also, the financial assistance from the Department of Civil Engineering, Indian Institute of Technology Guwahati, India is gratefully appreciated to carry out this research.

Cheers to the research scholar fraternity for creating a decent and sincere environment for research in the department. I also thank my colleagues, especially, Mr. Swaroop Mahato for motivation, insight discussions and cooperation, Dr. S. Kameshwar, Mr. Sudhi Sharma and Mr. M. Sajeer for providing the technical support and my pals, Dr. Sumit Agarwal, Dr. Ravi Kiran, Dr. Srikanth Vadlamudi, Dr. Khwairakpam Sachidananda and Mr. Kiran Singh for making my stay memorable. I wish a great future for all of my friends and colleagues.

Last but not least, one might not stand up without the support of his/her family, hence I would take this opportunity to thank my family who are the *raison d'être* for this degree. It was their love, faith, calmness, humbleness, support and long-lasting will that has helped me to eventually conclude a work worth sharing with others.

Amit Kumar Rathi
(11610409)
Department of Civil Engineering
Indian Institute of Technology Guwahati
Guwahati - 781039, India

Date: 27 May, 2019

This thesis is dedicated to
my beloved family.

Abstract

This thesis aims to develop high-fidelity polynomial dimension decomposition schemes for stochastic computation. It is achieved in multiple stages using efficient modelling of bases, decomposition terms, unknown coefficients and error terms. A new sequential support point generation scheme is also proposed in this thesis for efficient construction of the meta-model. Both, dimension decomposition and support points generation are developed for different non-intrusive applications to address the curse of dimensionality. The study first examines the performance of the conventional response surface method (RSM) constructed using least square regression technique which is widely used for optimization and reliability analysis. Its quality is improved using an adaptive scheme i.e. moving least square (MLS), where the unknown coefficients are determined by minimizing the weighted error at each support point. This, in turn, makes the approximation adaptive to the local variations. Different combinations of polynomial bases, design of experiment schemes and type of weight functions are studied to investigate the performance of the MLS based meta-modelling. The best combination is further applied for reliability based design optimization (RBDO). In this regard, a novel two-step adaptive RSM is proposed which bypasses the time exhaustive computational burden of RBDO. Two sets of separate response surfaces are constructed to determine the optimal design point and the response statistics necessary for the constrained optimization. The first step involves deterministic response surface for design optimization while the second step involves surrogate models for uncertainty quantification.

The MLS based adaptive determination of unknown coefficients is extended further using orthogonal polynomial bases to develop the stochastic response surface. It couples polynomial chaos expansion (PCE) with MLS technique that replicates the performance function better. In this thesis, Hermite polynomials are adopted as it transforms the limit state directly into the standard normal space where reliability analysis becomes straightforward. The time exhaustive conventional collocation based support points generation is replaced with Clenshaw-Curtis sparse grid scheme. It generates uniformly spaced points depending upon the level of hierarchy where the selection criteria is based on the linear norm as suggested by Smolyak. The input domain is populated sequentially by the sparse grid with an aim to create new points in the region of interest i.e. near the most probable failure point and/or near the maixma/minima. In case of reliability analysis, support points are generated iteratively near the failure region using the sub-grids hierarchy. This proposed algorithm for multi-level support point generation offers a tradeoff between the accuracy and efficiency of the reliability estimation. Continuous and differentiable penalty functions are imposed to determine multiple failure regions, if any, by repeating the optimization process. Once the surface is developed, reliability analysis is carried out using population based sampling schemes (e.g. importance sampling).

Finally, the accuracy of the meta-model is improved by representing it in terms of orthogonal subfunctions. In this context, finite difference based high dimensional model representation (HDMR) is used for dimension decomposition that commences from an initial reference point and progressively evolves in successive iterations. Most probable failure location is identified in every iteration and is used as the reference point for the following decomposition until it converges. Accordingly, the framework of HDMR is tuned to follow the sequential support point generation scheme. A distribution adaptive version of the sparse grid scheme is developed for support point generation. The unknown coefficients are determined using MLS where the bases of the subfunctions are defined by Hermite polynomials for efficient interpolation. The order of the decomposition is modified in each iteration to curtail the unnecessary terms in the proposed multiple decompositions. This judicious selection of lower order terms is particularly helpful in reducing the number of unknown coefficients in the proposed algorithm for *Adaptive Multiple Finite Difference HDMR* (AMFD-HDMR). In nutshell, this proposal provides an adaptive multi-order multi-level dimension decomposition technique for reliability analysis.

The issue of curse of dimensionality is further addressed by a novel approach using *Dimension Adaptive Fi-*

nite Difference HDMR (*d*AMFD-HDMR). It decomposes the original performance function into summands of smaller dimensions using a sparse formulation of HDMR. This formulation is suggested based on the individual contributions of all the dimensions while retaining only the significant mutual contributions of these dimensions. A sensitivity analysis is performed to screen the insignificant dimensions for better accuracy and efficiency. The support points are generated in a sparse grid framework based on the hierarchical tensor products of the sub-grids involving the *pdf* of the input variables. An additional feature (i.e. dimension adaptiveness) is introduced in the selection criteria of the sparse grid points in this new meta-modelling technique. It curtails the dimensions based on its significance and the subfunctions in this sparse formulation are modelled by MLS-PCE technique. In this process, it utilizes the benefits of orthogonality of the basis functions while providing an adaptive interpolation scheme. Once the meta-model is built, Monte Carlo simulation (MCS) is performed to bypass the time exhaustive computation of the original performance function.

In stochastic computation, the tractability of meta-models is also affected by the time required in training and approximating multiple realizations of MCS. These issues are different from the usual problem where the time consumption is only proportional to the multiple evaluations of the original limit state function. The MLS technique suffers such issues as it employs a scalar approach where matrices are inverted for each realization. To address this demerit, a novel surrogate modelling scheme [i.e. hybrid dimension adaptive high dimensional model representation (*hd*A-HDMR)] coupled with dimension adaptiveness in a multiple HDMR framework is proposed in this thesis. The hybrid scheme is suggested in this approach where the coefficients are determined using a Gaussian process. The global error of the multiple HDMRs is decomposed into the error terms of each subfunction. These individual terms are further modelled using correlations between the support points based on the Gaussian distribution. This results in additional new unknown coefficients which eventually leads to three different sets of unknown quantities in the proposed meta-modelling approach. They are associated with the PCE of the subfunctions in the dimension decomposition, the error terms and the multiple HDMRs. The overall computational advantage lies in its ability to determine all these unknown coefficients from the same set of support points. The thesis also suggests few algorithms for the different applications of *hd*A-HDMR e.g. reliability analysis, uncertainty quantification and RBDO.

Overall, each proposal is validated using various problems to demonstrate their performance. These problems include finite element model updating of an existing reinforced concrete road bridge, reliability analysis of portal frame, truss, edge-cracked plate, RBDO of passive tune mass damper and laminated composite plate. The accuracy and computational efficiency of the proposed models are established using MCS and other widely used reliability methods. The numerical analyses presented in this thesis clearly establishes that the proposed algorithms for surrogate modelling can be adopted for large class of practical reliability based design problems.

List of Publications

Journal Articles:

1. A. K. Rathi and A. Chakraborty, Reliability Based Performance Optimization of TMD for Vibration Control of Structures with Uncertainty in Parameters and Excitation, *Structural Control and Health Monitoring*, 2017, 28(1), e1857.
2. A. K. Rathi, S. Sharma and A. Chakraborty, Sequential Stochastic Response Surface Method using Moving Least Squares based Sparse Grid Scheme for Efficient Reliability Analysis, *International Journal of Computational Methods*, 2017, 1840017.
3. A. K. Rathi and A. Chakraborty, Dimension Adaptive Finite Difference Decomposition using Multiple Sparse Grids for Stochastic Computation, *Structural Safety*, 2018, 75, 119–132.

Book Chapter:

1. A. K. Rathi and A. Chakraborty, Robust Design of TMD for Vibration Control of Uncertain Systems Using Adaptive Response Surface Method, *In* Advances in Structural Engineering, Springer India, 1505-1517.

Conference Proceedings:

1. A. K. Rathi and A. Chakraborty, MLS based Sequential SRSM in Sparse Grid Framework for Efficient Uncertainty Quantification, *Proceedings of* 2$^{\text{nd}}$ ECCOMAS Thematic Conference on Uncertainty Quantification in Computational Sciences and Engineering (UNCECOMP 2017), 15-17 June, 2017, Rhodes Island, Greece.
2. A. K. Rathi, S. Sharma and A. Chakraborty, Sequential Stochastic Response Surface Method using Moving Least Squares based Sparse Grid Scheme for Efficient Reliability Analysis, *Proceedings of* 7$^{\text{th}}$ International Conference on Computational Methods (ICCM 2016), 01-04 August, 2016, Berkeley, CA, USA.
3. S. Sharma, A. K. Rathi and A. Chakraborty, Reliability Based Design of Nonlinear Composite Thin Plates, *Proceedings of* International Conference on Innovations in Structural Engineering (IC-ISE 2015), 14-16 December, 2015, Hyderabad, India.
4. A. K. Rathi and A. Chakraborty, Adaptive Response Surface based FE Model Updating for Operational Modal Analysis of RC Road Bridge, *Proceedings of* 4$^{\text{th}}$ Optimization and Stochastic Days (OSD 2014), 18-19 September, 2014, Bangalore, India.
5. S. Kameshwar, A. K. Rathi and A. Chakraborty, A Modified Gradient Based Reliability Analysis for Non-linear Non-algebraic Limit States Using Polynomial Chaos Expansion, *Proceedings of* International Congress on Computational Mechanics and Simulation (ICCMS 2012), 10-12 December, 2012, Hyderabad, India.

Contents

List of Figures

List of Tables

List of Abbreviations

AMFD-HDMR	Adaptive multiple finite difference high dimensional model representation
ANOVA	Analysis of variance
ARSM	Adaptive response surface method
AS-PCE	Adaptive sparse polynomial chaos expansion
CDF	Cumulative distribution function
Cov	Covariance
cov	Coefficient of variation
*d*AMFD-HDMR	Dimension adaptive multiple finite difference high dimensional model representation
DoE	Design of Experiment
dof	Degree of freedom
FE	Finite element
FORM	First order reliability method
FSDT	First order shear deformation theory
gPCE	Generalized polynomial chaos expansion
*hd*A-HDMR	Hybrid dimension adaptive high dimensional model representation
HDMR	High dimensional model representation
HO-SRSM	Higher order stochastic response surface method
KLE	Karhunen-Loève Expansion
LS	Least square
MCS	Monte Carlo Simulation
MDOF	Multiple degree of freedom
MLS	Moving least square
MLS-HDMR	Moving least square based high dimensional model representation
MPP	Most probable failure point
OLE	Optimal linear expansion
PCA	Principal component analysis
PCE	Polynomial chaos expansion
pdf	Probability density function
PSDF	Power spectral density function
RA	Reliability analysis
RBDO	Reliability based design optimization
RDO	Robust design optimization
RMS	Root mean square
RMSE	Root mean square error
RS-HDMR	Random sampling based high dimensional model representation
RSM	Response surface method

SDOF	Single degree of freedom
SORM	Second order reliability method
SPA	Saddlepoint approximation
SQP	Sequential quadratic programming
SRSM	Stochastic response surface method
TMD	Tuned mass damper
UDL	Uniformly distributed load
UQ	Uncertainty quantification

List of Major Symbols and Their Meanings

$\alpha_0, \alpha_i, \ldots$	Coefficients of polynomial chaos expansion
β_c	Reliability index
Δ^i	Difference in quadrature approximation
δ_i	Displacement at node i
$\delta_{\mathbf{x}_i}$	Euclidean distance of any arbitrary point from the i^{th} support point
δ_y	Isolator yield displacement
ϵ_1, ϵ_2	Residual error from 1^{st} and 2^{nd} order HDMR, respectively
Γ_p	Hermite polynomial basis of order p
γ_{xz}, γ_{yz}	Transverse shear strains
λ_w	Constant parameter in weight function
$\lambda_{\mathbf{x}}$	Scale reduction factor
μ_{x_i}	Mean of random variable x_i
ν_{12}	Poisson's ratio
$\phi_{\hat{\mathbf{x}}}$, $\phi_{\hat{\mathbf{y}}}$	Rotation along the transverse normal about $\hat{\mathbf{y}}$ axis and $\hat{\mathbf{x}}$ axis, respectively
$\Psi_i(\bullet)$	Matrix of the Hermite polynomial basis
ρ	Correlation coefficient
σ_{11}, σ_{22}	Stress
$\sigma_{x_i}, \sigma_{z_i}$	Standard deviation of random variable x_i and z_i, respectively
θ	Orientation angle of ply in composite plate
$\varphi_j(x_i)$, $\varphi_{j_1 j_2}(x_{i_1}, x_{i_2})$	Interpolation coefficients of HDMR
A	Force amplitude
A_i	Cross-section area of section i
$\mathbf{a}_i$	Vector of unknown coefficients in polynomial chaos expansion
b	Size of composite plate
$\mathbf{c}$	Reference point of finite difference HDMR, $\{c_1, c_2, \ldots, c_n\}$
c_f	Floor damping coefficient
c_i	Reference point coordinate of i^{th} variable
D_r	Influence radius of weight function
$\mathbb{E}[\bullet]$	Expectation operator
$\mathscr{E}_1, \mathscr{E}_2$	Permissible error for convergence of iteration
E_i	Elastic modulus of section i
$\mathfrak{F}$	Failure index
f_y	Isolator yield force
$f_Z(\mathbf{z})$	joint probability density function of $\mathbf{z}$

$f_Z^*(\mathbf{z})$	modified joint probability density function of $\mathbf{z}$ at $\mathbf{z}^*$
G_{12},G_{13},G_{23}	Shear modulus
$g(\bullet)$	Original performance function
$\hat{g}, \hat{g}(x_{i_1}), \hat{g}(x_{i_1}, x_{i_2})$	Value of $g(\bullet)$ at $\mathbf{c}$, $\{c_1, c_2, \ldots, c_{i_1-1}, x_{i_1}, c_{i_1+1}, \ldots, c_n\}$ and $\{c_1, c_2, \ldots, c_{i_1-1}, x_{i_1}, c_{i_1+1}, \ldots, c_{i_2-1}, x_{i_2}, c_{i_2+1}, \ldots, c_n\}$, respectively
$\tilde{g}(\bullet)$	Approximation of $g(\bullet)$
g_0	Zeroth order component function of HDMR
$\mathscr{H}_q$	Sparse grid quadrature expression
h	Thickness of composite plate
h_r	Positive integer factor used to generate points for RS-HDMR
$\mathbb{I}$	Set of unit space
$\mathscr{I}[\bullet]$	Indicator function which is either 0 or 1
I_i	Moment of inertia of section i
k	Positive integer factor used to generate points for RSM and HDMR
k_f, k_c	Floor stiffness and contact stiffness, respectively
m_f	Floor mass
$\mathbb{N}$	Set of natural numbers
n	Number of variables
n_b	Number of unknown coefficients in polynomial chaos expansion
n_c	Simulation size of importance sampling
n_s	Number of support points
m_i	Number of points in univariate direction i
o	Order of HDMR
P	Load
p	Degree of polynomial chaos expansion
p_f	Probability of failure
q	Level of sparse grid
$\mathbb{R}$	Set of real numbers
$S(\bullet)$	Total squared error of approximation
s_m	Standard deviation multiplication factor
T	Force period
T_{12}	Shear strength
U_{m_i}	Approximation by univariate quadrature rule for sparse grid
$\mathbf{u}$	Vector of standard normal pseudo random variables
u_0	Midplane displacements in $\hat{\mathbf{x}}$ direction
v_0	Midplane displacements in $\hat{\mathbf{y}}$ direction
$\mathbf{W}(\bullet)$	Weight function matrix for moving least square
$w(\bullet)$	Weight function for moving least square
w_0	Midplane displacements in $\hat{\mathbf{z}}$ direction
$w_{j,i}$	Weight function for univariate quadrature rule
X	Tensile strength
$\mathbf{x}$	Vector of random variables, $\{x_1\, x_2\, \ldots\, x_n\}$
$\mathbf{x}^{*,i}, \mathbf{z}^{*,i}$	Design point in original and standard normal space for iteration i, respectively
x_i	i^{th} random variable
Y	Compressive strength
$y(\bullet)$	Any arbitrary function, $y : [0,1]^n \to \mathbb{R}$
$\mathbf{z}$	Vector of standard normal random variables, $\{z_1\, z_2\, \ldots\, z_n\}$
z_i	i^{th} standard normal random variable

Chapter 1

Introduction

Structural designs are usually performed considering factors and conditions related to the safety of the system. These criteria are included to ensure desired level of reliability when the structure is exposed to its operational environment that are often uncertain in nature. The sources of these uncertainties are the variability in the mechanical properties of the system and loading, lack of information or knowledge, assumptions in the modelling, human error and so on. Deterministic quantification of these parameters are nearly impractical and hence, require their probabilistic descriptions. These uncertainties are classified into two categories, *viz.* *aleatory* and *epistemic*. The aleatory uncertainty includes randomly occurring events which can't be predicted beforehand whereas the epistemic uncertainty is due to lack of information or data. These categories can be defined as objective (i.e. aleatory) and subjective (i.e. epistemic) based on their nature. Hence, the popular design methodologies like Working Stress Design Method, Limit State Method and Plastic Design Method are governed by the safety related factors to consider the influence of these uncertainties. Thus, design methods are also classified under two categories, *viz.* Deterministic Design Methods and Probabilistic Design Methods [1] based on the phenomenon associated with the safety conditions of the structural system.

Primarily both, deterministic and probabilistic design philosophies vary based on the nature of the design variables. In the deterministic assessment, design variables are assumed at fixed values whereas in the probabilistic approach these variables are considered as random. The values of these random variables are either determined experimentally or through field experience. Deterministic designs are simpler and less cumbersome but it tends to provide either over or under performing designs. It doesn't consider any variation or uncertainty in the value of design variables based on the construction or manufacturing errors, defects etc. and assumes that each structure will have the same probability of failure i.e. equally reliable. In contrary, the probabilistic design approach considers uncertainty in the design variables and on this basis, it evaluates the performance function of the structural system for the probability of failure. This, in turn, ensures the desired level of safety of a structure which is judged on the basis of its failure probability.

In the past few decades, probabilistic methods incorporating uncertainty propagation through the design variables like load intensity, geometric properties, material strength etc. in conjunction with conventional structural analysis are developed. It demands high computational costs, however, with the advent of efficient computational facilities, these approaches become increasingly popular, especially for structural systems with high stakes (related to analysis, design and construction) to ensure safety. Different structures require different levels of reliability assessment based on the factors like importance, accuracy, computation etc. Thus, the field of structural reliability is classified into three major groups on the basis of safety analysis which is denoted by Level 1, Level 2 and Level 3 reliability methods. Level 1 reliability methods deal at the element level where the desired reliability is ensured by the use of partial safety factors. Presently, many design codes including Indian Standards specify the limit state design following this Level 1 design methodology. Level 2 methods consist of safety checks on the performance function defined at the desired point by limit state equation. The probability of failure of the system or the element is evaluated at this point. Finally, when the reliability analysis is executed on the complete system, it is called the Level 3 method. Besides these groups, structural reliability is also segregated into two domains based on the nature of randomness, i.e. time-invariant and time-varying reliability analysis. In the course of this study, the

author aims to explore time-invariant Level 2 reliability methods only.

As discussed earlier, the main objective of the reliability analysis is to assess the safety of the designed system considering uncertainty in the applied loads and/or the variables such as material strength, geometrical parameters etc. These variables are further referred as the random variables in this study. Hence, the analysis is done by considering the effects of these random variables on the performance which are designed by appropriate limit state equations. Let, a performance function $g(\mathbf{x})$ is evaluated for failure where $\mathbf{x} = \{x_1\, x_2\, \cdots\, x_i\, \cdots\, x_n\}$ is the vector of n random variables. It can be noted that if the function is evaluated as positive then the system is safe and vice versa. Hence, the complete design space is divided into safe and failure region by the limit state at $g(\mathbf{x}) = 0$ which serves as the intermediate boundary. The probability of failure denoted by p_f (i.e. $\mathscr{P}[g(\mathbf{x}) \leq 0]$) is evaluated by the integral of joint probability density function (*pdf*) of $\mathbf{x}$ [i.e. $f_X(\bullet)$] as expressed below

$$p_f = \int \cdots \int_{g(\mathbf{x})\leq 0} f_X(x_1, x_2, \ldots, x_i, \ldots, x_n)\, \mathrm{d}x_1 \mathrm{d}x_2 \cdots \mathrm{d}x_i \cdots \mathrm{d}x_n \tag{1.1}$$

The complement of the probability of failure is the *reliability* such that the summation of these two values results in unity. The reliability of the system is also depicted by an index β which was first defined by Cornell [2]. Later, it was redefined by Hasofer and Lind [2] addressing the lack of invariance in the previous proposal. As per this modified definition, the reliability index β is the shortest distance of the limit surface from the origin in the Standard Normal space and eventually, p_f is calculated as the area in the negative region which is expressed in the following form

$$p_f = \Phi(-\beta) \tag{1.2}$$

where, Φ represents the Standard Normal cumulative distribution function (CDF). It is accredited as the most widely accepted quantification of reliability in engineering. Thus, the reliability index corresponds to the most probable point of failure due to its shortest distance from the origin. Geometrically, this location on the limit surface is the closest failure point to the origin in the standard normal space. Hence, it can be defined as the point on the limit surface where the maximum value of the joint *pdf* of the random variables is obtained. This failure point is often regarded as the *design point*, *most probable failure point* (MPP) or the β point [3].

Using the above description, different methods of structural reliability analysis can be classified into three groups based on the approach and the computational effort associated with them. These groups are - population based, gradient based and polynomial approximation based reliability methods. The population or simulation based reliability methods generate a desired number of realizations using the combinations of the variables. Estimation of the failure probability is performed from the number of realizations which have failed to provide positive values of $g(\mathbf{x})$. Different techniques are developed for this purpose like Monte Carlo Simulation (MCS) [4], Importance Sampling [5], Directional Sampling [4], Latin Hypercube Sampling (LHS) [6] and Subset Simulation [7, 8]. These methods give more accurate estimation of p_f when adequate population is used. Among these methods, MCS is considered to be the most accurate if significant sample size is generated. Hence, it is usually considered as the reference or benchmark to compare the results from the other methods. Population based reliability methods are accurate but requires exorbitant computational cost while dealing with expensive finite element (FE) models, eventually making it less suitable for complex problems. This issue of computational expense to evaluate the probability of failure is addressed by the gradient based methods. These methods are based on the computation of the derivatives of the performance function with respect to the variables $\mathbf{x}$ and thus, serves as effective and faster techniques for optimization. First Order Second Moment (FOSM) Method [4], First Order Reliability Method (FORM) [4, 9] and Second Order Reliability Method (SORM) [10] are widely used gradient based techniques. These methods are applicable for an explicitly defined performance function where computation of the gradient is easier and hence, are limited to less complex problems. Also, design point based approximation of limit state performs poorly for large dimensions (say ≤ 20) [11]. This is due to the fact that in high dimensional problems, multiple regions contribute to failure which are otherwise overlooked by gradient based methods.

Finally, meta-model based methods can also be used for reliability analysis which generally have two steps. First step includes the replication of the limit state in the desired region followed by reliability analysis, bypassing the original $g(\mathbf{x})$ in this final step. The polynomial function based representation (a.k.a. *response surface method*) replaces the actual performance function that is often defined implicitly. This approximation

is done to replicate the original function near the design point to estimate the p_f that helps in reducing the computational cost and eases the reliability analysis. These methods include Response Surface Method (RSM) [12] and Stochastic Response Surface Method (SRSM) [13], along with their different modifications available in the literature. These polynomial approximation techniques are very attractive due to their less computational cost and simplicity. Both RSM and SRSM have proved to be very efficient in different domains of science and engineering and have actively engaged the researchers in the recent past to incorporate various modifications which are discussed in the following section.

1.1 Literature Review

Past few decades have witnessed remarkable development in the field of reliability. Researchers from different domains have contributed significantly in terms of quality and quantity for making it more robust, stable and logical. As this study is focused on the surrogate modelling based reliability analysis and uncertainty quantification, the methods developed here are tested with practical applications. The following subsections illustrate the current state-of-the-art in RSM, SRSM, High Dimension Model Representation (HDMR) and other surrogate modelling techniques developed in the recent past.

1.1.1 Response Surface Method

RSM based meta-modeling was first introduced by Box and Wilson [14] and has proved to be a promising technique for faster computation because of its simplicity and effectiveness for implicit functions [15]. Since then, it has been explored by many researchers to study the influence of different parameters, polynomial bases, sampling schemes and fitting techniques to solve the unknown coefficients. The primary objective of the researches is to improve the approximation near (or at) the design point within reasonable computational costs.

Faravelli [12] studied the performance of response surface method in reliability analysis of structural systems which was modelled in 3D nonlinear FE framework. Since the analytical form of the input–output relation was unknown, she suggested the use of polynomial response surface with complete quadratic bases. The response surface was generated using factorial scheme based support points where the actual FE model was solved. The unknown coefficients of the response surface were determined using least square technique which was improved by an optimal fit based on R^2 value and analysis of variance (ANOVA). This resulted in elimination of some of the cross terms with less significance. Although the study was based on stochastic FE analysis, it marked as one of the first implementation of RSM for reliability analysis in the field of structural engineering. Later, Bucher and Bourgund [16] proposed an efficient algorithm for RSM based reliability analysis. The original limit state function was represented by quadratic polynomials without cross terms. Initially, $2n+1$ support points were generated around the mean μ_{x_i} of the random variables which served as the centre point for the response surface. These points were spread along the axis of the random variables following $\mu_{x_i} \pm h_r \sigma_{x_i}$, where σ_{x_i} was the standard deviation of the i^{th} random variable and parameter h_r was a scaling factor. A general recommendation of $h_r = 3$ was prescribed in their study. Once the initial response surface was formed, design or failure point was evaluated to locate the new centre point for the next iteration. This new centre point was calculated using a linear interpolation technique. The second response surface was generated near this centre point and was further considered for reliability analysis. According to their algorithm, a total of $4n+3$ evaluations of the original performance function $g(\mathbf{x})$ were required. Their algorithm was one of the initial work on RSM in the field of structural reliability and is widely used as a benchmark. The method proves out to be fairly accurate and fast due to the polynomial approximation of the limit state near the design point with less number of function evaluation. However, the main demerit of this algorithm is that it assumes random variables as independent normally distributed and suffers ill-conditioning. Also, the accuracy of estimation of the failure probability remains unpredictable due to lack of convergence. Rajashekhar and Ellingwood [17] suggested few improvements to the aforementioned response surface algorithm. These improvements included additional quadratic polynomial cross terms, probability distribution based support points generation and stringent criterion for the fitting of the response surface. Additional cross terms increased the number of support points by $n(n-1)/2$ which were selected from 2^n factorial scheme. Instead of selecting the support points at the mean and on the axis of the random variables (as per Bucher and Bourgund [16]), the probability distribution of the random variables were considered to

include the tail end regions for sampling. Upper and lower tail ends were decided as per the sensitivity of the variable with respect to the limit state. Convergence criteria based on successive centre points was evaluated through interpolation. Liu and Moses [18] developed a sequential RSM for reliability analysis of complex limit state with large number of random variables. Their algorithm used the design point based criteria to govern the iterations of the response surface as suggested in the conventional RSM mentioned earlier.

Usually, the response surface is approximated around mean of the variables whereas the limit state lies away from it i.e. near tail end region. To address this issue for the effective generation of support points, Kim and Na [19] proposed gradient projection based sampling scheme. They selected linear response surface instead of quadratic basis functions and the reliability index β was evaluated using Rackwitz-Fiessler's algorithm [1] instead of MCS as the response surface was linear. They also conducted parametric study to determine the optimal scale factor h_r based on the sensitivity of β with respect to the curvature of the limit state. It was introduced to counter-check the error between the linear approximation and the actual failure surface near the design point. This vector projection based sampling scheme was further used by Das and Zheng [20] in an adaptive algorithm to improve the efficiency of the response surface. Initially, they employed an algorithm similar to Kim and Na [19] to locate an intermediate design point where the meta-model was built using quadratic basis without cross terms. The expression was modified using significant cross terms followed by reliability analysis using SORM. However, the method proved to be computational exhaustive for complex problems and also suffered ill-conditioning.

Guan and Melchers [21] presented parametric study on the sensitivity of support points and their impact on the quality of end result (i.e. p_f). They used $2n+1$ sample points, as discussed above, to develop the response surface with quadratic bases and the surface was constructed near the design point in an iterative manner. Initially, $2n$ points were generated as per $\mu_{x_i} \pm h_r \sigma_{x_i}$ where the parameter h_r was varied between 0.01 to 10.00. They studied the change in RSM with respect to the change in h_r and suggested the use of multiple h_r values to generate more sampling points for better fitting. In their study, they observed effective convergence for $h_r = 2$ or 3. However, the choice of h_r still depends on the nature of the limit state. Gomes and Awruch [22] presented a comparative study between different polynomial forms and sampling or experiment schemes, artificial neural network (ANN), FORM and MCS. The response surfaces considered in their study were quadratic with and without cross terms, and cubic without cross terms. They observed that quadratic polynomial basis without cross term using vector projecting sampling scheme was the most efficient combination. Further, their study showed an effective application of RSM coupled with neural network to reduce the computational burden. Similar study related to the use of neural network based RSM was presented by Hurtado [23].

Gayton *et al.* [24] proposed modified RSM for computationally expensive problems. Unlike conventional RSM, design points were evaluated on the basis of multiple sets of experiment or sampling points. They also used quadratic surface with cross terms and previous sampling points to locate the design point accurately. The algorithm had three steps – selection of search domain, reuse previous support points and refine the search domain. The first step was focused on predicting the search area for MPP which required $(n+4)$ support points. The response surface was formed using $(n+1)(n+2)/2+2$ support points based on the 3^n factorial design. These points were selected by angle-bisectors drawn from the mean of the variables in the search area. Statistical analysis was carried over to refine the search domain and the process was continued until the design point was located. However, convergence of their algorithm depended on the limit state function and the confidence interval of the search domain. An efficient algorithm for RSM was proposed by Romero *et al.* [25] where progressive lattice sampling scheme was employed to generate the complete quadratic polynomial. Gupta and Manohar [26] suggested an improved RSM based on multiple hypothetical spheres. The spheres were used to evaluate local failure points by shifting their origin on the axis of the variables. The radii of these spheres presented the local reliability index and helped to determine multiple MPPs in the limit state. A global response surface was fitted using these local spheres and the MCS was performed over it to obtain p_f.

All these studies presented above used least square regression to compute the unknown coefficients of RSM. It assigned uniform weights to all the support points generated in the RSM. As a consequence, modelling error was more giving unsatisfactory results, especially for inadequate support points in the vicinity of MPP. This issue was addressed by Kaymaz and McMohan [27] who proposed adaptive RSM. In this proposal, evaluation of the unknown coefficients were based on exponentially weighted regression instead of ordinary regression (i.e. least square technique). They used quadratic polynomial without cross terms and the support points were generated as per Gayton *et al.* [24]. Weights were assigned to the support points based on their Euclidian distances from the limit state. Support points close to the failure surface were given higher weights

which decreased exponentially for the points away from the surface which improved the quality of fitting. However, it suffered ill-conditioning when the support point lied on the limit state. To counter this numerical instability, Nguyen *et al.* [28] used double weights based on the relative difference of the limit state from the mean and distance of the sampling point from the centre point.

As mentioned earlier, RSM has proved to be an effective tool for reliability analysis, however it may face convergence issues, especially when dealing with nonlinear limit states. Wong *et al.* [29] observed such inconsistency in the results when applied for the nonlinear FE analysis. In their investigation on the performance of reinforce concrete beam, they observed divergence of the response surface where it generated impractical support points for h_r equal to 1 and 3. They summarized that this issue arose due to the non-smooth nature of the limit state. Their response surface approximation did not consider the cross terms. In order to address these issues, they proposed few improvements related to the selection of h_r as a function of the coefficient of variation of the random variables. Lee and Kwak [30] estimated p_f which required additional computational cost related to the estimation of the statistical moments of the performance function. RSM was used in the approximation of the limit state function in order to reduce the computational effort.

Another improvement of the RSM based on sampling points was suggested by Allaix and Carbone [31]. Their algorithm considered sampling along the tangents and the orthogonal directions of the regular polynomials upto degree 2 without the cross terms. They searched for the failure point using an iterative scheme over the rotated axial points. Gram-Schmidt orthogonalization was applied using direction cosines to generate these rotated support points. In spite of being an efficient and fast algorithm, RSM still has limitations when dealing with the nonlinear limit states. Kang *et al.* [32] and Taflanidis and Cheung [33] used moving least square technique to improve the performance. They considered weights as a function of distance of the sampling points from the intermediate centre points. Kang *et al.* [32] employed linear (initially) as well as quadratic (after the first iteration) response surfaces with axial sampling points where the weight was presented as spline functions. Taflanidis and Cheung [33] used complete quadratic terms with weights defined as exponential functions. Their results suggested better estimate of p_f by moving least square based regression.

Recently, RSM has emerged as an efficient tool for FE model updating [34]. It bypasses the computational cost needed in multiple runs of FE model. Also, it helps to evaluate the gradient for optimization which may be difficult otherwise. Ren and Chen [35] applied RSM for FE model updating of simply supported and box-culvert bridges. They optimized weighted residual error between the identified and modelled natural frequencies. It was noted that RSM based model updating converged faster than the sensitivity based updating techniques. Brehm *et al.* [36] studied RSM for updating cantilever truss and railway bridges. They used weights in the objective function which was defined by the energy based modal assurance criteria. They also used genetic algorithm and gradient based optimization for updating. Shahidi and Pakzad [37] proposed an unique updating scheme using RSM for linear as well as nonlinear problems. In their time domain FE model updating scheme, a generalized formation of RSM was defined where order and fitting were collectively judged from the individual response surface at each time step. In view of the application of RSM for model updating, Chakraborty and Sen [38] examined the effectiveness of MLS based approach over LS. In their study, conventional exponential weight function was used for MLS based RSM to update the properties of a ten-bar truss and culvert using synthetic data with error ranging from 10% to 30%.

In general, RSM has witnessed different applications in many engineering problems e.g. modal updating, design of RC structures, mechanical systems and aerospace structures among many others [39–42]. However, RSM, being a polynomial based regression scheme has problems in convergence and is not robust for nonlinear functions. It is also computationally inaccurate when dealing with high dimensional problems i.e. *curse of dimensionality*.

1.1.2 Stochastic Response Surface Method (SRSM)

In comparison to RSM, SRSM is convenient and convergent [43], whose accuracy depends on the order of the polynomial expansion. Gavin and Zaicenco [44] demonstrated the accuracy of SRSM in comparison to RSM and MCS. Their study was based on the reliability analysis of isolated systems under seismic loading. Shi *et al.* [45] used Hermite polynomials for reliability analysis which was accurate with less computational cost as compared to RSM and MCS.

The primary contribution for modelling uncertainties is due to polynomial chaos which was first introduced

by Weiner [46]. Later, Cameron and Martin [47] proved that the Hermite polynomials were orthogonal and convergent in $\mathcal{L}^2$ sense. Tatang [48] developed probabilistic collocation scheme for modelling implicit functions by PCE. It used Gauss quadrature points to evaluate the unknown coefficients of PCE. Further, Isukapalli [13] developed an efficient SRSM algorithm to model the uncertainty propagated in the output. He used Hermite polynomials for modelling the output uncertainties in terms of series expansion of random variables. He also developed close form expression for the transformations of some probability distributions e.g. lognormal, exponential, uniform. The unknown coefficients of the expansion were determined using sampling points based on collocation or regression schemes. He also developed an algorithm for efficient collocation. Thus, the limit state function was surrogated by an approximate polynomial expression defined in the standard normal space. His study was mostly concentrated on the uncertainty quantification of air quality modelling. This algorithm is considered as a benchmark in the literature and has been extensively used for structural reliability analysis. Although the uncertainty modelling using PCE is considered to be accurate, the primary drawback of PCE based technique is the curse of dimensionality, where the computational cost increases substantially with the higher number of random variables. Wei *et al.* [49] used sampling points based on monomial cubature rules where fewer points were required, thus making the method viable especially for computationally exhaustive models. Sudret and Der Kiureghian [50] modified stochastic FE analysis with FORM and importance sampling for reliability analysis. They employed Karhunen-Loève Expansion (KLE) with 5 terms to discretize the random field and observed limitation of FEM based reliability analysis for large uncertainty and short correlation length. It suffered accuracy as PCE with Galerkin approach failed to model the failure region of small probability and required higher order which, in turn, needed more computational time.

Xiu and Karniadakis [51] proposed a new technique to model the uncertainties by introducing Askey scheme where generalized PCE with different types of orthogonal polynomials were used. Their technique represented the non-Gaussian process in a better way as compared to Hermite expansions. Choi *et al.* [52] studied the efficiency and accuracy of generalized PCE with direct transformation techniques as proposed by Xiu and Karniadakis [51] and Isukapalli [13]. The generalized PCE with lower order was more efficient for non-normal variables whereas the direct transformation technique was more computationally efficient for other cases. They also proposed an efficient scheme by combining the transformation technique with Latin hypercube sampling. Ernst *et al.* [53] further studied the limitation of the generalized Hermite PCE for intrusive formulation.

Another efficient algorithm using Karhunen-Loève expansion and PCE for modelling the input-output relationship was presented by Huang *et al.* [54]. The unknown coefficients were obtained by means of collocation where the support points were obtained as different combinations of the roots of one order higher polynomials [13]. Liang *et al.* [55] presented a general collocation based SRSM using spreadsheet. However, their study didn't consider correlated random variables and the computation time required for convergence. Bressolette *et al.* [56] proposed a stochastic collocation scheme using Lagrange polynomials. This technique had better convergence and could be effectively used for reliability analysis and design but suffered large modelling error as the dimension increased. Ying [57] studied the performance of SRSM for reliability analysis in structural engineering. The collocation points were selected in high probability regions (i.e. near and symmetric to the origin) to reduce the error and actual function evaluations which ultimately improved the accuracy and lowered the computational cost.

Gavin and Yau [58] suggested to approximate the original limit state by higher order polynomials with cross terms. The order of the polynomials was restricted to limit the computation cost, ill-conditioning of the system equations and erroneous approximation of the limit state function outside the neighbourhood of the sampling points. In this context, they suggested Chebyshev polynomials whose order was selected based on their statistical and numerical significance. The degree of the polynomial for each random variable was determined irrespect of its correlation with others. After determining the degree of the polynomial for each random variable, all possibilities of mixed or cross terms were evaluated under predefined criteria so that the total number and individual degree of the cross term could be limited. Also, the cross terms were limited to only two random variables. The unknown coefficients were evaluated using either 3^n factorial sampling or by uniformly distributed random sampling depending upon the dimension of the problem. Finally, MCS was adopted to evaluate the probability of failure. The accuracy was tested by an adjusted R^2 value. Their work also included a parametric study on k with the fluctuation in the estimation of failure probability, the degree of the polynomial and adjusted R^2 for k ranging from 1 to 6. The method didn't consider correlation between the random variables and multiple failure regions.

Besides reliability analysis, PCE can also be used for sensitivity analysis in optimization problems. Hou *et*

al. [59] conducted sensitivity analysis of random functions where stochastic response surface was constructed to approximate the original function and its derivatives. As their analysis used integrals, it was applicable for functions with a low number of random variables i.e. ≤ 6. Schuëller and Pradlwarter [60] compared sampling methods (i.e. subset simulation and its variant) and spectral stochastic finite element method (SSFEM) for random field of embankment dam and observed better accuracy could be achieved by SSFEM. Ghanem *et al.* [61] extended the application of SSFEM combined with PCE by reducing the dimension for the same problem. KLE was adopted to limit the significant terms of the random field discretization to aide the stochastic model reduction. The idea arose from their observation that eigenvalues from KLE decay for short correlation length which reflects marginal or no significance of terms beyond certain limit. Maute *et al.* [62] proposed reduced order model for PCE based SSFEM applying multi point approximation based on sensitivity of displacement with respect to the variables which was evaluated using their derivatives. This required multiple updating of the reduced basis matrix by perturbations of the random variables. Like RSM, PCE can also be used for local approximation in the neighbourhood of MPP. This eases the computational burden due to higher dimensionality as demonstrated by Proppe [63]. Preliminarily, a higher order PCE is generated globally in order to estimate MPP. Following the global approximation, first order PCE is used for local approximation which is adaptively reformed. They used PCE with bi-orthogonal polynomials for simplifying the modelling of random fields. They performed reliability analysis by LHS based importance sampling over the MPP which was located by constrained optimization.

Blatman and Sudret [64] reduced the number of unknown coefficients to construct regression based sparse polynomial chaos approximation where less important terms were dropped based on their influence on the R^2 (i.e. coefficient of determination) value using stepwise regression technique. It required prior generation of support points through LHS which might result in larger sample size than actually required. Later, they prescribed sequential generation of LHS by refining the equally probable intervals for efficient stochastic computation [65]. They also used ANOVA based dimension reduction to decompose the sparse PCE based approximation [66]. Apart from regression based determination of unknown coefficients, they applied least angle regression technique with hyperbolic PCE [67] for random field problems. Hawchar *et al.* [68] used sparse PCE to study the time-dependent reliability using principal component analysis to reduce the number of time steps (i.e. dimension of the time-variant problem). Pan and Dias [69] applied sliced inverse regression over sparse PCE for uncertainty quantification of lognormally distributed random fields which were discretized by KLE. Blatman and Sudret [70] proposed an adaptive algorithm for detecting the significant PCE terms (i.e. sparse PCE) used to reduce the coefficients and subsequently reducing the computational cost. They demonstrated an example based on reliability analysis of nuclear reactor vessel subjected to thermal pressure shock by their proposed algorithm. In order to bypass the curse of dimensionality related to PCE, Hu and Youn [71] proposed a new adaptive PCE scheme for reliability analysis. Their work used adaptive sparse scheme for determining the order of PCE. High accuracy and convergence of their method were illustrated by numerical examples of reliability analysis and reliability based design optimization (RBDO).

Li *et al.* [72] proposed an improved SRSM for correlated non-normal random variables. They used Nataf transformation to convert the variables into the standard normal space and used collocation technique to find the coefficients of the Hermite polynomials. The number of collocation points were generated keeping in view of the stability of the system matrix. Mollon *et al.* [73] applied SRSM with collocation points for reliability analysis of compressed-air tunnel. They studied the structural stability of the tunnel entrance using friction angle and cohesion of the soil as random variables where SRSM helped in efficient calculation of the sensitivity and probability of failure.

Ahmed and Soubra [74] adopted subset simulation for reliability analysis of strip foundation on soil with spatial variation in elastic modulus. KLE was used to discretize the random field which followed lognormal distribution. In order to increase the efficiency, traditional subset simulation was improved by generating initial samples beyond a fixed distance from the origin in the standard normal space. This distance was optimally determined by a prior knowledge of the approximate probability of failure estimated on ad-hoc basis using SRSM. They showed that the traditional SRSM was a special case of their proposal when the distance they modelled was assumed to be zero.

Sasikumar *et al.* [75] studied the effect of random field on the reliability of composite plate using optimal linear expansion (OLE). The material properties of the layered composite plate were modelled by non-Gaussian distributions based on the experimental investigations [76]. Probability of failure was determined employing direct MCS which underestimated p_f in the random variable approach as compared to random field. The increase in correlation length also effected probability of failure which consequently improved the reliability of the plate. Use of OLE reduced the number of discretization terms through the construction of coarse

random field mesh. They also applied PCE based SSFEM to study the propagation of uncertainty in the composite plate [77]. It helped in overcoming the issue of singularity in OLE where inversion of correlation matrix becomes difficult for large correlation length. Later, they proposed a reduced order PCE based SSFEM where coarse equivalent stochastic model was established by considering the individual laminas as one layer. Tipireddy and Ghanem [78] proposed adaptive basis function based PCE for intrusive and non-intrusive formulations using projections where the random field was discretized by KLE with dominant term only. They applied sparse grid using Smolyak's construction to generate the support points. Generalized application of this proposal to reduce the dimension of more than one random variable was recently presented by Tsilifis and Ghanem [79].

1.1.3 Kriging

Besides RSM and SRSM based meta-modelling approach, Kriging has become popular among the engineers and researchers due its ability to optimally replicate a non-intrusive performance function [80]. It was first introduced in 1951 by Danie G. Krige, a South African engineer who developed it to predict the gold deposits [81]. Hence, the nomenclature of this method (i.e. Kriging) is accredited to him. The mathematical model of this technique was first proposed by Matheron [82] in 1963 for geostatistical analysis involving problems with spatial variability. Formation of the meta-model was based on the minimal variance in error where a simplified Kriging was considered without linear regression. Moreover, the contributions of different sets of experimental data or support points from the drilling locations were averaged such that the unknown coefficients were summed up to unity which eventually resulted in a weighted average. The primary advantage of this technique was its ability to estimate the first two statistical moments from the meta-model accurately. This method was also referred as the optimum interpolation by Cressie [83, 84].

Different Kriging techniques were developed in the recent past which could be broadly classified under the categories: Simple, Ordinary, Universal, Blind, Stochastic, Co or Multi-fidelity, Gradient and so on [85–90]. Simple Kriging considers a constant value of global behaviour of the meta-model which is known whereas ordinary Kriging assumes that the constant is unknown. Both, simple and ordinary Kriging are obsolete in the recent times whereas universal Kriging is one of the widely used technique which considers a regression model [91–93] in its formulation. Hence, it is also perceived as an extension of the previously discussed RSM. Another alternative is blind Kriging where the basis terms of the meta-model are not predefined as in its universal version [94]. It considers a Bayesian selection technique to determine the basis terms which effectively captures the variance at the support points for improvement of the surface.

Application of Kriging for uncertainty quantification and reliability analysis was first proposed by Romero *et al.* [25] and Kaymaz [95]. Kaymaz [95] performed reliability analysis as suggested by Bucher and Bourgund [16] coupled with universal Kriging using MATLAB® [96] based DACE toolbox [97]. A quadratic polynomial basis was considered in the meta-modelling and the support points were populated using CCD and the scheme suggested by Bucher and Bourgund [16]. Their study proved that Kriging based reliability analysis performed better than its polynomial counterpart (i.e. classical RSM [16]). It was also observed that the scaling parameter used in the Gaussian correlation function was highly sensitive which could effect the accuracy of the Kriging based surface. Moreover, different correlation functions (i.e. linear, exponential and Gaussian) were studied where these parameters were quantified using maximum likelihood optimization. They concluded that linear and exponential correlation functions were suitable for linear or nearly linear limit state whereas Gaussian model was preferable for nonlinear limit state. Van Beers and Kleijnen [80] employed support points generated from random perturbation to construct the Kriging based response surface. These perturbations were assumed to be following the properties of white noise. They applied least square based RSM to construct the meta-model with Kriging where leave-one-out cross-validation was performed to test the surface. Kleijnen *et al.* [98] used modified LHS scheme to generate support points for the construction of Kriging based response surface.

Schobi *et al.* [99] proposed meta-model based on PCE coupled with universal Kriging technique. The global approximation of the meta-model was characterized by the sparse PCE whereas local approximation was carried by the Kriging. The sparse polynomial expansion was built using hyperbolic truncation to limit the cross terms and LAR was further adopted to eliminate the insignificant terms in the expansion. The surface formed by their proposal was tested with leave-one-out cross-validation to avoid over-fitting. They developed two algorithms – the first one was straightforward (often referred as sequential PCE-Kriging) and the second algorithm formed an optimal meta-model using iterations to refine it. The second proposal (i.e.

optimal PCE-Kriging) was selected based on the minimum error in the leave-one-out cross-validation. The examples considered in their study were hypothetical performance functions with up to 20 input variables. The optimal PCE-Kriging was further adopted for reliability analysis of problems with maximum 10 random variables [100]. The support points were generated using LHS with an iterative enrichment based on the limit state margin. Dutta *et al.* [101] used sequential PCE with ordinary Kriging based meta-model to efficiently perform the RBDO of thin and flexible structures subjected to wind loading.

Wang *et al.* [102] used DACE Toolbox for global sensitivity analysis when the system had parametric uncertainty. In this model, the support points were generated using a low discrepancy sampling scheme in quasi-MCS and importance sampling framework. Gaussian correlation function was adopted for error estimation and the parameter of this function was optimized using maximum likelihood approach. The numerical examples considered in their study involved less number of random variables (i.e. ≤ 6). In particular, this study on uncertainty quantification using Kriging based sensitivity analysis proved to be fairly efficient as compared to commonly used Sobol indices. Jia and Taflanidis [103] proposed Kriging with principal component analysis (PCA) for risk analysis of hurricane. They adopted PCA to identify the significant dimensions to improve the accuracy of the Kriging based meta-model. This strategy reduced the dimensions significantly (i.e. from 10^4 to less than 50). They also observed that the Kriging reduced the computational cost. Gaspar *et al.* [104] presented parametric study using nonlinear FE model for reliability analysis and uncertainty quantification. They observed that the degree of polynomial basis in the Kriging based regression model had marginal effect on the overall accuracy. Hence, they advocated the use of ordinary Kriging over universal Kriging.

Zhang *et al.* [105] improved the efficiency of Kriging based meta-model by a sequential support point generation scheme in certain regions of interest (i.e. near limit state). They identified these regions of interest with the help of the probability of predicting negative value at any arbitrary location. The output was assumed to follow Gaussian distribution to calculate the probability and the region of interest was within 95% confidence interval (i.e. [2.5% 97.5%]). Overall, the concept employed in their study was similar to the one applied in the MPP based generation of support points by Kim and Na [19]. Once the support points were generated and refined to the region of interest, the best meta-model from the leave-one-out cross validation was considered further for the reliability analysis. Haeri and Fadaee [106] applied this technique to determine the probability of failure of the composite plate. They claimed marginal improvement in the results obtained from the neural network and its modified version with the radial basis function based meta-models. Both these studies used examples with higher p_f (> 0.01) and low dimension. Hence, the use of these techniques to determine low p_f of large dimensional problems still remain unanswered.

Echard *et al.* [107] proposed an efficient modification of Kriging based on sequential generation of the support points. Initially, a small size of randomly generated samples (say, MCS) were used, followed by more points in the regions with relatively high probability density. However, it faced few shortcomings due to the reduction in efficiency of the proposed sequential sampling strategy and the initial guess for sufficient generation of the support points from the MCS [108]. Jian *et al.* [109] investigated the accuracy and convergence criteria employed by Kriging for the reliability analysis. As the Kriging employed initial ensembles of simulated random variables, their proposal showed efficient sampling to reduce the variance in p_f estimation. Jiang and Li [110] combined Kriging with Active Subspace technique based on eigenvalue decomposition to address the high dimensional performance function. The decomposition gave reduced space with significant dimensions without any notable loss in the accuracy. However, their numerical study used examples having high p_f value (> 0.1) and hence, the performance of their model for low p_f was unobserved. Recently, a review of the developments of Kriging based meta-models for different applications was published by Kleijnen [111] highlighting the contributions in the risk and uncertainty quantification.

1.1.4 High Dimensional Model Representation

Unlike other meta-models discussed in the previous subsections, High Dimensional Model Representation is relatively new as it was first developed in 1990s. Rabitz *et al.* [112] proposed this technique based on orthogonal decomposition for large dimensional problems (i.e. the number of random variables $n > 10$). This decomposition or reduction technique is often used to represent high dimensional performance function into multiple component functions of low dimensions using ANOVA [113–117] and hence, it is called high dimensional model representation (HDMR). Similar decomposition technique based on the correlation between the input variables and the output function was given by Xu and Rahman [116]. Sobol' [114]

proposed an algorithm based on the intersecting hyper-planes which was widely known as cut-HDMR. In this model, the support points were evaluated in a defined grid which resulted in highly accurate HDMR model. Aliş and Rabitz [113] suggested inclusion of random sampling in the HDMR framework. In general, both deterministic sampling [118] and random sampling [119,120] were used by the researchers in the recent past.

Rao and Chowdhury [121] proposed an efficient algorithm for reliability analysis by utilizing HDMR in association with fast Fourier transform near MPP. In another paper [117], these authors studied finite difference HDMR for the reliability analysis where the interpolant was determined using MLS technique to demonstrate the efficiency of first and second order component functions. They also studied the ability of finite difference HDMR for handling piecewise continuous functions and reported that MLS based interpolation performed better than Lagrange interpolation [122]. Using this method, they also presented sensitivity analysis with respect to the variables and its derivatives [123]. Chowdhury *et al.* [117] studied finite difference HDMR for reliability analysis where they determined the interpolants using MLS technique. They considered till second order of HDMR for the approximation and demonstrated the efficiency using MLS for first and second order model representation. Chowdhury and Rao [124,125] studied different variations of HDMR using factorized functions instead of summand functions. Balu and Rao [126] used HDMR to solve problems with multiple design points. Sampling points for these models were selected axially as per weight functions, as suggested by Kaymaz and McMohan [27]. It helped to identify the reference points near the design points for developing the HDMR. Once the model was developed, the probability of failure was evaluated by fast Fourier transform. Ma and Zabaras [127] developed an adaptive algorithm for HDMR using sparse grid scheme. They identified important component functions to generate the adaptive HDMR based on its sensitivity with respect to the 0^{th} order component function. Luo *et al.* [128] proposed an efficient scheme to estimate the optimal order of the HDMR using the radial basis functions.

Chowdhury and Adhikari [118] proposed 1^{st} and 2^{nd} order HDMR with regular polynomial bases upto 2^{nd} degree for uncertainty quantification of random field problems. They evaluated uncertainty in the beam and plate modelling where the field was discretized by truncated KLE. Using HDMR, Chen *et al.* [129] developed 1^{st} order approximation for robust topology optimization by KLE based random field discretization. Using ANOVA based decomposition, Chakraborty and Chowdhury [130,131] proposed polynomial correlated function evaluation (PCFE) with orthogonal basis to solve both intrusive and non-intrusive problems. For intrusive application, Galerkin projections on the meta-model was considered whereas non-intrusive application was developed into analytical, semi-analytical and numerical solutions for the stochastic problems. The unknown coefficients of the expansion were determined using Homotopy algorithm. Later, they proposed modification by making the order of the polynomial and generation of the support points adaptive based on the sensitivity and distribution, respectively [131] for uncertainty quantification. Dey *et al.* [120] investigated the effect of uncertainty on the modal analysis of cantilever composite plate using random sampling based HDMR (RS-HDMR) [119]. This version of HDMR employed PCE with modified shifted Legendre polynomial bases to replicate the performance function. Support points were generated through quasi-random sampling such as Sobol' sequence to construct the meta model.

1.1.5 Other Meta-Model Techniques

Apart from the techniques reviewed in the above subsections, there are other meta-models often used in the field of optimization, uncertainty quantification and reliability analysis. Few of them are Radial Basis Function (RBF) [132,133], ANN [134], Support Vector Regression (SVR) [132], Multivariate Adaptive Regression Splines (MARS) [135], Splines [136] and so on. RBF [132,133] is an interpolation technique based on the weights or shape functions, hence it does not follow the regression model as in RSM, SRSM and Kriging. In this modelling technique, the basis functions are dependent of the distance between the two support points of the input variable. ANN [134] employs neurons based on interconnected multiple linear regression models, similar to the biological phenomenon of nervous system, where weights are assigned to train them. SVR [132] categorizes the support points based on hyperplanes which segregate the negative and positive values of the output. MARS [135] is a nonparametric regression based interpolation technique which employs splines as the basis function. Splines are formed using piecewise polynomial functions. The list of the meta-models along with the commonly employed DoE schemes [137–139] are given in Table 1.1. Also, the widely used fitting techniques required to construct these meta-models are tabulated for ready reference.

Table 1.1: Commonly used features of the meta-model techniques

Design of Experiment/ Sampling Schemes	Choice of Meta-models	Model Fitting Techniques
• Deterministic or classic schemes – Factorial (full or fractional) – Central composite – Alphabetical optimal (D etc.) – Box-Behnken – Plackett-Burman • Space-filling sampling methods – Simple grids – Latin hypercube – Orthogonal arrays – Hammersley Sequence – Uniform designs – Minimax and Maximin Hybrid methods • Directional simulation • Random sampling (pseudo or quasi) • Importance sampling • Discriminative sampling • Customized schemes (adaptive or sequential)	• Polynomial (regular or orthogonal) • HDMR or dimension decomposition • Kriging or Gaussian process • Least interpolating polynomials • Splines (linear, cubic etc.) and multivariate adaptive regression splines (MARS) • Radial basis functions (RBF) • Artificial neural network (ANN) • Support vector regression (SVR) • Knowledge base or decision tree • Hybrid or coupled surrogate models	• Least squares regression (ordinary, weighted or moving) • Best linear predictor/unbiased predictor (BLUP) • Log-likelihood • Multi-point approximation (MPA) • Sequential or adaptive meta-modelling • Back propagation (just for ANN) • Entropy (for decision tree)

1.2 Objectives

Literature review in the previous sections present a comprehensive survey of the past research works in the field of meta-model based optimization and reliability analysis. From this review, different areas emerge that demand further research to improve their potentials for high fidelity modelling of uncertainties. Some of these gap areas are mentioned below –

- The most important challenge among the meta-model base methods to this date is the curse of dimensionality. The detailed literature review suggests that majority of the papers illustrate their applications using low to moderate number of random variables.
- Global fitting of the meta-model with major emphasis on the local behaviour of the limit state function of complex engineering problems using interpolation or regression technique require further improvement in terms of accuracy and efficiency.
- Even for the local modelling of the limit state function, the proposed techniques in the literature often face numerical troubles which eventually lead to erroneous results.
- A large class of meta-models, try to replicate the nonlinear limit state, often require prior sensitivity analysis to adequately predict the degree of individual variables.

Most of the numerical techniques reported in the previous literatures aimed to build high-fidelity models with minimum computational cost that were proportional to the number of original function calls. In order to do so, theses methods either –

- omitted or modified certain terms in the polynomial series
- limited the number of independent variables through discretization of the random field or
- needed prior information of the limit states to determine the sensitivity with adequate accuracy and efficiency

Construction of these meta-models require support points generated from either deterministic sampling (i.e. collocation points, sparse grid) or random sampling (i.e. LHS, Sobol' sequence). It often employed a single generation of the support points. With this in view, the present study focuses on to

1. develop efficient non-intrusive adaptive algorithms to address the curse of dimensionality in the meta-modelling for uncertainty quantification and reliability analysis
2. reduce the number of original function evaluations required for the interpolations using effective and sequential generation schemes
3. develop an adaptive sparse meta-model with effective dimension reduction for high dimensional problems involving random field
4. study the application of the proposed modelling for reliability based design of high dimensional and complex problems

1.3 Organization of the Thesis

This thesis contributes towards the development of efficient high-fidelity meta-model for stochastic computation to quantify the reliability and the propagation of uncertainty in the response. The road map of this thesis following this first chapter which outlines the motivation for this study is given below –

- The 2^{nd} Chapter performs a comparative study between the local and global approximation approach of RSM with different support points schemes for deterministic optimization. A FE model updating problem is solved using these two approaches to compare their efficiency.
- Using the efficient version of RSM identified from the previous chapter, 3^{rd} Chapter extends the meta-model based application for random variables to quantify uncertainty and eventually, reliability analysis. Towards this direction, a two-step RSM based algorithm is developed for reliability based design optimization e.g. tuning passive controller working in the uncertain environment.
- In the 4^{th} Chapter, orthogonal polynomials are employed for meta-modelling using chaos based expansion. In this chapter, a sequential algorithm (i.e. Sequential SRSM) is developed using a hierarchial approach for efficient generation of the support points coupled with local approximation technique based on MLS. The performance of the proposed method is demonstrated using different benchmark and design problems for reliability analysis.
- Following these developments using orthogonal basis, 5^{th} Chapter suggests a new adaptive algorithm using HDMR where orthogonal terms or subfunctions are adopted to approximate the performance function. It explores the benefits of multiple constructions of the dimension decompositions for efficient and accurate modelling of the limit state.
- The efficiency of this method is further enhanced using a dimension wise adaptive version which forms a sparse multiple HDMR framework with modified sparse grid formulation. This proposal is further tested for stochastic FE analysis with spatial variability to address the issues with large dimensional problem which is presented in the 6^{th} Chapter.
- Use of MLS technique to determine the unknown coefficients results in solution of matrix inversion to minimize error at every realization. Hence, the meta-model suffers a significant computational burden due to scalar approach associated with the MLS technique. To address this, an alternate methodology is suggested where the error terms are modelled using random process. This eventually leads to the determination of three different sets of unknown coefficients which improves the computational efficiency. This is thoroughly explained in the 7^{th} Chapter.

- Finally, the salient contributions of this study are concluded in the 8^{th} Chapter along with the discussion on the plausible development of this study in the near future.

Chapter 2

Response Surface Method (RSM)

2.1 Introduction

In this chapter, basic formulation of the response surface method is discussed. Various orders of the polynomial bases are studied to determine the unknown coefficients and the performance of different support points generation schemes are reviewed. Using this formulation, benchmark problems are solved to compare the performance of different meta-models. Finally, a reinforced concrete road bridge is considered where finite element model is updated using response surface and field test data.

2.2 Response Surface Based Meta-modelling

Response surface is an approximate surface that maps the original performance function. It is typically a polynomial function in multi-dimensional space where the dimension represents the variables (i.e. $\mathbf{x} \in \mathbb{R}^n$) in the original function. It eases the exhaustive computational burden associated with the multiple evaluations of the original function which is often a complex FE model for reliability analysis and design optimization. RSM can be expressed as

$$\mathbf{g}(\mathbf{x}) = \mathbf{X}(\mathbf{x})\mathbf{a} + \mathbf{e}_{\mathrm{g}} \tag{2.1}$$

where, $\mathbf{g}$, $\mathbf{X}$, $\mathbf{a}$ and $\mathbf{e}_{\mathrm{g}}$ are the values of the original performance function, matrix of the RSM polynomial bases, coefficient vector and the error vector due to lack of fit, respectively. The generalized expression of RSM in Eq. 2.1 can be mathematically represented for the linear basis as

$$g(\mathbf{x}) = a_0 + \sum_{i=1}^{n} a_i x_i + \mathbf{e}_g \tag{2.2}$$

and for the quadratic basis without cross terms as

$$g(\mathbf{x}) = a_0 + \sum_{i=1}^{n} a_i x_i + \sum_{i=1}^{n} b_{ii} x_i^2 + \mathbf{e}_g \tag{2.3}$$

Above equation uses quadratic terms without considering the combined effects. However, it can be further modified with cross terms, if necessary and the complete quadratic surface is expressed as

$$g(\mathbf{x}) = a_0 + \sum_{i=1}^{n} a_i x_i + \sum_{i=1}^{n} b_{ii} x_i^2 + \sum_{i=1}^{n} \sum_{j>i}^{n} b_{ij} x_i x_j + \mathbf{e}_g \tag{2.4}$$

where, n is the number of variables. In general, the polynomial expansion used in RSM is limited to either linear or quadratic basis function [22]. The polynomial basis matrix is estimated by generating a specific pattern of support points following a particular DoE scheme. Using the values of $g(\mathbf{x})$ at these support points, Eq. 2.4 can be rearranged in the following form

$$\begin{Bmatrix} e_{g,1} \\ e_{g,2} \\ \vdots \\ e_{g,n_s} \end{Bmatrix} + \begin{bmatrix} 1 & x_{1,1} & \cdots & x_{n,1} & x_{1,1}x_{1,1} & x_{1,1}x_{2,1} & \cdots & x_{n,1}x_{n,1} \\ 1 & x_{1,2} & \cdots & x_{n,2} & x_{1,2}x_{1,2} & x_{1,2}x_{2,2} & \cdots & x_{n,2}x_{n,2} \\ \vdots & \vdots & \cdots & \vdots & \vdots & \vdots & \cdots & \vdots \\ 1 & x_{1,n_s} & \cdots & x_{n,n_s} & x_{1,n_s}x_{1,n_s} & x_{1,n_s}x_{2,n_s} & \cdots & x_{n,n_s}x_{n,n_s} \end{bmatrix} \begin{Bmatrix} a_0 \\ a_1 \\ \vdots \\ b_{nn} \end{Bmatrix} = \begin{Bmatrix} g(\mathbf{x}_1) \\ g(\mathbf{x}_2) \\ \vdots \\ g(\mathbf{x}_{n_s}) \end{Bmatrix} \tag{2.5a}$$

$$\Rightarrow \mathbf{X}(\mathbf{x})\mathbf{a} = \mathbf{g}(\mathbf{x}) - \mathbf{e}_g \tag{2.5b}$$

for quadratic basis. Similarly, it can be expressed for the linear basis by curtailing the additional terms associated with the quadratic polynomials. Original function evaluated at the support points are regressed to obtain the coefficients $\mathbf{a} = \{a_0\, a_1\, a_2 \cdots a_n \;\; b_{11}\, b_{12} \cdots b_{1n}\, b_{22} \cdots b_{nn}\}^{\mathsf{T}}$ of the polynomial set. Readers may refer to Myers *et al.* [140] for further details of this numerical technique. After the selection of basis (i.e. linear or quadratic), the unknown coefficients $\mathbf{a}$ are estimated by least square based curve fitting or its modified version (i.e MLS) which are discussed below.

2.2.1 Least Square Technique

This technique is commonly used for the regression analysis where it optimizes the square of error ε between the original function and the approximate surface. Using Eq. 2.5b, the square of the error can be expressed as

$$\varepsilon(\mathbf{a}) = \mathbf{e}_{\mathrm{g}}^{\mathsf{T}}\mathbf{e}_{\mathrm{g}} = (\mathbf{g} - \mathbf{X}\mathbf{a})^{\mathsf{T}}\,(\mathbf{g} - \mathbf{X}\mathbf{a}) \tag{2.6}$$

On minimizing Eq. 2.6 with respect to the unknown coefficients $\mathbf{a}$ gives the following expression for least square solution

$$\mathbf{a} = (\mathbf{X}^{\mathsf{T}}\mathbf{X})^{-1}\,(\mathbf{X}^{\mathsf{T}}\mathbf{g}) \tag{2.7}$$

The above expression of $\mathbf{a}$ is valid when $\mathbf{X}^{\mathsf{T}}\mathbf{X}$ is non-singular and is referred as ordinary least square technique.

2.2.2 Moving Least Square Technique

A major demerit of the aforementioned technique lies in its global fitting of the response surface which often results in large error. Once the coefficients $\mathbf{a}$ are evaluated, it remains fixed for every point in the design space. To address this issue, MLS technique is used which makes the coefficients evolving by assigning unequal weights to the support points. It updates the coefficients $\mathbf{a}(\delta_{\mathbf{x}})$ which become functions of the Euclidean distance $\delta_{\mathbf{x}}$. The inclusion of weights at the support points eventually modifies the summation of squared error in Eq. 2.6 as

$$\varepsilon = \sum_{i=1}^{n_s} w(\delta_{\mathbf{x}_i}) e_{g,i}^2 \tag{2.8}$$

where, $w(\delta_{\mathbf{x}_i})$ and $e_{g,i}$ denote the weight function and fitting error at the i^{th} support point, respectively. This modifies Eq. 2.6 by the weight matrix W as follows

$$\varepsilon(\mathbf{a}, \mathbf{x}) = \mathbf{e}_{\mathrm{g}}^{\mathsf{T}} W(\mathbf{x})\, \mathbf{e}_{\mathrm{g}} = (\mathbf{g} - \mathbf{X}\mathbf{a})^{\mathsf{T}} W(\mathbf{x})\, (\mathbf{g} - \mathbf{X}\mathbf{a}) \tag{2.9}$$

This adaptive estimation of $\mathbf{a}$ in MLS helps to model the local variation of $g(\mathbf{x})$ and hence performs better. The coefficient vector $\mathbf{a}$ is evaluated by minimizing the modified least square error in Eq. 2.9 which is

expressed as follows

$$\frac{\partial \varepsilon(\mathbf{a}, \delta_{\mathbf{x}})}{\partial \mathbf{a}} = -\mathbf{X}^{\mathsf{T}} W(\mathbf{x})[\mathbf{g} - \mathbf{X}\mathbf{a}] - [\mathbf{g} - \mathbf{X}\mathbf{a}]^{\mathsf{T}} W(\mathbf{x})\mathbf{X} = 0$$
$$\Rightarrow \mathbf{a}(\mathbf{x}) = (\mathbf{X}^{\mathsf{T}} W(\mathbf{x})\mathbf{X})^{-1}(\mathbf{X}^{\mathsf{T}} W(\mathbf{x}))\mathbf{g} \tag{2.10}$$

In the above equation, matrix W is given by

$$W(\mathbf{x}) = \begin{bmatrix} w(\delta_{\mathbf{x}_1}) & 0 & \cdots & \cdots & 0 \\ 0 & \ddots & & & \vdots \\ \vdots & & w(\delta_{\mathbf{x}_i}) & & \vdots \\ \vdots & & & \ddots & 0 \\ 0 & \cdots & \cdots & 0 & w(\delta_{\mathbf{x}_{n_s}}) \end{bmatrix} \tag{2.11}$$

If the variable weight factor w at each support points are fixed to unity, MLS technique converges to the ordinary least square technique. The most popular suggestion of the weight function is the exponential form which is given by

$$w(\delta_{\mathbf{x}_i}) = \begin{cases} \exp^{-\left(\frac{\delta_{\mathbf{x}_i}}{D_r \gamma_w}\right)^2}, & \text{if } \delta_{\mathbf{x}} \leq D_r \\ 0, & \text{if } \delta_{\mathbf{x}} > D_r \end{cases} \tag{2.12}$$

Here, it may be noted that the weight function varies with radial distance D_r which defines its domain of influence. For this purpose, the shape factor $\gamma_w = 0.3808$ [141] is used in Eq. 2.12 to control the decay of the weight function. From Eq. 2.12, it is evident that smaller value of D_r results in better fitting of the response surface due to the contribution of support points which are in the vicinity of the desired location. Thus, the coefficients determined based on these support points eventually reduces the error. Most and Bucher [142] have proposed different weight function based on the regularized scheme as follows

$$w(\delta_{\mathbf{x}_i}) = \begin{cases} \frac{\bar{w}(\delta_{\mathbf{x}_i})}{\sum_{j=1}^{n_s} \bar{w}(\delta_{\mathbf{x}_j})}, & \text{if } \delta_{\mathbf{x}_i}, \delta_{\mathbf{x}_j} \leq D_r \\ 0, & \text{if } \delta_{\mathbf{x}_i} > D_r \end{cases} \tag{2.13}$$

The individual weight function $\bar{w}(\delta_{\mathbf{x}_j})$ in the above equation is expressed as

$$\bar{w}(\delta_{\mathbf{x}_j}) = \frac{\left\{\left(\frac{\delta_{\mathbf{x}_j}}{D_r}\right)^2 + \delta_e\right\}^{-2} - (1+\delta_e)^{-2}}{\delta_e^{-2} - (1+\delta_e)^{-2}} \tag{2.14}$$

where, δ_e is considered as 10^{-5} [142]. Use of regularized weight function in RSM helps in assuming larger D_r as the shape function error is relatively less. Above formulation shows the advantage of MLS technique, especially for nonlinear surface where local approximation are carried out using weight functions as compared to the least square based RSM which uses global approximation.

2.3 Design of Experiment (DoE) Schemes

The unknown coefficients in the above formulations are determined using the response of the original performance function at the supports points generated using a definite DoE scheme. Thus, judicial choice of DoE is critical for the efficiency of RSM as the number of function evaluations affect the overall computational cost. That apart, the quality of fit is another criterion for the accuracy of the meta-model. In this study, four different DoE schemes are utilized to evaluate the coefficients of the RSM which are explained below.

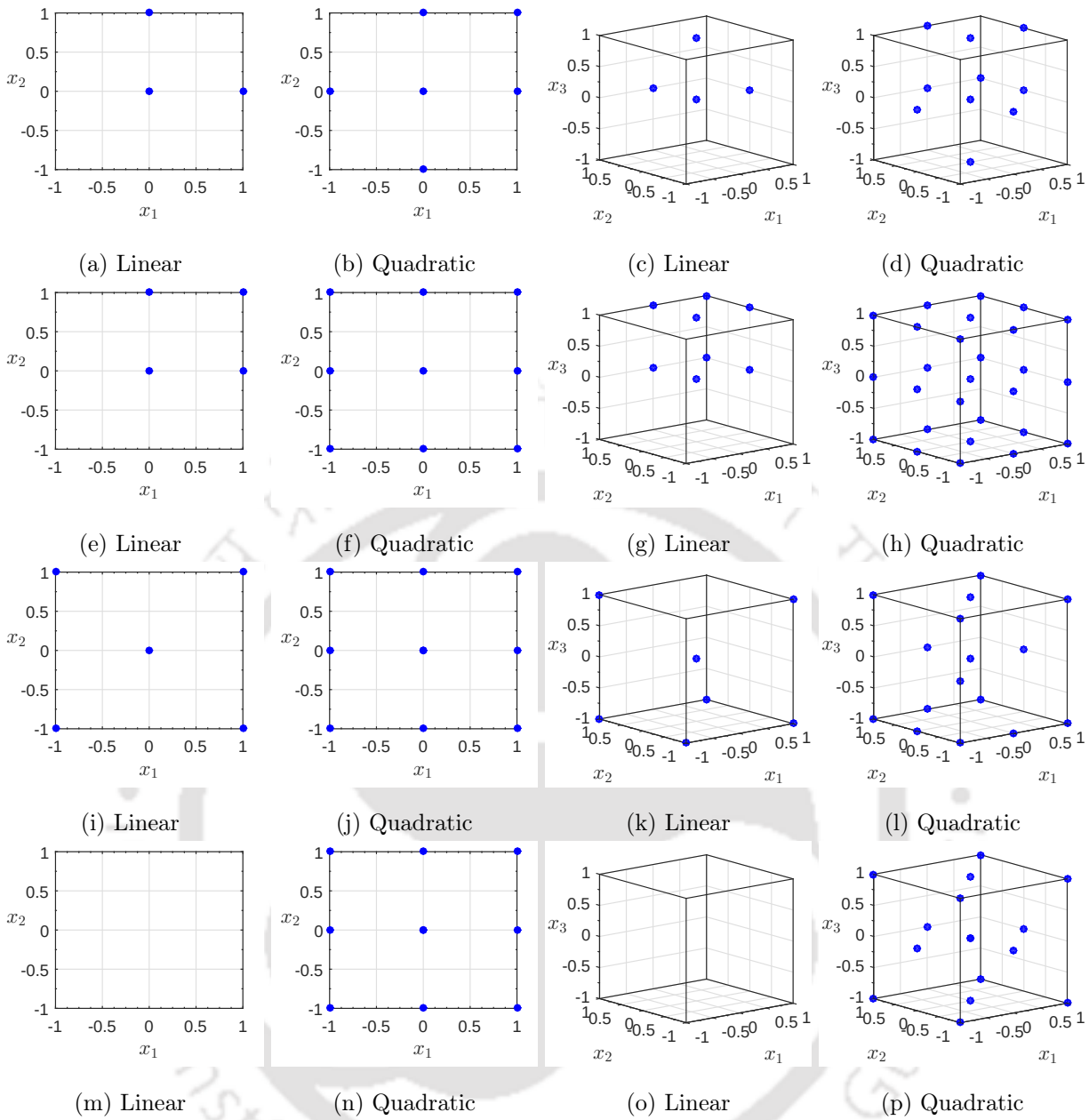

Figure 2.1: Support points generation by different DoE schemes: (a)–(d) Koshal Design, (e)–(h) Full Factorial Design, (i)–(l) D–Optimal design and (m)–(p) Central Composite Design (CCD) for linear and quadratic bases

2.3.1 Koshal Design

This scheme uses single parameter at a time to generate the DoE [143]. The sole benefit lies in the minimal generation of support points for the coefficient evaluation. This, in turn, effects the quality of the response surface. Fig. 2.1(a)–(d) depict the Koshal design for linear and quadratic polynomial bases which generate $(n+1)$ and $(n+1)(n+2)/2$ support points, respectively. It can be noted that the cardinality of the unknown coefficients vector $\mathbf{a}$ in RSM and n_s from this scheme are exactly equal.

2.3.2 Full Factorial Design

Unlike Koshal design where minimum support points are generated, full factorial design gives all possible combinations of the support points. This DoE scheme gives l_p^n support points where the level of factorial

design l_p is a non-zero integer with 1 for constant basis, 2 for linear basis and so on. The full factorial DoE scheme is shown in Fig. 2.1(e)–(h) for $l_p = 2$ and 3 (i.e. linear and quadratic basis, respectively). At the end of this section, it will be observed that all the DoE schemes discussed here, are subsets of full factorial design.

2.3.3 D-optimal Design

In this design scheme, variance of the error is minimized by choosing a subset of the full factorial design. This eventually helps to reduce the support points without compromising with the quality of meta-modelling for large number of parameters. The optimal criteria to improve the response surface is given by maximizing $|\mathbf{X}^\mathsf{T}\mathbf{X}|/(n_s)^n$ [140], where the number of support points required are defined by the user. In this study, 1.5 times the number of support points generated from the Koshal design is used. Thus, D-optimal design is same as full factorial design for number of parameters ≤ 2 as shown in Fig. 2.1(i)–(l). But further increase in number of parameter have a significant reduction in the number of support points.

2.3.4 Central Composite Design

Central composite design (CCD) scheme has radial as well as corner points along with the centre point where altogether $(1 + 2n + 2^n)$ support points are generated. In this study, *faced* central composite design is used where the radial points are situated at the middle of the adjacent corner points as shown in Fig. 2.1(m)–(p). Unlike full factorial design, this design generates less number of support points (but more than D-optimal design) with adequate fitting accuracy.

It is evident from Fig. 2.1 and Fig. 2.2 that the number of support points n_s generated by the Koshal design $\leq$ D-optimal design $\leq$ CCD $\leq$ full factorial design. Also, it can be noticed that for 2 parameters (i.e. $n = 2$) in linear approximation, D-optimal and full factorial designs have the same points. Moreover, for quadratic approximation, D-optimal, central composite and full factorial designs generate identical points. Fig 2.2 shows the number of support points n_s for different DoEs as the dimension (i.e. n) increases with respect to the linear and quadratic bases.

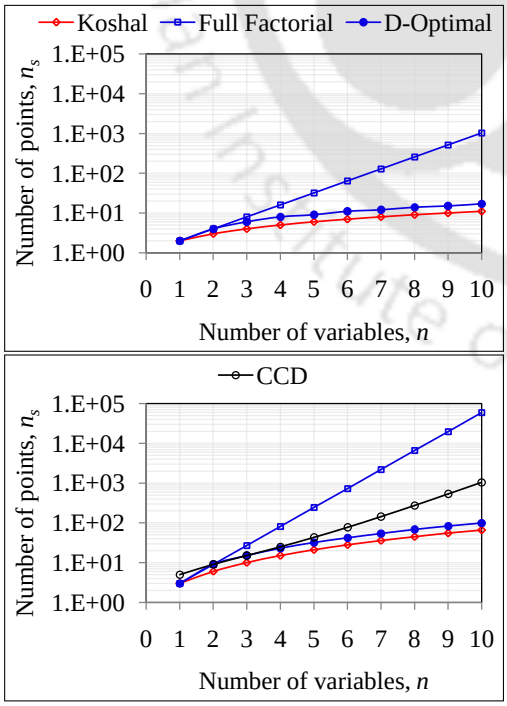

	n	Koshal	Full factorial	D-Optimal	CCD
Linear	1	2	2	2	
	2	3	4	4	
	3	4	8	6	
	4	5	16	8	
	5	6	32	9	
	6	7	64	11	
	7	8	128	12	
	8	9	256	14	
	9	10	512	15	
	10	11	1024	17	
Quadratic	1	3	3	3	3
	2	6	9	9	9
	3	10	27	15	15
	4	15	81	23	25
	5	21	243	32	43
	6	28	729	42	77
	7	36	2187	54	143
	8	45	6561	68	273
	9	55	19683	83	531
	10	66	59049	99	1045

Figure 2.2: Number of support points in different DoE schemes for linear and quadratic approximation

2.4 Numerical Study

In this section, RSM is used to solve two hypothetical problems of optimization and a FE updating using different regression techniques discussed in the previous sections. The response surface is developed in an iterative framework to determine the optimal locations of the given objective function. Here, the efficiency of the method is represented by the number of function evaluations to locate the optimal point whereas the accuracy is determined based on the converged optimal value of the objective function. Direct optimization using gradient based technique is employed as benchmark. Sequential quadratic programming (SQP) is adopted in this section for the constrained optimization where the input variables are bounded within the given limits. Following subsections illustrate the examples demonstrated in this chapter.

2.4.1 Optimization Examples

First, two example cases are discussed to demonstrate the performance of the RSM with different weight functions and DoE schemes. The objective functions considered in these examples are explicit with nonlinear input–output relationship which are discussed in the following subsections.

2.4.1.1 Example 1

In this example, a non-algebraic function is considered with two input variables (i.e. 2D) as expressed by

$$g(\mathbf{x}) = \log\left[1 + 3\left\{x_2 - (x_1^3 - x_1)\right\}^2 + \left(x_1 - \frac{4}{3}\right)^2\right] \tag{2.15}$$

The above equation gives a nonlinear objective function as shown in Fig. 2.3 which is optimized within the domain $x_1 \in [-2,\ 1]$ and $x_2 \in [-2,\ 2]$. The objective function contains one optimal location within the above specified bounds at [1 0] and the value of the objective function at this location is 0.105. The direct optimization of this objective function using SQP starting from a location on the boundary (say, $[-2\ -2]$) consumes 10 iterations to converge which is executed utilizing the in-built MATLAB [96] algorithm. Fig. 2.4(a) shows the convergence path followed by the gradient based optimization using central difference to estimate the gradients. Overall, this optimization process requires a total of 56 evaluations of the expression stated in Eq. 2.15 to accurately identify the optimal point. The values of the objective function corresponding to these evaluations and the minimized values after each iteration are presented in Fig. 2.4(b). This result is further considered as benchmark to compare the results obtained from the meta-model based approaches.

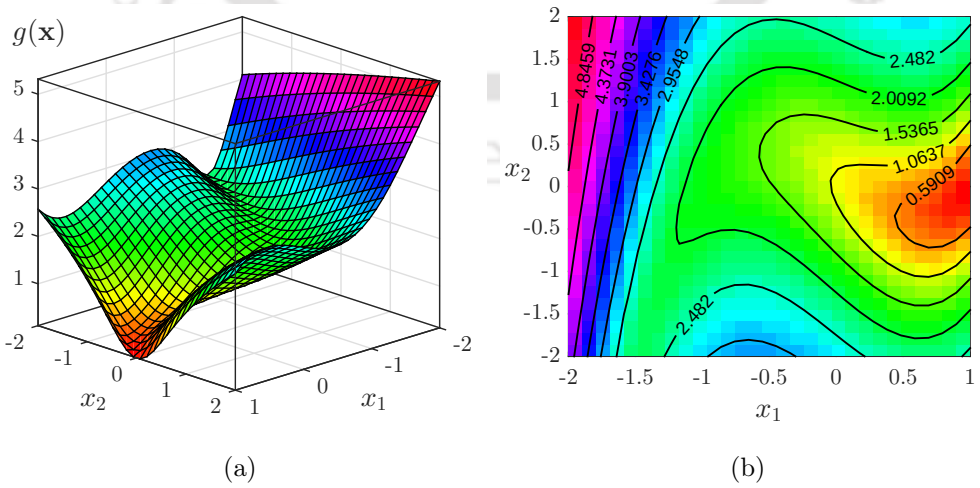

(a) (b)

Figure 2.3: Original surface of the objective function in Example 1 – (a) surface plot and (b) contour plot

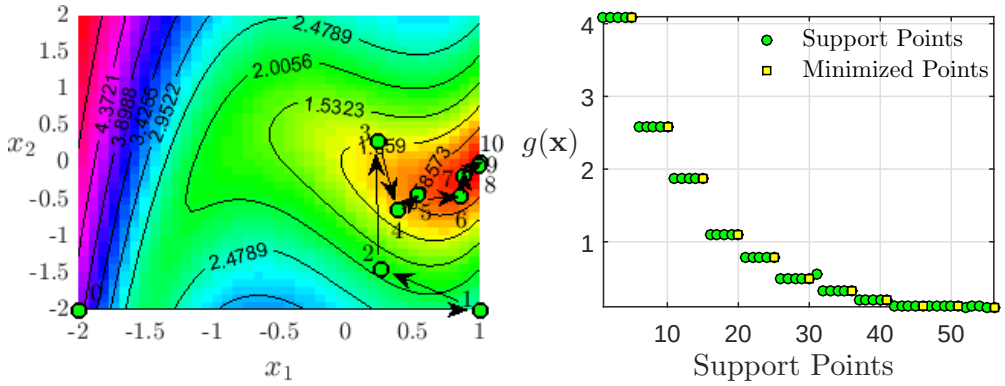

(a) (b)

Figure 2.4: (a) Optimization path followed by the gradient based method for Example 1 and (b) iteration wise convergence of the objective function value

Table 2.1: Minimized objective function values, number of iterations and function evaluations from the gradient based direct optimization and the different RSM schemes for Example 1

Optimization Method	Regression	Weight Type	Degree of the Basis Function	DoE	Iterations	Number of Runs	Minimized Objective Function Value
Direct Gradient	-	-	-	-	10	56	0.105
			1	Kos	5	18	1.413
			1	FF	3	14	0.735
RSM	LS	-	1	D-opt	7	31	1.807
			2	Kos	8	51	0.344
			2	CCD	8	73	0.363
			1	Kos	9	30	0.247
			1	FF	7	30	0.405
ARSM	MLS	Exponential	1	D-opt	7	41	0.527
			2	Kos	4	26	0.353
			2	CCD	2	18	0.336
			1	Kos	4	15	0.111
			1	FF	3	14	0.104
ARSM	MLS	Regularized	1	D-opt	9	52	0.109
			2	Kos	5	33	0.105
			2	CCD	2	18	0.111

Note: Here the number of runs gives the actual number of unique evaluations for the complete iteration process.

In the meta-model based approach, the optimized location is first determined using linear basis and accordingly, the response surface is formed using Eq. 2.2. Different DoE schemes, as discussed in § 2.3, are utilized to form the response surface where least square and MLS techniques are employed to evaluate the unknown coefficients. Table 2.1 presents the optimized results from the different combinations of DoE schemes and regression techniques used in this study. Least square based RSM involving Koshal, full-factorial and D-optimal based support points require 3 to 7 iterations to converge which calls Eq. 2.15 from 14 to 31 times. The optimized values of the objective function are 1.413, 0.735 and 1.807, respectively which yield relatively higher error. This is due to fact that linear approximation using least square based determination of the unknown coefficient vector $\mathbf{a}$ yields considerable error in fitting, especially for nonlinear surfaces. Fig 2.5

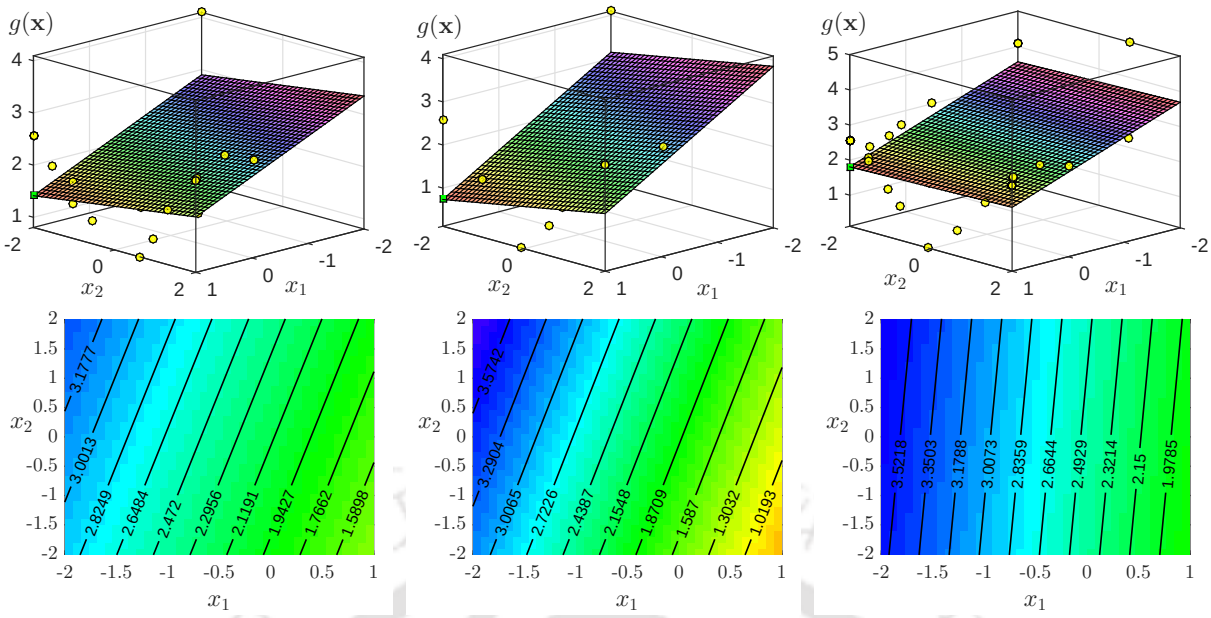

(a) (b) (c)

Figure 2.5: Least square technique based polynomial response surface with linear basis using (a) Koshal design, (b) full-factorial design and (c) D-optimal design, where the circled and squared data represent support points and minimized location, respectively

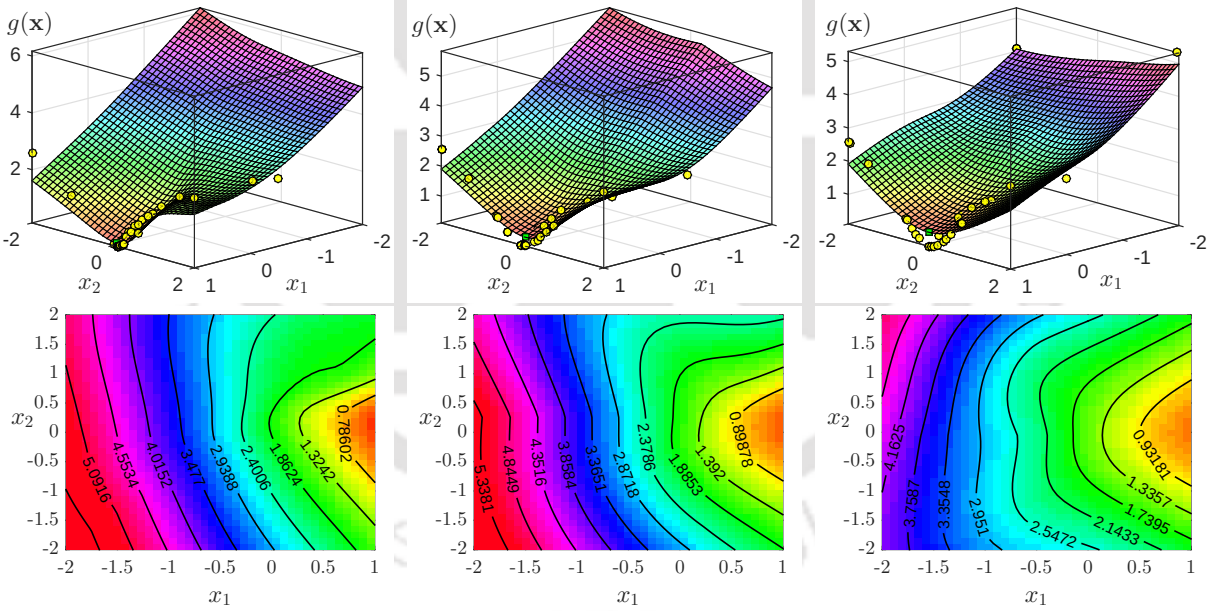

(a) (b) (c)

Figure 2.6: Least square technique based polynomial response surface with linear basis and exponential weight function using (a) Koshal design, (b) full-factorial design and (c) D-optimal design, where the rows in each case present the 3D and contour plots, respectively

depicts the response surfaces formed using support points from different DoE schemes and the identified optimized locations based on the meta-model after it converged as stated in Table 2.1. The surfaces formed are linear and the coefficient vector $\mathbf{a}$ remain unchanged throughout the domain. The fitting error is significant as majority of the support points does not lie on it, this means that the error is high even at the support points. However, this is abated in the MLS based determination of $\mathbf{a}(\mathbf{x})$ where these coefficients become function of the variable $\mathbf{x}$ as given in Eq. 2.10. Hence, evolving coefficients by minimizing the error

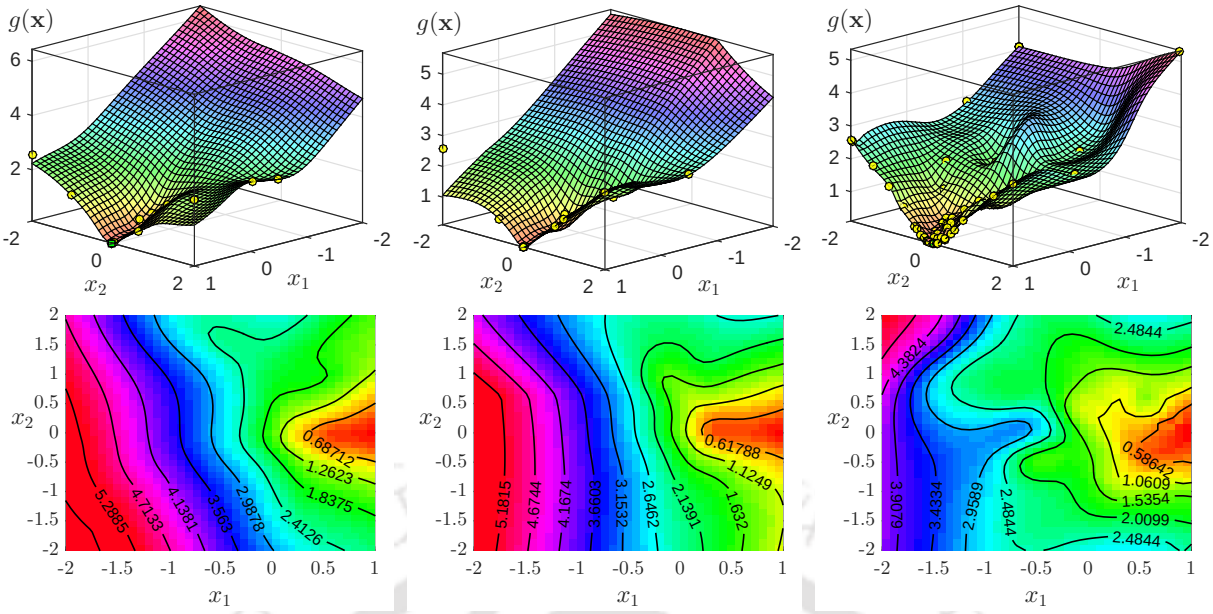

(a) (b) (c)

Figure 2.7: Least square technique based polynomial response surface with linear basis and regularized weight function using (a) Koshal design, (b) full-factorial design and (c) D-optimal design, where the rows in each case present the 3D and contour plots, respectively

at every point creates a nonlinear surface even using a linear basis function. Fig. 2.6 shows the response surfaces constructed using MLS technique with exponential weight function. Here, the influence radius D_r (i.e. $\sqrt{\{1-(-2)\}^2+\{2-(-2)\}^2}=5$) is considered in such a way that the contributions of all the support points are available for any arbitrary location in the given domain of $\mathbf{x}$. MLS technique considerably improves the optimized results as shown in Fig. 2.6 and Table 2.1 where the number of support points and the iterations for convergence are reported. However, it can be noticed in Fig. 2.6 that a few support points are not modelled adequately as these points are not included in the response surface. These fitting issues are further improved using regularized weight function as given in Eq. 2.13 and the response surfaces constructed using it are presented in Fig. 2.7. The results in Table 2.1 suggest that RSM using regularized weights provide the best results among the various options considered in this study. The number of support points for Koshal and full-factorial design are among the lowest while the D-optimal requires more support points. All of these response surfaces provide efficient results as compared to the gradient based direct optimization with appreciable accuracy in locating the minimal point and its value.

Further, the response surfaces are formed with higher degree of polynomial basis (i.e. quadratic) as per Eq. 2.4. In this case, the DoE formed using full-factorial, D-optimal and CCD schemes have similar locations in the bivariate domain. Hence, the results in Table 2.1 are shown for Koshal and CCD schemes as the above mentioned three schemes produce identical outcomes. The least square based RSM with full quadratic basis requires 51 and 73 support point evaluations for Koshal design and CCD, respectively. However, quadratic basis gives better estimation of the minimum location and consumes more function evaluation than the linear basis. Here, it may be noted that MLS based RSM employing exponential weight function makes marginal improvement in results with better efficiency, especially for CCD where only 18 support points are required. Furthermore, use of regularized weight function in MLS yields fairly accurate results with similar efficiency as reported earlier. Fig. 2.8 shows the response surfaces built using different approaches which infers the same outcome as discussed earlier where the fitting is improved with the introduction of weights, especially its regularized version. Overall, the regularized weight function based MLS technique outperforms other approaches considered in this study. For the quadratic basis, CCD scheme performs efficiently than Koshal design when used in MLS.

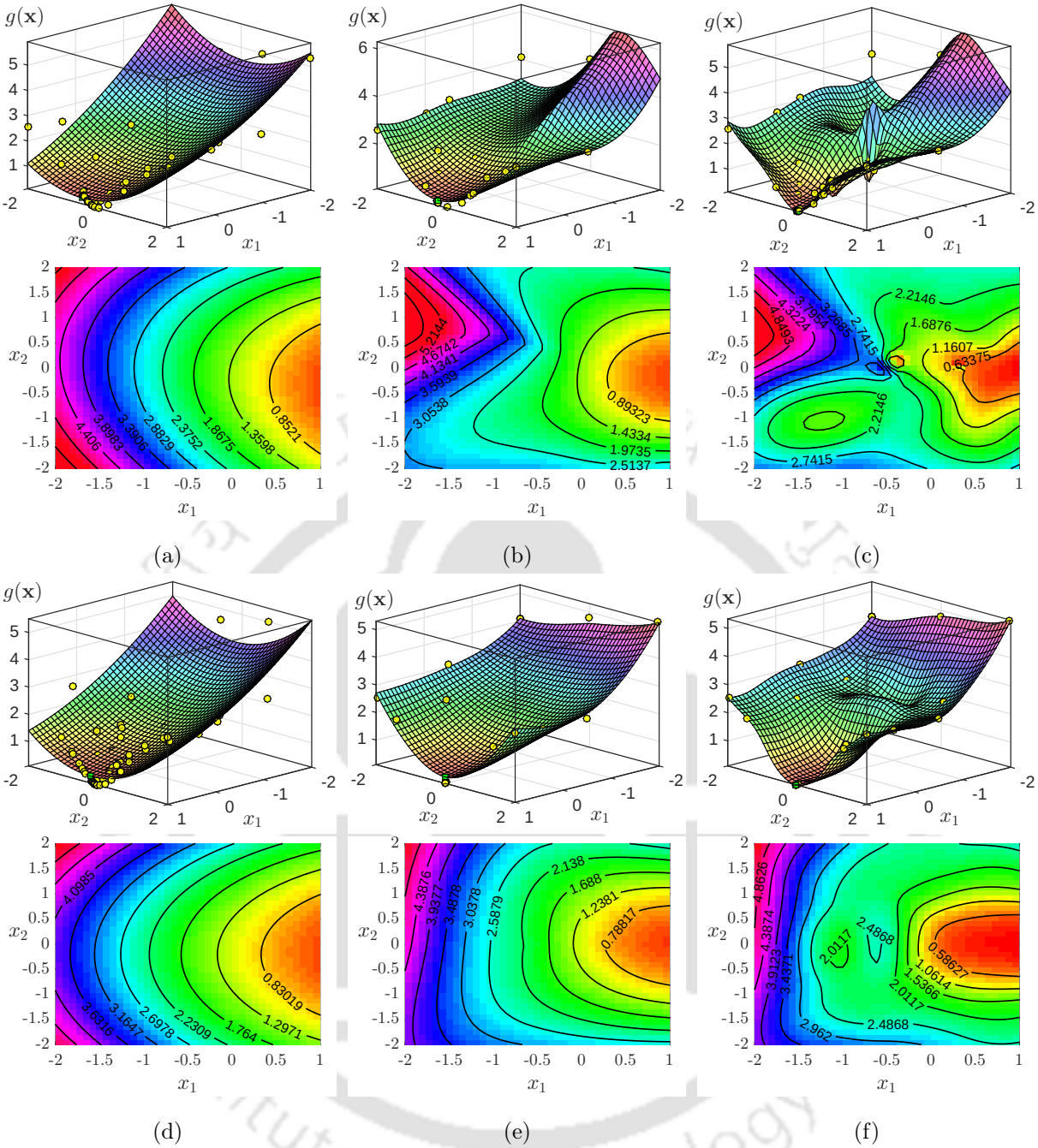

Figure 2.8: Complete quadratic response surface using (a) Koshal design and least square technique, (b) Koshal design and MLS technique with exponential weight function, (c) Koshal design and MLS technique with regularized weight function, (d) CCD and least square technique, (e) CCD and MLS technique with exponential weight function, and (f) CCD and MLS technique with regularized weight function, where the rows in each case present the 3D and contour plots, respectively

2.4.1.2 Example 2

The second example presented in this study is also a non-algebraic expression with three variables where the input-output relationship is defined by

$$g(\mathbf{x}) = (4x_2^2 + 2x_3^2 + 4x_1 + 1)\exp\left[\frac{x_1}{10}\right] \tag{2.16}$$

The range of the input variables (i.e. $\Omega_{\mathbf{x}}$) are considered to be $[-2,\ 2]$. Using gradient based optimization, the minima of this objective function in Eq. 2.16 is evaluated. Table 2.2 shows the optimized results and the iterations required to get it from a starting point $[-1\ +1\ -1]$. The iteration wise convergence is further demonstrated in Fig. 2.9 where the optimized results from each iteration is also given. The converged minima is at $[-2\ 0\ 0]$ and the corresponding value is -5.731. In total, this optimization process requires 45 evaluations of the objective function. Similar to the previous illustration, this example is also solved with different combination of response surfaces (i.e. linear and quadratic) to determine **a** and DoE schemes which

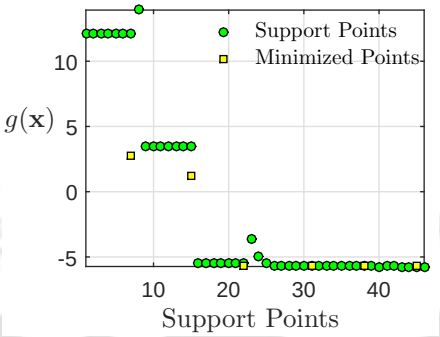

Figure 2.9: Iteration wise convergence of the objective function value in Example 2 using gradient based optimization

Table 2.2: Minimized objective function values, number of iterations and function evaluations from the gradient based direct optimization and the different RSM schemes for Example 2

Optimization Method	Regression	Weight Type	Degree of the Basis Function	DoE	Iterations	Number of Runs	Minimized Objective Function Value
Direct Gradient	-	-	-	-	5	45	-5.731
			1	Kos	20	86	11.915
			1	FF	4	35	-0.266
			1	D-opt	20	122	11.832
RSM	LS	-	2	Kos	5	51	-5.748
			2	FF	3	82	-6.569
			2	D-opt	2	33	-6.897
			2	CCD	3	46	-6.698
			1	Kos	16	76	-3.326
			1	FF	14	126	-3.452
			1	D-opt	10	70	-4.597
ARSM	MLS	Exponential	2	Kos	5	51	-5.702
			2	FF	3	82	-6.220
			2	D-opt	3	50	-6.157
			2	CCD	2	31	-6.206
			1	Kos	20	98	-5.739
			1	FF	14	125	-5.696
			1	D-opt	7	46	-5.759
ARSM	MLS	Regularized	2	Kos	5	51	-5.730
			2	FF	2	55	-5.731
			2	D-opt	4	67	-5.731
			2	CCD	2	31	-5.731

Note: Here number of runs gives the actual number of unique evaluations for the complete iterations.

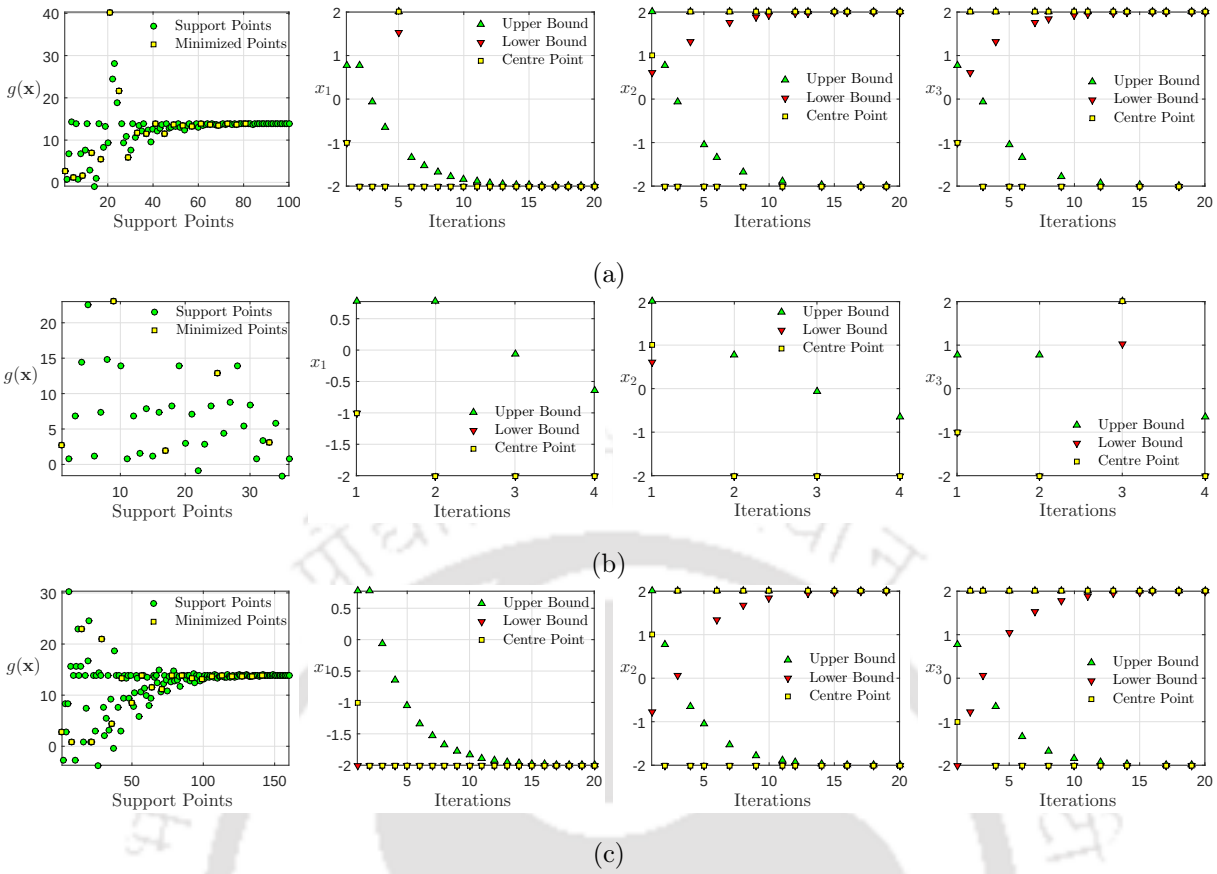

Figure 2.10: Optimization history of the objective function in Example 2 evaluated using RSM with least square technique and linear basis for (a) Koshal design, (b) full-factorial design and (c) D-optimal design

are discussed in the following paragraph.

Response surfaces using linear basis are formed using three DoE schemes (i.e. Koshal design, full-factorial design and D-optimal design). The convergence studies for the least square based coefficients are presented in Fig. 2.10 with respect to the objective function and the three input variables. For Koshal and D-optimal designs, variables x_2 and x_3 did not converged till 20 iterations which included 86 and 122 function calls, respectively. Although the response surface with full-factorial design converged in 4 iterations with 35 original function calls, but all of these cases converged to the locations other than the actual optima. Thus, the minimized values of the objective function are incorrect for all these cases. RSM is further applied with linear polynomial basis and MLS technique where weights are defined using the exponential function, as discussed earlier. Here, the value of influence radius D_r (i.e. $\sqrt{\{2-(-2)\}^2+\{2-(-2)\}^2+\{2-(-2)\}^2} \approx 6.93$) is selected as discussed in the previous example to determine the weights associated with the support points. This improves the meta-model based minimization process as the convergence is achieved (see Table 2.2) for all the DoE schemes considered in this study by evaluating $g(\mathbf{x})$ between 70 to 126 times. Still, it is observed that the converged locations differ from the results based on the gradient based optimization as shown in Fig. 2.11. The minimized values of the objective function from this surface is also subjected to modelling error. To improve this result, the exponential weight function is replaced by the regularized weight function and the same process is executed again. The efficiency of the RSM remains nearly consistent with 46 to 125 calls of actual $g(\mathbf{x})$ as reported in Table 2.2. However, the accuracy is improved in all the DoE cases where the optimal locations are nearly identified as presented in Fig. 2.12. It can be noted that the Koshal design uses 20 iterations to converge unlike the least square based RSM where the convergence is not achieved.

Following the improvement in the results, quadratic response surface is employed to perform the optimization. The DoE scheme considered here include Koshal design, full-factorial design, D-optimal design and CCD as the number of variables is 3 i.e. > 2. The polynomial surface with quadratic basis improves the result from its linear counterpart for all the cases as shown in Table 2.2. The Koshal design consistently performed for all the three response surface formed using least square, MLS with exponential weight and regularized

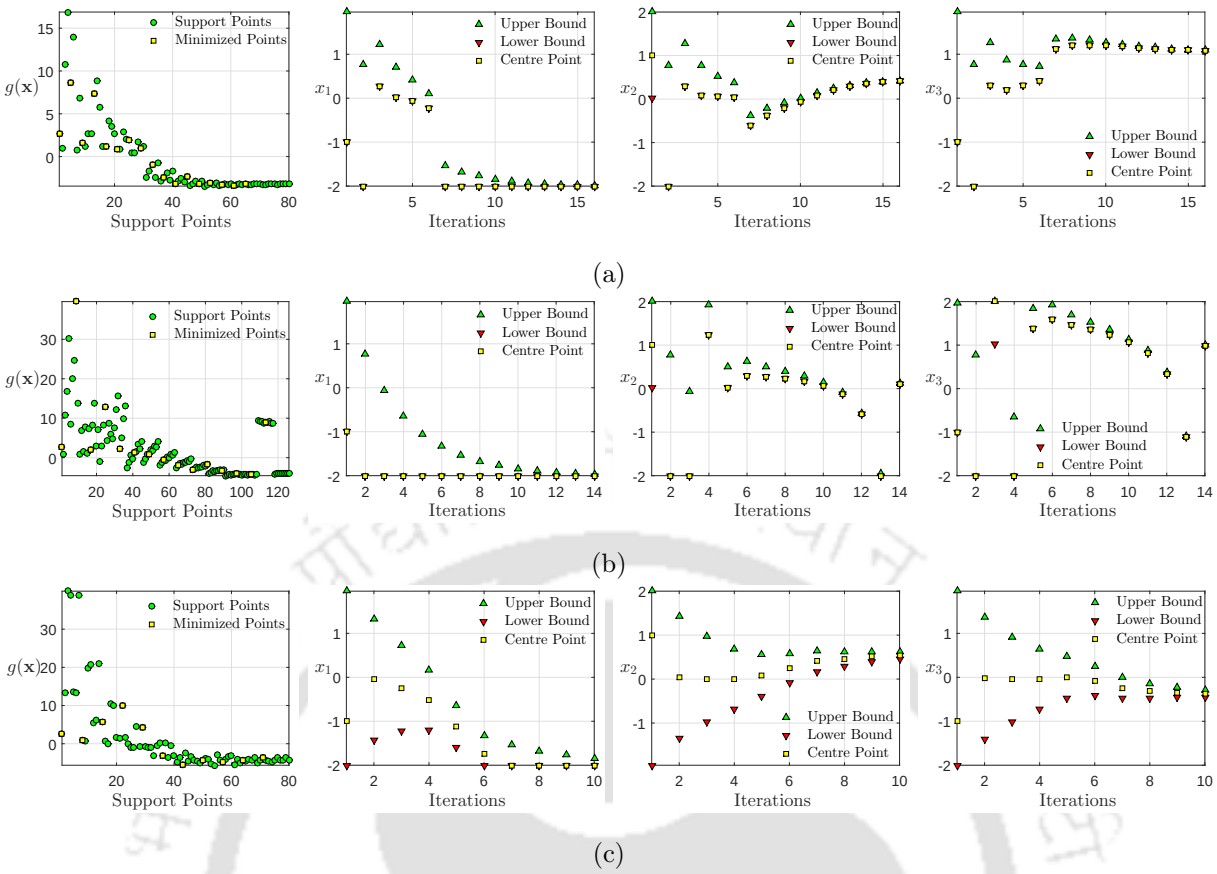

Figure 2.11: Optimization history of the objective function in Example 2 evaluated using RSM with MLS technique employing exponential weight and linear basis for (a) Koshal design, (b) full-factorial design and (c) D-optimal design

weight as shown in Figs. 2.13(a), 2.14(a) and 2.15(a), respectively. It requires 5 iterations followed by 51 function evaluations for all these response surfaces. In the case of MLS based RSM employing regularized weight, Koshal scheme provides efficient result as the optimization problem is solved with faster convergence evaluating less points than the linear basis. Figs. 2.13(b), 2.14(b) and 2.15(b) correspond to the results obtained from the full factorial design which show relatively scattered values of $g(\mathbf{x})$ at the support points. This wider spread than other DoE schemes infers that the full-factorial design considers every combination of coordinates in each iteration. CCD with MLS based RSM provides the fastest convergence in this study by calling 31 actual evaluations in 2 iterations which can be further depicted from Figs. 2.14(d) and 2.15(d). However, MLS based RSM with regularized weight function replicates the objective function better compared to the other options.

Overall, it can be summarized from these two examples that RSM with complete quadratic polynomial basis where the unknown coefficients are determined by the MLS technique utilizing regularized weight function is the best choice. It provides efficient results when coupled with CCD as the DoE scheme where the convergence is achieved with lesser number of function calls. Following these illustrative examples, this meta-modelling approach is tested for a practical application which involves updating of a structural model based on the actual test data.

2.4.2 FE Model Updating

The meta-model based optimization process discussed above is adopted for a field problem where the objective is to update the parameters of the numerical model such that it emulates the actual structure. A flowchart of the meta-model based updating process is presented in Fig. 2.16 which involves interaction between two different numerical solver platforms (i.e. ANSYS® and MATLAB®).

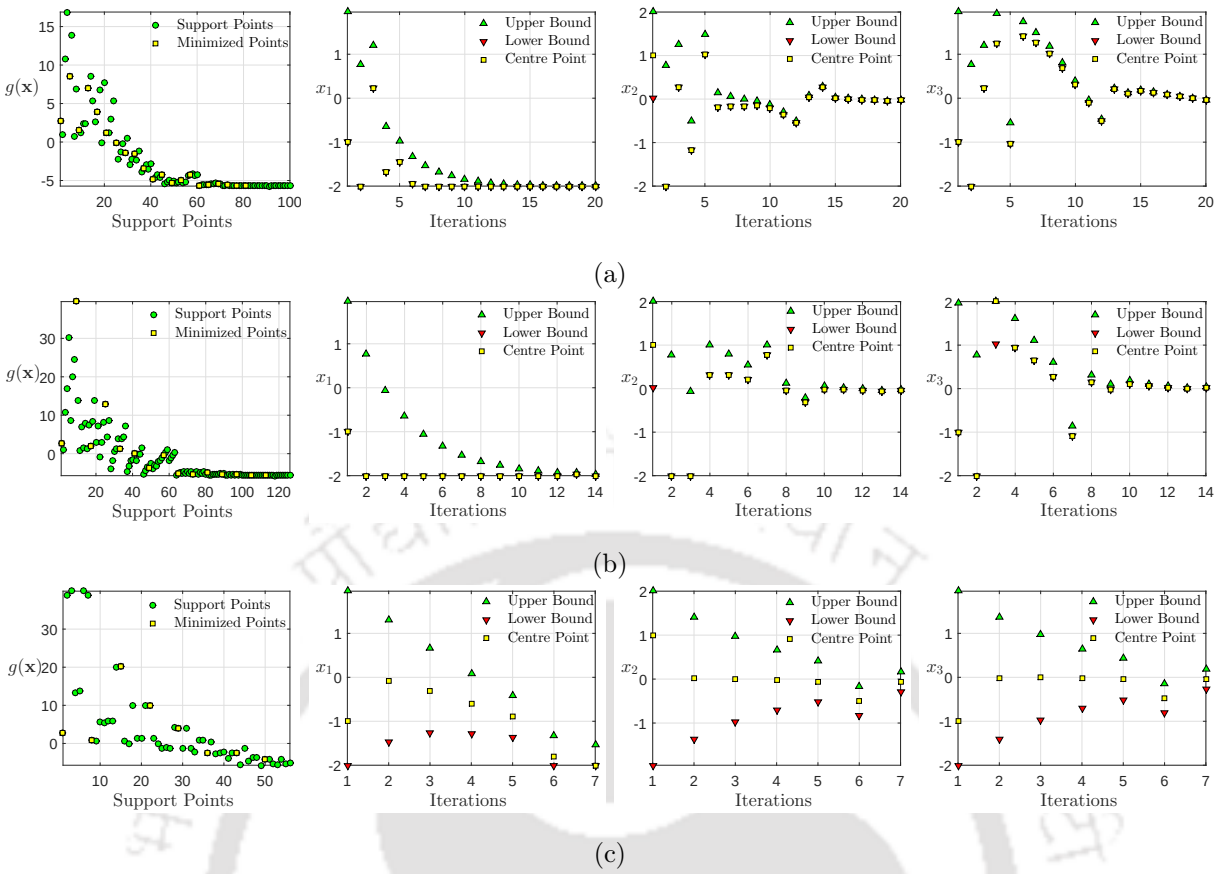

Figure 2.12: Optimization history of the objective function in Example 2 evaluated using RSM with MLS technique employing regularized weight and linear basis for (a) Koshal design, (b) full-factorial design and (c) D-optimal design

2.4.2.1 Description of RC Road Bridge and FE Model

The structure examined in this study is an existing reinforce concrete (RC) bridge near Indian Institute of Technology Guwahati in North Guwahati, Assam, India. Total length of the RC road bridge is 88.0m with 3 independent spans which are simply supported. The middle span is 39.0m long and the end spans stretch to 24.5m. It allows a two-way traffic flow with 7.5m in each lane. The full view of the longest span of the bridge is shown in Fig. 2.18(a). The bridge deck of the main span is resting over 4 prestressed longitudinal beams [see Fig. 2.18(b)] with 8 diaphragms which act as cross beams. The main span is considered in this study for further investigation. A three dimensional (3D) FE model is developed in ANSYS® using SHELL181 and BEAM188 elements [144] in the deck and the girders, respectively. The material properties are incorporated as per the Indian Standard [145] and the corresponding FE model made in ANSYS® as presented by Fig. 2.18(c).

2.4.2.2 Parameter Identification and Updating

The middle span of the RC road bridge is examined with sensors under traffic flow and the time history responses are recorded for further investigations using signal processing. To solve the modal identification problem, Hilbert-Huang transformation (HHT) technique [146] is used here. In this approach, signal is first decomposed into intrinsic modal function (IMF) by empirical mode decomposition. After the IMFs are evaluated, Hilbert transform is applied to obtain the instantaneous frequencies and phases. On time averaging of these instantaneous frequencies, the natural frequencies of the structure are identified as given by Mahato *et al.* [147].

Once the modal parameters (i.e. natural frequencies) are identified, FE model is updated using RSM. Generally, updating is executed for the parameters like material properties, dimensions etc. which play vital

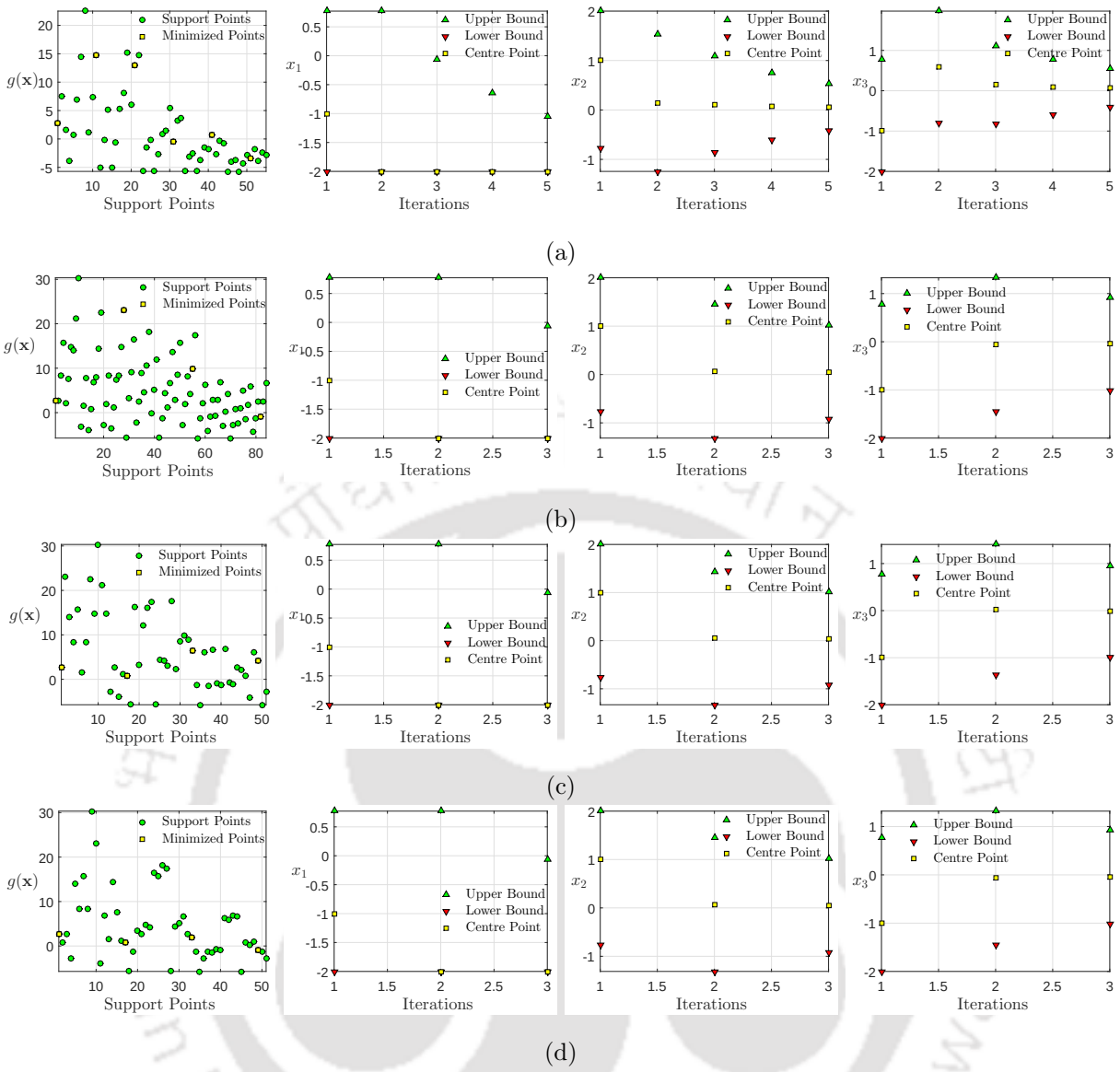

Figure 2.13: Optimization history of the objective function in Example 2 evaluated using RSM with least square technique and quadratic basis for (a) Koshal design (b) full-factorial design, (c) D-optimal design and (d) CCD

Table 2.3: Natural frequencies and corresponding mode shapes from FE model of RC road bridge

Sl. No.	Identified Natural Frequencies (Hz)	Updated Natural Frequencies (Hz)
Mode 1	3.04	3.06
Mode 2	7.74	7.61
Mode 3	13.81	13.39
Mode 4	19.72	19.86
Mode 5	26.66	26.68
Mode 6	28.32	27.99
Mode 7	29.48	28.73
Mode 8	30.92	30.72
Mode 9	31.63	33.48
Mode 10	34.60	34.07

role in the structural behaviour. With the selection of parameters $\mathbf{x}$, updating problem is solved to minimize

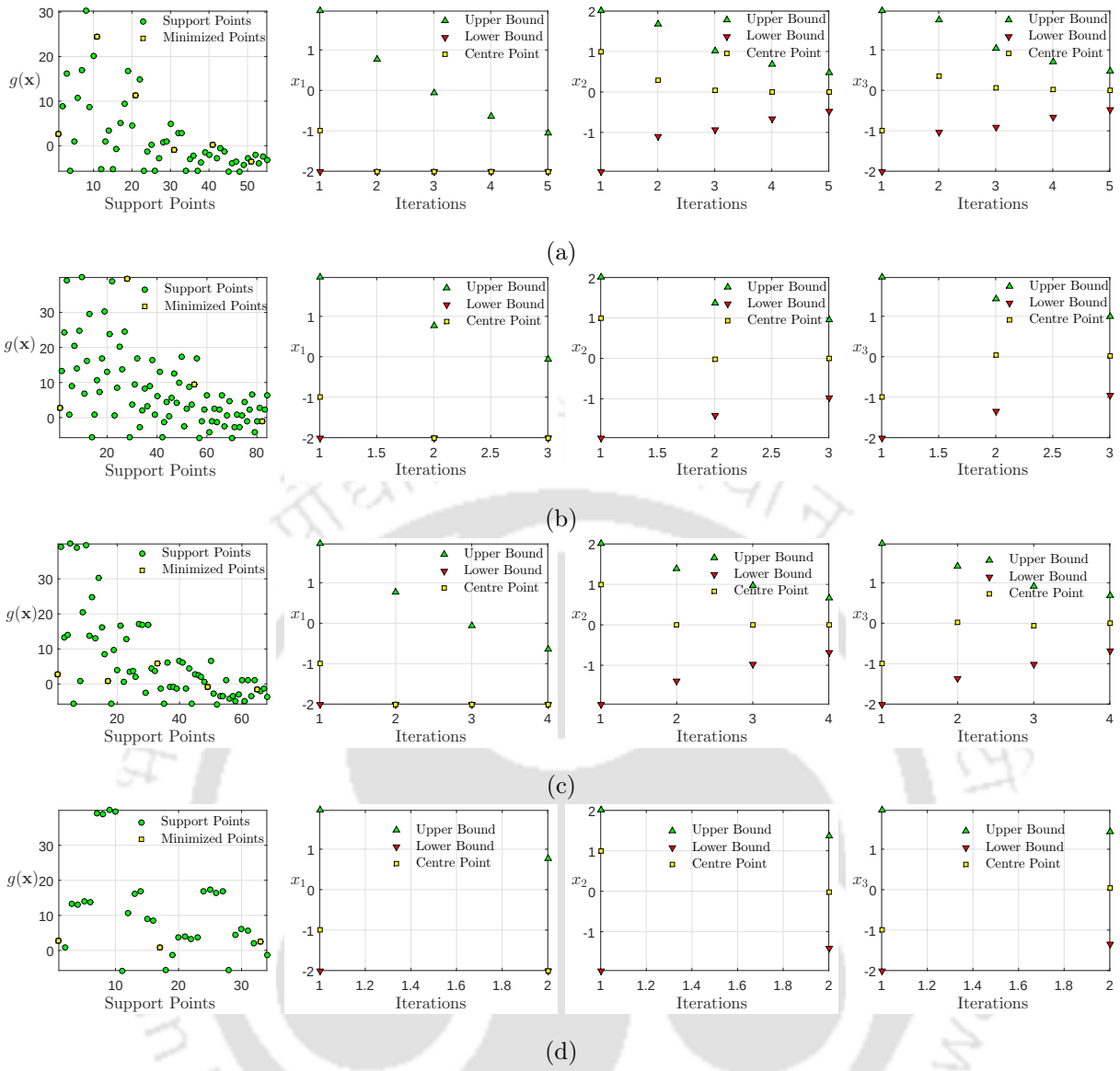

Figure 2.14: Optimization history of the objective function in Example 2 evaluated using RSM with MLS technique employing exponential weight and quadratic basis for (a) Koshal design (b) full-factorial design, (c) D-optimal design and (d) CCD

the residual error ϵ_u with respect to $\mathbf{x}$ i.e.

$$\begin{aligned} \min_{\mathbf{x}} \quad & \epsilon_u = \sqrt{\sum_{i=1}^{n_f} (\hat{f}_i(\mathbf{x}) - f_i)^2} \\ \text{where,} \quad & \mathbf{x} \in \Omega_{\mathbf{x}} \end{aligned} \tag{2.17}$$

In the above equation, $\hat{f}_i$ and f_i are i^{th} natural frequency identified from the operational modal analysis of the actual structure and the FE model, respectively. First n_f natural frequencies are considered for updating in this study where the parameters are bounded in the variable space $\Omega_{\mathbf{x}}$ with lower limit $\mathbf{x}_l$ and upper limits $\mathbf{x}_u$. RSM based meta-modelling is used to approximate the objective function (i.e. ϵ_u) for optimization. The details of RSM employed here is presented in the following section.

First ten natural frequencies identified from the operational modal analysis are reported in Table 2.3. The objective function in this updating problem considers the residual error ϵ_u in the first ten natural frequencies (i.e. n_f in Eq. 2.17 is equal to 10) between the identified and FE model. The parameters selected in this study for updating are elastic modulus E_c and density ρ_c of the reinforced concrete. These two parameters are bounded between $[2.5 \times 10^{10}, 5.0 \times 10^{10}]$ and $[1.8 \times 10^4, 2.5 \times 10^4]$, respectively to keep them realistic.

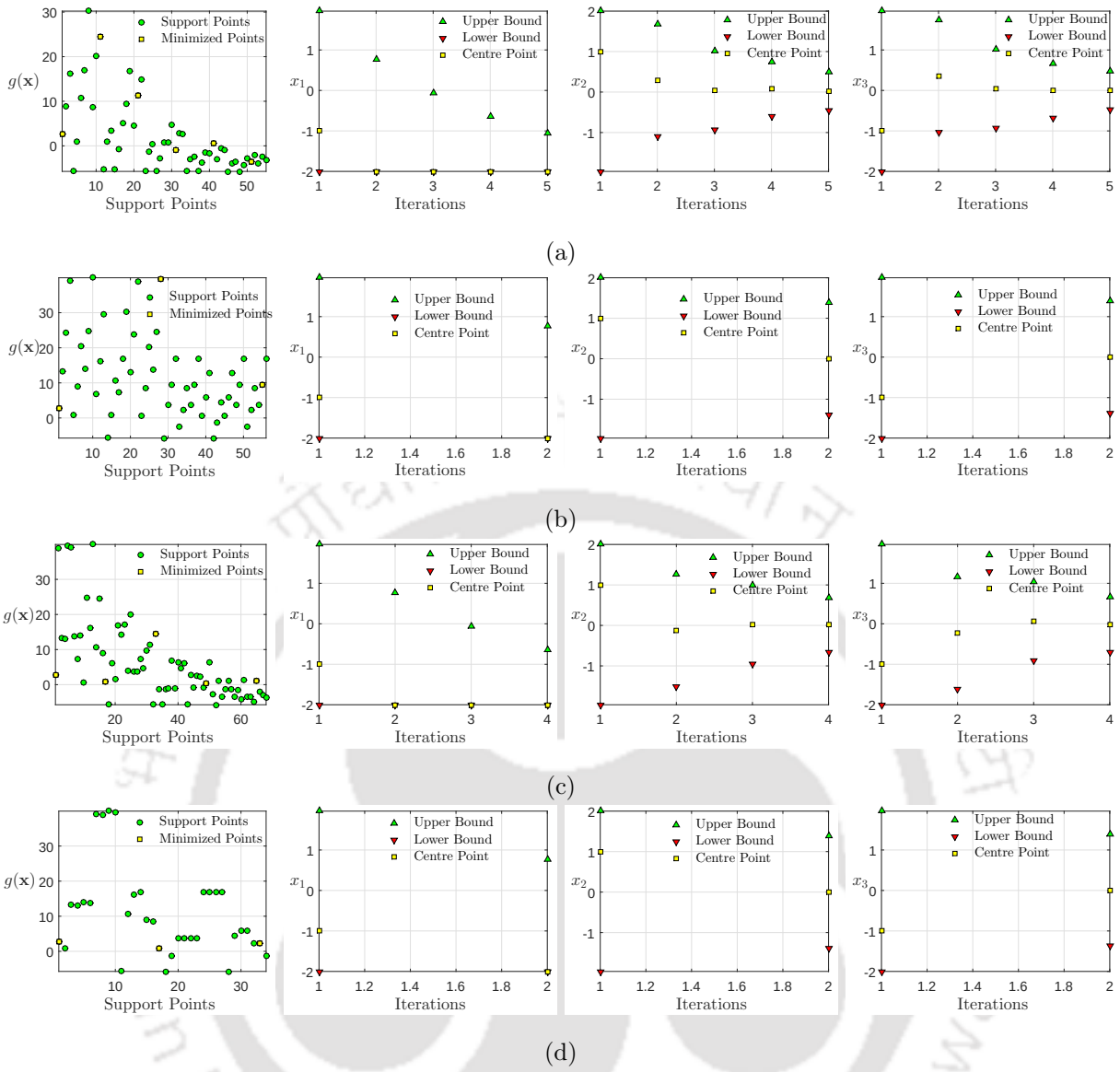

Figure 2.15: Optimization history of the objective function in Example 2 evaluated using RSM with MLS technique employing regularized weight and quadratic basis for (a) Koshal design (b) full-factorial design, (c) D-optimal design and (d) CCD

In this study, residual error is optimized to update the FE model using RSM based meta-models with different bases. A schematic flowchart of the complete updating procedure is presented in Fig. 2.16. To fit the response surface, initial range is chosen is such a way that the support points cover the entire domain. Additionally, steady convergence is ensured by setting the factor to 80%. This factor helps in reducing the domain of the new additional support points in each successive iteration. This reduction of bounds of E_c and ρ_c is shown in Fig. 2.19 for every iteration. Here, the lower and upper bound presents the extreme values of the parameter in the domain of support points generated for that iteration and the design point specifies the optimized point in that iteration. Moreover, one extra center point is generated as per the DoE and support points from the past iterations are used in regression for better fitting of the response surface. Linear scale transformation of the parameter in [0, 10] is performed to reduce the ill-conditioning of the matrices in the regression analysis. Thus, the radial distance D_r is defined as 14.14. The convergence criteria to stop the iteration is defined as 0.01% of variation in the parameters $\mathbf{x}$ (i.e. E_c and ρ_c) and the objective function. As discussed, RSM using least square and MLS regression techniques with linear as well as quadratic polynomial bases are executed with varying DoEs. DoE schemes such as the D-optimal and the full factorial have identical support points, for two parameters (i.e. $n = 2$) under linear approximation. Similarly, D-optimal, full factorial and central composite designs have identical support points for quadratic

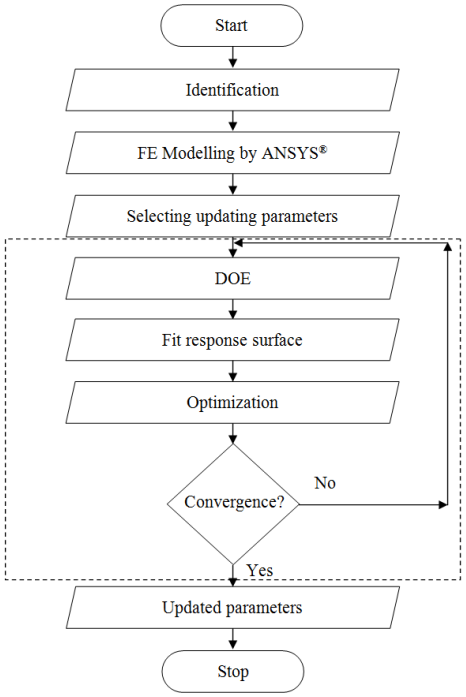

Figure 2.16: A flowchart of the RSM based updating scheme followed in this study

Table 2.4: Minimized objective function values, number of iterations and FE model runs from the direct gradient optimization and the different RSM schemes

Optimization Method	Regression	Weight Type	Degree of the Basis Function	DoE	Iterations	Number of Runs	Minimized Objective Function Value
Direct Gradient	-	-	-	-	7	38 (38)	2.1688
ARSM	LS	-	1	D-Opt	11	67 (60)	2.1316
			1	Kos	9	46 (30)	2.1319
			2	CCD	6	67 (56)	2.1317
			2	Kos	6	49 (38)	2.1315
ARSM	MLS	Exponential	1	D-Opt	11	67 (62)	2.1317
			1	Kos	9	46 (30)	2.1319
			2	CCD	2	23 (20)	2.1320
			2	Kos	6	49 (38)	2.1315
ARSM	MLS	Regularized	1	D-Opt	5	31 (29)	2.1318
			1	Kos	9	46 (30)	2.1319
			2	CCD	2	23 (20)	2.1320
			2	Kos	6	49 (38)	2.1312

Note: Here (.) gives the actual number of FE model runs for the complete iterations.

approximation. Hence, all these cases show similar results. A comparative study is performed for RSM based on least square and moving least square with exponential and regularized weights for different polynomial bases and DoE.

Here, the response surfaces are fitted individually for all the ten natural frequencies then the objective function (see Fig. 2.20) is optimized by gradient based method. Fig. 2.20 shows nonlinear relation of the

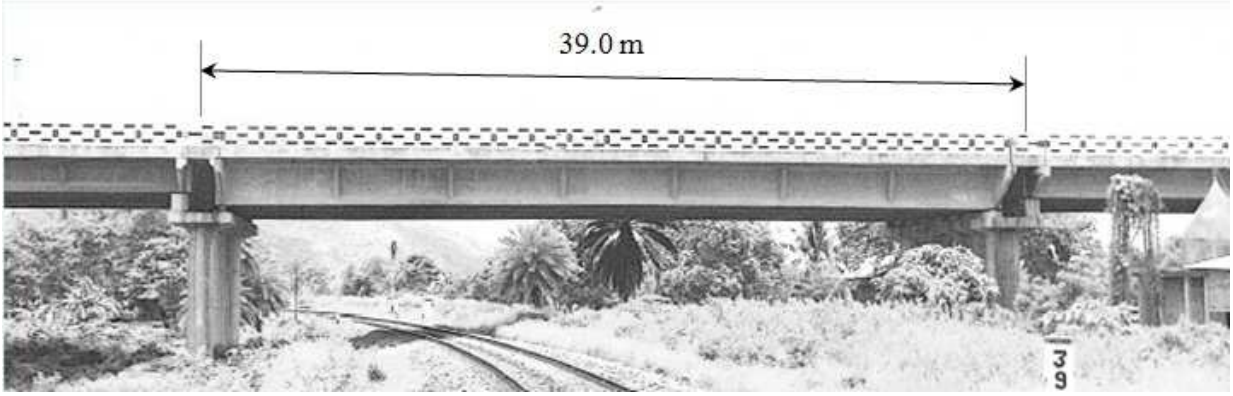

(a)

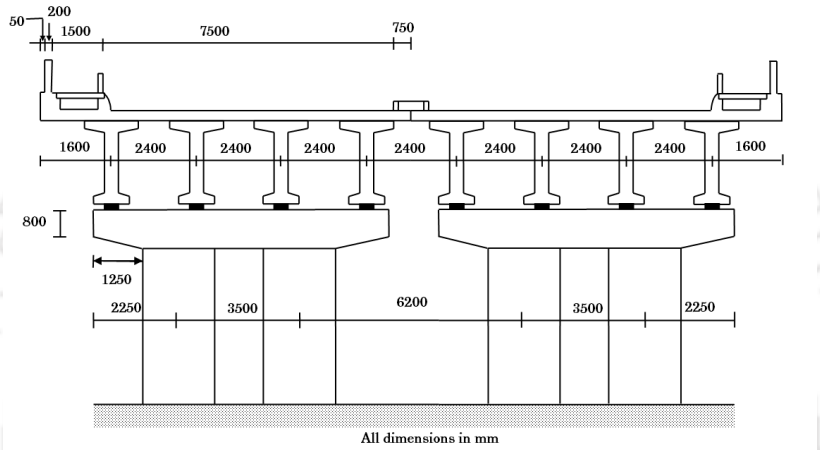

(b)

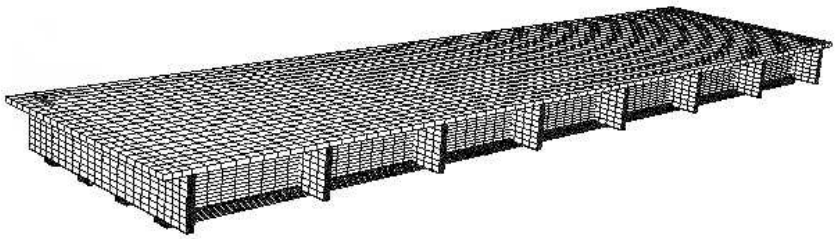

(c)

Figure 2.17: View of (a) the RC road bridge, (b) the cross-section of the bridge and (c) the FE Model made in ANSYS®

residual error ϵ_u with respect to the updating parameters. The outcomes of this updating problem solved for different cases are presented in Table 2.4. It is observed that the convergence was achieved for all these RSMs and the differences in the end results are insignificant. Results show that least square and moving least square with exponential weight function have similar number of iterations, FE solutions and minimized objective function value for linear approximation. But for quadratic approximation, CCD converges faster for MLS based RSM by dropping the number of iterations from 6 to 2 and subsequently, reducing the FE solutions from 67 to 23. Thus, 65% reduction in FE solutions is noticed. Similarly for MLS with regularized weight function, D-optimal design also shows faster convergence with 5 iterations and 31 FE solutions as compared to 11 iterations and 67 FE solutions for both least square and moving least square using exponential weight function based RSM. In all the six cases of Koshal scheme (see Table 2.4), it can be noticed that there is no change in the number of iterations and support points. This is plausibly due to the fact that

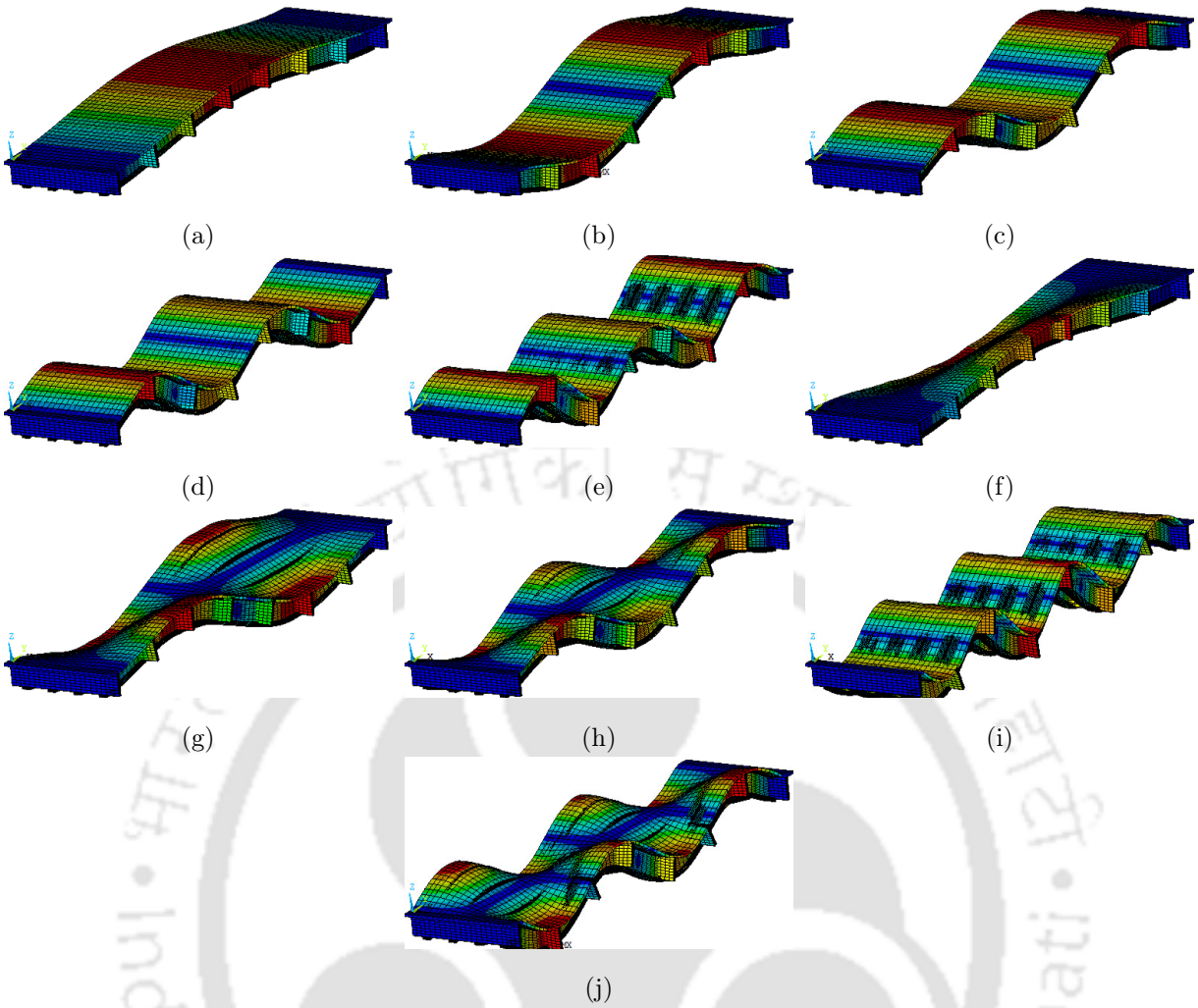

Figure 2.18: First ten mode shapes of the RC bridge from ANSYS®

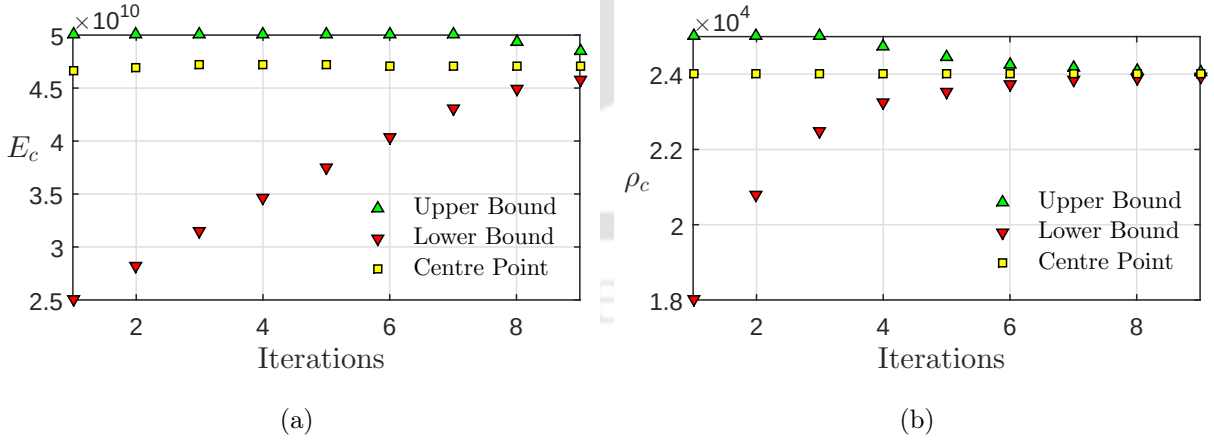

Figure 2.19: Reduction in the bounds of the updating parameter (i.e. E_c and ρ_c) with succeeding iterations of ARSM

this DoE scheme generates minimal support points for coefficient evaluation and subsequently, the effect of weight function in MLS is not significant. Thus for similar polynomial bases, minimum value of the objective functions are almost identical in each iterations. The increase in support points, as in the case of D-optimal design (also, full factorial and central composite designs) shows a significant improvement in MLS based RSM, especially with regularized weights. Moreover, direct gradient based optimization without employing

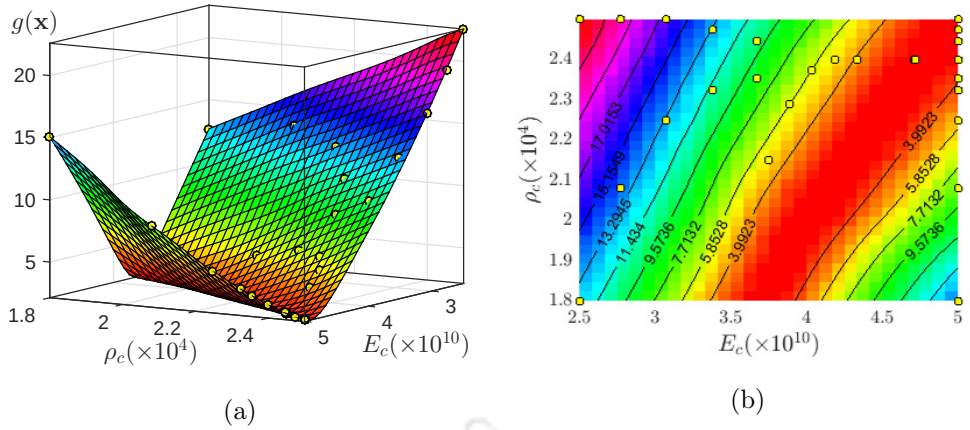

Figure 2.20: Objective function with respect to the updating parameters along with support points generated in ARSM

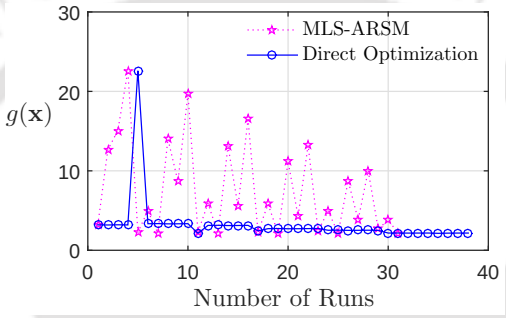

Figure 2.21: Convergence of the objective function with MLS based RSM and gradient based optimization

RSM is also performed for elucidating the effectiveness of meta-modelling. It is observed that RSM formed by least square converges slower than the direct gradient based optimization. Similar conclusions can be drawn for Koshal design based support points generation. But, quadratic polynomial approximation using exponential and regularized weight functions show speedy convergence for CCD (also, D-optimal and full factorial designs). Additionally, linear approximation based on regularized weight function shows better efficiency than direct gradient based optimization. A comparison of convergence between them is presented in Fig. 2.21. In this study, duplicate FE solutions are avoided which reduces the actual FE solutions that are represented in the first brackets in Table 2.4. The numerical studies and discussion presented above justify the use of MLS based response surface meta-modelling for solving the optimization problems e.g. FE model updating.

2.5 Summary

This chapter deals with the application of RSM in optimization and model updating of RC road bridge. For this purpose, response surface methodology surrogates the physically time consuming FE model analysis for multivariate input-output relations. A comparative study is performed using least square based RSM and MLS based RSM with exponential and regularized weight functions for linear and quadratic bases. Also, the efficiency of different DoE schemes are studied in this chapter. The summary of this work is as follows

- It is noted that MLS based RSM performs better than least square based RSM. Also, the regularized weighted MLS based RSM is more efficient than the exponentially weighted MLS based RSM.
- Selection of DoE scheme for the support points generation is critical. Koshal design shows no difference in the number of the FE solutions and the optimized results with least square and MLS based RSM in the present study. Whereas D-optimal, full factorial and central composite designs show considerable difference in the meta-models using MLS based RSM.

- As compared to gradient based optimization for FE model updating, MLS based RSM converged faster except for exponentially weighted linear polynomial basis and Koshal design.

With this in view, the performance of RSM is proposed to be studied further with DoE schemes like central composite design and regularized weight function for high dimensional problems.

Chapter 3

RSM for Reliability Analysis

3.1 Introduction

The RSM in deterministic framework, as discussed in the previous chapter, can also be employed for reliability assessment. In this regard, the response surface is built using random variables to estimate the probability of failure of the structure. This, in turn, helps to reduce the computational effort associated with the estimation of reliability. With this in view, the present chapter discusses the use of RSM and its modified version for reliability analysis and design. To do so, a new proposal using two-step RSM is introduced to solve the design optimization of a structure subjected to uncertainty. Numerical results are presented in this work to clearly demonstrate the computationally efficiency of the proposed algorithm for reliability based design optimization.

3.2 Response Surface Formulation for Reliability Analysis

Let us consider a performance function $g(\mathbf{x})$ with input variable $\mathbf{x}$ which constitutes deterministic as well as random variables. The input variable vector can be denoted in two subset vectors $\mathbf{x}_d$ and $\mathbf{x}_r$ for deterministic and random variables, respectively. It can be noted that if there are no deterministic variable(s), then $\mathbf{x}$ is equal to $\mathbf{x}_r$. In that case, the response surface $\tilde{g}(\mathbf{x})$ is formed by considering the random variables only.

As suggested in Chapter 2, the response surface is generated for reliability assessment by assuming a domain $\Omega_{\mathbf{x}}$ of the associated variables. Either of the Eqs. 2.2, 2.3 or 2.4 can be utilized to construct linear or quadratic meta-model. Since, the response surface for reliability analysis is constructed in the standard normal space (i.e. with respect to $\mathbf{z}$), the vector $\mathbf{x}$ needs to be transformed into standard normal space $\mathbf{z}$. This transformation can be performed using different approaches such as Rosenblatt transformation [4], Morgenstern model [148], Nataf model [148] and so on. These approaches employ marginal transformations which are discussed below in brief –

- *Rosenblatt Transformation:* It is based on one-to-one CDF mapping which is given by

$$\begin{aligned}
\Phi(z_1) &= F_{X_1}(x_1) \\
\Phi(z_2) &= F_{X_2}(x_2|X_1 = x_1) \\
&\vdots \\
\Phi(z_i) &= F_{X_i}(x_i|X_1 = x_1, X_2 = x_2, \ldots, X_{i-1} = x_{i-1}) \\
&\vdots \\
\Phi(z_n) &= F_{X_n}(x_n|X_1 = x_1, X_2 = x_2, \ldots, X_{n-1} = x_{n-1})
\end{aligned} \tag{3.1}$$

for correlated random variables. Here, $F_X(\bullet)$ and $\Phi(\bullet)$ denote the CDF of the random variable $\mathbf{x}$ and the CDF of the standard normal random variable $\mathbf{z}$, respectively. For uncorrelated random variables, the above expression is simplified to

$$\mathbf{x} = F_{\boldsymbol{X}}^{-1}[\Phi(\mathbf{z})] \tag{3.2}$$

In general, determination of the conditional CDF of the random variables is not always numerically possible. Thus, use of this transformation for correlated cases is practically difficult for many problems. In this regard, correlation coefficient based transformation models can be applied to ease the computational difficulties which is discussed in the next method.

- *Morgenstern Model:* Let the marginal CDFs for bivariate case be defined as $F_{X_i}(x_i)$ and $F_{X_j}(x_j)$ which are used to give the Morgenstern distribution such that [148]

$$F_{X_iX_j}(x_i, x_j) = F_{X_i}(x_i)F_{X_j}(x_j)[1 + \rho'_{ij}\{1 - F_{X_i}(x_i)\}\{1 - F_{X_j}(x_j)\}] \tag{3.3}$$

and

$$f_{X_iX_j}(x_i, x_j) = f_{X_i}(x_i)f_{X_j}(x_j)[1 + \rho'_{ij}\{1 - 2F_{X_i}(x_i)\}\{1 - 2F_{X_j}(x_j)\}] \tag{3.4}$$

where, $f_{X_iX_j}(x_i, x_j) = \partial F_{X_iX_j}(x_i, x_j)/\partial x_i \partial x_j$ is the joint *pdf*. It can be noted that this model is applicable when the value of joint *pdf* is not negative. It eventually gives the modified correlation coefficient $\rho'_{ij} \in [-1, +1]$ which is evaluated by solving the expression given below

$$\rho_{ij} = \int_{-\infty}^{+\infty}\int_{-\infty}^{+\infty}\left(\frac{x_i - \mu_{x_i}}{\sigma_{x_i}}\right)\left(\frac{x_j - \mu_{x_j}}{\sigma_{x_j}}\right) f_{X_iX_j}(x_i, x_j)\,\mathrm{d}x_i\mathrm{d}x_j \tag{3.5}$$

The range of accuracy of this transformation for different correlation structure is limited.

- *Nataf Model:* Another popular method is the Nataf transformation [148] which is given by

$$f_{\boldsymbol{X}}(\mathbf{x}) = f_{X_1}(x_1)f_{X_2}(x_2)\cdots f_{X_n}(x_n)\frac{\varphi_n(\mathbf{z}, \mathcal{R}')}{\varphi(z_1)\varphi(z_2)\cdots\varphi(z_n)} \tag{3.6}$$

where, $\mathcal{R}' = \mathrm{Cov}[\boldsymbol{Z}^\mathsf{T}, \boldsymbol{Z}] = \mathbb{E}[\boldsymbol{Z}^\mathsf{T}\boldsymbol{Z}] = [\rho'_{ij}]$, $\forall\ i, j = 1, 2, \ldots, n$. Here, it may be noted that Cov and $\mathbb{E}$ represent the covariance and expectation operators, respectively. The individual correlation between the transformed random variables $\mathbf{z}$ is evaluated using

$$\rho'_{ij} = \int_{-\infty}^{+\infty}\int_{-\infty}^{+\infty}\left(\frac{x_i - \mu_{x_i}}{\sigma_{x_i}}\right)\left(\frac{x_j - \mu_{x_j}}{\sigma_{x_j}}\right)\varphi_2(x_ix_j, \rho_{ij})\,\mathrm{d}x_i\mathrm{d}x_j \tag{3.7}$$

where, ρ_{ij} is the element of $\mathcal{R} = \mathrm{Cov}[\boldsymbol{X}^\mathsf{T}, \boldsymbol{X}]$. However, this transformation is not accurate near the boundary of the correlation coefficient (i.e. near -1 or $+1$).

After the formation of the response surface in the standard normal space $\mathbf{z}$, gradient based technique is applied to locate the failure point. Hence, similar to the previous chapter, this application of RSM also invokes two iteration loops. The outer loop remains the same where new support points are generated iteratively whereas the inner loop finds the location of MPP instead of minimizing the objective function as expressed in Eq. 2.17. The MPP is determined using Rackwitz-Fissler's algorithm [1] which is given by

$$\mathbf{z}_{D,it} = \frac{[\mathbf{z}_{D,it-1}\nabla\tilde{g}(\mathbf{z}_{D,it-1})^\mathsf{T} - \tilde{g}(\mathbf{z}_{D,it-1})]}{\|\nabla\tilde{g}(\mathbf{z}_{D,it-1})\|^2}\nabla\tilde{g}(\mathbf{z}_{D,it-1})^\mathsf{T} \tag{3.8}$$

In the above equation, $\mathbf{z}_{D,it}$ is the optimized MPP over the response surface for the iteration it. The above expression can be derived from either by sequential quadratic programming (SQP) or by Newton-Raphson's method [149, 150]. This design point is evaluated in the iteration it requires further refinement to get better estimation of the failure. In this regard, Bucher and Bourgund [16] suggested extrapolation to find the location of the new design point for the next iteration. The expression for the improved design point that

lies on the limit surface is given as follows

$$\mathbf{x}_{N,it+1} = \mathbf{x}_{N,it} + [\mathbf{x}_{D,it} - \mathbf{x}_{N,it}] \frac{g(\mathbf{x}_{N,it})}{g(\mathbf{x}_{N,it}) - g(\mathbf{x}_{D,it})} \tag{3.9}$$

Thus, the outer loop utilizes this new design location $\mathbf{x}_{N,it+1}$ to generate the response surface for the successive iteration. Although, Bucher and Bourgund [16] limited the number of iteration to two, it can be extended until the convergence is achieved. This convergence is usually evaluated between the successive design points and the actual functional value at these locations. For practical applications, the permissible error is considered in the range of 10^{-2} to 10^{-3}.

The final response surface $\tilde{g}(\mathbf{x})$ is constructed once the aforementioned convergence test is satisfied to locate the most probable failure point $\mathbf{x}^*$. Following this iterative procedure, reliability analysis is performed to estimate the probability of failure p_f. Different techniques for reliability analysis can be applied such as FORM, SORM, MCS, LHS, importance sampling and so on. One of the popular method is MCS that demands adequate sample size to carry out the reliability assessment. Using this methods, the probability of failure p_f is evaluated as

$$p_f \approx \frac{1}{n_c} \sum_{i=1}^{n_c} \mathscr{I}[\tilde{g}(\mathbf{x}_i) < 0] \tag{3.10}$$

where, n_c is the sample size of the simulation. In the above equation, $\mathscr{I}[\bullet]$ is a binary indicator function (i.e. either 0 or 1) based on the condition stated within the third bracket.

Here, it may be noted that the aforementioned approach of meta-modelling forms a global approximation of the actual performance function and eventually, the error associated with it can be significant. This is due to the fact that global error minimization fails to capture any local variation. Hence, an adaptive scheme is proposed by Kaymaz and McMahon [27] that minimizes the weighted norm of the error which is further discussed in the following section.

3.2.1 Adaptive Response Surface Method (ARSM)

In many occasions, global approximation fails to replicate the limit state accurately which results in either over- or under-estimation of the probability of failure. Thus, accurate replication of the limit state is the key task in the meta-model based reliability assessment. Due to this reason, improving the accuracy near the design point, in particular, remains a critical issue. To address this issue, weights are assigned at the support points which abate the error in approximation and makes the polynomial surface adaptive to the local variation, if any. The weight for this purpose is given by [27]

$$w(\mathbf{x}_i) = \exp\left(-\frac{g(\mathbf{x}_i) - \mathbf{x}_{\text{best}}}{\mathbf{x}_{\text{best}}}\right) \tag{3.11}$$

where, $\mathbf{x}_{\text{best}}$ represents the location of the support point which is closest to the limit state (i.e. it fulfils $\min[|g(\mathbf{x})|]$). This modifies the error estimation in Eq. 2.6 to

$$\varepsilon = \sum_{i=1}^{n_s} w(\mathbf{x}_i) e_{g,i}^2 \tag{3.12}$$

Minimizing the total error in the above equation by following the steps in § 2.2.1, the coefficient vector $\mathbf{a}$ obtained as follows

$$\mathbf{a} = (\mathbf{X}^\mathsf{T} W \mathbf{X})^{-1} (\mathbf{X}^\mathsf{T} W) \mathbf{g} \tag{3.13}$$

Above expression is often called weighted regression where $W = \text{diag}[w(\mathbf{x}_1)\, w(\mathbf{x}_2) \cdots w(\mathbf{x}_i) \cdots w(\mathbf{x}_{n_s})]$. It can be noted that difference between the Eqs. 2.10 and 3.13 lies in the definition of the weight function $w(\bullet)$. In Eq. 3.11, the weight function is invariant to the approximation at any arbitrary point. This mean that once the weights are assigned, it remain unchanged throughout the response surface construction. However, this is not the case in the MLS based RSM where the weight function varies with respect to the distance

of the support points and any arbitrary location. Hence, the determination of the unknown coefficients **a** becomes independent of the location of the arbitrary point in the weighted regression. In the present study, adaptive response surface using MLS based regression due to its superior quality to map the nonlinear limit state is adopted.

Once the adaptive response surface is formed, any model of structural reliability assessment can be applied to obtain the final probability of failure. This approach can be further extended to RBDO problems which require multiple estimation of p_f as discussed in the following section.

3.3 Proposed Design Optimization Using RSM

Previous subsections describe the formulation of RSM and its adaptive version that can be used for optimization and reliability analysis. Here, it may be noted that reliability analysis involves random variables as opposed to deterministic variables in optimization. However, reliability based design optimization needs both deterministic and random variables. This, in turn, demands construction of the response surface using deterministic as well as random variables. In actual case, RBDO is also subjected to constraints as described in the following model

$$\begin{aligned} &\text{Minimize} && g(\mathbf{x}_d,\ \mathbf{x}_r) && \text{w.r.t. } \mathbf{x}_d \\ &\text{Subjected to :} && g_o \geq \mu_g(\mathbf{x}_d^*,\ \mathbf{x}_r) + \beta_c\ \sigma_g(\mathbf{x}_d^*,\ \mathbf{x}_r) \\ & && \mathbf{x}_d \in \Omega_{\mathbf{x}_d} \end{aligned} \tag{3.14}$$

In the above equations, g_o represents the threshold that demarcates the safe and failure regions. Parameters μ_g and σ_g in Eq. 3.14 represent the mean and standard deviation of the output while $\Omega_{\mathbf{x}_d}$ specifies the domain of the design variables. Thus, the above formulation tries to minimize $g(\bullet)$ subjected to a specific β_c (i.e. given reliability) at an optimal variance σ_g^2. In this context, the mean $\mu_g(\mathbf{x}_d^*,\ \mathbf{x}_r)$ and standard

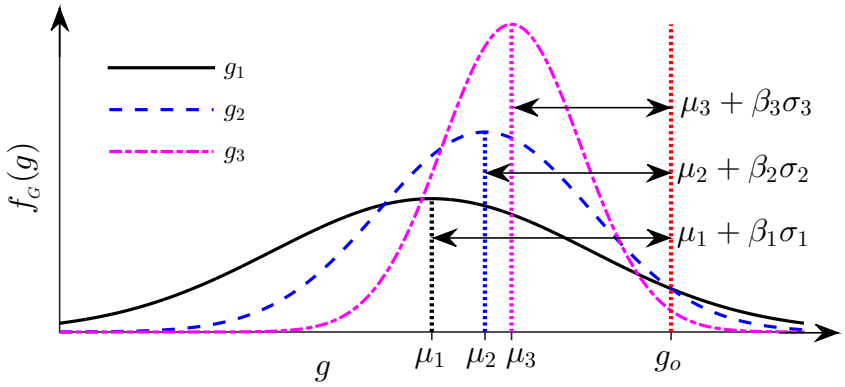

Figure 3.1: Typical *pdf*s in different iterations of RBDO where g_i represents the i^{th} design

deviation $\sigma_g(\mathbf{x}_d^*,\ \mathbf{x}_r)$ of $g(\bullet)$ are evaluated statistically by generating adequate realizations of the random variables $\mathbf{x}_r$ with specified *pdf* at every deterministic design point $\mathbf{x}_d^*$. To ease this computational burden, a new two-step response surface approximation is proposed for both optimization as well as moment evaluation at every $\mathbf{x}_d$. This approach is described in the following sections.

3.3.1 Two-step ARSM for RBDO

The RBDO problem described in Eq. 3.14 demands to satisfy constraint condition (i.e. reliability or probability of failure) for optimal choice of the design variables $\mathbf{x}_d$. This, in turn, requires the evaluation of the first two moments. The constraint condition reveals that the failure surface is at a distance $\beta_c\sigma_g$ from the mean μ_g as shown in Fig. 3.1. The area under the curve beyond the point g_o is the probability of failure (i.e. $\mathscr{P}[g(\mathbf{x}) \geq g_o]$). Now, by considering a predefined value of β, the controller parameters can be optimized for the robust design as described in Eq. 3.16. On minimizing the parameters, resulting design will ensure the predefined reliability as compared to the conventional design which has no control over the uncertainty.

Fig. 3.1 shows the schematic *pdf* of the performance function for three different designs (i.e. Design-1, Design-2 and Design-3). It is clear that Design-3 has less probability of failure compared to Design-1 and Design-2. This is due to the fact that the variance in Design-3 (i.e. σ_3^2) is less than that in Design-1 and Design-2 (i.e. σ_1^2 and σ_2^2, respectively) even when the variations in mean μ_g in all the cases are negligible. This sets the goal for the reliability based design optimization. In other words, the reliability based design has less probability of failure due to better control over the dispersion of the performance function value as compared to the deterministic design which is exposed to uncertainty. It is due to the skewed *pdf* leading to reduction in variance of the performance function without significant change in the mean value as compared to the deterministic design. Although FOSM is used to evaluate the reliability, present formulation is open to adopt any other model to estimate p_f.

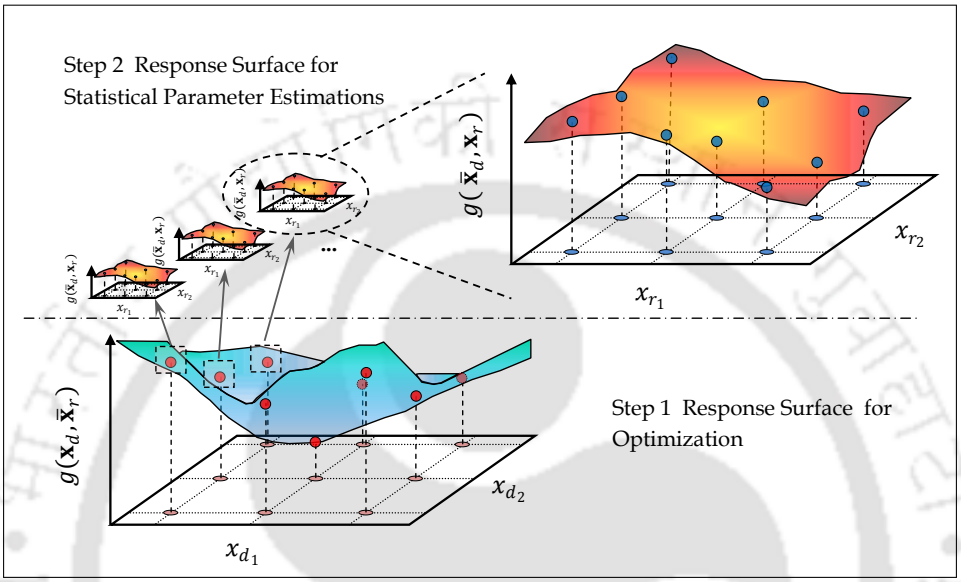

Figure 3.2: A schematic illustration of the proposed two-step ARSM used for RBDO

An illustration of the response surfaces in this two-step ARSM algorithm is presented in Fig. 3.2. One distinct advantage of the ARSM algorithm is speedy and accurate estimation with less chances of ill-conditioning as compared to the global RSM. The main cause behind ill-conditioning is over-fitting. In this context, over-fitting occurs due to – higher order polynomial, less number of support points and large number of input variables. However, in the present analysis linear or quadratic polynomial basis is used with adequate number of support points. Moreover, the constrained stochastic optimization considered in the present analysis has moderate number of random variables. Hence, the chances of over-fitting in this case is less. This issue is further verified with simulation results. A stepwise sequential algorithm of the proposed scheme for parameter optimization is shown in the flowchart given in Fig. 3.3. Initially, the domain of $\mathbf{x}_d$ (i.e. $\Omega_{\mathbf{x}_d}$) and the statistical properties of $\mathbf{x}_r \in \Omega_{\mathbf{x}_r}$ (i.e. mean $\mu_{\mathbf{x}_r}$, standard deviation $\sigma_{\mathbf{x}_r}$, *pdf* and correlation coefficient, if any) are defined. Additionally, the desired reliability index β_c for the threshold level g_o are also defined by the user. Assuming an initial design point $\mathbf{x}_d^* \in \Omega_{\mathbf{x}_d}$, n_s support points of $\mathbf{x}_d$ are generated following any suitable DoE scheme. On these points, response surface using MLS as per Eq. 2.10 is constructed which corresponds to step 1 as shown in Fig. 3.2. For this purpose, the values of the random variables $\bar{\mathbf{x}}_r$ is fixed at some characteristic values (e.g. $\mu_{\mathbf{x}_r}$ in the present study). Simultaneously, at each of these support points for $\mathbf{x}_d$, another set of support points for $\mathbf{x}_r$ using a DoE scheme is generated and the values of $g(\bullet)$ are evaluated to estimate μ_g and σ_g. Using these support points, the second response surface is developed by adopting the MLS technique as in step 1. Therefore, number of step 2 response surfaces formed is equal to n_s. MCS technique is adopted for the moments estimation using response surface in step 2. The purpose of selecting the meta model based approach solely lies at this step where computational burden for uncertainty quantification using original differential equation is huge, especially for complex finite element model of large structures. Once the μ_g and σ_g for each n_s support points of $\mathbf{x}_d$ are obtained, constrained RBDO is solved using the response surface in step 1 by gradient based optimization (e.g. SQP [151]) to evaluate the new design point $\mathbf{x}_d^*$. These steps are repeated with the new design point $\mathbf{x}_d^*$ to get a better approximation until the convergence is achieved. The convergence criteria used in this study are $\left|(g_{it} - g_{it-1})/g_{it-1}\right| \leq 0.01\%$ and $\left|(\mathbf{x}_{d,it}^* - \mathbf{x}_{d,it-1}^*)/\mathbf{x}_{d,it-1}^*\right| \leq 0.01\%$. In this framework, two processes run sequentially in each iteration until terminating criteria is achieved. The proposed algorithm is explained in the flowchart in Fig. 3.3.

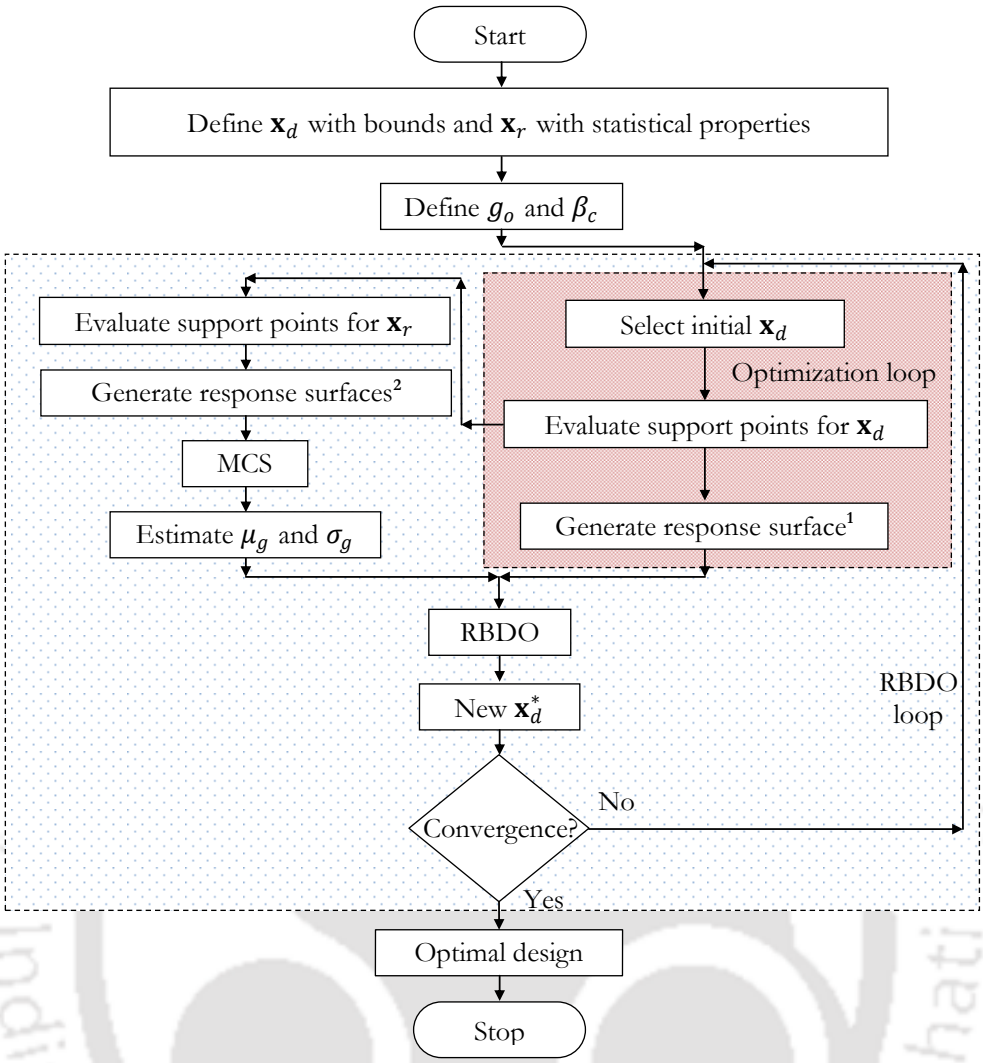

Figure 3.3: A flowchart of the proposed RBDO using two-step ARSM ([1] and [2] refer to first and second step response surfaces, respectively)

Here, the key steps are as follows –

- **Initialize:** Generate initial design point $\mathbf{x}_{d,0}^*$ within bounds $[\mathbf{x}_{d,L}, \mathbf{x}_{d,U}]$ and assume $\bar{\mathbf{x}}_r$ for random variables.
- **Step 1:** Generate support points as per DoE pattern with center at $\mathbf{x}_{d,it}^*$. Using these support points, MLS based response surface is constructed for optimization with respect to $\mathbf{x}_d$. In this context, the support points from previous iterations can be included for better approximation.
- **Step 2:** Generate second series of response surface using $\mathbf{x}_r$ at each support points in the Step 1 to evaluate statistical moments (i.e. μ_g and σ_g^2) necessary for satisfying constraint equation. In this context, MCS is performed on the second response surface which is easy and faster to implement.
- **Optimization:** New $\mathbf{x}_{d,it+1}^*$ is evaluated using gradient based optimization on the response surface at Step 1.
- **Convergence Check:** Stopping criteria is checked as mentioned before. If the criteria is satisfied then the iteration is terminated else Step 1 is recalled. It may be noted that it represents the current iteration and the permissible errors $\mathscr{E}_1$ and $\mathscr{E}_2$ are preselected prior to optimization.

Based on this model, numerical study is conducted to show the efficiency of the proposed algorithm (see Fig. 3.2) which is presented in the following section.

3.4 Numerical Results and Discussion

In this section, numerical modelling of adaptive response surface and its application for reliability analysis and reliability based design optimization are discussed. For this purpose, the original performance function is evaluated at different support points generated by different schemes. In this study, CCD [14] is used for error minimization as suggested in Chapter 2. Fig. 3.4 shows a typical distribution of the support points in CCD scheme. A total of $(1 + 2n + 2^n)$ support points are generated in each iteration. The functional values at these points are used to estimate the error. Using MLS based surface fitting in each iteration, the

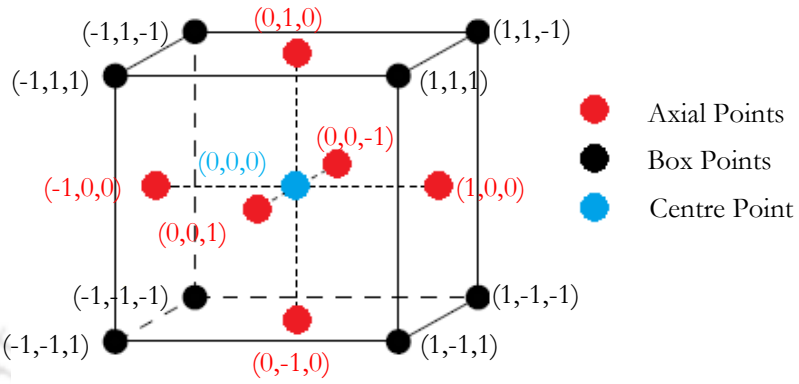

Figure 3.4: A typical distribution of support point as per CCD scheme with centre point, box points and axial points

model is improved based on the new design point $\mathbf{x}_d^*$ evaluated after each iteration. Further, to compare the improvement in reliability, three different optimization schemes are discussed for minimizing $g(\bullet)$ with respect to $\mathbf{x}_d$ which are as follows:

- **Design 1 - Deterministic Design Optimization:** The objective in this design scheme is to

$$\begin{aligned} &\text{Minimize} && g(\mathbf{x}_d,\ \bar{\mathbf{x}}_r) && \text{w.r.t. } \mathbf{x}_d \\ &\text{Subjected to :} && \mathbf{x}_d \in \Omega_{\mathbf{x}_d} \end{aligned} \tag{3.15}$$

  where, the deterministic parameters of the system are $\mathbf{x}_d \in [\mathbf{x}_{d,L},\ \mathbf{x}_{d,U}]$, while $\bar{\mathbf{x}}_r$ represents a fixed value of $\mathbf{x}_r$ (e.g. mean or 95 percentile value). Here, subscripts L and U specify lower and upper bounds of $\mathbf{x}_d$. Optimizing $\mathbf{x}_d$ gives the best design parameters for the deterministic case when no randomness is associated with the other system parameters $\mathbf{x}_r$. Thus, it is known as deterministic design optimization (DDO).

- **Design 2 - Robust Design Optimization:** Contrary to the above scheme, RDO incorporates the randomness in the objective function. In this case, the objective function is defined by the mean of $g(\bullet)$ which is given by

$$\begin{aligned} &\text{Minimize} && \mu_g(\mathbf{x}_d,\ \mathbf{x}_r) && \text{w.r.t. } \mathbf{x}_d \\ &\text{Subjected to :} && \mathbf{x}_d \in \Omega_{\mathbf{x}_d} \end{aligned} \tag{3.16}$$

  Again, $\mathbf{x}_d$ is the deterministic variable while $\mathbf{x}_r$ has randomness described by their respective *pdf*.

- **Design 3 - Reliability Based Design Optimization:** The description of this design scheme is earlier provided in § 3.3. The same is applied here for comparison with the other design schemes described above.

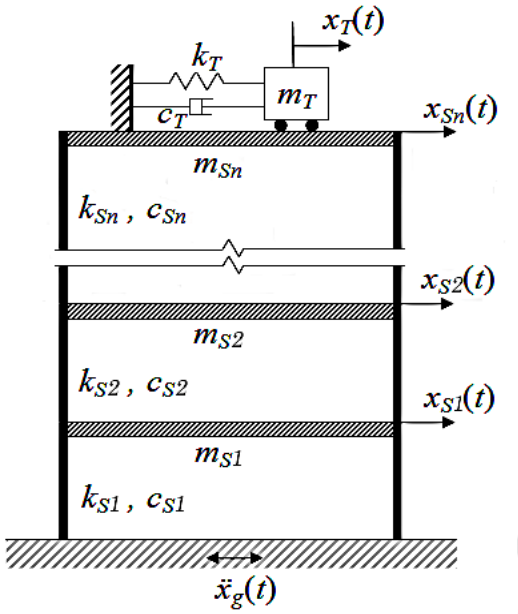

Figure 3.5: MDOF primary system with TMD

3.4.1 RBDO of Tune Mass Damper (TMD)

Fig. 3.5 shows the multi degree of freedom (MDOF) system with TMD considered in this example. The displacement vector $x(t) = \{x_T(t)\ x_{Sn}(t)\ \ \ldots\ x_{S2}(t)\ x_{S1}(t)\}^{\mathsf{T}}$ with respect to base has $(n+1)$ elements where subscripts T and S_i represent TMD and i^{th} structural DOF, respectively. The system is excited by the ground acceleration $\ddot{x}_g(t)$ which has $\mathbf{M}$, $\mathbf{C}$ and $\mathbf{K}$ $(\in \mathbb{R}^{(n+1)\times(n+1)})$ as mass, damping and stiffness matrices. Equation of motion for the linear time invariant system in Fig. 3.5 can be expressed in state-space as

$$\dot{z}(t) = \mathbf{A}z(t) + \mathbf{B}u(t) \tag{3.17}$$

In the above equation, $z(t) = \{x(t)^{\mathsf{T}}\dot{x}(t)^{\mathsf{T}}\}^{\mathsf{T}}$ is the state variable where $z(t) \in \mathbb{R}^{2(n+1)}$ and $u(t) \in \mathbb{R}^{(n+1)}$ is the input excitation vector. The system matrix $\mathbf{A}$ and input matrix $\mathbf{B}$ can be expressed as follows

$$\mathbf{A} = \begin{bmatrix} \mathbf{0} & \mathbf{I} \\ \mathbf{A}_k & \mathbf{A}_c \end{bmatrix} \tag{3.18a}$$

$$\mathbf{B} = \begin{bmatrix} \mathbf{0} \\ \mathbf{I} \end{bmatrix} \tag{3.18b}$$

where, $\mathbf{0}$ and $\mathbf{I}$ are zero and identity matrices, respectively. Other sub-matrices $\mathbf{A}_k$ and $\mathbf{A}_c$ are $-\mathbf{M}^{-1}\mathbf{K}$ and $-\mathbf{M}^{-1}\mathbf{C}$ respectively. In this formulations, $(\dot{})$ represents derivative with respect to time t. The base acceleration $\ddot{x}_g(t) \in u(t)$ is modelled as a filtered white noise which is generally defined by the Kanai-Tajimi spectrum [152, 153]. It is modelled as the response of a second order linear filter excited by a zero mean Gaussian white noise whose governing equation is

$$\ddot{x}_f(t) + 2\eta_g\omega_g\dot{x}_f + \omega_g^2 x_f = -f(t) \tag{3.19a}$$

$$\ddot{x}_g(t) = \ddot{x}_f(t) + f(t) = -(2\eta_g\omega_g\dot{x}_f + \omega_g^2 x_f) \tag{3.19b}$$

where, the ground is modelled as a SDOF filter with frequency ω_g and critical damping ratio η_g subjected to white noise $f(t)$ of intensity S_o. The output power spectral density function (PSDF) from the SDOF ground

filter acts as the input PSDF for the MDOF system which can be expressed as [154]

$$S_{ff}(\omega) = S_o \frac{1 + 4{\eta_g}^2(\frac{\omega}{\omega_g})^2}{(1-(\frac{\omega}{\omega_g})^2)^2 + 4{\eta_g}^2(\frac{\omega}{\omega_g})^2} \tag{3.20}$$

The Kanai-Tajimi spectrum described in the above equation can be alternatively assembled in the $\mathbf{A}_k$ and $\mathbf{A}_c$ as

$$\mathbf{A}_k = \left[\begin{array}{ccc|c} & & & \omega_g^2 \\ & -[\mathbf{M}^{-1}\mathbf{K}] & & \vdots \\ & & & \omega_g^2 \\ \hline 0 & \cdots & 0 & -\omega_g^2 \end{array}\right] \tag{3.21a}$$

$$\mathbf{A}_c = \left[\begin{array}{ccc|c} & & & 2\eta_g\omega_g \\ & -[\mathbf{M}^{-1}\mathbf{C}] & & \vdots \\ & & & 2\eta_g\omega_g \\ \hline 0 & \cdots & 0 & -2\eta_g\omega_g \end{array}\right] \tag{3.21b}$$

Above modifications of $\mathbf{A}_k$ and $\mathbf{A}_c$, increase the dimension from $(n+1)$ to $(n+2)$. Accordingly, the dimensions of Eq. 3.17 to Eq. 3.18b are altered. Using the above formulation, one can evaluate the transfer function $\mathbf{H}(\omega)$ of the system by applying Fourier transformation on both sides of Eq. 3.17 which is given by

$$\mathbf{H}(\omega) = (i\omega\mathbf{I} - \mathbf{A})^{-1}\mathbf{B} \tag{3.22}$$

where, i is $\sqrt{-1}$. Generally, TMD is tuned to the first natural frequency of the uncontrolled primary system. The tuning is done using the design variable $\mathbf{x}_d = \{\omega_r \ \eta_T\}^\mathsf{T}$ for a fixed mass ratio m_r of TMD, where ω_r is dimensionless ratio of the natural frequencies of TMD and primary structure while η_T denotes the critical damping ratio of TMD. The optimal tuning parameters are found out by minimizing suitable objective function of interest. Few literatures [155–159] are available that provide both close-form solution and numerical evaluation of the controller parameters for various structural and operational conditions. However, once the parameters are optimized and the controller is set into action, the designer has limited or no control over this passive devices. In this context, it may be noted that every system has inherent uncertainty that affect the performance of the controller once tuned in a deterministic framework. With this in view, present study aims to tune the controller by minimizing the root mean square (RMS) response of the primary system where uncertainty is embedded in the optimization problem. For this purpose, the stochastic responses of the combined system are evaluated first. The response of the MDOF-TMD system described by Eq. 3.17 can be written as

$$z(t) = z(t_0) + \int_{t_0}^{t} (\mathbf{A}\, z(\tau) + \mathbf{B}\, u(\tau))\, d\tau \tag{3.23}$$

where, t_0 denotes the initial time. The output correlation matrix $\mathbf{R}$ for zero time-lag (i.e. $\mathbf{R}_{zz}(t)$) can be expressed as

$$\mathbf{R}_{zz}(t) = \mathbb{E}[z(t)\, z^\mathsf{T}(t)] \tag{3.24}$$

where, $\mathbb{E}[\bullet]$ represents the expectation operator. On differentiating the correlation matrix $\mathbf{R}_{zz}(t)$ with respect to t, one gets

$$\frac{d}{dt}\mathbf{R}_{zz}(t) = \mathbb{E}[\dot{z}(t)\, z^\mathsf{T}(t)] + \mathbb{E}[z(t)\, \dot{z}^\mathsf{T}(t)] \tag{3.25}$$

Substituting the expression of $\dot{z}(t)$ from Eq. 3.17 and by simplifying, it can be shown that

$$\frac{d}{dt}\mathbf{R}_{zz}(t) = \mathbf{A}\, \mathbb{E}[z(t)\, z^\mathsf{T}(t)] + \mathbf{B}\, \mathbb{E}[u(t)\, z^\mathsf{T}(t)] + \mathbb{E}[z^\mathsf{T}(t)\, z(t)]\, \mathbf{A}^\mathsf{T} + \mathbb{E}[z(t)\, u^\mathsf{T}(t)]\, \mathbf{B}^\mathsf{T} \tag{3.26}$$

Further, multiplying Eq. 3.23 by $u^{\mathsf{T}}(t)$ and taking expectation on both side, one can obtain the cross-correlation between $z(t)$ and $u(t)$ which is given by

$$\mathbb{E}[z(t)\, u^{\mathsf{T}}(t)] = \mathbb{E}[z(t_0)\, u^{\mathsf{T}}(t)] + \int_{t_0}^{t} (\mathbf{A}\, \mathbb{E}[z(\tau)\, u^{\mathsf{T}}(t)] + \mathbf{B}\, \mathbb{E}[u(\tau)\, u^{\mathsf{T}}(t)])\, d\tau \tag{3.27}$$

It may noticed from Eq. 3.27 that the initial conditions defined at t_0 are independent of the excitation and time. Therefore, one gets

$$\mathbb{E}[z(t_0)\, u^{\mathsf{T}}(t)] = \mathbb{E}[z(t_0)]\, \mathbb{E}[u^{\mathsf{T}}(t)] = \mathbb{E}[z(t_0)] \times 0 = 0 \tag{3.28}$$

Similarly, as $z(\tau)$ is independent of $u(t)$, it leads to

$$\mathbb{E}[z(\tau)\, u^{\mathsf{T}}(t)] = \mathbb{E}[z(\tau)]\, \mathbb{E}[u^{\mathsf{T}}(t)] = \mathbb{E}[z(\tau)] \times 0 = 0 \tag{3.29}$$

Furthermore, the excitation $u(t)$ is a zero mean white noise process and thus, the auto-correlation can be expressed as

$$\mathbb{E}[u(\tau)\, u^{\mathsf{T}}(t)] = 2\pi S_0 \delta(t-\tau) \tag{3.30}$$

where, $\delta(\bullet)$ denotes Dirac's delta function. Substituting $\mathbb{E}[z(t_0)\, u^{\mathsf{T}}(t)]$, $\mathbb{E}[z(\tau)\, u^{\mathsf{T}}(t)]$ and Eq. 3.30 in Eq. 3.27, one gets

$$\mathbb{E}[z(t)\, u^{\mathsf{T}}(t)] = \int_{t_0}^{t} \mathbf{B}\, 2\pi S_0 \delta(t-\tau)\, d\tau = \frac{1}{2}\mathbf{B}\, 2\pi S_0 \tag{3.31}$$

Integrating $\delta(\bullet)$ over $[t_0,\ t]$ evaluates $\frac{1}{2}$ as the function is even. Similarly, $\mathbb{E}[u(t)\, z^{\mathsf{T}}(t)]$ from Eq. 3.26 can also be estimated as $\frac{1}{2}\, 2\pi S_0 \mathbf{B}^{\mathsf{T}}$. Substituting these in Eq. 3.26 gives

$$\frac{d}{dt}\mathbf{R}_{zz}(t) = \mathbf{A}\, \mathbf{R}_{zz}(t) + \mathbf{R}_{zz}(t)\, \mathbf{A}^{\mathsf{T}} + 2\pi S_0 \mathbf{B}\mathbf{B}^{\mathsf{T}} \tag{3.32}$$

With $t \to \infty$, process $z(t)$ approaches to stationarity and subsequently, mean and covariance of the process becomes independent of t. Thus, the following Lyapunov equation is formed for statistical moments

$$\mathbf{A}\mathbf{R}_{zz} + \mathbf{R}_{zz}\mathbf{A}^{\mathsf{T}} + 2\pi S_0 \mathbf{B}\mathbf{B}^{\mathsf{T}} = 0 \tag{3.33}$$

Above equation is solved for evaluating the correlation matrix $\mathbf{R}_{zz}$ using in-built Lyapunov equation solver algorithm in MATLAB® [96]. Once the auto-correlation is obtained by solving the Lyapunov equation, one can evaluate the RMS value of the response $z(t)$ at every DOF. Therefore, the RMS value at the top floor of the primary structure can be expressed as

$$\sigma^{c}_{x_{Sn}} = \sqrt{\mathbf{R}_{zz}(2,2)} \tag{3.34}$$

Similarly, RMS value of the displacement at the top storey without TMD (i.e. $\sigma^{uc}_{x_{Sn}}$) can be evaluated by $\sqrt{\mathbf{R}_{z_o z_o}(1,1)}$, where $z_o(t)$ denotes the state space variable without TMD.

Above formulation is used for designing the TMD for optimal reliable control. In this analysis, RMS value of the response is used to evaluate the optimal TMD parameters. A dimensionless objective function $J(\bullet)$ using the ratio of RMS values of the displacement at the top storey with and without TMD systems is defined as follows

$$J(\mathbf{x}_d, \mathbf{x}_r) = \frac{\sigma^{c}_{x_{Sn}}}{\sigma^{uc}_{x_{Sn}}} \tag{3.35}$$

Where, $\mathbf{x}_d$ represents the deterministic design variables of TMD and $\mathbf{x}_r$ represents random variables associated with the primary system which are described by their respective *pdf*. Two different primary system models are studied in this work which are explained below.

Table 3.1: Details of system parameters for SDOF model

Random Variables	Mean Values	Units
ω_S	9.700	rad/s
η_S	0.020, 0.050	-
ω_g	12.100	rad/s
η_g	0.400	-
S_o	0.025	m^2/s^3

3.4.1.1 Validation Exercise

In this section, numerical analysis is carried out to study the performance of the proposed algorithm to evaluate the optimal parameters of TMD operating in presence of uncertainty. The TMD is attached to a SDOF system subjected to base excitation as demonstrated in the previous section. The uncertainties are caused by the primary system and excitation parameters as specified in Table 3.5 which shows the mean values of the uncorrelated and uniformly distributed random variables. It may be noted that the proposed algorithm is not restrictive to any kind of probability distribution and correlation between the random variables. Thus, it can be adopted for generalized case i.e. non-normal and correlated random variables. Also, to study the effect of detuning, three different level of covs (i.e. 10%, 20% and 30%) are considered here. These covs are used to examine the design and performance of TMD. Two different damping cases of the primary system (i.e. $\eta_S = 2\%$ and 5%) are considered here. The controller is designed for frequency ratio ω_r and damping ratio η_T for a given mass ratio m_r.

Using the values, the proposed algorithm is applied for reliability based optimization of these TMD parameters. In this study, the initial design point for optimization is assumed at [0.060 0.010] and support points are generated in its surrounding using the CCD scheme for fitting the response surface. The use of meta-model helps in optimization and to estimate the moments of controller's performance function by circumnavigating the solution of Eq. 3.17. This numerical study demonstrates a simple linear system, however, it can be extended to complex time exhaustive finite element models. In this context, it may be noticed that the execution of response surface is significantly less time consuming than solving a finite element model. In the proposed algorithm, robustness of the design is controlled by the constraint condition which is governed by the threshold value J_o, mean and standard deviation of J. Here, the threshold value J_o is considered to be 1 which indicates complete detuning of the controller. This means that the RMS value of the controlled system is equal to the uncontrolled one. In optimization, the response surface is formed adaptively as it is updated in each successive iteration near the new design point. As two optimization variables are used in

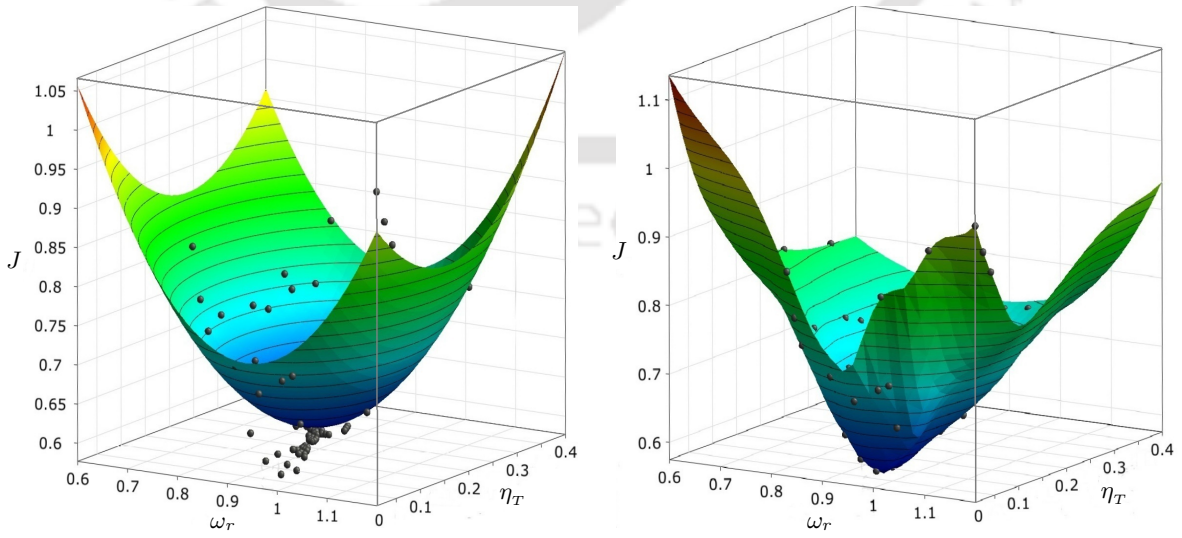

Figure 3.6: ARSM approximation of performance function using (a) least square technique and (b) MLS technique where • represents the support points

this study, altogether 9 support points are generated at each design point based on the CCD scheme for Stage-1 response surface. Further, 43 support points are generated with respect to 5 random variables (i.e. $1+2\times5+2^5$) at each 9 support points for Stage-2 response surfaces. Estimation of the unknown coefficients (as per Eqs. 2.7 and 2.10) are done by least square as well as MLS technique. The response surfaces from both these techniques are shown in Fig. 3.6. It can be noticed that the LS based response surface poorly replicates the objective function as the actual values at the support points are lying out of the modelled surface. Whereas the MLS based approximation using normalized weight function performs much better. Thus, the unknown coefficients evaluated by MLS are used for further analysis.

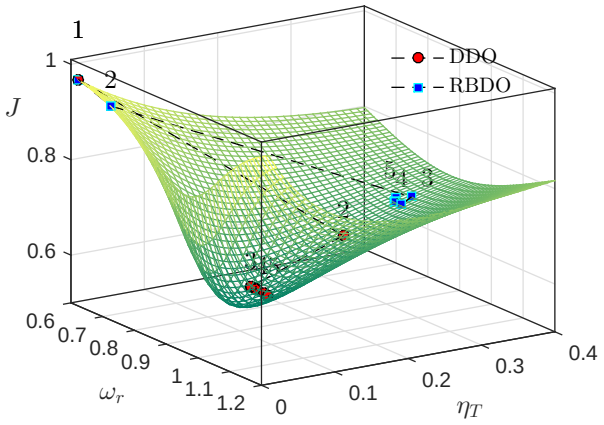

Figure 3.7: Optimized design points at each iteration

Initially, the controller design is conducted with no randomness in the primary system and the excitation (i.e. deterministic case is solved by minimizing the performance function). For this purpose, only the Stage-1 of RSM is used for optimization and the Stage-2 RSM is discarded as no randomness is considered in this design. Thus, it can be called as deterministic design optimization (DDO). Later, the proposed algorithm is applied for reliability based design of the controller. The design from both these methods are compared to address the effect of uncertainty. The design points from both these optimizations in each iteration are demonstrated in Fig. 3.7. The deterministic optimization converges to the minima of the performance function. However, due to the presence of uncertainty in the system, the RBDO design converges to a distinctly different location. The value of optimized ω_r in case of reliability based design is lower than the deterministic design. This analysis is conducted for 5 different mass ratios ranging from 1% to 5% which are shown in Fig. 3.8 and 3.9. The value of ω_r decreases with the increase in mass ratio of the controller due to the decrease in the first natural frequency as the mass of the TMD increases. At different levels of uncertainty, similar trend of optimized design with varying mass ratio can be noticed. Also, with the increase in covariance (i.e. from 0.1 to 0.3), the optimized value of ω_r decreases as more detuning effect is present. To reduce this effect, higher value of damping ratio in TMD is chosen (see Fig. 3.10 and 3.11). From the Fig. 3.7, one can notice slight decrease of ω_r to obtain optimal performance for higher damping ratio in the controller. The damping ratio of TMD is optimized at higher value in reliability based design to significantly reduce the standard deviation of the output as shown in Fig. 3.12(b). Fig. 3.12(a) shows the mean value of the performance function which has relatively less variation for higher damping ratio as compared to the deterministic design. Eventually, trivial change in the mean and noticeable reduction in variance improves the overall reliability of the controller performance. Further, the effect of detuning caused by the uncertainty does not show any specific trend for different values of cov. As the cov decreases, the deterministic and reliability based optimal design of TMD approach the same point. Higher values of cov shows a considerable effect of detuning as the designed values differ where ω_r from RBDO follows same trend as the DDO (i.e. it decreases with increase in mass ratio of TMD) while the optimized η_T shows a reverse trend. This is due to the fact that increase in mass of TMD results in better performance and reliability of the controller.

The effect of detuning on the deterministic design is quantified by estimating the statistical moments (i.e. mean and standard deviation). Table 3.2 and 3.3 show these moments for varying cov and mass ratio m_r. It is obvious that the effect of detuning is more for higher cov (say 0.3). Increase in uncertainty in the system and excitation parameters observes a significant decrease in standard deviation in the reliability based design as compared to deterministic design. This significantly improves the reliability of the controller performance

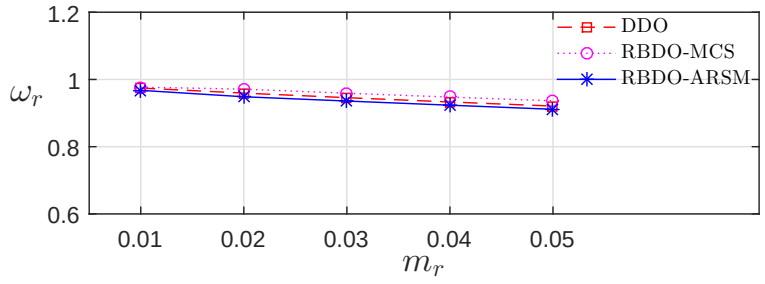

(a)

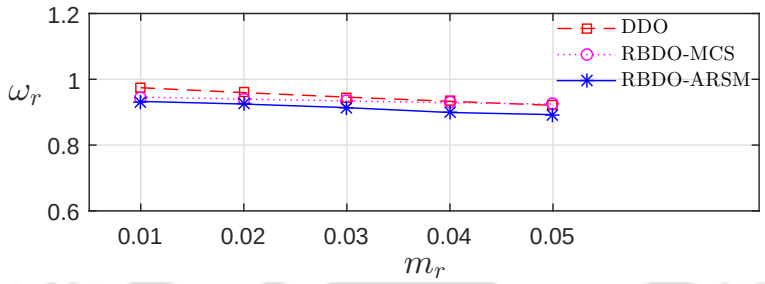

(b)

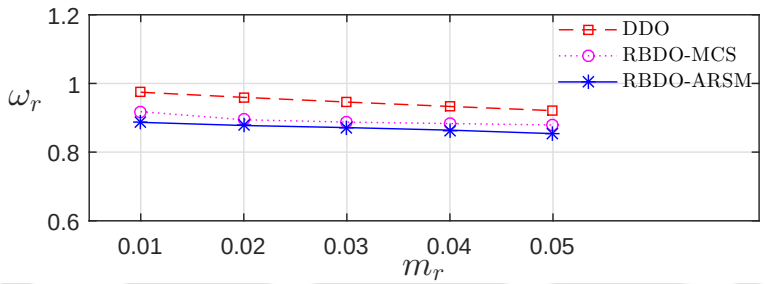

(c)

Figure 3.8: Variation in the optimum frequency ratio ω_r with respect to mass ratio m_r for (a) 10%, (b) 20% and (c) 30% uncertainty when $\eta_S = 0.02$

Table 3.2: Mean and standard deviation of performance function (μ_J and σ_J) with respect to mass ratio m_r for damping ratio $\eta_S = 0.02$ and varying uncertainties

m_r	cov	DDO		RBDO-MCS		RBDO-ARSM	
		μ_J	σ_J	μ_J	σ_J	μ_J	σ_J
0.01	0.1	0.7954	0.0713	0.7865	0.0534	0.7820	0.0545
	0.2	0.8690	0.0925	0.8712	0.0322	0.8643	0.0339
	0.3	0.9046	0.0917	0.9087	0.0255	0.9055	0.0240
0.02	0.1	0.7024	0.0655	0.7024	0.0655	0.6948	0.0601
	0.2	0.7926	0.1072	0.7801	0.0550	0.7713	0.0572
	0.3	0.8441	0.1162	0.8403	0.0399	0.8316	0.0421
0.03	0.1	0.6437	0.0568	0.6437	0.0568	0.6381	0.0547
	0.2	0.7370	0.1091	0.7164	0.0709	0.7088	0.0728
	0.3	0.7973	0.1268	0.7825	0.0544	0.7725	0.0569
0.04	0.1	0.6023	0.0493	0.6023	0.0494	0.5979	0.0498
	0.2	0.6935	0.1064	0.6725	0.0819	0.6680	0.0830
	0.3	0.7591	0.1314	0.7360	0.0660	0.7257	0.0686
0.05	0.1	0.5710	0.0435	0.5710	0.0435	0.5678	0.0461
	0.2	0.6584	0.1019	0.6432	0.0892	0.6414	0.0871
	0.3	0.7269	0.1326	0.6983	0.0754	0.6884	0.0779

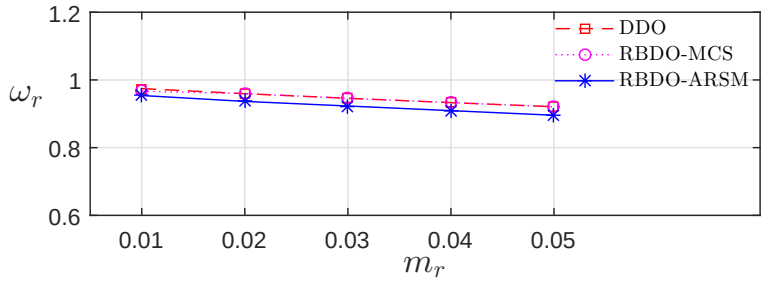

(a)

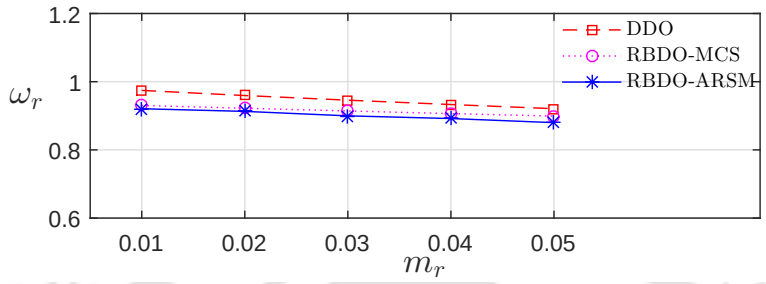

(b)

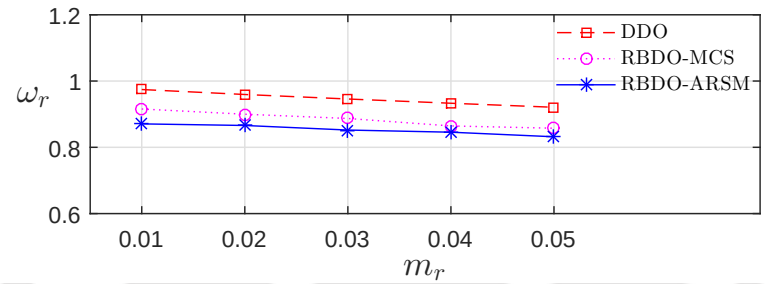

(c)

Figure 3.9: Variation in the optimum frequency ratio ω_r with respect to mass ratio m_r for (a) 10%, (b) 20% and (c) 30% uncertainty when $\eta_S = 0.05$

Table 3.3: Mean and standard deviation of performance function (μ_J and σ_J) with respect to mass ratio m_r for damping ratio $\eta_S = 0.05$ and varying uncertainties

m_r	cov	DDO		RBDO-MCS		RBDO-ARSM	
		μ_J	σ_J	μ_J	σ_J	μ_J	σ_J
0.01	0.1	0.9002	0.0307	0.8984	0.0254	0.8957	0.0258
	0.2	0.9350	0.0432	0.9448	0.0138	0.9399	0.0156
	0.3	0.9523	0.0436	0.9630	0.0106	0.9582	0.0121
0.02	0.1	0.8434	0.0337	0.8434	0.0337	0.8391	0.0320
	0.2	0.8914	0.0574	0.8975	0.0256	0.891	0.0274
	0.3	0.9185	0.0621	0.9308	0.0188	0.9216	0.0223
0.03	0.1	0.8028	0.0329	0.8028	0.0329	0.7989	0.0328
	0.2	0.8571	0.0638	0.8573	0.0357	0.8497	0.0376
	0.3	0.8909	0.0731	0.9025	0.0251	0.8930	0.0280
0.04	0.1	0.7716	0.0313	0.7716	0.0313	0.7679	0.0328
	0.2	0.8285	0.0667	0.8237	0.0441	0.8161	0.0460
	0.3	0.8672	0.0801	0.8755	0.0311	0.8669	0.0333
0.05	0.1	0.7465	0.0297	0.7465	0.0297	0.7433	0.0330
	0.2	0.8042	0.0675	0.7961	0.0510	0.7896	0.0526
	0.3	0.8466	0.0847	0.8508	0.0373	0.8409	0.0399

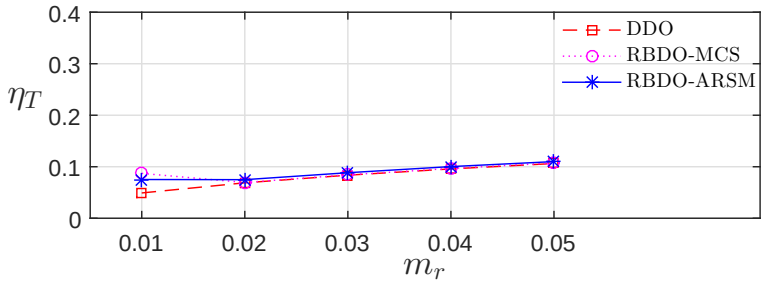

(a)

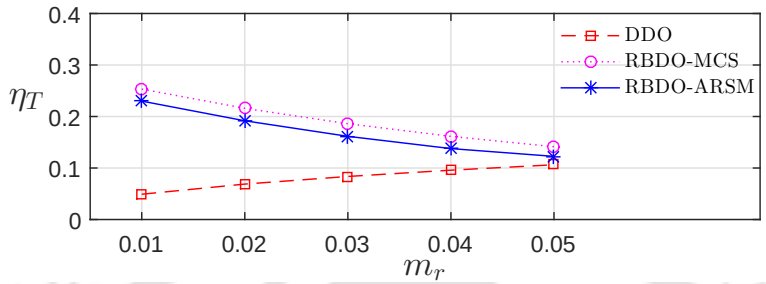

(b)

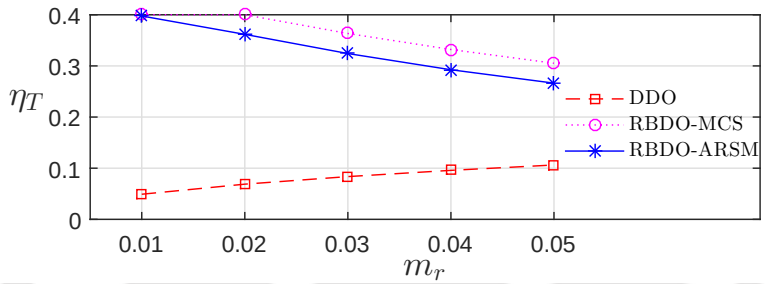

(c)

Figure 3.10: Variation in the optimum damping ratio η_T with respect to mass ratio m_r for (a) 10%, (b) 20% and (c) 30% uncertainty when $\eta_S = 0.02$

Table 3.4: Percentage error in the approximation of the performance functions and its statistical properties

m_r	cov	Error (%)		
		J	μ_J	σ_J
0.01	0.1	0.5	0.6	2.1
	0.2	1.2	0.8	5.3
	0.3	0.3	0.4	5.9
0.02	0.1	0.7	1.1	8.2
	0.2	1.7	1.1	4.0
	0.3	1.8	1.0	5.5
0.03	0.1	0.2	0.9	3.7
	0.2	1.4	1.1	2.7
	0.3	2.3	1.3	4.6
0.04	0.1	0.2	0.7	0.8
	0.2	0.4	0.7	1.3
	0.3	2.4	1.4	3.9
0.05	0.1	0.5	0.6	6.0
	0.2	1.1	0.3	2.4
	0.3	2.3	1.4	3.3

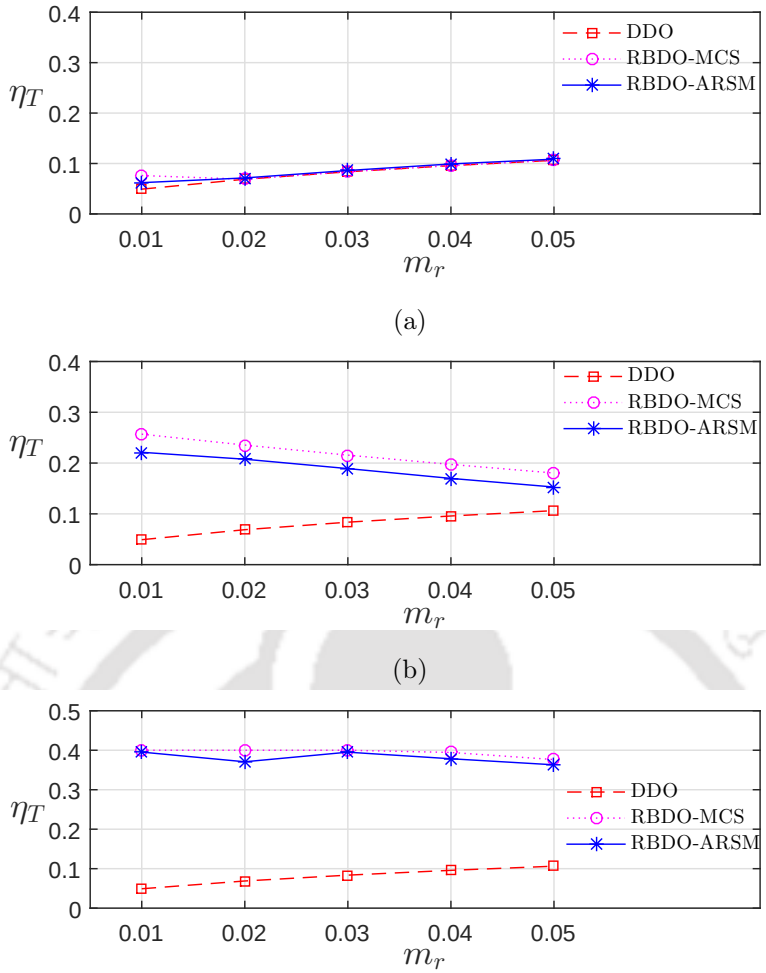

Figure 3.11: Variation in the optimum damping ratio η_T with respect to mass ratio m_r for (a) 10%, (b) 20% and (c) 30% uncertainty when $\eta_S = 0.05$

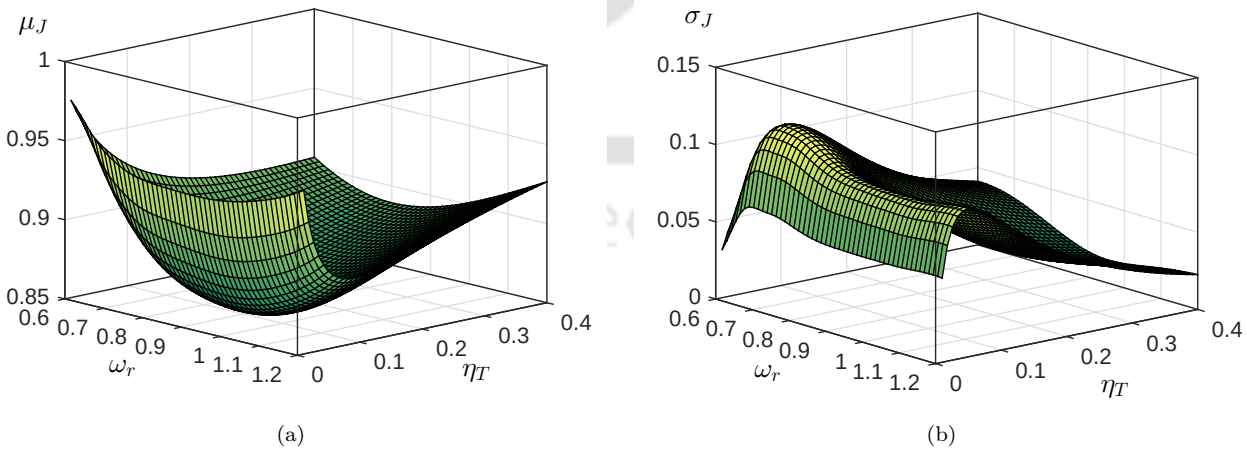

Figure 3.12: (a) Mean and (b) standard deviation of performance function J

as the changes in the mean value are not significant. From Table 3.2 and 3.3, one can notice the decrease in the standard deviation value with the rise in cov level for the reliability based design, which is opposite to the deterministic design. This reverse phenomenon is caused due to the improvement in reliability as

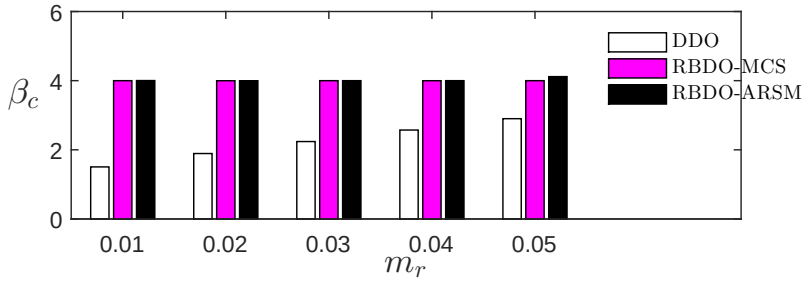

(a)

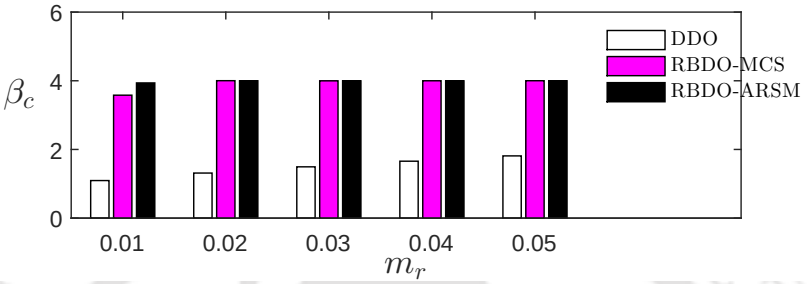

(b)

Figure 3.13: Variation in the sigma level β_c with respect to mass ratio m_r for 30% uncertainty when $\eta_S = 0.02$

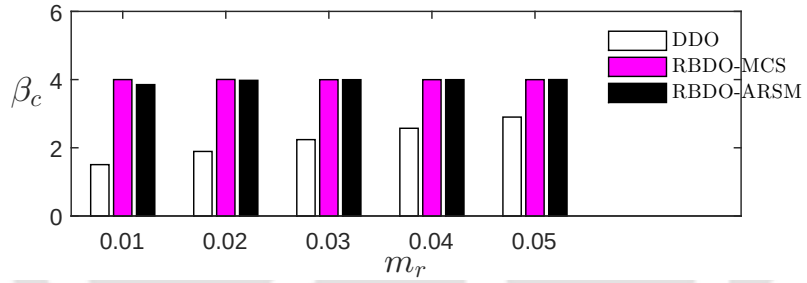

(a)

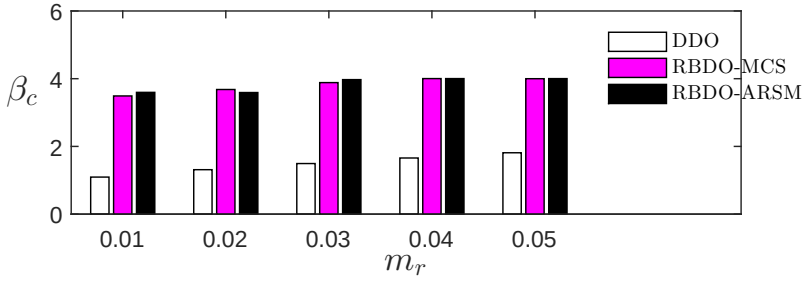

(b)

Figure 3.14: Variation in the sigma level β_c with respect to mass ratio m_r for 30% uncertainty when $\eta_S = 0.05$

the mean value of the performance function is closer to the threshold value J_o. This overall effect of the statistical moments helps in improving the sigma level of the TMD which is given in Figs. 3.13 and 3.14. The sigma level β_c is quantified for the J_o used in this study. A few designs as per the proposed algorithm are not able to achieve the desired β_c factor equal to 4 as the design variable of TMD has reached to its limit value. It can be noticed that the β_c factor obtained by RBDO is significantly more than the deterministic design which gives the global minima of J by not considering effect of uncertainties. This eventually makes the design with higher failure probability due to stepper nature of the performance function. Whereas the optimal design gives better reliability. In TMD design, the sigma level achieved by RBDO is most effective

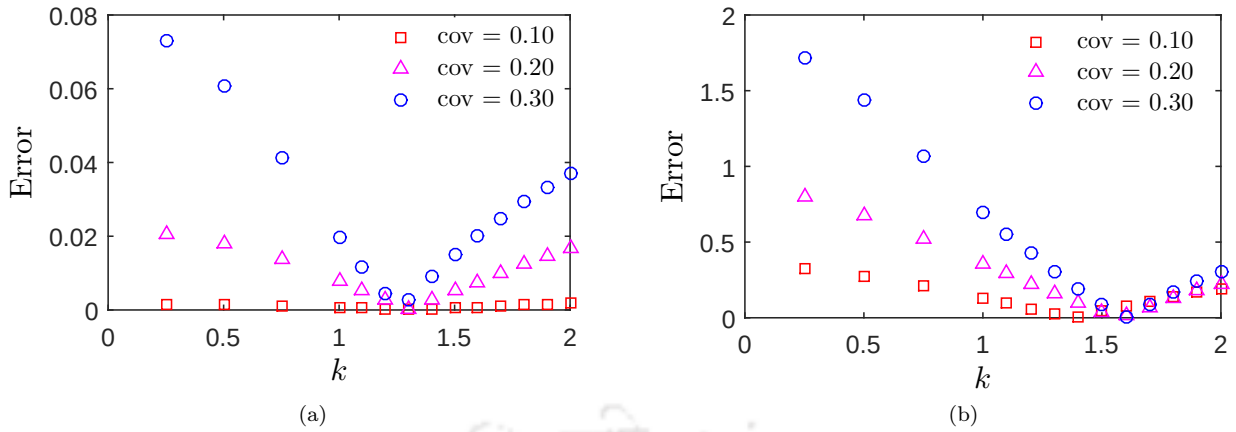

Figure 3.15: Error in the estimation of the (a) mean and (b) standard deviation

due to the inclusion of weighted sum of first two statistical moments in the optimization. This also helps in avoiding design cases where a series of optimal solutions or fronts are evaluated ranging from optimal mean to optimal standard deviation. One can notice improvement in β_c due to lower probability of failure with increase in m_r. Lower value of the β_c factor makes the corresponding design more vulnerable during the operations. Thus, the effectiveness of the proposed optimization method is elucidated with comparison to its deterministic counterpart, as shown in Fig. 3.13 and 3.14. It can be noted that cov equal to 0.1 is not shown as the design variation is trivial and the β_c factor is more than the desired value.

In Figs. 3.8 and 3.9, one can notice the small difference between simulation and the proposed algorithm using Eq. 3.16. Similar observations can be made in Figs. 3.10 and 3.11 for the damping ratio of TMD. These mismatch are caused by the error in numerical estimation of the statistical moments due to lack of fitting of the meta-model. This modelling error is more prominent as the covariance (i.e. level of uncertainty) increases which results in higher domain for searching and fitting the response surface. Table 3.4 shows the percentage error in replicating the performance function J in Stage-1 response surface and subsequent error in moments estimation in Stage-2. The results in this table shows that MLS based algorithm offers excellent meta-model with error less than 2.5%. Moreover, estimation of mean and standard deviation (i.e. μ_J and σ_J) are also accurate with maximum error of 1.4% and 8.2%, respectively. Relatively higher error in variance estimation is attributed to improper local mapping in Stage-2. However, the domain is selected in such as way that the error in variance estimation remains well within the allowable limit (in this case 10%).

The results show that less than 2.5% error is witnessed in the approximation of the performance function by MLS based meta-model. Also, the critical part of estimation of the mean and standard deviation (i.e. μ_J and σ_J, respectively) show a maximum error of 1.4% and 8.2%, respectively. Error in standard deviation is higher as the lack of proper fitting of meta-model resulting in incomplete mapping of the domain of the original function as limited support points are generated following the CCD scheme. This has resulted into misfit of highly nonlinear original surface which is reflected in the error of variance estimation. But one can notice that these errors are generally less that 5% (with none exceeding 9%) as well as Figs. 3.13 and 3.14 show a close match in the sigma level of reliability based designs. Similar trend of error in mean and standard deviation area noticed for linear as well quadratic polynomial bases. Hence, one can conclude that the proposed algorithm for reliability based design of TMD is efficient for all practical purpose. This elucidates the preference of proposed RBDO method to design the controllers. In this context, proper placing of the support points play a vital role on modelling error, especially in the Stage-2 which is fitted once using CCD scheme where points are generated by $\mu \pm k\sigma$. The factor k identifies the domain of these support points. Overall the proposed two-step response surface algorithm offer excellent performance in solving reliability based design optimization problem. Fig. 3.15 shows the sensitivity analysis performed with respect to this multiplication factor. From this figure, it can be noticed that in comparison with k, σ_J estimation is more sensitive. The optimal scale factor for μ_J estimation is 1.3 while that for σ_J varies between 1.5 to 1.7 which support the conclusion that a wider domain in necessary for more accurate estimation of standard deviation.

3.4.1.2 Reliability Based Design Optimization

The above discussion proves the accuracy of the proposed algorithm for reliability based design optimization. In this section, the proposed method is applied to a passive controller which observes contradicting functions for optimization of the design parameters. With this in view, it is tested with different design phenomena such as deterministic design and robust design (i.e. *Design-1* and *Design-2*, respectively) to show its merit. A numerical study of the aforementioned design optimizations is performed for a 3DOF-TMD system considering the effect of uncertainty in it. The TMD is designed with respect to the optimal values of $\mathbf{x}_d$ for a given mass ratio of TMD where the random variables $\mathbf{x}_r$ in the study are elastic modulus E_S and density ρ_S of material in primary structure, modal damping ratio of the primary system η_S, natural frequency of soil ω_g, damping ratio of soil η_g and magnitude of the white noise intensity S_0. All these variables along with their respective mean values, *pdf*s and bounds are listed in the Table 3.5. The performance of TMD

Table 3.5: Properties of deterministic and random variables for MDOF-TMD system

	Variables	$\mu_{\mathbf{x}_r}$	$\mathbf{x}_{d,l}$	$\mathbf{x}_{d,u}$	*pdf*
$\mathbf{x}_d$	ω_r	-	0.60	1.20	-
	η_T	-	0.01	0.40	-
$\mathbf{x}_r$	E_S	1.10E2 GPa	-	-	Uniform
	ρ_S	8000 kg/m^3	-	-	Uniform
	η_S	0.02, 0.05	-	-	Uniform
	ω_g	18.85 rad/s	-	-	Uniform
	η_g	0.60	-	-	Uniform
	S_0	0.02 m^2/s^3	-	-	Uniform

is studied for two different mean values of damping in the primary structure. These are 2% and 5% with uniform *pdf* as mentioned in the Table 3.5. Although the random variables for this numerical analysis are considered to be uniform, proposed formulation does not impose any restriction on the type (i.e. uniform or any other distribution) and the nature (i.e. correlated or uncorrelated) of the random variables. For the most general case (i.e. correlated non-normal random variables), desired set of random numbers can be simulated accordingly prior to the constraint optimization. Three different level of uncertainties are considered in this study with cov equal to 10%, 20% and 30%. During the construction of response surfaces, the range of variables (i.e. random or deterministic) are normalized between 0 to 10. This preconditioning of the variables is performed to reduce the possibility of any numerical instability in solving Eq. 2.10 caused by large matrix inversion. Accordingly, the influence radius D_r of weight function in Eq. 2.13 is assumed as 15 and 25 for Stage-1 and Stage-2 response surfaces, respectively. These values are considered to cover the entire domain by the influence radius. Support points are generated for $\mathbf{x}_d$ in Stage-1 RSM using CCD scheme as discussed in § 2.3. Stage-2 response surface is constructed at each $\mathbf{x}_d^*$ to evaluate μ_J and σ_J which is described as μ_g and σ_g in § 3.3, respectively. For this purpose, MCS is adopted on the Stage-2 surfaces with a sample size $n_s = 1000$. Optimization of $\mathbf{x}_d$ is performed using gradient based technique on Stage-1 response surface for three different design schemes i.e. DDO, RDO and RBDO presented as *Design-1*, *Design-2* and *Design-3* in this chapter, respectively. DDO or *Design-1* is a special case which requires formation of only Stage-1 response surface. For RBDO, the threshold parameter J_o is assumed to be 1 which corresponds to complete detuning of the passive controller. The aim of the optimization is to evaluate $\mathbf{x}_d^*$ for which μ_J lies far left from J_o in the probability distribution plot. Besides this, the reliability based optimization also ensures best possible reduction in σ_J so that the area under the tail end on the right side of J_o is minimized as shown in Fig. 3.1. Combination of these two statistical parameters (i.e. μ_J and σ_J) dictate the design output for maximum reliability (or minimum failure) which is depicted by the parameter β_c, often called as the sigma level.

The randomness in $\mathbf{x}_r$ has a significant effect on the performance of TMD which leads to complete or partial detuning of the controller. It is caused by the perturbations in natural frequencies of the primary system due to the variation in the system parameters (i.e. $\mathbf{x}_r$). Thus, quantification of this detuning effect and the remedial measures against this adverse condition needs to be incorporated in the controller design. Fig. 3.16 shows the transfer function $\mathbf{H}(\omega)$ of the top floor for controlled and uncontrolled systems with mean of η_S equal to 2% and 5%. It shows the peak amplitude at first natural frequency ω_{n1} which is used to tune the controller in this analysis. Effect of TMD to control the vibration energy of the primary structure is quantified by reduction in the area under the transfer functions. The effect of variation will be more

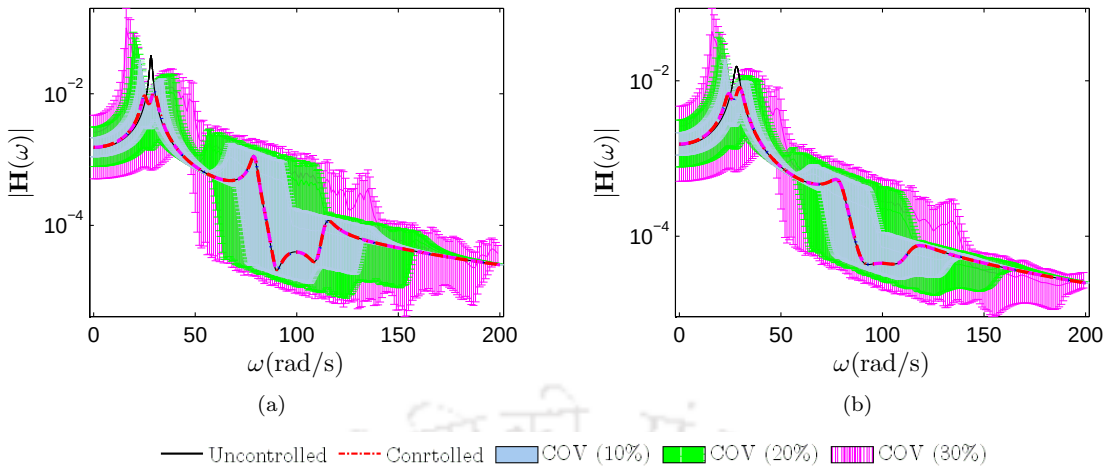

Figure 3.16: Transfer function of the 3DOF system with and without TMD under varying uncertainties with (a) mean of $\eta_S = 2\%$ and (b) mean of $\eta_S = 5\%$

prominent near ω_{n1} as the magnitude and area under $\mathbf{H}$ is relatively more in the vicinity of ω_{n1} as compared to the other natural frequencies. Additionally in Fig. 3.16, varying covs of $\mathbf{x}_r$ from 10% to 30% are shown with the deterministic design of TMD which shows the effect of cov. These variations in the transfer function often shows increase in the magnitude of the controlled natural frequencies for the coupled system. This is attributed due to the lack of tuning caused by the perturbations which alter the natural frequencies of the primary system. Thus, the effect of uncertainties associated with the transfer function is vital for effective performance of TMD. Similarly, the effect of uncertainties are also reflected in terms of statistical properties of the performance function $J(\bullet)$. For comparison, mean and standard deviation of J (i.e. μ_J and σ_J) are estimated for different covs and are shown in Fig. 3.17. The mean of J shows a concave nature having higher values towards the bounds with respect to ω_r for all the uncertainty levels. This signifies that the optimal mean value of J in terms of ω_r, generally, lies in the range of 0.85 to 0.95 for lower uncertainty level and 0.75 to 0.95 for higher uncertainty. On the other side, the mean of J with respect to lower damping ratio of TMD shows higher value and subsequently, decreases with increase in damping ratio until optimality is reached. It increases with higher damping ratio of the controller, however, this increase is relatively less as compared to values at low damping ratios. Similarly to ω_r, the optimal range of damping ratio of TMD may be considered between range 0.05 to 0.10 for lower uncertainty level which shifts between 0.10 and 0.30 for higher uncertainty. Also, in the case of standard deviation of J, it can be noticed that magnitude of σ_J is higher for low damping ratio of TMD. This means that low damping in the controller significantly effects the variation in performance function. Let us consider optimized design point such that it lies in the vicinity of two maxima as shown in Fig. 3.17(b). It is known that ω_r is dependent on the natural frequency of the primary system and the controller. The properties of the primary system are dictated by the mass and stiffness of the structure which are random in real life. Thus, the tuning natural frequency of primary system is liable to be uncertain because of the random environment. This phenomenon leads to variation in optimal frequency ratio of TMD and in case of lower damping in the controller (as in the case of *Design-1*), adverse effect on the performance of the controller is possible. This condition worsens with increase in the level of cov from 10% to 30% where it can be noticed that two maxima are replaced by a region of high variance [see Fig. 3.17(f)]. But, with the increase in η_T, the variance of J decreases. This particular tradeoff is caused by the effect of higher damping offered by TMD which effectively absorbs the variations. Similar sensitivity towards the design parameters is witnessed for both the mean values of η_S (i.e. 2% and 5%). Additionally, conflicting nature of the statistical properties can be justified due to the presence of high standard deviation values in the vicinity of optimal μ_J. This can effect the overall reliability of the controller as the area under the failure region will be more, as demonstrated in Fig. 3.1. Thus, standard deviation significant effects the optimal design of the controller under random environment. In this context, optimal design of TMD with constraints based on mean and standard deviation is used in this study. This is discussed in the upcoming paragraph where the TMD is designed using proposed algorithm and compared with other methods.

Different formulations are used to estimate the TMD design variables $\mathbf{x}_d$. At first, design optimization is carried out in deterministic framework (i.e. *Design-1*) and optimal values of $\mathbf{x}_d$ are obtained as given in

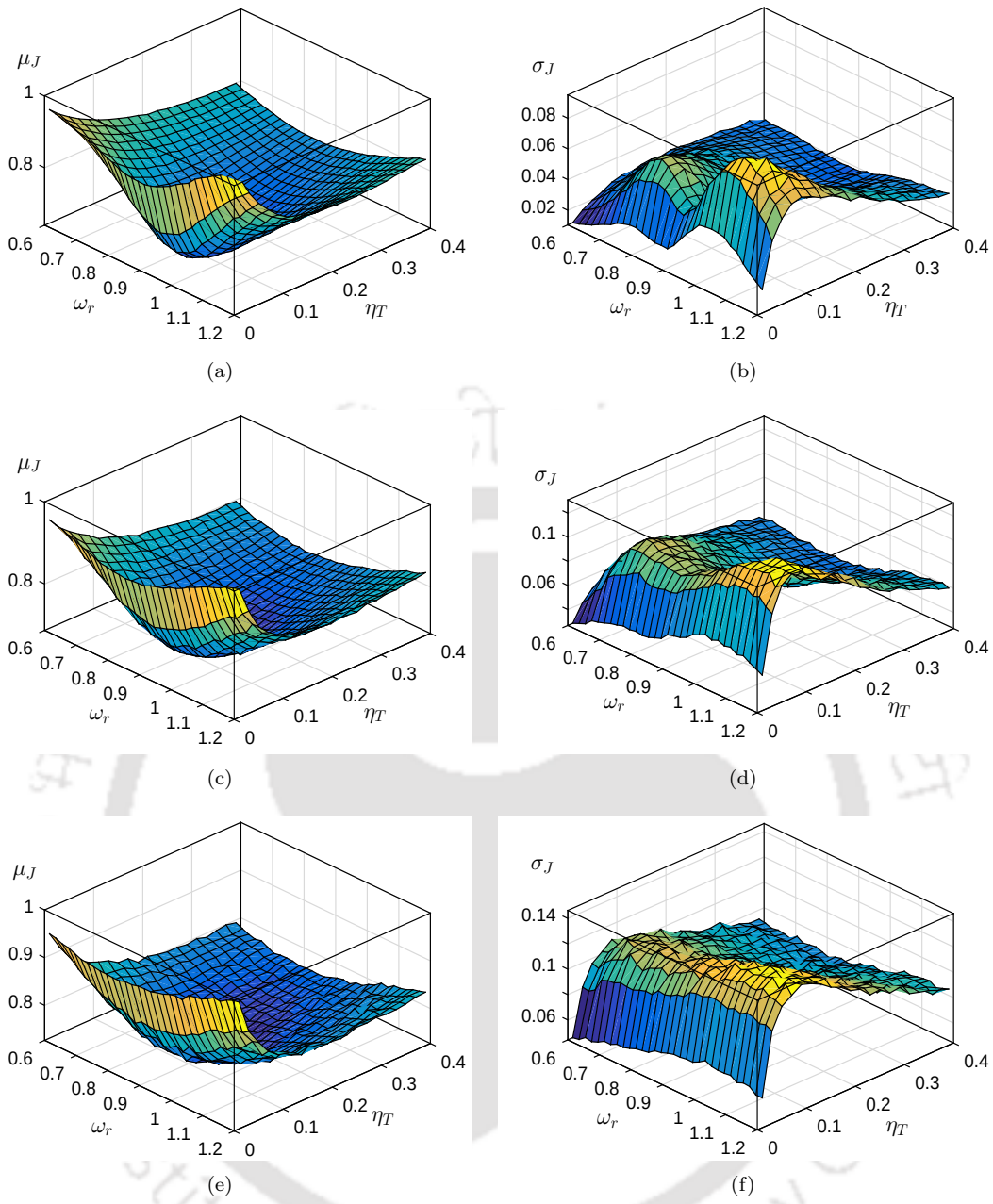

Figure 3.17: Mean and standard deviation of the TMD percentage reduction for mean of $\eta_S = 2\%$ with (a) & (b) cov = 10%, (c) & (d) cov = 20% and (e) & (f) cov = 30%

Eq. 3.15. For this purpose the values of $\mathbf{x}_r$ is fixed at their respective mean values and the only Stage-1 response surface is invoked. After this, *Design-2* for robust optimization of TMD parameters is carried out. Unlike conventional optimization, RDO uses the randomness associated with $\mathbf{x}_r$ as defined earlier by their respective *pdf*s and minimizes the mean of J to obtain optimal $\mathbf{x}_d$. Finally, constraint reliability based design of TMD parameters are carried out that employees the proposed two-step RSM using MLS based local approximations. For this purpose, the first two moments are obtained from Stage-2 response surfaces to satisfy the constraint condition. Fig. 3.18 and Fig. 3.19 show the optimal parameters (i.e. $\mathbf{x}_d = \{\omega_r \ \eta_D\}^\mathsf{T}$) obtained from the three different design models.

Optimized natural frequency ω_r decreases gently with the increase in mass ratio of TMD m_r for both conventional optimization as well as robust optimization. This is due to the increase in the mass of TMD which reduces the first natural frequency of the controlled system. However, increase in cov effects the optimized ω_r value as noticed in Fig. 3.18(e) and (f). It is due to the fact that uncertainty leads to higher σ_J and eventually, leads to the detuning of controller designed in a deterministic framework. In general,

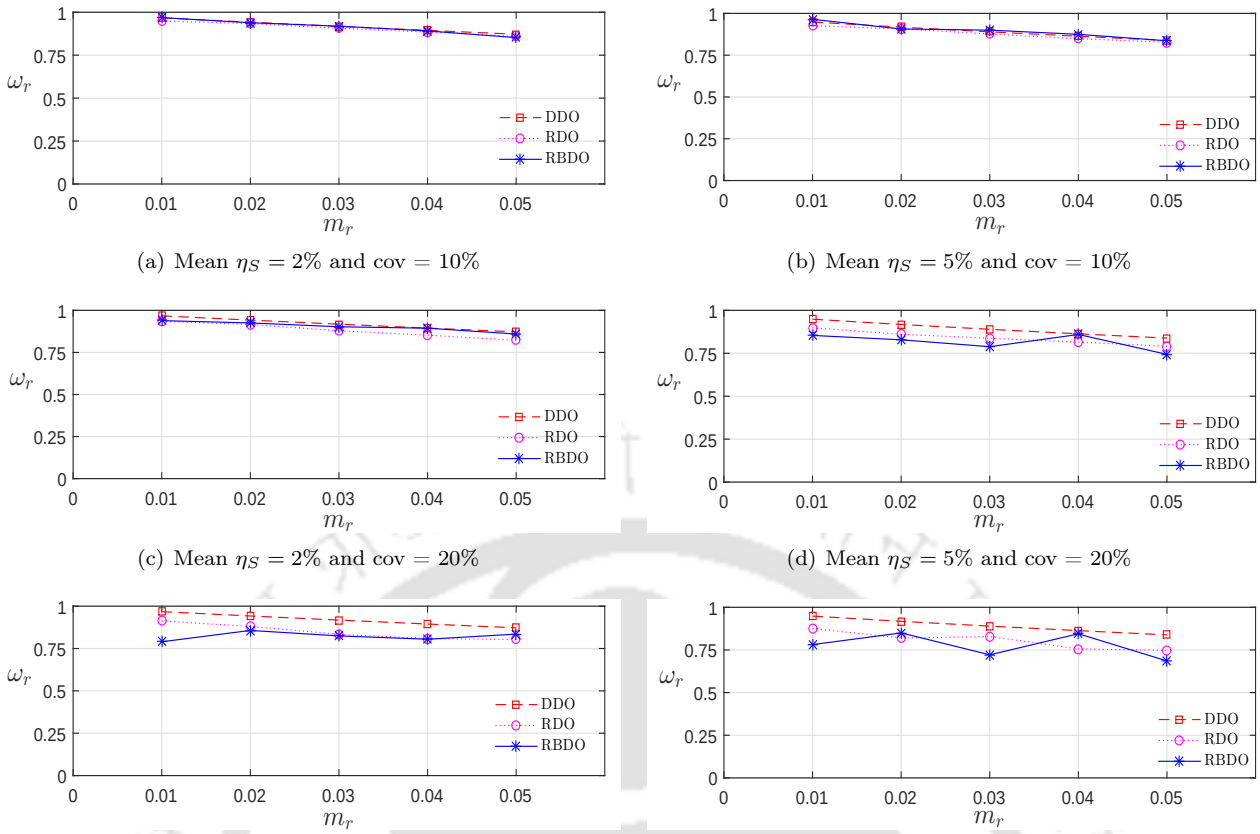

(a) Mean $\eta_S = 2\%$ and cov $= 10\%$

(b) Mean $\eta_S = 5\%$ and cov $= 10\%$

(c) Mean $\eta_S = 2\%$ and cov $= 20\%$

(d) Mean $\eta_S = 5\%$ and cov $= 20\%$

(e) Mean $\eta_S = 2\%$ and cov $= 30\%$

(f) Mean $\eta_S = 5\%$ and cov $= 30\%$

Figure 3.18: Optimized frequency ratio ω_r evaluated using different optimization frameworks for different levels of cov

conventional optimization usually results in values say $\omega_r \approx 1.0$ (i.e. resonance) whereas the reliability based optimization framework does not follow this monotonous trend (i.e. its optimized values are critically governed by the factors β_c, μ_J and σ_J). Conventional design shows nearly linear increase in the optimized η_T value following the mass ratio. Similar trend is followed for the RDO where the amount of damping of TMD increases with rise in uncertainty. Thus, the location of minimum mean is not exactly at the minima of J but slightly away towards the lower and upper bound of ω_r and η_T, respectively. Optimized η_T based on the proposed method results in a mixed behaviour due to the aforementioned reasons. Fig. 3.19 shows an acute demand of the optimized damping of TMD, generally, for higher uncertainties. This demand is due to nearly flat surface of J towards higher damping ratio of TMD which leads to a reduced effect of randomness on the performance of TMD. From the above discussion, particularly for low uncertainty, it can be concluded that conventional (i.e. *Design-1*), robust (i.e. *Design-2*) and reliability (i.e. *Design-3*) based optimizations give nearly same designs. However for the robust and reliability based designs, rise in the level of cov results the decrease in frequency ratio and increase in damping ratio of the controller from the deterministic optimized design values.

The overall performance in the random environment can be quantified on the basis of the statistical parameters. In this context, a detailed presentation of mean and standard deviation of J at the design points $\mathbf{x}_d^*$ (i.e. $\mu_{J(\mathbf{x}_d^*, \mathbf{x}_r)}$ and $\sigma_{J(\mathbf{x}_d^*, \mathbf{x}_r)}$) are shown in Fig. 3.20 and Fig. 3.21, respectively. Following the nature of the performance function, mean μ_J decreases with ascending mass of the TMD whereas it decreases with descending η_S. The mean from the conventional optimization, robust and reliability based designs (i.e. *Design-1*, *Design-2* and *Design-3*, respectively) observes comparatively little variation. Obviously, *Design-2* has the best value of μ_J among all and is generally followed by the mean evaluated from *Design-3*) and the conventional design. However, a few exceptions are noticed where the proposed method yield higher mean as compared to the conventional design. This is either caused the favourable attainment of desired reliability β_c or due to the unsmooth nature of mean (see Fig. 3.17) as a result of statistical estimation by generation of new set of random numbers in each time instant. In all the cases, standard deviation σ_J evaluated over

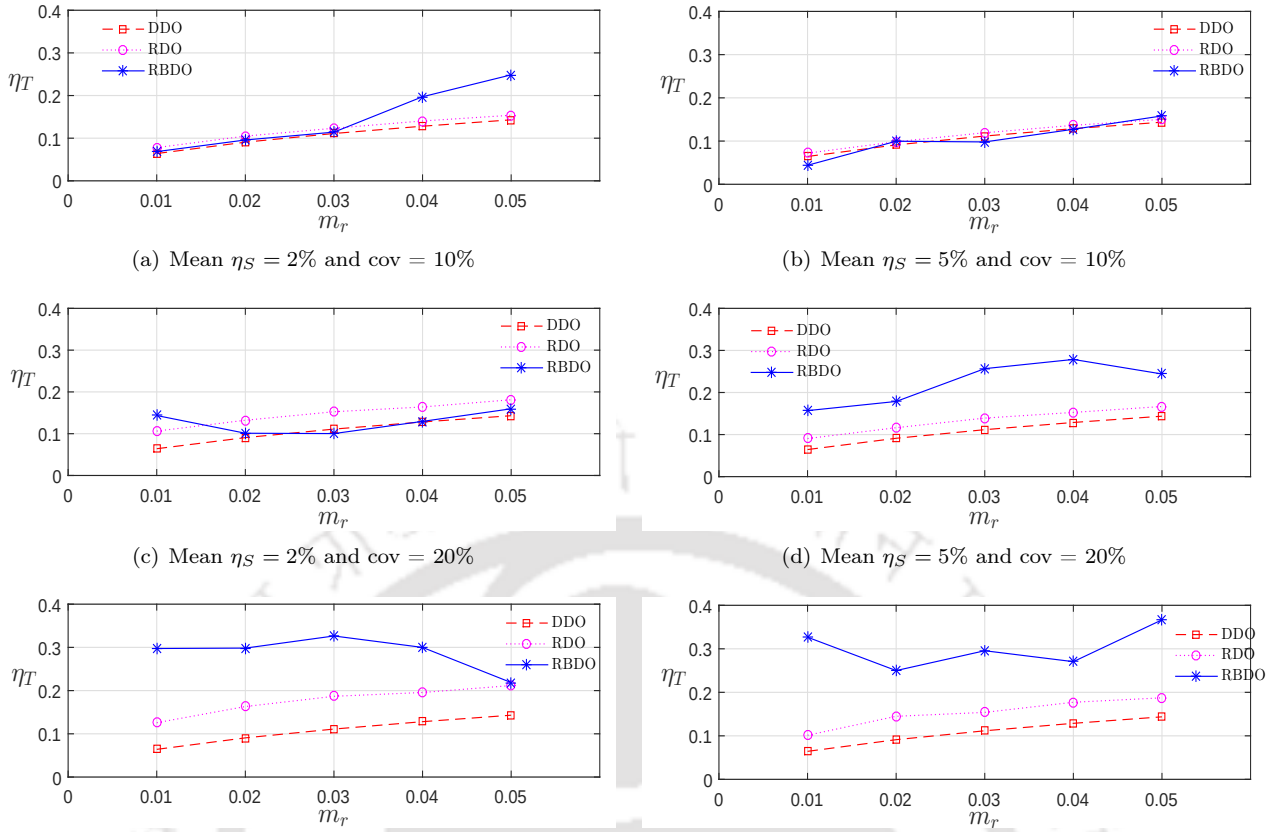

(a) Mean $\eta_S = 2\%$ and cov $= 10\%$

(b) Mean $\eta_S = 5\%$ and cov $= 10\%$

(c) Mean $\eta_S = 2\%$ and cov $= 20\%$

(d) Mean $\eta_S = 5\%$ and cov $= 20\%$

(e) Mean $\eta_S = 2\%$ and cov $= 30\%$

(f) Mean $\eta_S = 5\%$ and cov $= 30\%$

Figure 3.19: Effect of uncertainties on optimized damping ratio of TMD η_T evaluated using different optimization frameworks

the conventional optimum designs are highest. It is due to the presence of steep slope in the proximity of the optimized J affects the performance of controller under the system and loading uncertainties resulting in high variance. Fig. 3.21 shows a mixed trend of the standard deviation by conventional and robust design with respect to m_r due to the sensitivity of J with the random variables. Moreover, damping of the primary system helps to reduce the variation in the performance of TMD under uncertainty. Robust design based standard deviation exhibits better performance than conventional design but less than the proposed reliability based design. *Design-3* evaluates the $\mathbf{x}_d^*$ with low standard deviation for higher reliability. In contrast to DDO and RDO, the proposed reliability based framework includes the influence of the standard deviation in optimizing the design point. For cov of 20% and 30%, the standard deviation as per reliability based design show an increasing trend due to the decrease of mean at design point with respect to m_r when β_c is fixed at 4. This nature is opposite to other methods considered in this study. It can be explained as in case of cov $= 20\%$ and $\eta_S = 2\%$, the reliability as specified by the constraint (i.e. $\beta_c = 4$) is achieved by the conventional optimization as well as RDO for m_r over 2%. Hence, the σ_J from reliability based optimization starts following the trend of the robust and conventional design based standard deviations. This behaviour is also noticed for lower uncertainty where $\beta_c > 4$ for the conventional and robust designs (see Fig. 3.21).

Revisiting the above discussion and Fig. 3.17, a fairly conflicting nature of the mean and standard deviation of the performance of TMD can be inferred. For further understanding about these two parameters, multi-objective Non-dominated Sorting in Genetic Algorithm-II (NSGA-II) is invoked for Pareto optimization of μ_J and σ_J. It gives an optimal set of Pareto solutions for the two conflicting objective functions in Fig. 3.22 which are compared with the design points $\mathbf{x}_d^*$ from DDO, RDO and RBDO. Low uncertainties do not account for significant changes in the mean and standard deviation and thus, the design points lie on the Pareto front. Increase in cov to 20% and 30% shows the deviation of the conventional optimized design point from the optimal front. Still both the robust and reliability based optimized designs (i.e. $\mathbf{x}_d^*$ from *Design-2* and *Design-3*, respectively) remain on the Pareto front. RDO follows the apex point of the Pareto front as it reflects the best value of the mean. Whereas, RBDO shows a tradeoff in design location on the

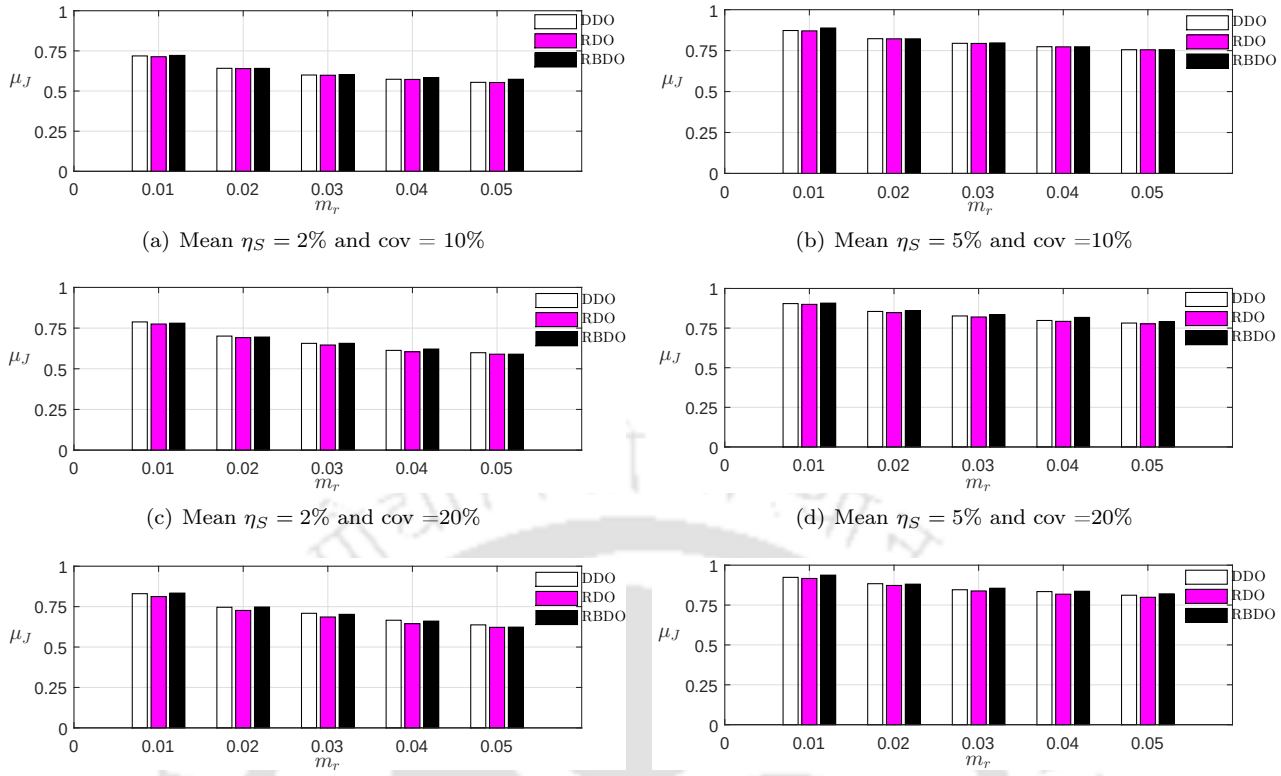

(a) Mean $\eta_S = 2\%$ and cov $= 10\%$

(b) Mean $\eta_S = 5\%$ and cov $=10\%$

(c) Mean $\eta_S = 2\%$ and cov $=20\%$

(d) Mean $\eta_S = 5\%$ and cov $=20\%$

(e) Mean $\eta_S = 2\%$ and cov $=30\%$

(f) Mean $\eta_S = 5\%$ and cov $=30\%$

Figure 3.20: Statistical estimation of mean of J with respect to different optimized design points for varying m_r and cov

Table 3.6: Reliability constraint β_c evaluated from optimized designs of the 3DOF-TMD system from different optimization frameworks

Mean η_S	cov	m_r	β_c		
			DDO	RDO	RBDO
2%	0.20	0.01	2.25	2.97	3.84
		0.02	3.18	3.87	3.98
	0.30	0.01	1.51	1.94	2.90
		0.02	1.99	2.61	3.75
		0.03	2.23	2.92	3.87
		0.04	2.66	3.37	4.03
		0.05	2.86	3.49	4.12
5%	0.20	0.01	1.95	2.40	3.14
		0.02	2.46	2.81	3.40
		0.03	2.76	3.02	3.70
		0.04	3.00	3.33	3.57
		0.05	3.26	3.41	3.61
	0.30	0.01	1.24	1.45	2.26
		0.02	1.35	1.78	2.30
		0.03	1.59	1.83	2.26
		0.04	1.65	2.01	2.26
		0.05	1.79	2.14	2.35

Pareto front to compensate the reliability constraint. Minor offsetting of design associated to the proposed method in Fig. 3.22 is due to unsmooth nature of mean and standard deviation and estimation error in the

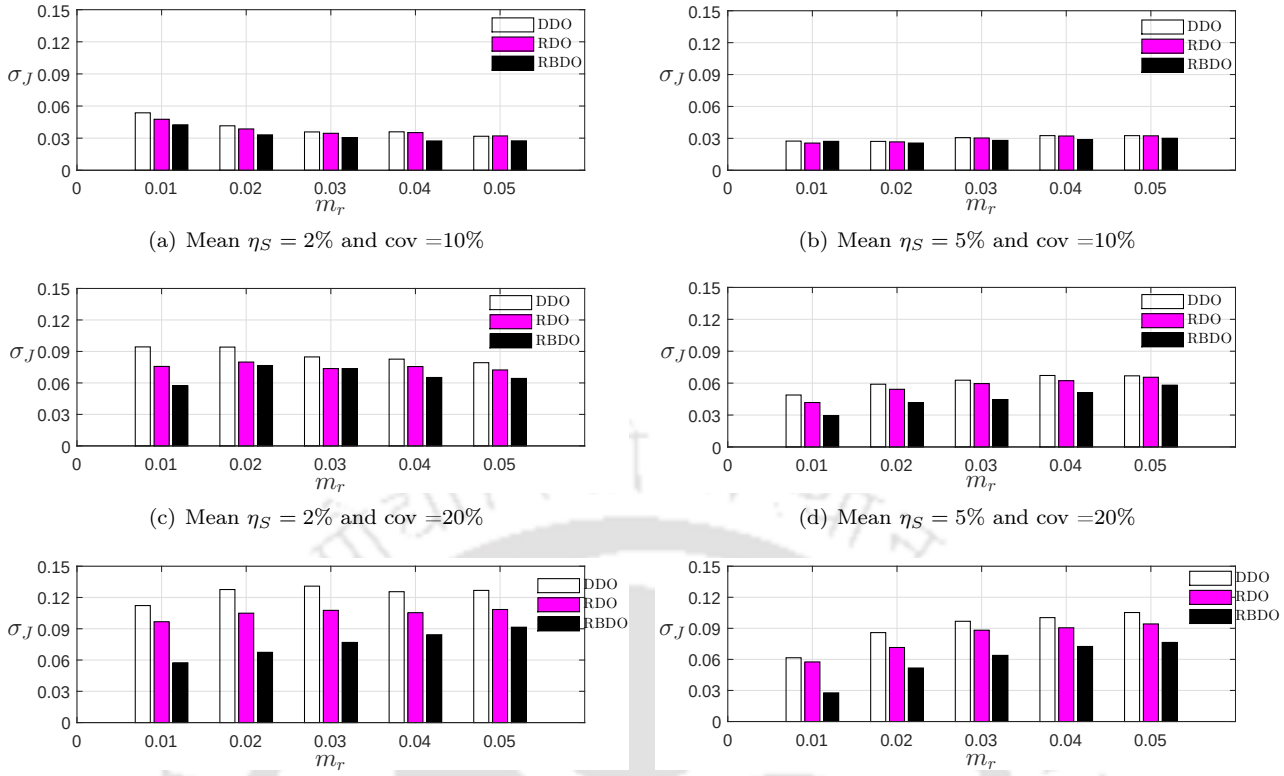

(a) Mean $\eta_S = 2\%$ and cov $=10\%$

(b) Mean $\eta_S = 5\%$ and cov $=10\%$

(c) Mean $\eta_S = 2\%$ and cov $=20\%$

(d) Mean $\eta_S = 5\%$ and cov $=20\%$

(e) Mean $\eta_S = 2\%$ and cov $=30\%$

(f) Mean $\eta_S = 5\%$ and cov $=30\%$

Figure 3.21: Standard deviation of TMD performance at optimized design locations

meta-models. It can be concluded that the robust and reliability based designs of TMD are the elements of the Pareto front.

In this context, the prime concern of this study is to improve the reliability of the TMD. Improvement is intended by means of constraint optimization. Basically, it selects the design points with marginal deviation of mean value. This is achieved by a tradeoff between the statistical moments (i.e. μ_J and σ_J). Fig. 3.23 shows the probability density function $f_J(j)$ of J at $\mathbf{x}_d^*$ from different optimizations included in this study, where low level of uncertainty experiences trivial change in the distribution. For cov of 30%, a clear deviation is witnessed in Fig. 3.23 as compared to other designs.

Constraint β_c evaluated from DDO and RDO are compared with RBD and are listed in Table 3.6. Reliability levels are improved with increasing mass of the TMD for DDO and RDO which are reflected in the increase of β_c value. Although the variance of the performance function is low for higher η_S, but the controller has lower reliability. This is due to higher mean value at $\eta_S = 5\%$ as compared to 2%. The listed data shows the conclusive proof where RBDO shows an average 51% improvement in β_c as compared to 21% from RDO. Even with respect to the RDO based β_c, the proposed design accounts for an average appreciation of 24%. Maximum improvement of β_c in RBDO is 91% whereas the *Design-2* has witnessed 32% from the conventional design. Hence, the obtained results clearly justify the merit of the proposed approach for reliability based design where the systems are subjected to contradicting objectives. In this context, the meta-modelling technique helps in providing accurate design and reducing the associated computational burden attached with the RBDO process.

3.5 Summary

A new reliability based design optimization using meta-modelling technique is presented in this chapter. For this purpose, a two-step response surface based algorithm is proposed. TMD operating in uncertain environment is considered for numerical validation with three different optimization schemes (*viz.* DDO,

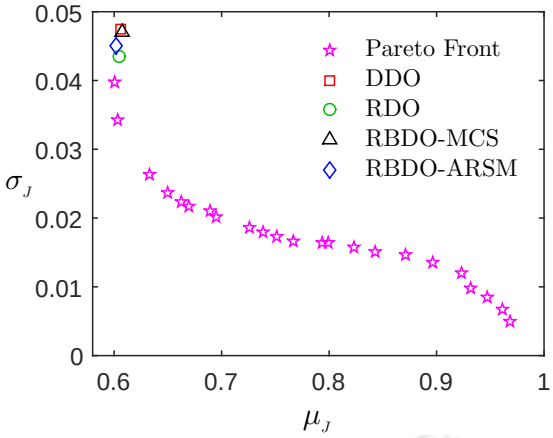

(a) Mean $\eta_S = 2\%$ and cov $= 10\%$

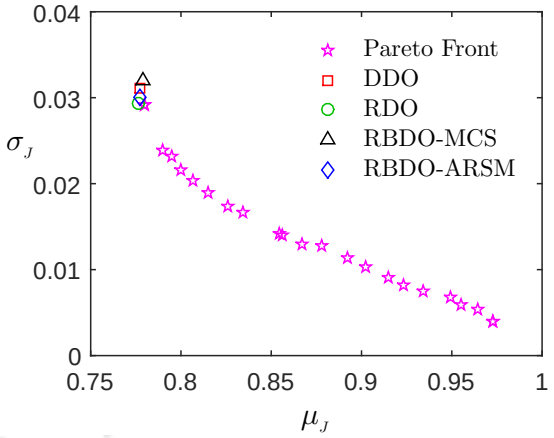

(b) Mean $\eta_S = 5\%$ and cov $= 10\%$

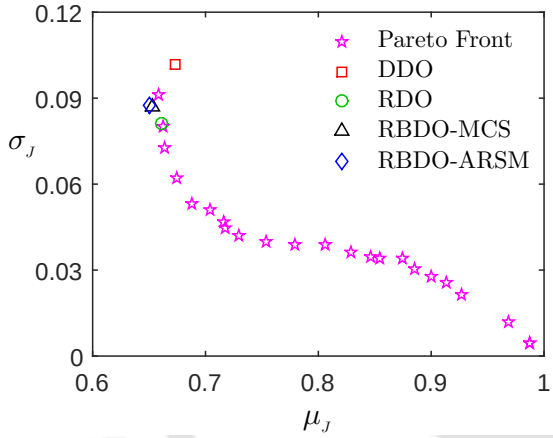

(a) Mean $\eta_S = 2\%$ and cov $= 20\%$

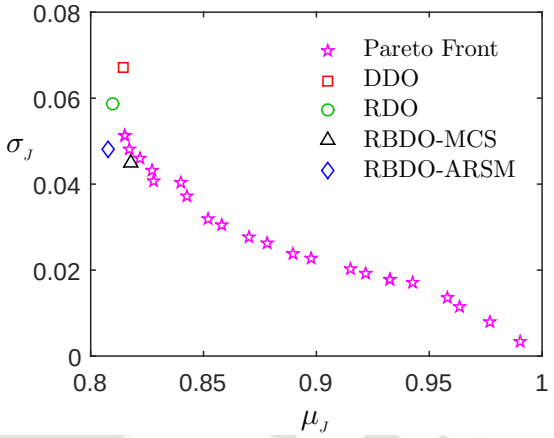

(b) Mean $\eta_S = 5\%$ and cov $= 20\%$

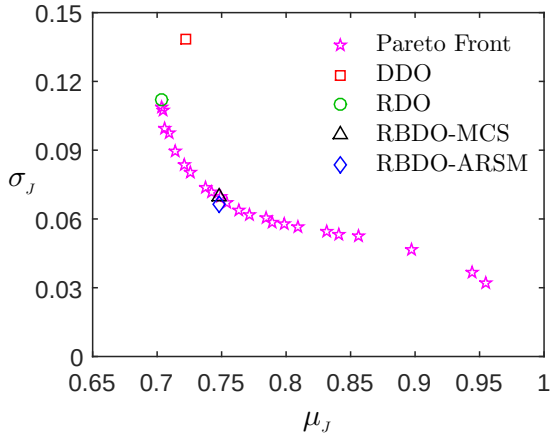

(a) Mean $\eta_S = 2\%$ and cov $= 30\%$

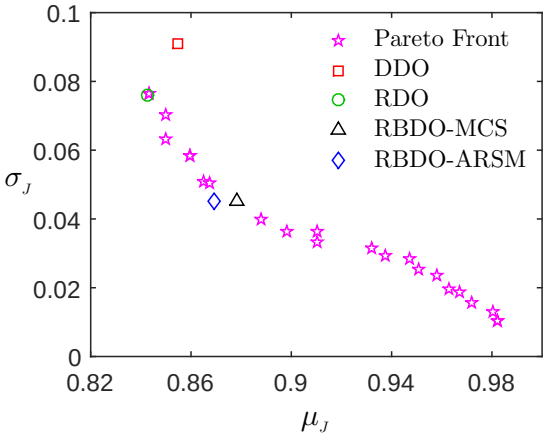

(b) Mean $\eta_S = 5\%$ and cov $= 30\%$

Figure 3.22: Pareto front of multi-objective (*viz.*, mean and standard deviation of performance function J) optimization corresponding to three covs

RDO and RBDO) to show the efficiency of the proposed meta-model based algorithm. The first two moments (i.e. mean and variance) of the response are used to evaluate the reliability of the controller. These moments are estimated using MCS on the meta-models that bypasses time exhaustive solution of the original system equations. For better fitting of the response surface, regularized weights are used in MLS scheme and the constrained conditions are developed in such a way that they ensure the desired level of reliability when operating in the random environment. The performance with DDO, RDO and RBDO are comprehensively studied and the optimal design points are evaluated that enhances the overall reliability of the passive

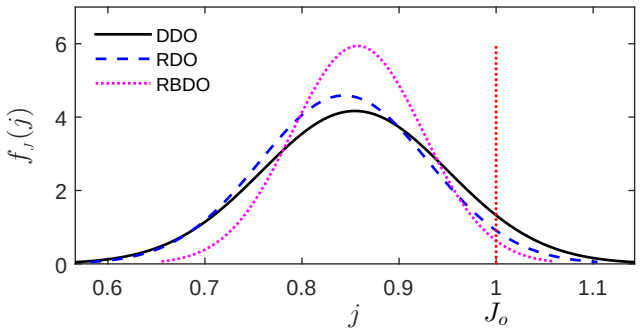

Figure 3.23: Probability density function of J by different optimization frameworks

controller. Moreover, behaviour of design parameters and different level of uncertainties are studied. The major conclusions from this numerical study are as follows

- Use of MLS based RSM for optimization and estimate of statistical moments help in bypassing multiple solutions of the performance function required for the simulation. Thus, inclusion of the proposed meta-model approach assists in application of time consuming uncertainty quantification required in stochastic design optimization. The present proposal is generic which can be applied for problems with correlated non-normal random variables.
- Mean and standard deviation of the controller performance function have a conflicting nature on the global minima in RDO. In this context, the proposed two-step RSM based optimization helps to reduce the standard deviation which, in turn, improves the robustness of the controller.
- For problems with conflicting performance functions e.g. mean and standard deviation of TMD, Pareto front gives various design points as in the front set. Robust design strategy focused on mean minimization ends at the tail of this design set which suffers large variance. This issue escalates with the increase in the level of uncertainties. To address it, the proposed method employs a reliability based objective which selects the best design from the front set as per the designer's requirement.
- Variation due to uncertainty in the system parameters show a significant change in natural frequency and transfer function of the controller system. It adversely affects the performance of TMD designed by deterministic approach. Whereas, the proposed optimal design of TMD performs better as it ensures reliability of the device operating in the random environment.

Moreover, it can be noted that application of regular polynomials often suffers ill-conditioning while performing the matrix inversion [160]. The issue is severe when the basis matrix size is large due to a large dimensional problem. Hence, as a remedy, orthogonal polynomials can be applied which is discussed in the next chapter.

Chapter 4

Stochastic Response Surface Method

4.1 Introduction

The aforementioned formulation of ordinary polynomial based response surface is extended in this chapter to avoid ill-conditioning, if any. Orthogonal polynomial scheme is employed to condition the basis matrix used in the meta-model. Moreover, the curse of dimensionality associated with the previously discussed DoE schemes is also addressed here. A hierarchial support point generation scheme is adopted to enhance the efficiency of the meta-modelling technique. Using this technique, a new sequential sparse grid scheme is proposed based on the optimization which is performed on the response surface in every iteration. The formulation of the proposed approach is logically developed as stated in the following sections.

4.2 Stochastic Response Surface Methodology

In Stochastic Response Surface Method (SRSM), the original performance function $g(\bullet)$ is replaced by the summation of orthogonal polynomials described in terms of the random variables. It utilizes the polynomial chaos expansion which is defined by the nonlinear functional of arguments $\mathbf{z}$ that is convergent in mean-square sense [161]

$$g(\mathbf{z}) = \alpha_0\Gamma_0 + \sum_{i_1=1}^{\infty}\alpha_{i_1}\Gamma_1(z_{i_1}) + \sum_{i_1=1}^{\infty}\sum_{i_2=1}^{i_1}\alpha_{i_1i_2}\Gamma_2(z_{i_1}, z_{i_2}) + \cdots \tag{4.1}$$

In the above equation, Γ_p is the polynomial chaos expression of the random variables $\mathbf{z} = \{z_{i_1}\, z_{i_2}\, \cdots\, z_{i_p}\}$ with degree p and are associated with the unknown coefficients $\alpha_0, \alpha_{i_1}, \alpha_{i_1i_2}, \ldots, \alpha_{i_1i_2\ldots i_p}$. On truncating the PCE till p^{th} degree for practicality, provides the approximate representation of the original performance function as follows [13]

$$g(\mathbf{z}) \approx\ \alpha_0 + \sum_{i_1=1}^{n}\alpha_{i_1}\Gamma_1(z_{i_1}) + \sum_{i_1=1}^{n}\sum_{i_2=1}^{i_1}\alpha_{i_1i_2}\Gamma_2(z_{i_1}, z_{i_2}) + \ldots + \sum_{i_1=1}^{n}\sum_{i_2=1}^{i_1}\cdots\sum_{i_p=1}^{i_{p-1}}\alpha_{i_1i_2\ldots i_p}\Gamma_p(z_{i_1}, z_{i_2}, \ldots, z_{i_p}) \tag{4.2}$$

Rewriting Eq. 4.2 in the compact form gives

$$g(\mathbf{z}) \approx \sum_{i=0}^{p}\acute{\alpha}_i\mathbf{\Gamma}_i(\mathbf{z}) = \mathbf{\Xi}(\mathbf{z})\mathbf{b} \tag{4.3}$$

where, $\mathbf{\Gamma}_i(\mathbf{z})$ is a set of orthogonal polynomials defined using random variables $\mathbf{z}$ such that $\mathbf{\Gamma}_0 = 1$, $\mathbb{E}[\mathbf{\Gamma}_i] = 0$ and $\mathbb{E}[\mathbf{\Gamma}_i\mathbf{\Gamma}_j] = 0$, $\forall\, i \neq j$. Also in the above equation, $\acute{\alpha}_i \in \mathbf{b} = \{\alpha_0\, \alpha_1\, \ldots\, \alpha_n\, \alpha_{11}\, \alpha_{21}\, \ldots\, \alpha_{nn\ldots n}\}^{\mathsf{T}}$ represents

Table 4.1: Commonly used different orthogonal polynomials and the associated weight functions $W_P(\bullet)$ to develop them using Gram-Schmidt orthogonalization

Polynomial name	$W_P(x)$	Support range	*pdf*
Legendre	1	$(-1, +1)$	Uniform
Chebyshev	$(1-x^2)^{\pm 1/2}$	$[-1, +1]$	Uniform
Jacobi	$(1-x)^{a_1}(1+x)^{a_2}, \quad \forall\, a_i > -1$	$[-1, +1]$	Beta
Laguerre	$\exp(-x)$	$[0, +\infty)$	Gamma
Hermite	$\exp(-x^2)$	$(-\infty, +\infty)$	Gaussian

the unknown coefficients associated with the basis $\mathbf{\Gamma}_i \in \mathbf{\Xi}(\mathbf{z})$.

Different basis functions are used in the literature which are determined using Gram-Schmidt orthogonalization [160]. It usually considers the polynomial expansion of the form $\Gamma_p(z) = a'_{p,0} f_0(z) + a'_{p,1} f_1(z) + \cdots + a'_{p,p-1} f_{p-1}(z) + z^p$, where the coefficients $a'_{p,i}$ are determined by

$$a'_{p,i} = \frac{\int_{a_l}^{a_u} W_P(z) z^p f_i(z)\, \mathrm{d}z}{\int_{a_l}^{a_u} W_P(z) f_i^2(z)\, \mathrm{d}z}, \qquad i = 0,\, 1,\, 2,\, \ldots,\, p-1 \tag{4.4}$$

using the weighted least square minimization and the basis term f_i represents a polynomial function of degree i. The above expression is derived assuming the orthogonality between the different bases i.e. $\int_{a_l}^{a_u} W_P(z) f_{i_1}(z) f_{i_2}(z)\, \mathrm{d}z = 0,\ \forall\ i_1 \neq i_2$, here, a_l and a_u represent the lower and upper bounds of the support range. A few of the orthogonal polynomials proposed in the literature (e.g. Legendre, Laguerre, Hermite, Chebyshev) [52,58] for different applications are given in Table 4.1. Among them, Hermite polynomial scheme is popular in reliability analysis and stochastic finite element modelling. In this study, Hermite polynomial is used by adopting the weight function W_P as shown in the Table 4.1. On simplifying the above expression, the basis function of Hermite polynomial takes the following form

$$\Gamma_p(z_{i_1}, z_{i_2}, \ldots, z_{i_p}) = \exp\left(\frac{1}{2}\mathbf{z}\mathbf{z}^{\mathsf{T}}\right)(-1)^p \frac{\partial^p \exp\left(-\frac{1}{2}\mathbf{z}\mathbf{z}^{\mathsf{T}}\right)}{\partial z_{i_1} \partial z_{i_2} \ldots \partial z_{i_p}} \tag{4.5}$$

This polynomial type is considered due to the fact that it is analogous to the Gaussian density function with the range from $-\infty$ to $+\infty$. Thus, it helps in directly transforming the limit state to the standard normal space which eases the reliability analysis. Fig. 4.1 shows different polynomial bases formed using the above expression for a uni-dimensional case. Using Eq. 4.5 in Eq. 4.3, the number of unknown coefficients n_b can be calculated for the polynomial degree p and the number of random variables n as

$$\begin{aligned} n_b &= 1 + \frac{n!}{(n-1)!\,1!} + \frac{(n+1)!}{(n-1)!\,2!} + \ldots + \frac{(n-1+p)!}{(n-1)!\,p!} \\ &= \frac{(n+p)!}{n!\,p!} \end{aligned} \tag{4.6}$$

Generally, these unknown coefficients are determined using collocation or regression technique. Thus, a total of $\frac{(n+p)!}{n!\,p!}$ coefficients need to be determined which, in turn, demands to develop same number of simultaneous equations [13]. In this study, MLS technique is adopted which has weight functions that decays with the Euclidian distance between the support points. Once the stochastic meta-model is constructed, it can be used to determine the uncertainty propagation from the input to the output and structural reliability.

4.3 MLS based SRSM

The unknown coefficients are determined using regression analysis [13] in this study. However, instead of single global meta-model, MLS technique is adopted similar to its application in the ARSM. This helps to incorporate the local changes which are often neglected owing to large modelling error. Thus, local variations are addressed by the MLS based regression in the SRSM framework. Following Eq. 2.8 to evaluate the second

norm of the error associated with the SRSM based approximation yields

$$\begin{aligned}\varepsilon(\mathbf{b},\mathbf{z}) &= \sum_{i=1}^{n_s} w(\delta_{\mathbf{z}_i})[\Xi_i(\mathbf{z})\mathbf{b} - g(\mathbf{z}_i)]^2 \\ &= [\boldsymbol{\Xi}(\mathbf{z})\mathbf{b} - \mathbf{g}(\mathbf{z})]^{\mathsf{T}} W(\mathbf{z})[\boldsymbol{\Xi}(\mathbf{z})\mathbf{b} - \mathbf{g}(\mathbf{z})] \end{aligned} \tag{4.7}$$

where,

$$W(\mathbf{z}) = \mathrm{diag}[w(\delta_{\mathbf{z}_1}), w(\delta_{\mathbf{z}_2}), \ldots, w(\delta_{\mathbf{z}_{n_s}})] \tag{4.8}$$

is the weight matrix. Using this modified regression technique, the unknown coefficients $\mathbf{b}$ can be expressed as follows

$$\mathbf{b}(\mathbf{z}) = \left[\boldsymbol{\Xi}^{\mathsf{T}}\, W(\mathbf{z})\, \boldsymbol{\Xi}\right]^{-1} \left[\boldsymbol{\Xi}^{\mathsf{T}}\, W(\mathbf{z})\right] \mathbf{g} \tag{4.9}$$

Here, each row of the matrix $\boldsymbol{\Xi}$ represents the polynomial basis corresponding to the location of the support points. Thus, the unknown coefficients vector $\mathbf{b}$ depends on $\mathbf{z}$ in the MLS formulation due to its moving character. The matrix $W(\mathbf{z})$ in the above equation consists of elemental weight function w which is given by the Eq. 2.13. This evolving character of MLS modifies Eq. 4.2 where the coefficients are evaluated separately at each realization. Thus, making the approximation adaptive to the local variation which is as follows

$$\begin{aligned} g(\mathbf{z}) \approx\ & \alpha_0(\mathbf{z}) + \sum_{i_1=1}^{n} \alpha_{i_1}(\mathbf{z})\Gamma_1(z_{i_1}) + \sum_{i_1=1}^{n}\sum_{i_2=1}^{i_1} \alpha_{i_1 i_2}(\mathbf{z})\Gamma_2(z_{i_1}, z_{i_2}) \\ & + \ldots + \sum_{i_1=1}^{n}\sum_{i_2=1}^{i_1}\cdots\sum_{i_p=1}^{i_{p-1}} \alpha_{i_1 i_2 \ldots i_p}(\mathbf{z})\Gamma_p(z_{i_1}, z_{i_2}, \ldots, z_{i_p}) \end{aligned} \tag{4.10}$$

and rewriting the above expression in the matrix form, one gets

$$g(\mathbf{z}) \approx \sum_{i=0}^{p} \acute{\alpha}_i(\mathbf{z})\boldsymbol{\Gamma}_i(\mathbf{z}) = \boldsymbol{\Xi}(\mathbf{z})\mathbf{b}(\mathbf{z}) \tag{4.11}$$

where, $\boldsymbol{\Xi}(\mathbf{z})$ consists of the Hermite polynomial basis of degree $\leq p$. Although, this evolving regression technique improves the performance of the meta-model significantly, it still suffers computational challenges for large dimensional problems with multiple optima. Besides this, computational cost for the large dimensions has remained a major challenge to the designers. Thus, there is a constant demand for a more efficient technique for reliability estimation that involves less function evaluations and subsequent computational cost without compromising with the quality of the end results. With this in view, present study aims to demonstrate sequential development of the stochastic response surface where the support points are generated using an efficient sparse grid technique.

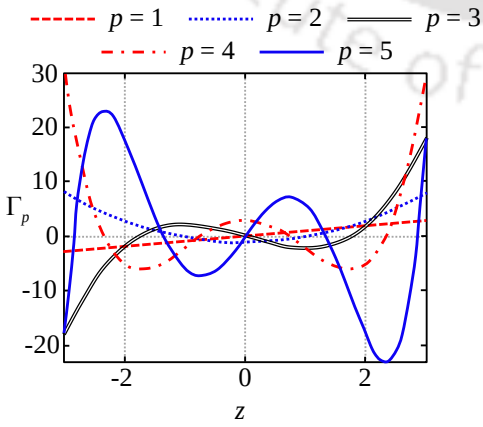

p	$\Gamma_p(z)$
0	1
1	z
2	$z^2 - 1$
3	$z^3 - 3z$
4	$z^4 - 6z^2 + 3$
5	$z^5 - 10z^3 + 15z$

Figure 4.1: A representation of different degrees of polynomial basis based on the Hermite scheme for univariate expansion

4.4 Sequential SRSM with Sparse Grid Scheme

The details of the proposed sequential SRSM using MLS based PCE in a sparse grid framework is presented below.

4.4.1 Sequential SRSM

It may be noted from Eq. 4.2 that stochastic response surface is constructed by Hermite polynomials with unknown coefficients which are evaluated using support points generated by different techniques namely - collocation method, Latin hypercube design, monomial cubature rule among many others [162]. Location of these points are fixed prior to the determination of the coefficients to construct the polynomial basis matrix $\boldsymbol{\Xi}$. Hence, the number of support points n_s should be at least equal to the number of unknown coefficient (i.e. n_b). Thus, the support points generation may be dense or sparse depending on the number of random variables n and the degree of the polynomial p. However, as the support points are denser, computational cost rises making SRSM less effective. On the other hand, more support points in the vicinity of the limit state [i.e. $g(\mathbf{x}) = 0$] help to achieve better accuracy to estimate the probability of failure [163]. Therefore, customizing the number of support points n_s in a single iteration becomes a difficult task. To overcome this problem, the present study uses an iterative scheme where the support points are generated only in the region where it is required. This is done by optimizing the Gaussian space of the approximated surface to find out the most probable failure point (or design point) as

$$\begin{aligned} &\text{Find :} && \mathbf{z} \\ &\text{Minimize :} && |\mathbf{z}|_2 \\ &\text{Subjected to :} && \tilde{g}(\mathbf{z}) = 0 \end{aligned} \tag{4.12}$$

Above optimization is executed over the approximated surface [i.e. $\tilde{g}(\bullet)$] which imposes no restriction on the choice of the optimization tool. Hence, different searching tools like gradient based methods or population based algorithms can be adopted to perform this task. The accuracy of the optimization largely depends on the accuracy of the meta-modelling. Although, the accuracy of the meta-model increases with number of support points, a tradeoff between the number of points and modelling error is adopted to optimize the computational cost. In this study, sequential quadratic programming (SQP) routine inbuilt in MATLAB® [96] is used to solve Eq. 4.12 to evaluate the design point $\mathbf{z}^*$ in the Gaussian space.

From the above discussion, it is evident that the ideal condition requires more points in the failure region and less elsewhere. This, in turn, improves the efficiency of the reliability method by limiting the number of function calls in order to reduce the cost of computation. To explain this phenomenon, Fig. 4.2 demonstrates the points generated by the full grid formation using collocation method. These points almost uniformly cover the domain as the degree of PCE increases [162]. This might lead to inclusion of points that are insignificant for the estimation of the probability of failure and lead to excessive computational burden.

Thus, to minimize the function calls (i.e. the number of support points), the proposed method progressively generate the surface that is initiated at a predefined point. Without loss of generality, this initial design point is considered to be the mean values of the random variables (i.e. $\mu_{\mathbf{x}}$). The support points are located around this design point, preferably with the extent to incorporate the failure region (i.e. $g(\mathbf{x}) \leq 0$). PCE is constructed using Eq. 4.2 of degree p for n random variables. In this context, the number of support points must be greater than or equal to n_b for solving the PCE based approximation by MLS technique as explained in Eq. 2.10. This localized least square whose coefficients change from one point to another helps to map the original surface better as opposed to its traditional counterpart (i.e. least square). Hence, less support points are required as the number of unknown coefficients n_b are reduced due to lower degree PCE than conventional SRSM. After constructing the approximate surface $\tilde{g}(\mathbf{x})$, constrained optimization problem in Eq. 4.12 is solved to identify the failure region and the corresponding new optima. The new deign point is further used to generate more support points as explained earlier. In order to generate more support points near the limit state [i.e. $\tilde{g}(\mathbf{x}) = 0$], the spatial extent of the support points in every iteration it is reduced by factor $\lambda_{it}^{\mathbf{x}}$ (< 1.0). The value of this reduction factor depends on the convergence and the accuracy to be

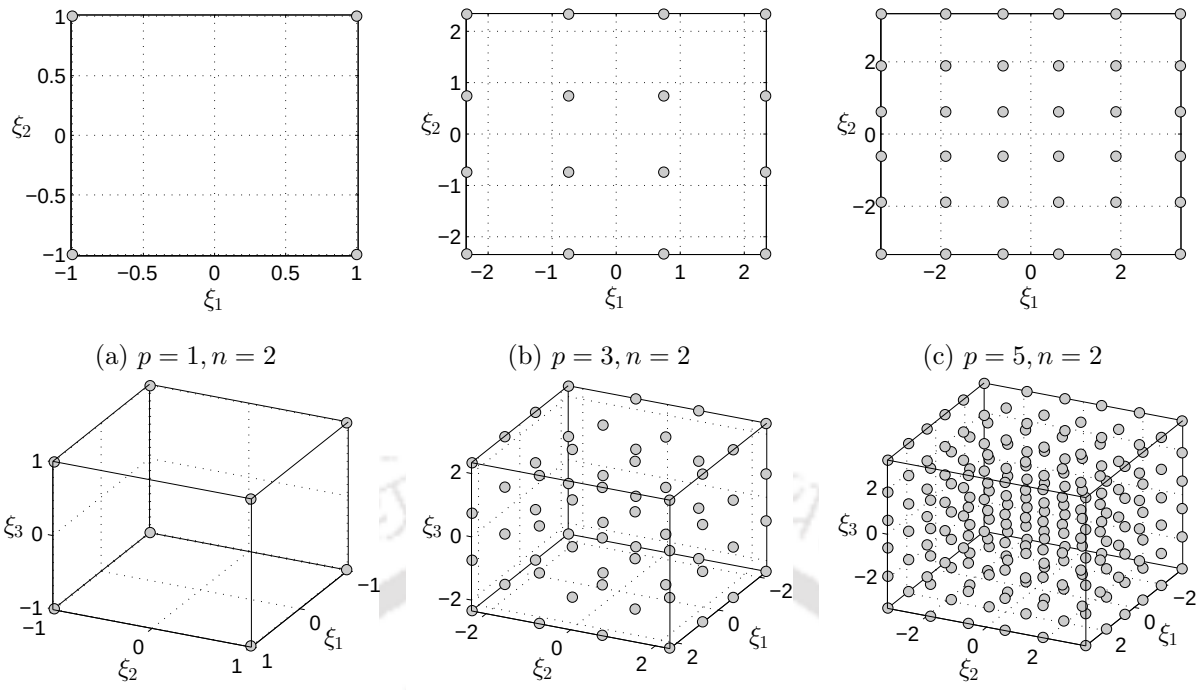

(a) $p = 1, n = 2$ (b) $p = 3, n = 2$ (c) $p = 5, n = 2$

(d) $p = 1, n = 3$ (e) $p = 3, n = 3$ (f) $p = 5, n = 3$

Figure 4.2: Collocation points with different degrees and dimensions

attained. After every iteration, convergence of the solution is checked by

$$|\tilde{g}(\mathbf{x}^{*,it-1}) - \tilde{g}(\mathbf{x}^{*,it})| \leq \breve{e}_1 \tag{4.13}$$

$$|\mathbf{x}^{*,it-1} - \mathbf{x}^{*,it}| \leq \breve{e}_2 \tag{4.14}$$

where, $\breve{e}_1$ and $\breve{e}_2$ are the permissible errors, typically in the range of 10^{-2} to 10^{-3}.

Following the convergence, original limit state is checked for multiple failure points or regions. This is performed by introducing penalty function or bulge $\breve{g}$ over the approximate surface $\tilde{g}$ which modifies the stochastic response surface as [164]

$$\tilde{g}_m(\mathbf{z}) = \tilde{g}(\mathbf{z}) + \sum_{i=1}^{n_p} \breve{g}_i(\mathbf{z}) \tag{4.15}$$

In the above equation, n_p denotes the number of most probable failure points and the penalty function $\breve{g}$ is given by [164]

$$\breve{g}_i(\mathbf{z}) = \begin{cases} \frac{\varrho|\mathbf{z}^{*,i}|_2 \cdot |\nabla\tilde{g}(\mathbf{z}^{*,i})|_2 \cdot (r_i^2 - |\mathbf{z}-\mathbf{z}^{*,i}|_2^2)^2}{[(\gamma_p|\mathbf{z}^{*,i}|_2)^2 - (\varrho|\mathbf{z}^{*,i}|_2)^2]^2} & \text{if } |\mathbf{z}-\mathbf{z}^{*,i}|_2 \leq r_i \\ 0 & \text{elsewhere} \end{cases} \tag{4.16}$$

at the failure location. The parameter ϱ in Eq. 4.16 is assumed to be 0.75 and influence radius of the bulge r_i is estimated by $\gamma_p|\mathbf{z}^{*,i}|_2$. Two stopping criteria for this problem are devised as follows

$$\cos^{-1}\left[\frac{\mathbf{z}^{*,i+1}.\mathbf{z}^{*,i}}{|\mathbf{z}^{*,i+1}|_2|\mathbf{z}^{*,i}|_2}\right] \leq \theta_p \tag{4.17}$$

$$|\mathbf{z}^{*,i+1} - \mathbf{z}^{*,i}|_2 \leq |\mathbf{z}^{*,i}|_2 \tag{4.18}$$

to identify new failure point(s), if any, where the half-angle θ_p is formed hypothetical between the foot of bulge and the failure point. As suggested by Der Kiureghian and Dakessian [164], $\theta_p = 66°$ and $\gamma_p = 1.10$ are considered in the present study. Once the convergence is achieved as per Eqs. 4.13, 4.14, 4.17 and 4.18, reliability is estimated using importance sampling technique.

4.4.2 Sparse Grid Scheme

It may ne noted that non-intrusive formulation requires training of meta-model through support points evaluated over the predefined locations in the design space. Number of these support points primarily dictate the computational viability of the meta-model in terms of accuracy and cost. This requires a tradeoff between the permissible error and the computational effort. Therefore, an efficient but sparse formulation of the support points is employed in this study using Smolyak's algorithm [165]. It considers an interpolation using quadrature rule of the form

$$\mathscr{U}^i(g) = \sum_{j=1}^{n_{s,i}} \breve{w}_i^{(i,j)} . g(x_i^{(i,j)}) \tag{4.19}$$

for univariate case which is extended to multi-dimensional interpolation as

$$\begin{aligned}(\mathscr{U}^{i_1} \otimes \mathscr{U}^{i_2} \otimes \cdots \otimes \mathscr{U}^{i_n})(g) &= \sum_{j_1=1}^{n_{s,1}} \sum_{j_2=1}^{n_{s,2}} \cdots \sum_{j_n=1}^{n_{s,n}} (\breve{w}_1^{(i_1,j_1)} \otimes \breve{w}_2^{(i_2,j_2)} \otimes \cdots \otimes \breve{w}_n^{(i_n,j_n)}) . g(x_1^{(i_1,j_1)}, x_2^{(i_2,j_2)}, \ldots, x_n^{(i_n,j_n)}) \\ &= \sum_{\mathbf{j}} \breve{\mathbf{w}}_{\mathbf{n}}^{(\mathbf{i},\mathbf{j})} g(\mathbf{x}_{\mathbf{n}}^{(\mathbf{i},\mathbf{j})}) \end{aligned} \tag{4.20}$$

In the above equation, $i \in \mathbb{N}$ represents interpolant index, $n_{s,i}$ is the number of grid points for a given random variable x_k and the coefficient $\breve{w}_k^{(i,j)} \equiv \breve{w}_k^{(i,j)}(x_k^{(i,l)}) = \delta_{jl}$ with $l \in [1\ n_{s,i}]$. The full-grid interpolation may require exhaustive computational effort which is reduced by curtailing the sub-grids using Smolyak's algorithm. It is a multi-step interpolation which includes the lower grids controlled by level q [166]. Hence, the sparse grid interpolation is given by [167]

$$\mathscr{A}_{q,n}(g) = \sum_{|\mathbf{i}|_1 \leq q+n-1} (\Delta^{i_1} \otimes \Delta^{i_2} \otimes \cdots \otimes \Delta^{i_n})(g) = \mathscr{A}_{q-1,n}(g) + \underbrace{\sum_{|\mathbf{i}|_1 = q+n-1} (\Delta^{i_1} \otimes \Delta^{i_2} \otimes \cdots \otimes \Delta^{i_n})(g)}_{\Delta\mathscr{A}_{q,n}(g)} \tag{4.21}$$

with multi-index set $\mathbf{i} = \{i_1\, i_2 \ldots i_n\}$, $|\mathbf{i}|_1 = \sum \mathbf{i}$ and $\Delta^i = \mathscr{U}^i - \mathscr{U}^{i-1}$, where $\mathscr{U}^0 = 0$. This shows that Smolyak's algorithm for sparse grid interpolation is constructed by sequentially adding the interpolants based on the hierarchy q. To perform the interpolation as given in Eq. 4.21, support points are generated as follows [167]

$$\Delta\mathscr{H}_{q,n} = \bigcup_{|\mathbf{i}|_1 = q+n-1} (x_{1,\Delta}^{(i_1)} \otimes x_{2,\Delta}^{(i_2)} \otimes \ldots \otimes x_{n,\Delta}^{(i_n)}) \tag{4.22}$$

for interpolant $\Delta\mathscr{A}_{q,n}(g)$, where $x_{k,\Delta}^{(i_l)} = x_k^{(i_l)} \setminus x_k^{(i_l-1)}$ with $x^{(0)} = \emptyset$. Based on the level of interpolation i, number of grid points in each direction (i.e. for each random variable) are evaluated using

$$n_{s,i} = \begin{cases} 1 & \text{if } i = 1 \\ 2^{i-1} + 1 & \text{when } i > 1 \end{cases} \tag{4.23}$$

and the associated coordinates of these points are obtained by

$$x^{(i,j)} = \begin{cases} 0.5 & \forall\ j = 1 \quad \text{when } n_{s,i} = 1 \\ \dfrac{j-1}{n_{s,i}-1} & \forall\ j = 1, \ldots, n_{s,i} \quad \text{if } n_{s,i} > 1 \end{cases} \tag{4.24}$$

which forms a tree-like (or dendriform) structure [167]. Following the above equations, a case of two variables x_1 and x_2 with different combinations of interpolation levels denoted by indices i_1 and i_2, respectively is illustrated in Fig. 4.3(a). For brevity, the figure shows combinations with $i_1, i_2 \leq 5$ which are represented by nodes. Sparse grid level q is assigned to construct the points and summation of indices (i.e. $|\mathbf{i}|_1 = i_1 + i_2$) is computed for each combination. As presented in Eq. 4.22, sparse grid points $\Delta\mathscr{H}_{q,n}$ are generated using the combinations such that $q = |\mathbf{i}|_1 - n + 1$. Fig. 4.3(a) marks these nodes having equal to $|\mathbf{i}|_1$ through separate

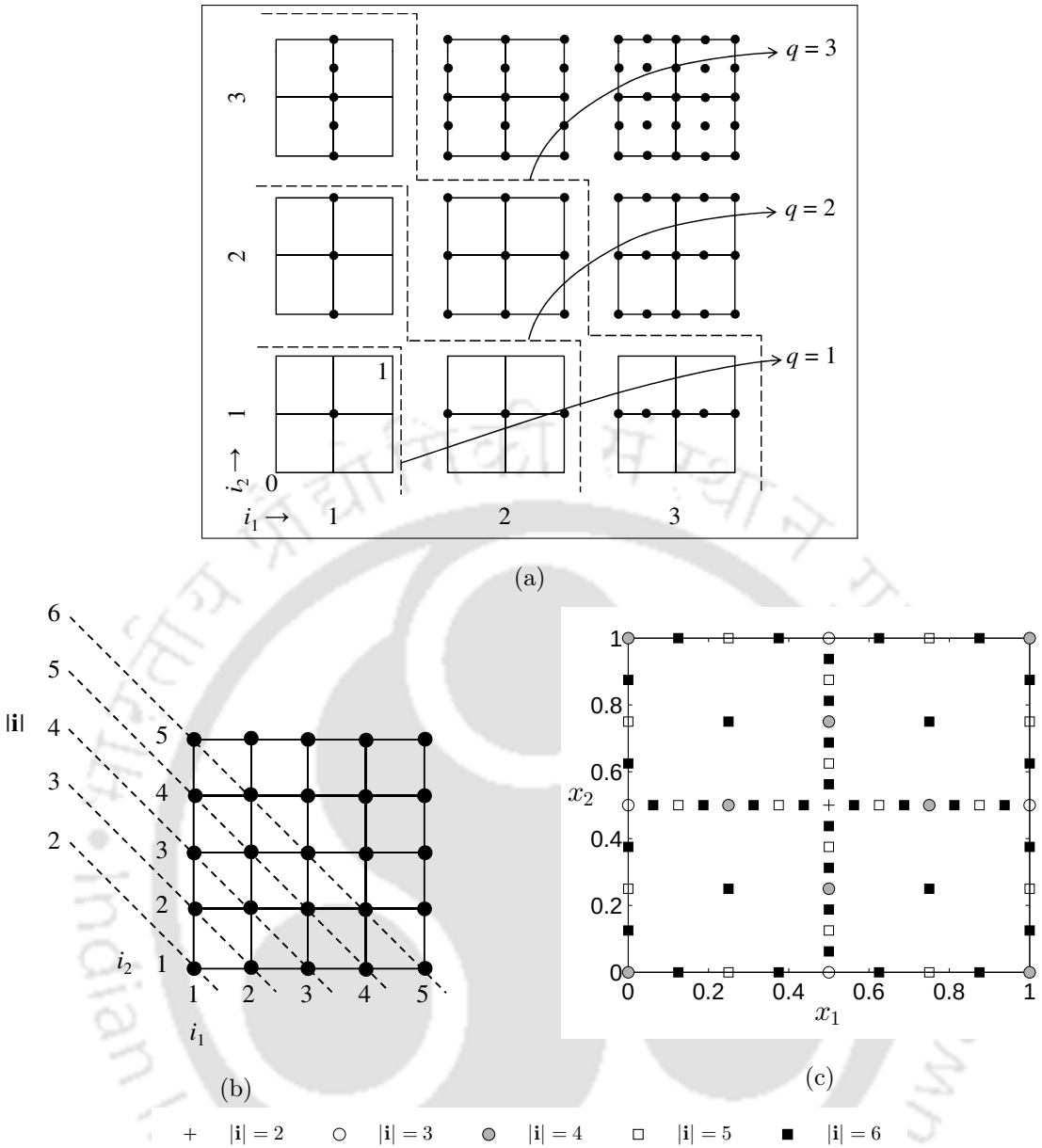

Figure 4.3: (a) A schematic presentation of the product grid, (b) sparse grid interpolation and (c) associated grid points

dash lines. Using Eq. 4.23, number of points for individual interpolation combinations are calculated and the coordinates of these points are obtained from Eq. 4.24 in the unit space. Fig. 4.3(b) shows the points generated at different sparse grid level q based on the index summation $|\mathbf{i}|_1$ with first point starting from center. It can be observed that the points formed in $\Delta\mathscr{H}_{q,n}$ are exclusive and unique as the points are not repeated in any predecessor and successor levels. However, in the present study, sparse gird points are formed using $\mathscr{H}_{q,n}$ which is defined as union of all points from the levels $\leq q$. Fig. 4.4 shows the Clenshaw-Curtis sparse grid generated for various q values. On the contrary to a full grid scheme as shown in Fig. 4.2, sparse grid scheme fills the domain (in this case, unit space) non-uniformly. Thus, creating large voids between adjacent points. The proposed sequential method attempts to fill such voids in the vicinity of the limit state only, as the space far away from the critical region does not contribute much in reliability estimation.

In general, coefficients in Eq. 4.19 are determined using piecewise multi-linear function as the basis for

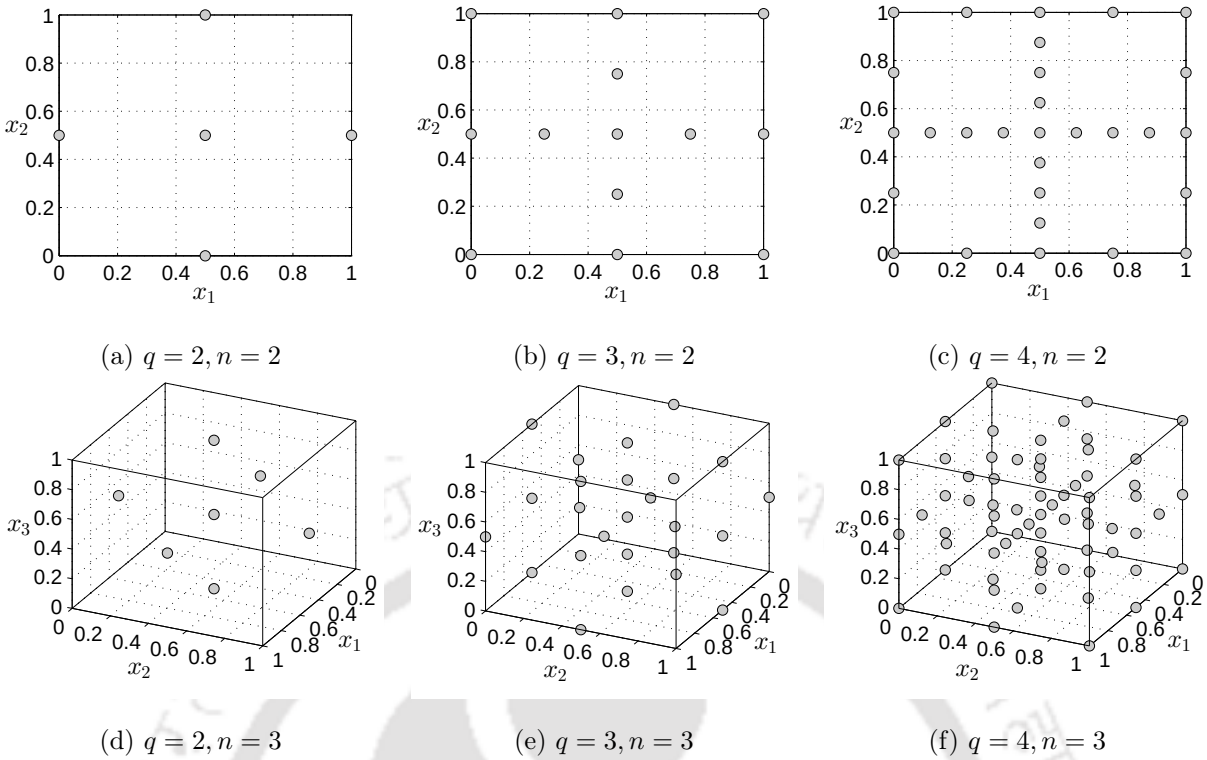

(a) $q = 2, n = 2$ (b) $q = 3, n = 2$ (c) $q = 4, n = 2$

(d) $q = 2, n = 3$ (e) $q = 3, n = 3$ (f) $q = 4, n = 3$

Figure 4.4: Support points generated by Clenshaw-Curtis sparse grid scheme

interpolation over the sparse grid points which is expressed as [165]

$$\breve{w}_i^{(i,j)} = \begin{cases} 1 & \text{for } j = 1 \text{ if } n_{s,i} = 1 \\ 1 - (n_{s,i} - 1)|x - x_i^{(i,j)}| & \text{if } |x - x_i^{(i,j)}| < (n_{s,i} - 1)^{-1} \\ 0 & \text{elsewhere} \end{cases} \tag{4.25}$$

In the present study, the use of piecewise multi-linear basis function is replaced with MLS based SRSM by substituting Eq. 4.11 into Eq. 4.19. This modifies the interpolation expression given in Eq. 4.19 as

$$\mathscr{U}^i(g) = \sum_{j=1}^{n_{s,i}} \Xi_j^i(z)\mathbf{b}(z) \tag{4.26}$$

Above equation clearly shows that the weight $\breve{w}_i^{(i,j)}$ which served as the basis function in Eq. 4.19 is replaced by MLS formulation with regularized weight function w embedded in $\mathbf{b}$. This shows that proposed method retains the advantage of selective tensor product as per Eq. 4.21 to limit the number of support points and introduces the benefits of MLS based SRSM in the same framework.

The proposed formulation describes sparse grid as a multi-step process which gives 1, 4, 8, 16 and 36 support points with respect to $|\mathbf{i}|_1 = 2, 3, 4, 5$ and 6 for $n = 2$. This indicates that as the level q increases, the number of support points grows factorially between the adjacent levels. This curse of dimensionality also makes the sparse grid formulation less attractive for stochastic computation. Few methods have been discussed in the literature like selecting index set $\mathbf{i}$ based on the weighted tensor product [168], adaptive selection of points near the non-smooth regions [167] and so on, to make it efficient. These methods employ multiple level-wise generation within a single process of sparse grid construction to address the local variations. However, present study introduces a new alternative based on the optimization of the output function g in order to generate multiple sparse grids. The objective function can be defined based on the desired output (e.g. limit state, maxima, minima). For example, if reliability analysis is the main goal, the objective function can be defined as per Eq. 4.12. This objective function needs support points near the most probable failure point (or design point) which is optimized iteratively. Thus, the minimized value $\mathbf{z}^{*,it}$ obtained from Eq. 4.12 serves as

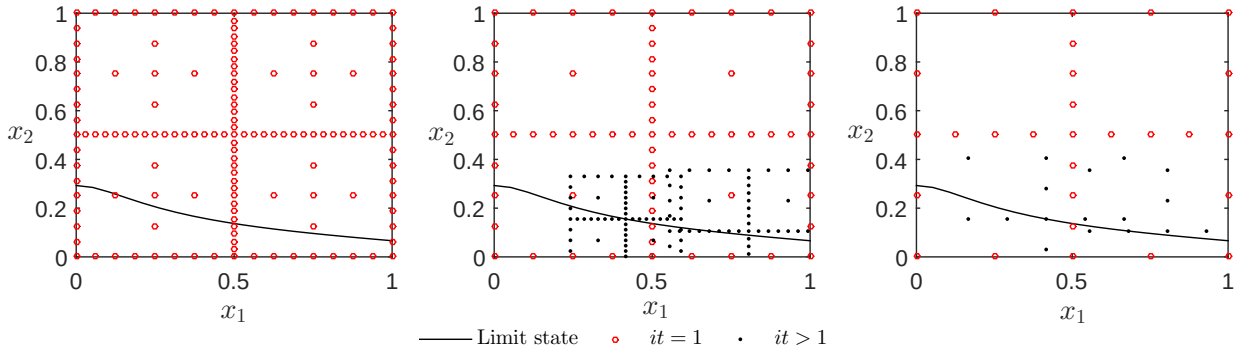

(a) $n_s = 145$ (b) $n_s = 155$ (c) $n_s = 46$

Figure 4.5: Generation of points using (a) single sparse grid of $\mathscr{H}_{6,2}$, (b) multiple sparse grids of $\mathscr{H}_{5,2}$ and (c) multiple sparse grids of $\mathscr{H}_{4,2}$ for $it = 1$ and $\mathscr{H}_{3,2}$ for $it > 1$

the new center point to generate additional support points for the next iteration. Consequently, it populates the design space with additional points in multiple iterations near the limit state as shown in Fig. 4.5. It can be noted that for $it > 1$, the coordinates of the new sparse grids are squeezed by factor $\lambda_{it}^{\mathbf{x}}$ to effectively map the local variations near the limit state. Efficiency of this optimization based generation is illustrated using three cases presented in Fig. 4.5(a), 4.5(b) and 4.5(c). The first case adopts single generation of the sparse grid using $q = 6$, the second case implements Eq. 4.12 with level $q = 5$ till $it = 3$ and the last case employs different sparse grid levels $q = 4, 3, 3$ with respect to iteration 1, 2, 3. Resulting population of the support points near the limit state is observed to be in the order of case 1 < case 3 < case 2. However, total number of support points generated within the domain is least for case 3 as compared to case 1 and case 2. Hence, it can be inferred that a logical tradeoff for multiple sparse grids yields an efficient generation of the support points fulfilling the desired objective.

Based on this discussion, it can be concluded that stochastic computation over the original performance function increases the computational burden which can be bypassed through MLS based SRSM by considering $\tilde{g}(\mathbf{z})$ instead of $g(\mathbf{x})$ in Eq. 4.12 which is demonstrated with the help of numerical results in the section below.

4.4.3 Reliability Assessment

Once the convergence is achieved as described in the previous section, reliability analysis is carried out to estimate the probability of failure p_f. Based on the support points generated sequentially in every iteration, approximate surface $\tilde{g}(\mathbf{x})$ is constructed. In this context, it may be noted that support points generated in every iteration along with the corresponding values of the original function are used to construct the global response surface. Using this surface, proposed method estimates the most probable failure point $\mathbf{x}^*$. Here, importance sampling [5] is chosen with appropriate sample size to carry out the reliability assessment. The probability of failure p_f is evaluated as

$$p_f \approx \frac{1}{n_c} \sum_{i=1}^{n_c} \frac{\mathscr{I}[\tilde{g}(\mathbf{x}^i) \leq 0] f_{\mathbf{x}}(x^i)}{f_{\mathbf{x}}^*(x^i)} \tag{4.27}$$

where, n_c is the sample size of the simulation. In the above equation, $\mathscr{I}[\bullet]$ is a discrete indicator function with binary output (i.e. either 0 or 1) based on the condition stated in the third bracket. Additionally, $f_{\mathbf{x}}(x)$ is the joint probability density function (*pdf*) of the random variables and $f_{\mathbf{x}}^*(x)$ denotes the modified *pdf* applied as the weight to shift the simulation in the vicinity of the most probable failure point. Readers may refer [5] for further details of this technique.

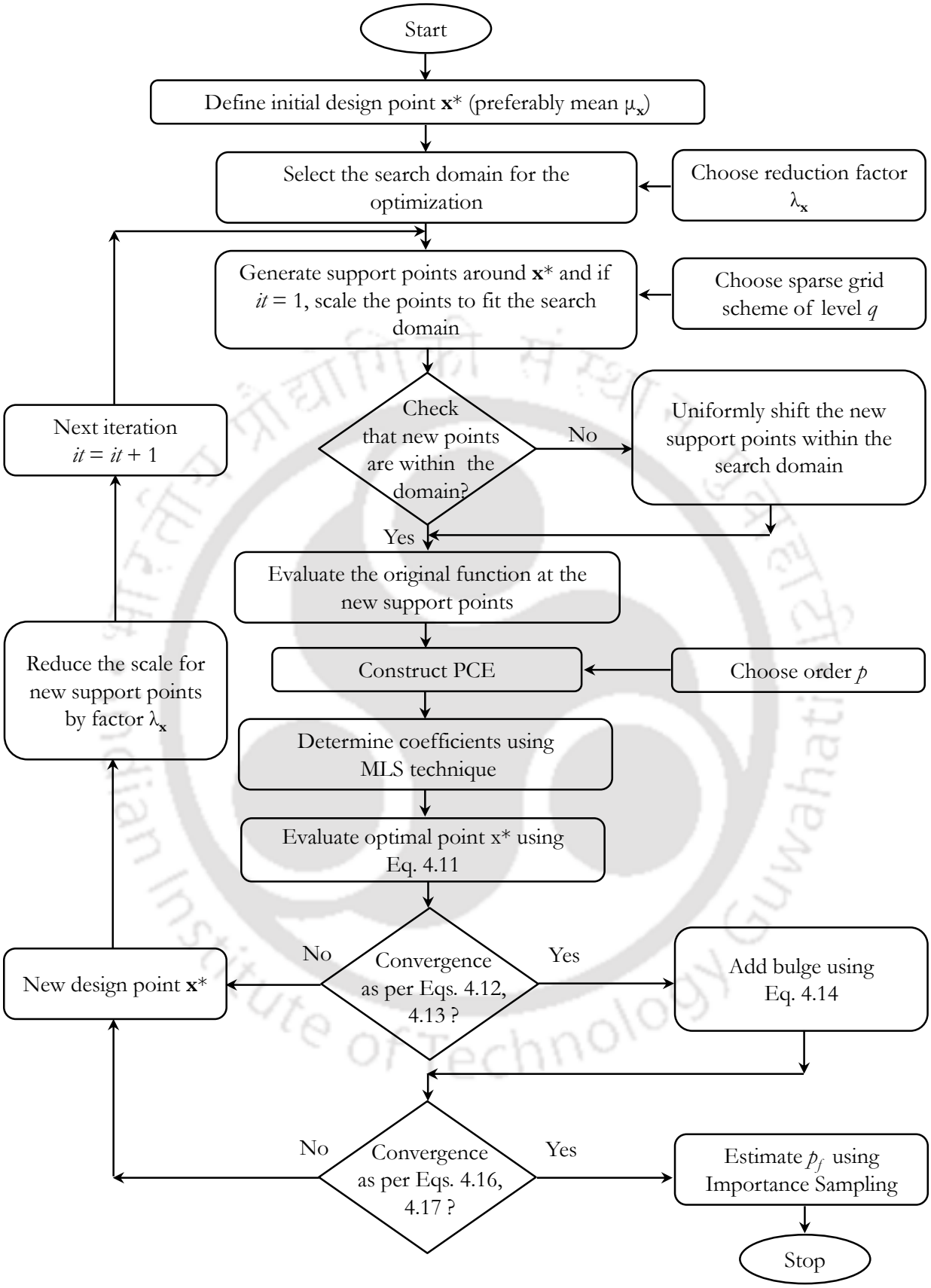

Figure 4.6: Flowchart of the proposed sequential SRSM

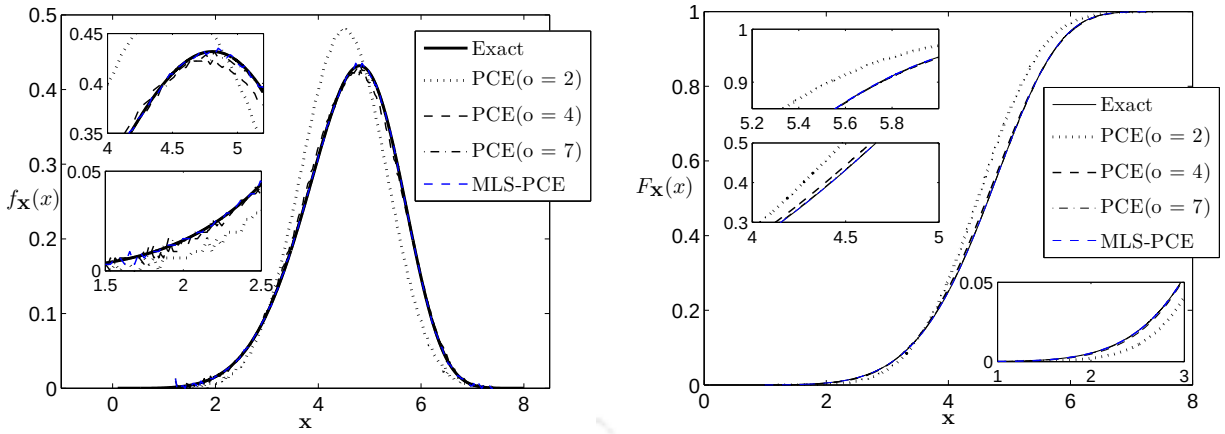

(a) (b)

Figure 4.7: Comparison of (a) *pdf* and (b) CDF of a random variable following Weibull distribution evaluated from different methods

4.5 Numerical Results and Discussion

The proposed sequential SRSM discussed in the previous section is considered here for numerical analysis. Fig. 4.6 shows the flowchart of the proposed method. In the present study, the degree of the polynomial is fixed at two to capture the higher order nonlinearity and uncertainty when used in MLS framework. To demonstrate the rationality behind this claim, Weibull distribution with mean and variance as 4.60 and 0.85, respectively is considered for a quick check. The effective range of [0 8] is subdivided in eight equidistant segments. Fig. 4.7 shows the *pdf* and CDF of the Weibull distribution using conventional PCEs of different degree and proposed MLS-PCE. As the degree increases, conventional PCE matches with the exact expression. It is noted that 7^{th} degree PCE is adequate to map the Weibull distribution while the same accuracy is achieved using second degree MLS-PCE. Thus, using second degree PCE in MLS framework, the proposed sequential SRSM is tested with different benchmark problems from the literature representing different level of complexities. Results obtained from the proposed method are compared with other methods (e.g. FORM, SORM, HO-SRSM, SRSM, MCS) to demonstrate its efficiency and accuracy. Finally, two design problems involving nonlinear FE analysis are presented to demonstrate the advantage and superiority of the proposed algorithm for reliability based design.

4.5.1 Validation Study

As stated above, benchmark examples are solved first to demonstrate the efficiency and accuracy of the proposed method for reliability analysis of explicitly defined performance functions. Three benchmark examples are considered including hypothetical and actual limit states. A detailed discussion on the numerical results are given below.

4.5.1.1 Example 1: Franke's Test Surface

In this example, a bivariate performance function is considered which is given by

$$\begin{aligned} y(\mathbf{x}) \;=\; & 0.75\exp\{-0.25(9x_1-2)^2-0.25(9x_2-2)^2\} \\ & +0.75\exp\left\{-0.0204(9x_1-2)^2-0.10(9x_2-2)^2\right\} \\ & +\;0.50\exp\{-0.25(9x_1-7)^2-0.25(9x_2-3)^2\} \\ & -0.25\exp\{-(9x_1-4)^2-(9x_2-7)^2\}-0.25 \end{aligned} \tag{4.28}$$

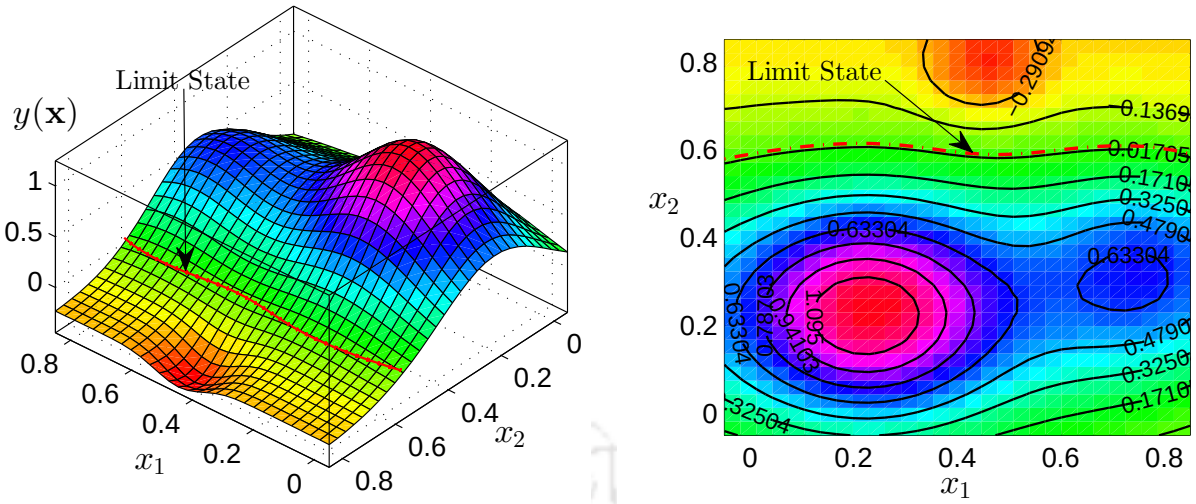

(a) (b)

Figure 4.8: (a) Surface plot and (b) contour plot of the Franke's test surface with limit state

where, x_1 and x_2 are independent Gaussian random variables with mean $\mu_{\mathbf{x}} = 0.40$ and standard deviation $\sigma_{\mathbf{x}} = 0.10$. The function in Eq. 4.28 is a modified version of the original Franke's test surface where the limit for failure is set to 0.25 [117]. It is widely considered as a benchmark problem for testing the interpolation of scattered data. Fig. 4.8(a) shows the profile of the original surface which has two maxima and one minima. The complexity of this example can be observed from the contour plot given in Fig. 4.8(b) which shows the limit state lies between the two maxima and one minima.

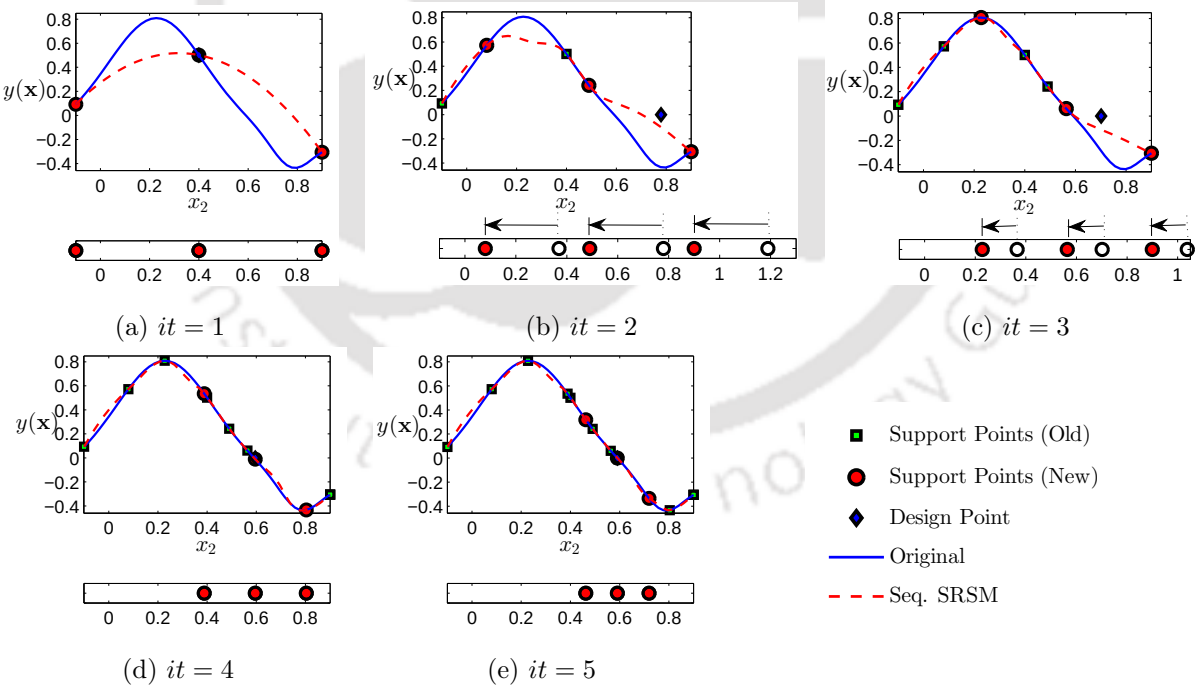

(a) $it = 1$ (b) $it = 2$ (c) $it = 3$

(d) $it = 4$ (e) $it = 5$

Figure 4.9: Sequential generation of the support points using the sparse grid scheme

To demonstrate the generation of sequential SRSM, Franke's test surface is simplified by cutting the surface using an imaginary plane through the mean value of the random variable x_1 as shown in Fig. 4.9. This, reduces the test surface to a 1D function of the random variable x_2. As stated in the flowchart (i.e. Fig. 4.6), the process commences from the mean of the random variable (i.e. μ_{x_2}) which is assumed as the initial design point. The support points using Clenshaw-Curtis sparse grid of level q are generated around this

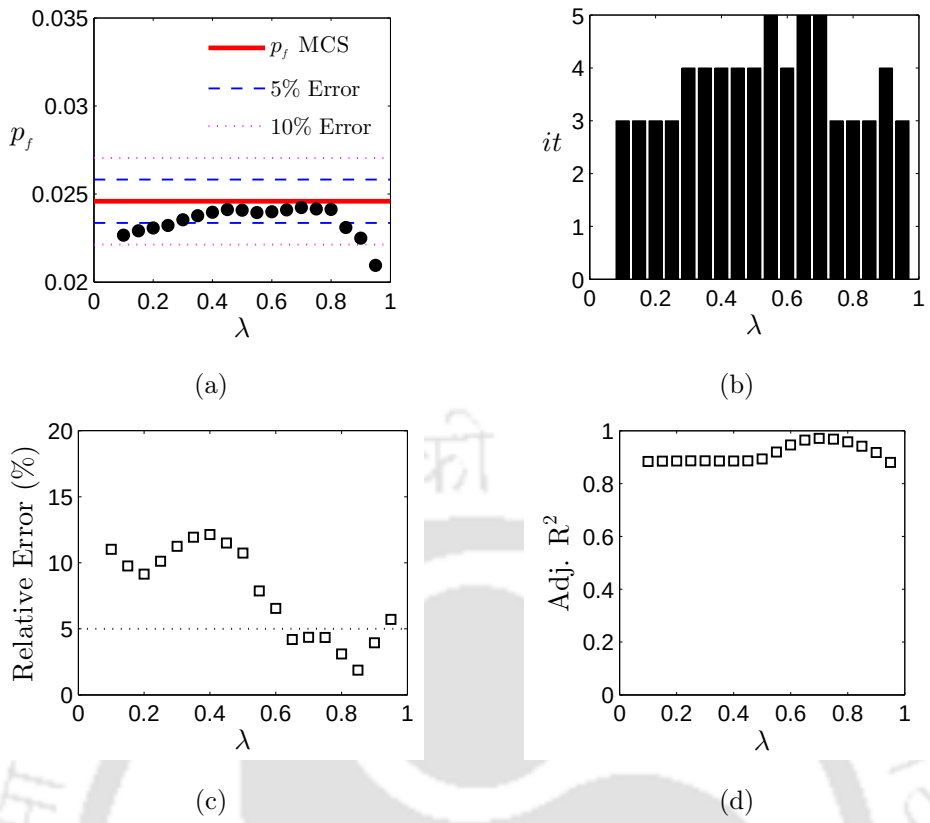

Figure 4.10: Sensitivity analysis for different $\lambda_{\mathbf{x}}$ values in Franke's function with respect to (a) probability of failure, (b) iterations, (c) relative error and (d) adjusted R^2

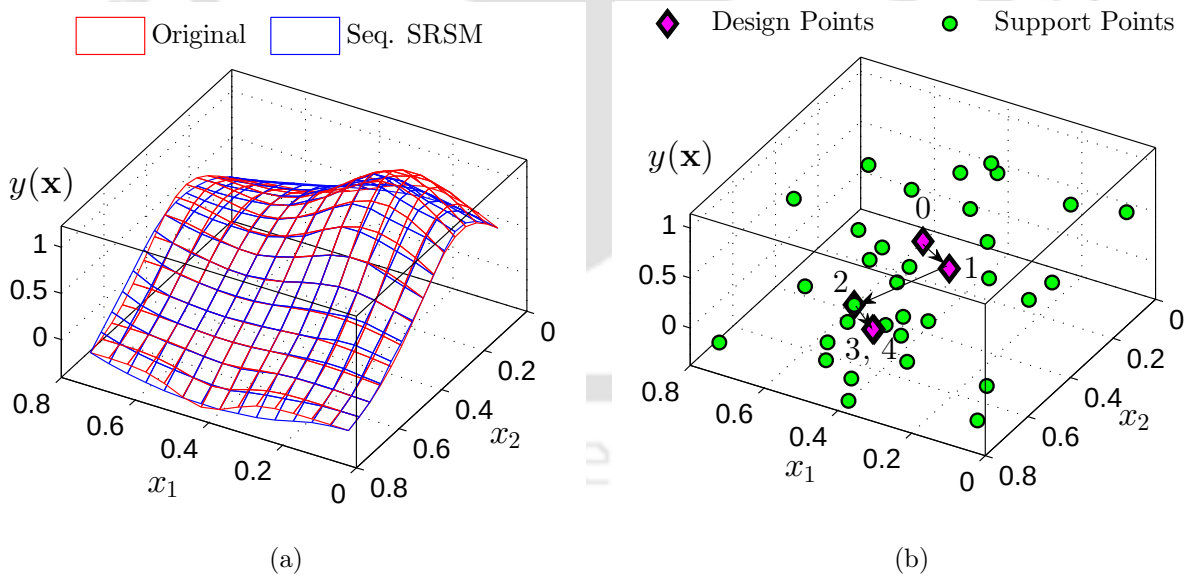

Figure 4.11: Franke's test surface: (a) sequential SRSM and (b) the support points generated by the sparse grid scheme

design point. Lower and upper bounds of the support points are assumed in such a way that it is sufficient enough to accommodate the limit state condition [i.e. $y(\mathbf{x}) = 0$]. It may be noted that the sequential SRSM employs Hermite polynomials which are in Gaussian space. Hence, the limits of the random variable x_2 in the standard normal space is considered to be $[-5,\ 5]$. Based on the sparse grid level $q = 2$, three equidistant support points are generated in the first iteration as shown in Fig. 4.9(a). In this context, the support points for z_2 are generated in the standard normal space and converted into its original space defined by x_2. Using

Table 4.2: Comparison of probability of failure for the Franke's function

Method	Degree	p_f	Function calls	Error (%)	Remark
MCS	-	0.02459	10^6	-	-
FORM	-	0.02714	36	10.37	-
SORM	-	0.02386	56	2.97	-
SRSM	4	0.03489	25	41.89	-
	6	0.03142	49	27.78	-
	8	0.02968	81	20.70	-
	10	0.02812	121	14.36	-
HO-SRSM	-	0.02647	70	7.65	$p = [6, 7]$
Seq. SRSM	2	0.02446	36	0.53	$q = 3^{(\text{for } it=1,2)}$ and $q = 2^{(\text{for } it=3,4)}$

these three points, an approximate surface with PCE of degree $p = 2$ is constructed using MLS technique as discussed earlier. Eq. 4.12 is optimized to determine the next optimal location (i.e. new design point) for generating more support points. In the following iteration $it = 2$, additional support points are generated around the new design point using $q = 2$. Here, the extent (i.e. difference between the bounds) of the new support points is reduced from the previous one by a factor $\lambda < 1$ so that more points are segregated near the design point. In this case, $\lambda = 0.80$ is adopted which is observed to give quick convergence. Locations of these new support points are shown in Fig. 4.9(b). It can be observed that one support point lies beyond the domain $[-5, 5]$. Therefore, the position of all new support points are shifted uniformly to fit within the given limits. This uniform shifting is done to maintain the symmetry of the new support points. However, if the initial guess on bounds does not contain the limit state [i.e. $y(\mathbf{x}) = 0$], the bounds may be suitably readjusted to incorporate the failure region. Once the position of the new support points are shifted as shown in Fig. 4.9(b), Eq. 2.10 is solved to determine the unknown coefficients at these points. The response surface is improved using old as well as new support points. Again the optimization is executed to determine the next location for $it = 3$ as in Fig. 4.9(c). This eventually helps to concentrate the support points near the failure region for faster convergence. In this case, the convergence is achieved in five iterations using 15 function calls. However, only 13 actual function calls are executed because $it = 2$ and 3 have two common points. Fig. 4.9(d) and 4.9(e) show the performance function (i.e. original and proposed) after convergence. A close match is observed between them which justifies the accuracy of the proposed algorithm. It may be noted that penalty functions like bulging [164] can be adopted in the proposed algorithm for determining multiple failure points (or multiple maxima/minima) in the limit state, if any.

Sequential development of the response surface requires adequate sparse grid level as the number of support points grow rapidly with each successive iteration. Thus, considering higher q value (say 4, 5, ...) may result in more function calls whereas low value of q may not provide better approximation as it contains the axial points only. A tradeoff is suggested in this study such that the computational cost for the support points and accuracy can be balanced in the iterative framework. Two different sparse grid levels are employed in the first few iterations and for all the successive iterations. This means iteration one and two use $q = 3$ while the successive iterations consider $q = 2$ until the convergence is achieved. Besides the sparse grid level, choice of scale reduction factor λ also plays a critical role in the sequential SRSM. Using the suggested sparse grid levels, Franke's function is solved for different λ values. Fig. 4.10 shows the estimated probability of failure, iterations required to converge, average error in approximation and adjusted R^2 obtained in the sequential stochastic response surface. Evaluation of the relative error in the approximation and the adjusted R^2 are done by generating a test sample of size 100 uniformly over the domain. It is observed that λ values from 0.30 to 0.85 give fair estimation of p_f (i.e. error is within $\pm 5\%$) whereas the relative error and adjusted R^2 improve from 0.60 to 0.90. The convergence is achieved between three to five iterations for λ values from 0.10 to 0.95. In this study, λ is considered to be 0.80 as it is found to offer optimal results. This leads to a total of four iterations and 36 actual function calls. Fig. 4.11 shows the approximation achieved and the support points generated in the proposed sequential SRSM for the bivariate Franke's test surface. This example is also solved by different methods for reliability estimation and the results from these methods are summarized in Table 4.2. In this study, MCS is assumed to be the most accurate estimation of the probability of failure which gives $p_f = 0.02459$ with one million samples (i.e. $n_c = 10^6$). Solutions using

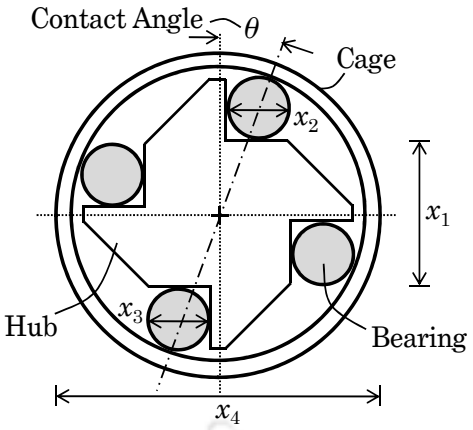

Figure 4.12: Fortini's clutch assembly

FORM and SORM converge after 36 and 56 function calls and p_f estimated are 0.02714 and 0.02386 with 10.37% and 2.97% error, respectively. Additionally, it is observed that the initial choice in FORM and SORM (e.g. $x_1^* = 0.20$ and $x_2^* = 0.20$) may lead to computational difficulty to achieve convergence and eventually yield erroneous results. Conventional SRSM is executed with PCE of degree four, six, eight and ten for both these variables. It requires 25 to 121 function calls to estimate p_f with error 14.36–41.89% as shown in the Table 4.2. HO-SRSM [58] solves the problem with the degree $p = 6$ and 7 for the random variables x_1 and x_2, respectively, giving $p_f = 0.02647$ (i.e. 7.65% error) with 70 function calls. Sequential SRSM performs the reliability analysis using 36 function evaluations which gives better estimation of p_f with error equal to 0.53%.

4.5.1.2 Example 2: Fortini's Clutch

Next example is the Fortini's clutch assembly [30] which consists of a hub and four roller bearings placed in a cage as shown in Fig. 4.12. The clutch is designed against the overturning based on the contact angle θ formed by the vertical axis passing through the center of the hub with a line connecting the centers of the opposite roller bearings. Thus, the limit state can be defined as

$$g(\mathbf{x}) = \underbrace{\cos^{-1}\left[\frac{x_1 + 0.5(x_2 + x_3)}{x_4 - 0.5(x_2 + x_3)}\right]}_{\theta} - 0.08726 \tag{4.29}$$

where, x_1, x_2, x_3 and x_4 are the independent random variables with statistical properties mentioned in Table 4.3. In order to avoid overturning of the clutch and operate smoothly, the contact angle θ must lie within 5° (i.e. 0.08726 radian). Table 4.4 summarizes the probability of failure, error in estimation and number of function calls obtained from various methods. MCS estimates $p_f = 0.00130$ with a sample size of

Table 4.3: Statistical properties of variables in Fortini's clutch assembly

Random variables	Mean (μ_x)	Standard deviation (σ_x)	Distribution
x_1(mm)	55.29	7.93 $\times 10^{-2}$	Beta
x_2(mm)	22.86	4.30 $\times 10^{-3}$	Gaussian
x_3(mm)	22.86	4.30 $\times 10^{-3}$	Gaussian
x_4(mm)	101.60	7.93 $\times 10^{-2}$	Rayleigh

10^5 which is referred as the benchmark. Gradient based methods (i.e. FORM and SORM) diverge [30] and are unable to estimate the probability of failure. Conventional SRSM computes probability of failure using degrees $p = 3$, 5 and 7 estimating the p_f as 0.00116, 0.00120 and 0.00118, respectively with inaccuracies ranging from 7.69% to 10.77% in spite of having significant number of support points (i.e. $n_s = 256$, 1296 and 4096, respectively). It is further solved using HO-SRSM with the degree of the polynomials in Eq. 4.29 as five, two, two and five respectively. It consumes 192 support points to offer $p_f = 0.00094$ with error nearly

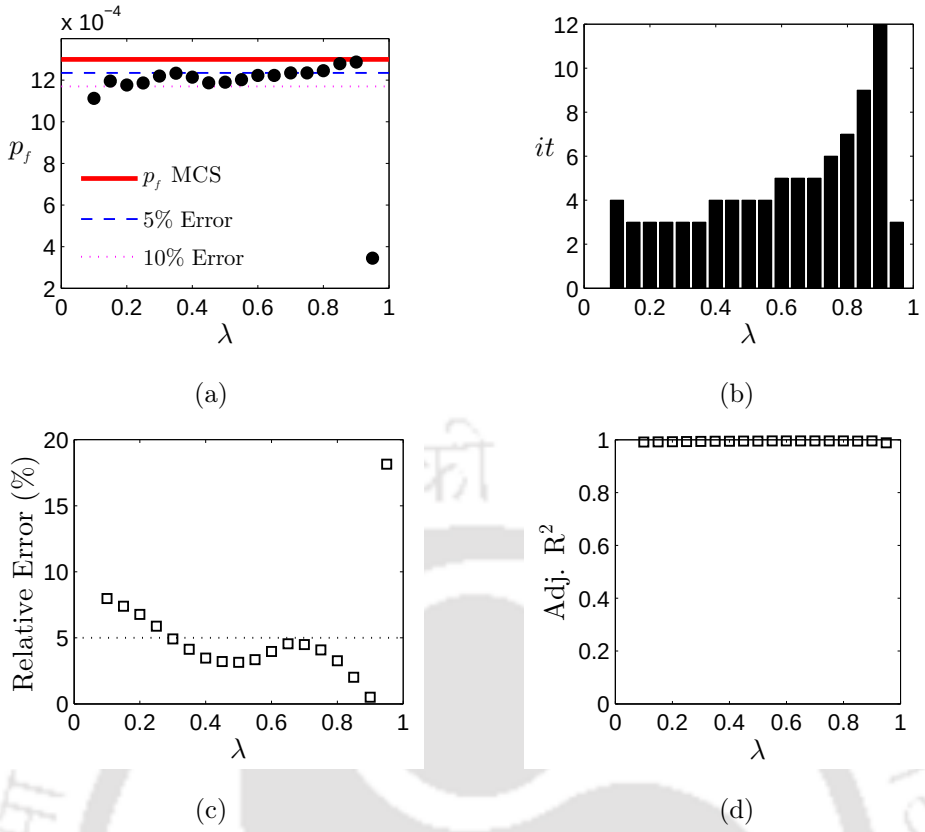

Figure 4.13: Sensitivity analysis for different $\lambda_{\mathbf{x}}$ values in Fortini's clutch with respect to (a) probability of failure, (b) iterations, (c) relative error and (d) adjusted R^2

28%. Xiong *et al.* [163] also showed the application of DW-SRSM for a similar problem with Gaussian random variables. They performed 70 original function evaluations using collocation and LHS schemes with error ranging from 0.2% to approximately 8.0%. Finally, p_f is estimated using the proposed method for different values of sparse grid level q as shown in Table 4.4. A mixed usage of q is demonstrated where the initial few iterations adopt higher value of q as compared to the following iterations. Five cases are shown in Table 4.4, including three cases where $q = 3$ in the initial few iterations which is reduced to 2 until the convergence is achieved. The results show the efficiency and accuracy of sequential SRSM using first and second degree PCE with different combinations of spare grid levels. It can be noticed that successive iterations produce new support points and the algorithm demands more computational cost which may impose serious restrictions for large problems. Thus, a tradeoff between the level and the accuracy is made involving intermittency criteria to choose an optimal level for the specific problem. In this context, $q = 3$ in first two iterations followed by $q = 2$ in successive iterations is found to produce optimal result. Sensitivity analysis based on the reduction factor λ is also carried out for this problem as shown in Fig. 4.13. Over a wide range of λ, the p_f estimation is within 10% but most accurate results are observed over the range $[0.60,\ 0.90]$. Based on this sensitivity analysis, λ is assumed to be 0.80. It is observed that this value of λ offers optimal results for most of the problems. Therefore, $\lambda = 0.80$ is recommended for general purpose unless any other value is selected from the sensitivity analysis by the designer for a specific application.

4.5.1.3 Example 3: Non-differentiable Function

In this example, a hypothetical limit state is examined which is expressed as [117]

$$g(\mathbf{x}) = 35 - \sum_{i=1}^{2} x_i^2 - \sum_{j=3}^{6} x_j - \frac{x_7 x_8 x_9}{\max(1, x_{10})} \tag{4.30}$$

Table 4.4: Estimated p_f of the Fortini's clutch assembly using different reliability methods

Method	Degree	p_f	Error (%)	Function calls	Remark
MCS	-	0.00130	-	10^5	-
FORM	-	-	-	-	-
SORM	-	-	-	-	-
SRSM	3	0.00116	10.77	256	-
	5	0.00120	7.69	1296	-
	7	0.00118	9.23	4096	-
HO-SRSM	-	0.00094	27.77	192	$p = [5, 2, 2, 5]$
Seq. SRSM	2	0.00125	3.85	164	$q = 3^{(\text{for } it=1,\ldots,4)}$
	2	0.00130	0.00	132	$q = 3^{(\text{for } it=1,2,3)}$; $q = 2^{(\text{for } it=4)}$
	2	0.00124	4.62	100	$q = 3^{(\text{for } it=1,2)}$; $q = 2^{(\text{for } it=3,4,5)}$
	2	0.00130	0.23	68	$q = 3^{(\text{for } it=1)}$; $q = 2^{(\text{for } it=2,3,4)}$
	1	0.00128	1.54	36	$q = 2^{(\text{for } it=1,\ldots,4)}$

In the above limit state, max(•) gives the largest value among the set in the first bracket. Due to this reason, $g(\mathbf{x})$ is non-differentiable which creates difficulty to apply gradient based reliability analysis (e.g. FORM, SORM). Table 4.5 shows the statistical properties of the ten uncorrelated random variables. As usual MCS result with 10^6 samples is used for reference as shown in Table 4.6. Conventional SRSM is performed with degree $p = 2$ and 3 for all the random variables which demands 59046 and 1048576 support points, respectively. This makes the process very expensive as the second case (i.e. $p = 3$) requires more function calls than MCS. Besides fixed degree of PCE for all random variables as in the previous two cases, SRSM with variable degrees are also tried and tabulated here. Different degrees of these PCE for ten random variables are shown in the third case of SRSM. The result obtained in this case with 19440 function calls has

Table 4.5: Random variables in the non-differentiable function

Random variables	Mean (μ_x)	Standard deviation (σ_x)	*pdf*
x_1, x_2	-0.200	1.200	Gaussian
x_3	2.500	0.400	Gaussian
x_4, x_5, x_6	2.500	1.400	Gaussian
x_7	1.000	1.000	Gaussian
x_8	1.230	0.350	Gaussian
x_9	0.980	0.023	Gaussian
x_{10}	2.000	1.000	Gaussian

1.01% error. Although the result is fairly accurate, the cost of computation is significantly high. HO-SRSM is further used to calculate the probability of failure which is estimated to be 0.000430 (i.e. 8.59%) with 1804 support points, consuming relatively less computational cost. It results in huge reduction of n_s and enhanced accuracy as compared to previously discussed cases of $p = 2$ and 3. This, in turn, clearly indicates that the unnecessary support points in full grid schemes might reduce the efficiency. Sequential SRSM further reduces the computational cost to 504 function calls (i.e. nearly 72% reduction from HO-SRSM). Additionally, the accuracy of the proposed method (i.e. error is 2.27%) is also well within the acceptable limits for all practical purpose proving the efficiency of this method in terms of accuracy and computational cost.

4.5.2 Application to Structural Problems

The benchmark examples presented in the previous section have proved the performance of the proposed algorithm. Hence, implicit performance functions associated to actual engineering problems are further investigated for reliability assessment. Four different FE problems are considered with correlation between the random variables, fatigue mechanics and dynamic analysis to demonstrate the performance of the proposed algorithm.

Table 4.6: Estimated p_f for different cases in the non-differentiable function

Method	Degree	p_f	Function calls	Error (%)	Remark
MCS	-	0.000396	10^6	-	-
FORM	-	0.000076	115	80.81	-
SORM	-	0.000353	295	10.94	-
SRSM	2	0.000422	59046	6.57	-
	3	0.000417	1048576	5.30	-
	-	0.000400	19440	1.01	$p = [2, 2, 1, 1, 1, 1, 2, 2, 2, 4]$
HO-SRSM	-	0.000430	1804	8.59	$p = [2, \ldots, 2, 4]$
Seq. SRSM	2	0.000387	504	2.27	$q = 3^{(\text{for } it=1,2)}$ and $q = 2^{(\text{for } it=3,4)}$

4.5.2.1 Problem 1: Multi-storey Portal Frame with Static Lateral Load

In this example, a three-bay five-storey portal frame is solved for reliability analysis against a serviceability criteria under lateral loading as shown in Fig. 4.14. The failure criteria is described in terms of horizontal displacement $u(\mathbf{x})$ of the top floor and the limit state is defined as [130]

$$g(\mathbf{x}) = u_o - u(\mathbf{x}) \tag{4.31}$$

where, u_o is the threshold value of the horizontal displacement. Here, eight different beam and column elements are used with random properties (i.e. cross-section area, moment of inertia and Young's modulus) shown in Fig. 4.14 and Table 4.7. In addition to these random variables, lateral loads acting on the frame are also random. The properties of these random variables are listed in Table 4.8. It may be noted that the random variables are correlated and the correlation matrix is as follows

$$\rho_{\mathbf{x}} = \begin{pmatrix} 1 & & & & & & & & \\ 0.90 & 1 & & & & & & & \\ 0 & 0 & 1 & & & & & & \\ 0 & 0 & 0.95 & 1 & & & & & \\ 0 & 0 & 0.95 & 0.95 & 1 & & & & \\ 0 & 0 & 0 & 0 & 0 & 1 & & & \\ 0 & 0 & 0 & 0 & 0 & 0.13 & 1 & & \\ \vdots & \vdots & \vdots & \vdots & \vdots & \vdots & \ddots & \ddots & \\ 0 & 0 & 0 & 0 & 0 & 0.13 & \cdots & 0.13 & 1 \end{pmatrix} \tag{4.32}$$

Index notation in Eq. 4.32 follows the order of the random variables as specified in Table 4.8. Static analysis of the frame for a given realization of the random variables is performed using ANSYS V13.0 [144]. MCS with a sample size of 10^5 is found to provide converged result and is considered as benchmark to check the accuracy of the other methods. Table 4.9 shows the probability of failure for different allowable limits u_o ranging from 0.025m to 0.055m for design purpose.

FORM consumes 176 to 352 function calls to evaluate the probability of failure for different threshold values. Although, the number of function calls in FORM are least among all the methods, the error in p_f estimation ranges from nearly 8% to 40% as shown in the Table 4.9. In SORM, the demand for function calls escalates due to the evaluation of the Hessian matrix. This results in 1709 to 1885 calls of ANSYS [144] solver including the evaluation of the failure point. Error in estimation of p_f is still high, ranging from approximately 10% to 36%. This shows that both the gradient based methods perform poorly in this case. SRSM of degree $p = 2$ requires large number of function calls (i.e. $(p+1)^{21} = 1.046\text{E}10$) as the problem has 21 random variables. This makes it computationally expensive than the MCS due to the curse of dimensionality and hence, it is not used in this present study. It also shows the limitation of SRSM for reliability analysis using collocation

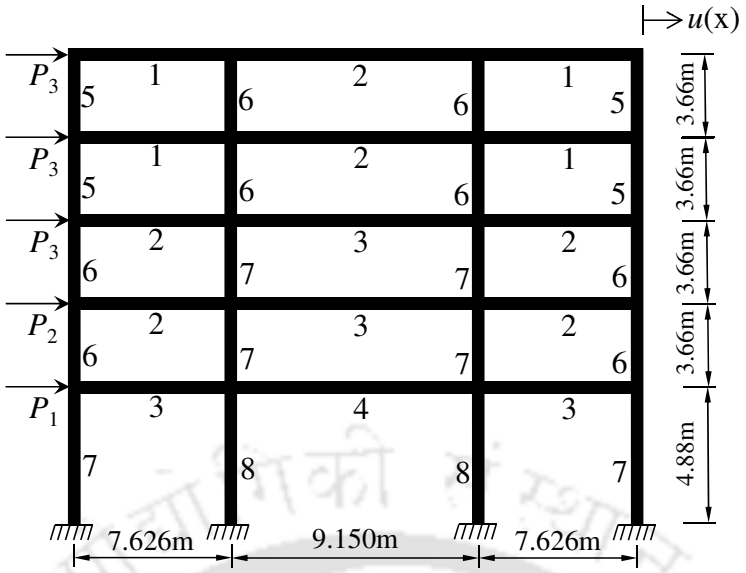

Figure 4.14: A multi-storey multi-bay building subjected to lateral loads

Table 4.7: Element properties in the multi-storey multi-bay building

Element type number	Area	Moment of inertia	Young's modulus
1	A_5	I_5	E_1
2	A_6	I_6	E_1
3	A_7	I_7	E_1
4	A_8	I_8	E_1
5	A_1	I_1	E_2
6	A_2	I_2	E_2
7	A_3	I_3	E_2
8	A_4	I_4	E_2

scheme to solve high-dimensional problems. HO-SRSM calls 4014 FE evaluations but performs poorly with error ranging from 12.42% to 86.56% for different threshold levels. On the contrary, the proposed sequential SRSM can solve this high-dimensional problem involving only eight iterations to converge. As stated earlier, first two iterations are carried out with $q = 3$ which generates 925 points in each iteration. Successive iteration consumes additional 43 function calls for $q = 2$. Using 2108 function evaluations, sequential SRSM results in significant improvement of p_f estimation (i.e. error $< 4\%$). This example clearly demonstrates the merits of the proposed scheme over the gradient based methods or other variants of PCE based techniques (i.e. SRSM and HO-SRSM) reported in the literature.

4.5.2.2 Problem 2: Three-storey Base Isolated Building Excited by Dynamic Load

A three-storied building, resting on the base isolators as shown in Fig. 4.15(a) are characterized by its yield force and displacement (i.e. f_y and δ_y, respectively), is presented here for reliability analysis. Each floor is considered to be rigid with mass m_f and columns are massless with stiffness k_f and damping d_f. The building is additionally guarded with snubbers having stiffness k_c to prevent excessive lateral deformation of the base isolators. It is activated as the horizontal displacement of the bottom floor exceeds δ_c as shown in Fig. 4.15(a). A secondary system is placed on the second storey of the building which has two degree of freedom (DOF) with mass (m_1 and m_2), stiffness (k_1 and k_2) and damping (d_1 and d_2). The combined system has six DOF which is subjected to ground acceleration $\ddot{u}_g(t)$ as shown in Fig. 4.15(b). Support motion is characterized by the sinusoidal pulse with amplitude A_p and time period T_p. Random variables considered in this case along with their statistical properties are listed in Table 4.10.

Performance function for this problem includes multiple serviceability criteria based on the inter-storey drift of the primary structure, absolute acceleration of the mass m_2 and relative motion of mass m_1 with respect

Table 4.8: Details of random variables in the multi-storey multi-bay building

Random variables	Units	Mean	Standard deviation	*pdf*
$E_1 \rightarrow x_1$	kN/m^2	2.174 $\times 10^{+7}$	1.915 $\times 10^{+6}$	Lognormal
$E_2 \rightarrow x_2$	kN/m^2	2.380 $\times 10^{+7}$	1.915 $\times 10^{+6}$	Lognormal
$P_1 \rightarrow x_3$	kN	71.175	28.470	Rayleigh
$P_2 \rightarrow x_4$	kN	88.970	35.590	Rayleigh
$P_3 \rightarrow x_5$	kN	133.454	40.040	Rayleigh
$A_1 \rightarrow x_6$	m^2	0.313	0.056	Lognormal
$A_2 \rightarrow x_7$	m^2	0.372	0.074	Lognormal
$A_3 \rightarrow x_8$	m^2	0.506	0.093	Lognormal
$A_4 \rightarrow x_9$	m^2	0.558	0.112	Lognormal
$A_5 \rightarrow x_{10}$	m^2	0.253	0.093	Lognormal
$A_6 \rightarrow x_{11}$	m^2	0.291	0.102	Lognormal
$A_7 \rightarrow x_{12}$	m^2	0.373	0.121	Lognormal
$A_8 \rightarrow x_{13}$	m^2	0.419	0.139	Lognormal
$I_1 \rightarrow x_{14}$	m^4	8.134 $\times 10^{-3}$	1.038 $\times 10^{-3}$	Lognormal
$I_2 \rightarrow x_{15}$	m^4	1.151 $\times 10^{-2}$	1.298 $\times 10^{-3}$	Lognormal
$I_3 \rightarrow x_{16}$	m^4	2.137 $\times 10^{-2}$	2.596 $\times 10^{-3}$	Lognormal
$I_4 \rightarrow x_{17}$	m^4	2.596 $\times 10^{-2}$	3.029 $\times 10^{-3}$	Lognormal
$I_5 \rightarrow x_{18}$	m^4	1.082 $\times 10^{-2}$	2.596 $\times 10^{-3}$	Lognormal
$I_6 \rightarrow x_{19}$	m^4	1.410 $\times 10^{-2}$	3.461 $\times 10^{-3}$	Lognormal
$I_7 \rightarrow x_{20}$	m^4	2.328 $\times 10^{-2}$	5.625 $\times 10^{-3}$	Lognormal
$I_8 \rightarrow x_{21}$	m^4	2.596 $\times 10^{-2}$	6.490 $\times 10^{-3}$	Lognormal

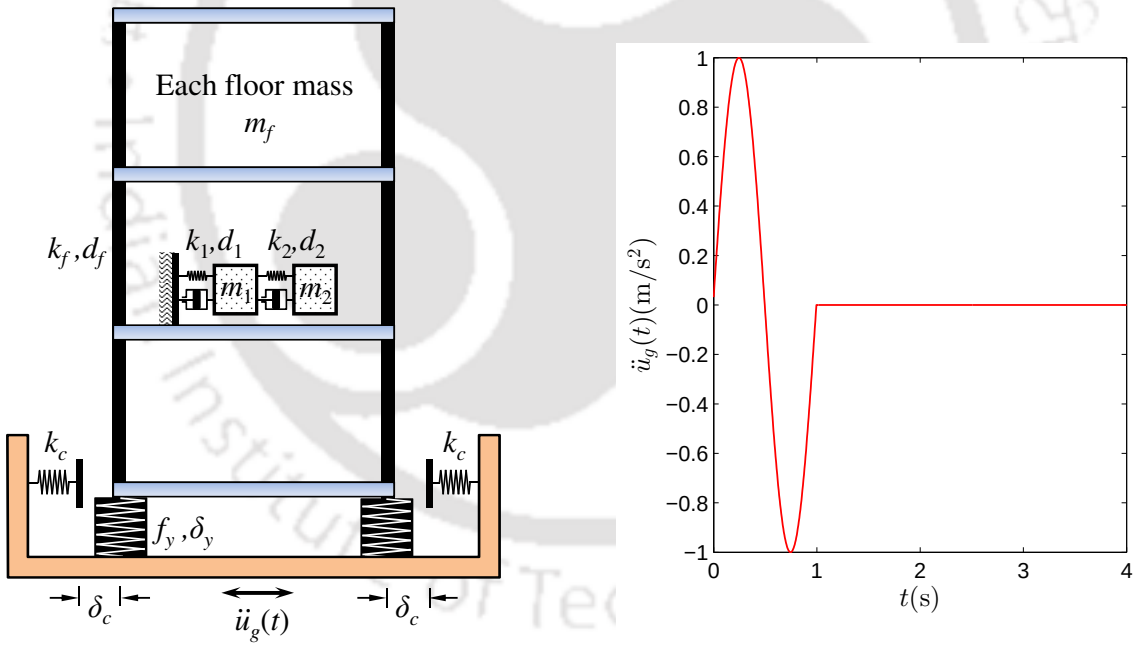

(a) (b)

Figure 4.15: Three-storey base isolated building with secondary system: (a) schematic diagram and (b) base excitation

to the floor displacement on which it is mounted. Combined effects of these criteria are considered to form the limit state which is expressed as [58]

$$g(\mathbf{x}) = 12.5(0.04 - \max_t |u_{f_i}(t) - u_{f_{i-1}}(t)|)_{i=2,3,4} + (0.5 - \max_t |\ddot{u}_g(t) + \ddot{u}_{m_2}(t)|) + 2(0.25 - \max_t |u_{f_2}(t) - u_{m_1}(t)|) \tag{4.33}$$

Table 4.9: Estimated p_f from different reliability methods in the multi-storey multi-bay building

u_o (m)	MCS	FORM	SORM	SRSM	HO-SRSM	Seq. SRSM
0.025	0.22099	0.24315	0.24895		0.19354	0.22067
		(10.03)	(12.65)		(12.42)	(0.14)
0.030	0.08974	0.10222	0.10732		0.06420	0.09009
		(13.91)	(19.60)	Number	(28.46)	(0.40)
0.035	0.03193	0.03696	0.04020	of	0.01740	0.03114
		(15.77)	(25.91)	function	(45.49)	(2.45)
0.040	0.01008	0.01182	0.01366	calls	0.00407	0.01019
		(17.28)	(35.53)	are	(59.61)	(1.13)
0.045	0.00319	0.00343	0.00360	very	0.00089	0.00320
		(7.62)	(13.11)	large	(72.21)	(0.44)
0.050	0.00100	0.00092	0.00110		0.00019	0.00101
		(8.21)	(10.12)		(80.74)	(0.84)
0.055	0.00039	0.00023	0.00030		0.00005	0.00037
		(39.96)	(23.10)		(86.56)	(3.61)

Note: Values in parentheses represent the error percentage in estimation with respect to MCS.

Table 4.10: Details of random variables in the base isolated building

Random variables	Unit	Mean	Standard deviation	*pdf*
$m_f \rightarrow x_1$	kg	$6.0 \times 10^{+3}$	$6.0 \times 10^{+2}$	Lognormal
$d_f \rightarrow x_2$	N/m	$6.0 \times 10^{+4}$	$1.2 \times 10^{+4}$	Lognormal
$k_f \rightarrow x_3$	N-s/m	$3.0 \times 10^{+7}$	$3.0 \times 10^{+6}$	Lognormal
$f_y \rightarrow x_4$	N	$2.0 \times 10^{+4}$	$4.0 \times 10^{+3}$	Lognormal
$\delta_y \rightarrow x_5$	m	5.0×10^{-2}	1.0×10^{-2}	Lognormal
$k_c \rightarrow x_6$	N/m	$3.0 \times 10^{+7}$	$9.0 \times 10^{+6}$	Lognormal
$T_p \rightarrow x_7$	s	1.0	0.2	Lognormal
$A_p \rightarrow x_8$	m/m/s	1.0	0.5	Lognormal

Note: x_1, x_2, ..., x_8 are independent.

In the above equation, $u_{f_i}(t)$, $u_{m_1}(t)$ and $u_{m_2}(t)$ represent the horizontal displacements of i^{th} floor, secondary masses m_1 and m_2 respectively. As usual, MCS generates sample size of 10^5 to determine the probability

Table 4.11: Estimated p_f from different reliability methods in the base isolated building

Method	Degree	p_f	Function calls	Error (%)	Remark
MCS	-	0.1939	10^5	-	-
FORM	-	0.2276	90	17.37	-
SORM	-	0.1384	202	28.63	-
SRSM	2	0.1951	6561	0.61	-
HO-SRSM	-	0.1987	4196	2.46	$p = [2, 2, 2, 2, 3, 6, 2, 3]$
SRSM-SPA [169]	-	0.1995	93	1.81	-
Seq. SRSM	1	0.1961	51	1.17	$q = 2^{(\text{for } it=1,2,3)}$
	2	0.1950	307	0.54	$q = 3^{(\text{for } it=1,2)}$; $q = 2^{(\text{for } it=3)}$

of failure which is 0.1939. Considering this result as reference, gradient based methods are executed which yield significant errors as shown in Table 4.11. FORM overestimates the probability of failure which suggests that the limit state is convex in this example [2]. Quadratic approximation using SORM fails to capture the curvature properly as it underestimates the p_f with large error. This shows that the gradient based methods are not reliable for solving this example. In contrary to these methods, performance of the meta-model based methods like SRSM and HO-SRSM are fairly accurate with errors $\leq 3\%$. However, the number of function evaluations required for these methods are large which make them computationally expensive. It

has been reduced by weighted SRSM with saddlepoint approximation (SRSM-SPA) demonstrated by Huang *et al.* [169] which requires 93 function evaluations resulting in 1.81% error. However, the proposed sequential SRSM needs less function calls (i.e. $n_s = 51$) compared to these methods without compromising the quality of the end result (i.e. error $< 1.81\%$). The accuracy is further improved to 0.54% with PCE degree $p = 2$ requiring 307 function calls. This proffers that the proposed method can efficiently solve complex nonlinear limit state obtained from multiple serviceability criteria often faced in the actual field conditions.

4.5.2.3 Problem 3: Geometrically Nonlinear Composite Plate

In this case, the design of a carbon-epoxy composite plate is carried out using the proposed algorithm. The composite plate, as shown in Fig. 4.16, consists of laminates stacked in proper sequence with different orientations. In the present work, geometrically nonlinear composite plate is studied for reliability analysis where the properties and dimensions of the laminates are assumed to be identical. It is analyzed using first order shear deformation theory (FSDT) where transverse normal is allowed to rotate. This, helps to include transverse shear strains in equilibrium equation where the displacement field is given by [170]

$$\left.\begin{aligned} u(\hat{x},\hat{y},\hat{z}) &= u_0(\hat{x},\hat{y}) + \hat{z}\phi_{\hat{x}}(\hat{x},\hat{y}) \\ v(\hat{x},\hat{y},\hat{z}) &= v_0(\hat{x},\hat{y}) + \hat{z}\phi_{\hat{y}}(\hat{x},\hat{y}) \\ w(\hat{x},\hat{y},\hat{z}) &= w_0(\hat{x},\hat{y}) \end{aligned}\right\} \tag{4.34}$$

In the above equation, mid-plane displacements u_0, v_0 and w_0 are associated to $\hat{x}$, $\hat{y}$ and $\hat{z}$ directions,

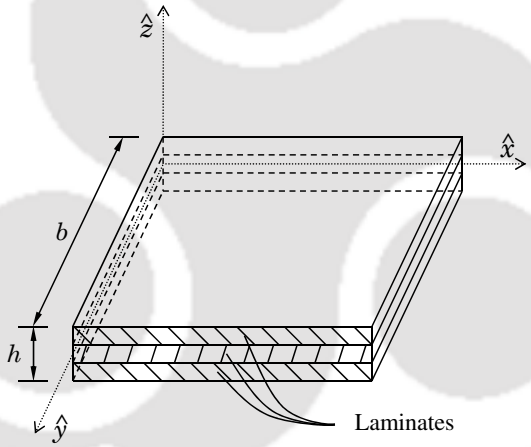

Figure 4.16: A schematic diagram of the composite plate

respectively. The rotation with respect to transverse normal denoted by $\phi_{\hat{x}}$ is about $\hat{y}$ and similarly, $\phi_{\hat{y}}$ is about $\hat{x}$. Using thin plate condition where rotations are determined by slopes of the transverse deflection and applying von-Karman assumptions, Eq. 4.34 yields [170]

$$\begin{bmatrix} \varepsilon_{\hat{x}\hat{x}} \\ \varepsilon_{\hat{y}\hat{y}} \\ \gamma_{\hat{x}\hat{y}} \end{bmatrix} = \begin{bmatrix} \varepsilon^m_{\hat{x}\hat{x}} \\ \varepsilon^m_{\hat{y}\hat{y}} \\ \gamma^m_{\hat{x}\hat{y}} \end{bmatrix} + \hat{z} \begin{bmatrix} \varepsilon^f_{\hat{x}\hat{x}} \\ \varepsilon^f_{\hat{y}\hat{y}} \\ \gamma^f_{\hat{x}\hat{y}} \end{bmatrix} \tag{4.35a}$$

$$\boldsymbol{\gamma} = \begin{bmatrix} \gamma_{\hat{x}\hat{z}} \\ \gamma_{\hat{y}\hat{z}} \end{bmatrix} \tag{4.35b}$$

where, $\gamma_{\hat{x}\hat{z}}$ and $\gamma_{\hat{y}\hat{z}}$ represent shear strains. In Eq. 4.35, superscripts m and f denote membrane and flexural components, respectively. Geometric nonlinearity caused by large deformation gives rise to additional higher

order terms in the strain field. This modifies the membrane strain to [170]

$$\left.\begin{aligned} \varepsilon^m_{\hat{x}\hat{x}} &= u_{0,\hat{x}} + \tfrac{1}{2}(w_{0,\hat{x}})^2 \\ \varepsilon^m_{\hat{y}\hat{y}} &= v_{0,\hat{y}} + \tfrac{1}{2}(w_{0,\hat{y}})^2 \\ \varepsilon^m_{\hat{x}\hat{y}} &= u_{0,\hat{y}} + v_{0,\hat{x}} + w_{0,\hat{x}}\; w_{0,\hat{y}} \end{aligned}\right\} \tag{4.36}$$

Here, the constitutive equation for a laminate is expressed as

$$\begin{Bmatrix} \sigma_1 \\ \sigma_2 \\ \tau_{12} \\ \tau_{23} \\ \tau_{13} \end{Bmatrix} = \begin{bmatrix} Q_{11} & Q_{12} & 0 & 0 & 0 \\ Q_{21} & Q_{22} & 0 & 0 & 0 \\ 0 & 0 & Q_{66} & 0 & 0 \\ 0 & 0 & 0 & Q_{44} & 0 \\ 0 & 0 & 0 & 0 & Q_{55} \end{bmatrix} \begin{Bmatrix} \varepsilon_1 \\ \varepsilon_2 \\ \gamma_{12} \\ \gamma_{23} \\ \gamma_{13} \end{Bmatrix} \tag{4.37}$$

where, Q_{ij} represents the plane stress reduced stiffness coefficients. In Eq. 4.37, these coefficients are defined along the material axes of the laminate which can be transformed into the global axes by

$$\breve{\mathbf{T}} = \mathbf{T}\mathbf{Q}\mathbf{T}^{\mathsf{T}} \tag{4.38}$$

where, $\mathbf{T}$ is the transformation matrix. This leads to inclusion of coupling terms in the formulation of the orthotropic laminate. Thus, the constitutive equation for a composite plate by adding the laminates to get an equivalent single layer is given as

$$\begin{bmatrix} \mathbf{N} \\ \mathbf{M} \end{bmatrix} = \begin{bmatrix} \mathbf{A} & \mathbf{B} \\ \mathbf{B} & \mathbf{D} \end{bmatrix} \begin{bmatrix} \varepsilon^m \\ \varepsilon^f \end{bmatrix} \tag{4.39}$$

where, $\mathbf{N}$ and $\mathbf{M}$ are the force and moment resultants, respectively. Also, $\mathbf{A}$ is the extensional stiffness matrix, $\mathbf{B}$ represents the bending-extension coupling stiffness matrix and $\mathbf{D}$ denotes the bending stiffness matrix. Here, incremental formulation of total Lagrangian is adopted to develop the geometric nonlinear equilibrium equation [170]. Hence, the virtual work equation of the undeformed plate with volume V and area A is given by

$$\int_V (\mathrm{d}\varepsilon^{\mathsf{T}}\, \sigma\, \mathrm{d}V) = \int_V (\rho_c\, \mathrm{d}u^{\mathsf{T}}\, g_c\, \mathrm{d}V) + \int_A (\mathrm{d}u^{\mathsf{T}}\, p_c\, \mathrm{d}A) \tag{4.40}$$

where, $\mathrm{d}\varepsilon$ is the virtual Green strain vector, $\mathrm{d}u$ gives the virtual displacement, σ represents Piola-Kirchoff stress vector, ρ_c is the mass density of the material, g_c is the body force per unit mass and p_c denotes the pressure applied on the plate. The displacement field can be discretized using finite elements which is given by

$$\bar{u} = \sum_{i=1}^{n_n} [\Omega_i I]\mathbf{q}_i \tag{4.41}$$

where, I is the identity matrix, Ω_i denotes the shape function for any arbitrary node i and $\mathbf{q}_i = \{u_i\ v_i\ w_i\ \phi_{xi}\ \phi_{yi}\}^{\mathsf{T}}$ represents the nodal displacements. Extending the above equation for the complete thickness yields the elemental nonlinear equilibrium equation as

$$\psi(\mathbf{q}) = \sum_{i=1}^{n_e} \left[\int_a (\breve{\mathbf{B}}^{\mathsf{T}}\, \bar{\sigma}\, \mathrm{d}a) - \bar{\mathbf{P}}_e \right] = 0 \tag{4.42}$$

where, $\breve{\mathbf{B}}$ denotes the strain-displacement matrix with nonlinear terms, $\psi(\mathbf{q})$ represents the summation of external and internal forces, $\bar{\sigma}$ gives the force and moment resultant and $\bar{\mathbf{P}}_e$ is the total external force at the element level. This nonlinear equilibrium equation can be evaluated to get the displacement vector q. In the present study, Newton-Raphson iterative technique [170] is used to solve this nonlinear equilibrium equation.

Using this FE model of a geometrically nonlinear plate, fragility analysis is carried. Table 4.12 shows the statistical properties of the random variables used in this example. Here, modified Tsai-Hill failure

criterion [75] is adopted to define the limit state which is an extension of the von-Mises distortion energy theory. The limit state based on the modified Tsai-Hill failure index $\mathfrak{F}$ is expressed as

$$g(\mathbf{x}) = 1 - \underbrace{\left\{\left(\frac{\sigma_{11}}{X}\right)^2 + \left(\frac{\sigma_{22}}{Y}\right)^2 - \left(\frac{\sigma_{11}\sigma_{22}}{X^2}\right) + \left(\frac{\sigma_{12}}{T_{12}}\right)^2\right\}}_{\mathfrak{F}} \tag{4.43}$$

where, σ_{11}, σ_{22} and σ_{12} are the laminate stresses along the respective material coordinates whereas X, Y and T_{12} represent the longitudinal, transverse and shear strengths, respectively. As shown in Eq. 4.43, limit state represents the condition when the failure index $\mathfrak{F}$ of any laminate exceeds unity.

Table 4.12: Statistical properties of the random variables in the nonlinear composite plate

Random variables	Units	Mean	cov (%)	*pdf*	Parameters	
$\nu_{12} \rightarrow x_1$	-	0.281	7.5	Lognormal	-	-
$G_{12} \rightarrow x_2$	GPa	4.500	8.8	Lognormal	-	-
$X_t \rightarrow x_3$	GPa	2.409	6.7	Lognormal	-	-
$X_c \rightarrow x_4$	GPa	1.148	18.1	Lognormal	-	-
$T_{12} \rightarrow x_5$	GPa	0.083	5.0	Lognormal	-	-
$E_1 \rightarrow x_6$	GPa	154.900	5.9	Weibull	158.820	21.6
$E_2 \rightarrow x_7$	GPa	8.700	9.5	Weibull	9.055	12.9
$Y_t \rightarrow x_8$	GPa	0.046	20.0	Weibull	0.050	5.7
$Y_c \rightarrow x_9$	GPa	0.196	15.3	Weibull	0.209	7.7

Table 4.13: Estimated p_f for different reliability methods in the nonlinear composite plate

Method	Degree	p_f	Function calls	Error (%)	Remark
MCS	-	0.1906	10^4	-	-
FORM	-	0.1965	220	3.10	-
SORM	-	0.1963	751	2.99	-
SRSM	-	0.2187	1280	14.74	$p = [1,1,1,1$ $1,1,1,4,1]$
	-	0.2632	1536	38.09	$p = [1,1,1,1$ $1,1,1,5,1]$
HO-SRSM	-	0.1900	3324	0.31	$p = [2,2,2,2$ $2,5,3,5,2]$
Seq. SRSM	2	0.1975	456	3.64	$q = 3^{(\text{for } it=1,2)}$ and $q = 2^{(\text{for } it=3,4,5)}$

A square carbon-epoxy composite plate is considered of dimension 1m $\times$ 1m and thickness 0.010m. The plate is simply supported in all four sides with uniformly distributed load of 0.090MPa acting downwards. The laminates are placed with orientation [0°/90°/0°]. To perform the FE analysis, nine noded quadrilateral element with a mesh size 8×8 is used. The random variables in this study are elastic modulus E_1 and E_2, shear modulus G_{12}, Poisson's ratio ν_{12} and strength parameters X_t, X_c, Y_t, Y_c and T_{12}. Their statistical parameters and *pdf* are adopted from Sasikumar *et al.* [75] and are mentioned in Table 4.12. Using these parameters, the reliability of the plate against modified Tsai-Hill failure criterion is evaluated by the methods described in the previous examples and the results are shown in Table 4.13. As usual, the MCS is conducted with 10^4 samples and is considered as the benchmark for further analysis. Gradient based methods (i.e. FORM and SORM) gives satisfactory results with 220 and 751 function calls respectively. The probability of failure estimated in these two cases have error around 3.1% and 2.99%. A marginal improvement in the second order method is noticed. However, the quality of the results largely depends on the initial guess which is a known drawback of the gradient based techniques. With these results in hand, SRSM and its

modified versions are tried. First, the conventional SRSM is tried with degree two and three that need 19683 and 262144 function calls. These are well above the function calls required for MCS. As each function call needs to solve nonlinear FE code to check the failure criterion involving significant computation time, these methods are not feasible. Moreover, the results from the SRSM have 14.74% and 38.09% error for two different combination of the degrees of random variables which are not satisfactory at all. Once the performance of the conventional SRSM is studied, HO-SRSM is tried with different degrees. It is found to converge with $p_f = 0.19$ that has 0.31% error with 3324 function calls. Finally, proposed sequential SRSM is used to study the reliability. The proposed method with $q = 3$ in the first two iterations followed by $q = 2$ converges after 5 iterations with error of 3.84%. It requires 456 function calls which is more than FORM but well below that required for SORM and HO-SRSM. This clearly justifies the superiority of the proposed method for actual design problems involving complex FE models as in this case.

4.5.2.4 Problem 4: Edge-cracked Plate with Axial and Shear Stresses

In this example, nonlinear plane strain problem is demonstrated where the reliability of the damaged plate is evaluated using the proposed algorithm. An edge-cracked plate exposed to unidirectional tensile and shear stresses (i.e. σ_∞ and τ_∞, respectively) at one end is solved for reliability. Fig. 4.17(a) shows the configuration of the plate along with its boundary conditions. It has a horizontal crack of length a_c at the middle. Deformation of edge-cracked plate with remote tensile and shear stresses involve mixed-mode fracture. It contains modes I and II of fracture mechanics which reflect opening and in-plane shear failure [171]. The shear intensity factors for these modes (i.e. K_{I} and K_{II}, respectively) are calculated using level set method [172]. The plate is analyzed in plane strain condition using the extended finite element method (XFEM) [173] involving four noded quadrilateral elements. This modified version of FE analysis has advantages to model crack or other localized discontinuities. XFEM avoids mesh refinement required at the crack location due to stress concentration which can be seen in Fig. 4.17(b) near the edge-crack tip. Traditional approach needs to conform the crack geometry for meshing and update it as the crack path evolves. This leads to a more computationally exhaustive FE analysis which is alleviated by XFEM. Fig. 4.17(b) shows that XFEM consists of two types of nodes, namely classical nodes and enriched nodes. Classical nodes are shown in the Fig. 4.17(b) without any marking whereas the enriched nodes are marked along the crack. Additional *enrichment functions* are incorporated on these nodes to model the discontinuity due to crack [172]. The

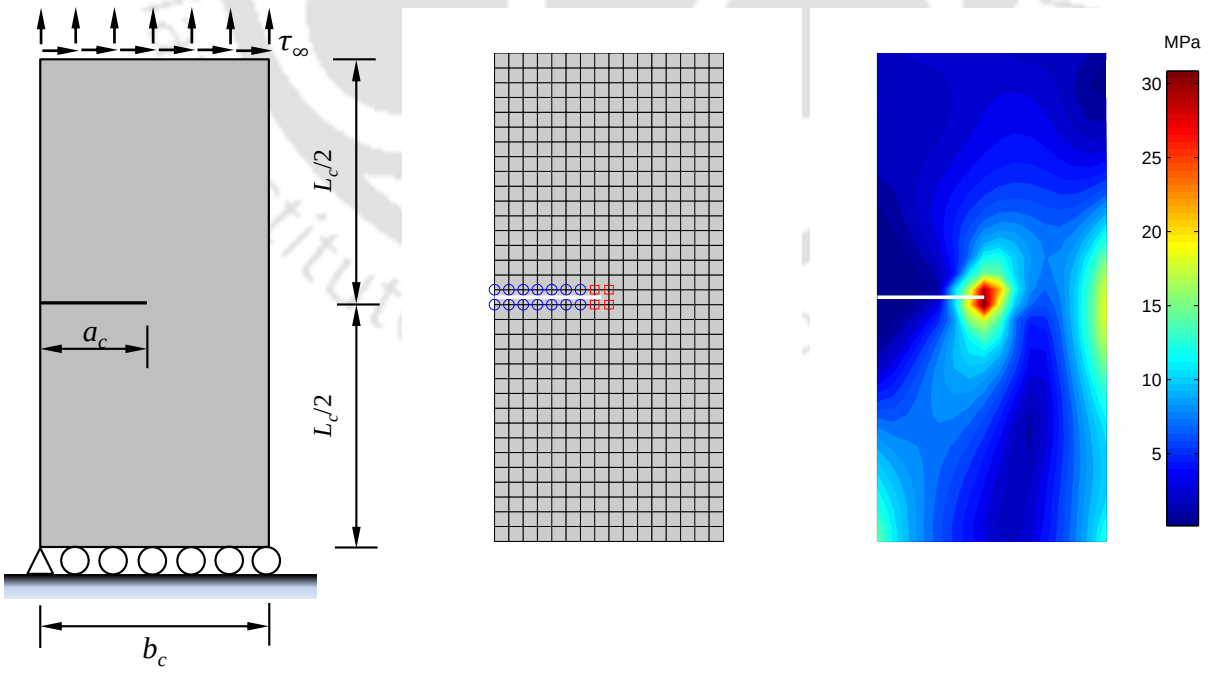

(a) (b) (c)

Figure 4.17: Edge-cracked plate with remote tensile and shear stresses: (a) schematic diagram of support condition, geometry and loads; (b) mesh details and (c) von-Mises stress contour

nodes along the crack are selected for enrichment using Heaviside step function as [172]

$$h(\mathbf{x}) = \begin{cases} +1 & \text{Above Crack} \\ -1 & \text{Below Crack} \end{cases} \tag{4.44}$$

These nodes are depicted in the Fig. 4.17(b) with a circle. Another set of nodes are highlighted by square which surrounds the crack tip. These nodes are also enriched but with a different function as Heaviside step function cannot be used for partially cracked elements. Here, the enrichment function is an asymptotic displacement field near the crack tip which is given by

$$\phi_s(x)|_{s=1,\ldots,4} = \left[\sqrt{r_o}\sin\frac{\hat{\theta}}{2},\ \sqrt{r_o}\cos\frac{\hat{\theta}}{2},\ \sqrt{r_o}\sin\hat{\theta}\sin\frac{\hat{\theta}}{2},\ \sqrt{r_o}\sin\hat{\theta}\cos\frac{\hat{\theta}}{2}\right] \tag{4.45}$$

where, r_o and $\hat{\theta}$ represents the local polar coordinates of the element. Both these enrichment functions (i.e. Eqs. 4.44 and 4.45) reflect the true field of the crack elements which are either completely or partially cut by the crack [172]. Thus, the displacement field is modified as

$$\mathrm{u}^h(\mathrm{x}) = \sum_{i\in\mathcal{N}} n_i(\mathrm{x})u_i + \sum_{j\in\mathcal{N}_h} n_j(\mathrm{x})h(\mathrm{x})\mathrm{u}_{a_j} + \sum_{k\in\mathcal{N}_\phi} n_k(\mathrm{x})\sum_{s=1}^{4}\phi_s(\mathrm{x})\mathrm{u}^s_{b_k} \tag{4.46}$$

where, $n_i(\mathrm{x})$ and u_i represent the shape function and nodal displacement, u_{a_j} and $\mathrm{u}^s_{b_k}$ are associated with the enriched nodes along the crack and at the crack tip, respectively. This, in turn, modifies the stiffness matrix to incorporate the additional degrees of freedom and is given by

$$\mathbf{K} = \begin{bmatrix} \mathbf{K}_{uu} & \mathbf{K}_{ua} & \mathbf{K}_{ub} \\ \mathbf{K}_{au} & \mathbf{K}_{aa} & \mathbf{K}_{ab} \\ \mathbf{K}_{bu} & \mathbf{K}_{ba} & \mathbf{K}_{bb} \end{bmatrix}. \tag{4.47}$$

here, subscripts u, a and b denotes the corresponding degrees of freedom associated with the traditional FE, Heaviside enriched nodes and crack tip.

Table 4.14: Properties of the random variables in the edge-cracked plate

Random variables	Unit	Mean	Standard deviation	*pdf*
$a_c \rightarrow x_1$	m	3.50	0.404	Uniform
$b_c \rightarrow x_2$	m	7.50	0.289	Uniform
$\sigma_\infty \rightarrow x_3$	N/m	1.00	0.100	Normal
$\tau_\infty \rightarrow x_4$	N/m	1.00	0.100	Normal
$E \rightarrow x_5$	MPa	30.00	3.000	Lognormal
$\nu \rightarrow x_6$	-	0.25	0.025	Lognormal

In this study, the performance function of the edge-cracked plate is given by a failure criterion based on mixed-mode fracture using maximum circumferential stress theory [171] as

$$g(\mathbf{x}) = K_{th} - \left[K_{\mathrm{I}}(\mathbf{x})\cos^2\frac{\theta(\mathbf{x})}{2} - \frac{3}{2}K_{\mathrm{II}}\sin\theta(\mathbf{x})\right]\cos\frac{\theta(\mathbf{x})}{2} \tag{4.48}$$

where, K_{th} represents the threshold fracture toughness which is measured from experiments [116] and the crack propagation angle $\theta_c(\mathbf{x})$ is evaluated using

$$\theta_c(\mathbf{x}) = \begin{cases} 2\tan^{-1}\left(\frac{1-\sqrt{1+8[K_{\mathrm{II}}/K_{\mathrm{I}}]^2}}{4K_{\mathrm{II}}/K_{\mathrm{I}}}\right) & \text{if } K_{\mathrm{II}} > 0 \\ 2\tan^{-1}\left(\frac{1+\sqrt{1+8[K_{\mathrm{II}}/K_{\mathrm{I}}]^2}}{4K_{\mathrm{II}}/K_{\mathrm{I}}}\right) & \text{if } K_{\mathrm{II}} < 0 \end{cases} \tag{4.49}$$

The properties of these random variables $\mathbf{x}$ in the present problem are listed in Table 4.14. Probability

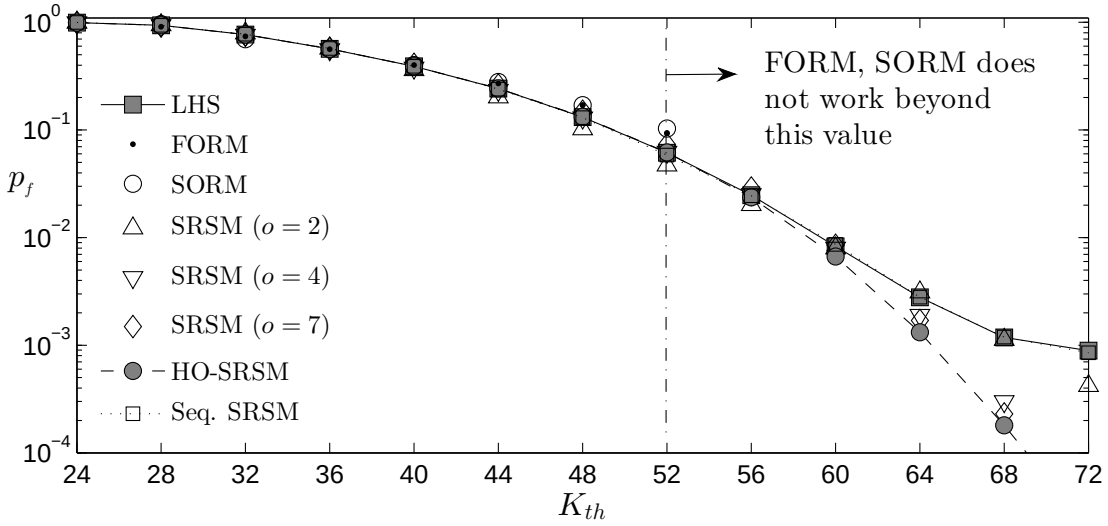

Figure 4.18: Fragility curve with respect to fracture toughness

of failure is estimated for performance function $g(\mathbf{x})$ given in Eq. (4.48) with different threshold fracture toughness values. Fig. 4.18 illustrates the p_f estimated from different methods. In this case, LHS is used as it requires smaller sample size to get the result as accurate as in MCS. Results from LHS are evaluated using 10^5 function calls and the p_f values are considered as benchmark to compare the accuracy of different methods. Gradient based approaches (i.e. FORM and SORM) consume 56 to 154 and 284 to 382 function

Table 4.15: Percentage of error in the estimated p_f with respect to LHS for different cases in the edge-cracked plate

K_{th}	FORM	SORM	SRSM			HO-SRSM	Seq. SRSM
			$p = 2$	$p = 4$	$p = 7$		
24	-	-	0.09	0.05	0.16	0.03	0.12
28	2.75	2.93	0.73	0.40	1.46	0.16	0.02
32	3.59	9.42	2.95	0.97	1.40	0.04	0.65
36	0.84	0.62	0.92	1.77	1.02	0.12	0.60
40	2.71	2.73	7.34	3.20	4.16	0.10	0.03
44	11.57	15.01	16.81	3.49	7.93	0.39	1.17
48	28.92	29.14	22.62	1.67	13.23	0.76	1.00
52	52.07	67.80	23.62	1.39	19.22	0.65	4.98
56	-	-	18.32	1.56	16.62	4.45	1.06
60	-	-	3.69	3.41	2.27	19.77	3.94
64	-	-	11.40	32.04	39.00	52.65	0.45
68	-	-	4.07	74.58	80.76	85.00	0.47
72	-	-	53.37	96.29	97.53	97.30	4.30

calls, respectively. Both these methods face non-convergence for threshold value $K_{th} \geq 52$ as shown in the Fig. 4.18. In this context, it may be noted that gradient based techniques perform satisfactorily in the high values of p_f while practical design is carried out for low p_f values, typically in the range of 10^{-3} to 10^{-4}. SRSM of degrees two, four and seven are also applied for solving this performance function which require 729, 15625 and 262144 XFEM evaluations. Among these degrees, $p = 2$ performs better near the low p_f values (i.e. $K_{th} \geq 64$) whereas, elsewhere SRSM with $p = 4$ estimates p_f accurately as shown in Table 4.15. This under-performance of $p = 4$ and 7 near the tail end is plausible due to over-fitting by higher degrees. Moreover, it may be noted that traditional SRSM is not reliable as different degrees perform differently. Similar results can be noted with HO-SRSM which also experiences nearly accurate ($\leq 5\%$ error) estimation of p_f up to $K_{th} = 52$ using 698 function calls. This method also under-performs with higher degree ($p = 4$ and 7) in the area where $K_{th} \geq 60$. Contrary to these meta-models, sequential SRSM yields $\leq 5\%$ error throughout the fragility curve as shown in the Fig. 4.18. Similar to previous examples, it considers $q = 3$ for

the first two iterations using 170 function calls followed by $q = 2$ adding 13 functions calls in every successive iterations. Altogether, it utilizes 170 to 248 function evaluations to estimate the p_f for different K_{th}. From these results, it can be inferred that the proposed method is able to estimate the probability of failure accurately using optimal computational cost for complex problems involving time exhaustive nonlinear FE analysis.

4.6 Summary

An efficient reliability analysis using sequential development of the stochastic response surface is demonstrated here. In the recent past, few literatures, as discussed in Chapter 1, have tried different ways to populate support points using a sequential generation which still requires further improvements for efficiency. These past literatures have either attempted to search the input space for limit state or sequentially generate the tensor product of sample sub-grids. A novel idea is presented in this study where an efficient combination of both is illustrated for the reliability analysis using MLS based SRSM coupled with sparse grid interpolation scheme. In this process, global response surface is developed using MLS based PCE as it provides better fitting due to its moving character, even for low polynomial degree. The orthogonality offered by basis functions help in the stability of the meta-model. Clenshaw-Curtis sparse grid scheme generates support points using selective tensor product based on the hierarchy. The sequential development of the meta-model is performed by locating the most probable failure point. This helps in producing more support points using the sparse grid scheme in its vicinity. The degree of the polynomials and the level of the sparse grid are adjusted so that it offers significant flexibility to optimize the computational cost without compromising with the accuracy of the end result. In this context, any standard optimization tool may be adopted as the proposed method imposes no restriction. Continuous and differentiable penalty function such as bulge can be introduced to find multiple failure points, if any. Using the proposed algorithm, different benchmark problems with varying level of complexities are solved to demonstrate the level of accuracy along with the computational cost involved in the reliability analysis. Finally, two reliability based design problems involving nonlinear FE analysis are considered. All these results clearly prove the superiority of the proposed method for large class of practical problems compared to other methods available in the literature. Overall, it proves to be an effective tool for reliability analysis for problems with large dimensions and other associated complexities. With simple modifications, the proposed method can be adopted for problems with multiple performance functions, spatial variation and uncertainty quantification.

Chapter 5

High Dimensional Model Representation (HDMR)

5.1 Introduction

Reliability analysis and subsequent design optimization of large real-life structures are often complex and offer several challenges e.g. formulation of limit state to accommodate different design criteria, optimization scheme for economic design, computational cost among many others. The issue of computational cost is generic for problems involving expensive FE models among these challenges. It arises due to either the large ensemble required for population based methods to evaluate the low probability of failure or the strong correlation between the dimensions (i.e. number of input variables) and the number of support points in the surrogate reliability methods. In case of polynomial based meta-models, the efficiency is often dictated by the degree of the polynomial which faces contradicting objectives – number of support points and accuracy of fit. Although this contradiction is prevalent in the approximation methods, adequate accuracy can be attained using less number of support points using orthogonal terms. In this context, dimension decomposition based meta-model approach (e.g. HDMR) has gained a lot of attention in the recent past due to its versatility. This is studied here and a new algorithm is proposed for accurate approximation of the limit state followed by efficient estimation of the probability of failure.

5.2 Formulation of HDMR

Dimension decomposition or HDMR and its variants developed in the recent past have become an efficient tool for uncertainty quantification and reliability analysis of problems with large number of random variables [115, 117, 118]. Efficiency of these techniques depend on the quality of approximation of the original performance function. It also aims to achieve a notable reduction in computational complexity by avoiding insignificant correlations between the higher order terms in input and output. Here, the term *correlation* means the mutual effect of the variables which is distinct and not related to its usual definition in statistical sense [112]. In this formulation, a multivariate function is expressed by series of component functions that are sequentially summed based on the hierarchy. These component functions represent the individual as well as combined effects of the input variables denoted by their *order*. Hence, it simplifies a multidimensional output to a sum of functions having fewer variables within the acceptable accuracy [112]. This makes it an attractive meta-modelling technique especially for problems with large dimensions.

Assume an integrable function $g(\bullet)$ defined in a unit hypercube of dimension n (i.e. $\mathbb{I}^n$). Decompose this multidimensional function into the summands of different dimensions with finite hierarchical expansion based

on the analysis of variances (ANOVA). The symbolic expression of this decomposition is as follows [127]

$$g(\mathbf{x}) = \sum_{j \subset \{1,2,\ldots,n\}} g_j(\mathbf{x}_j) \tag{5.1}$$

where, $\mathbf{x}_j$ represents the subset of the variables, $\{x_{j_1}\, x_{j_2} \cdots x_{j_o}\}$ for $j = \{j_1, j_2, \ldots, j_o\}$. Thus, Eq. 5.1 can be expanded into

$$\begin{aligned} g(\mathbf{x}) = g_0 + \sum_{i_1=1}^{n} g_{i_1}(x_{i_1}) + \sum_{i_1=1}^{n} \sum_{i_2 \geq i_1}^{n} g_{i_1 i_2}(x_{i_1}, x_{i_2}) + \ldots \\ + \sum_{i_1=1}^{n} \cdots \sum_{i_o \geq i_{o-1}}^{n} g_{i_1 i_2 \ldots i_o}(x_{i_1}, x_{i_2}, \ldots x_{i_o}) + \ldots + g_{12\ldots n}(x_1, x_2, \ldots, x_n) \end{aligned} \tag{5.2}$$

Summands in the above expression depicts the influence of the corresponding variables and their combind effect to get the function $g(\mathbf{x})$. The first function g_0 in Eq. 5.2 is of order zero and denotes mean response. The second term is the univariate function $g_{i_1}(x_{i_1})$ of variable x_{i_1} which is independent from the other variables. This first order component function can be nonlinear depending upon the output function $g(\mathbf{x})$. The bivariate function $g_{i_1 i_2}(x_{i_1}, x_{i_2})$ is a second order term which represents the interactive responses of the variables x_{i_1} and x_{i_2} in $g(\mathbf{x})$. Similarly, with the increase in the subset of the variables for the higher order summands, corresponding effects of the associated variables on $g(\mathbf{x})$ are considered. The last component $g_{12\ldots n}(x_1, x_2, \ldots, x_n)$ is of n^{th} order and provides a collective residual effect of all the variables $x_1, x_2, \ldots, x_n$ on the output $g(\mathbf{x})$. For a given problem, the order of the summands in Eq. 5.2 (say, up to o^{th} order term) is suitably determined by the designer. In general, an order ≤ 3 is found to be sufficient for most of the problems [113]. This is justified based on the practical implementations as the influences of higher order terms are normally negligible and its inclusion may result in slow convergence. Hence, a computationally efficient and reduced order approximation of the the output function $g(\mathbf{x})$ can be obtained using the HDMR. The application of this methodology is not just restricted to weak contributions of the higher order input variable correlations but can be extended to address its strong contributions without any difficulty.

Based on the methods adopted to determine the component functions, it can be broadly classified as – *ANOVA-HDMR* [174] and *Finite Difference-HDMR* [114]. A brief discussion is given on these approaches in the following sections.

5.2.1 ANOVA-HDMR

The HDMR constructed using the analysis of variance is often employed for randomly generated support points and hence, this approach is also referred as Random Sampling based HDMR [119]. The component functions of this HDMR are evaluated by forming subfunctions through an integral or unconditional averaging which is given by

$$g_0 = \int_{N_n} g(\mathbf{x}) \mathrm{d}\mathbf{x} \tag{5.3a}$$

$$g_{i_1}(x_{i_1}) = \int_{N_{n-1}} g(\mathbf{x}) \mathrm{d}\mathbf{x}_{i_1} - g_0 \tag{5.3b}$$

$$g_{i_1 i_2}(x_{i_1}, x_{i_2}) = \int_{N_{n-2}} g(\mathbf{x}) \mathrm{d}\mathbf{x}_{i_1 i_2} - g_{i_1}(x_{i_1}) - g_{i_2}(x_{i_2}) - g_0 \tag{5.3c}$$

for 0^{th}, 1^{st}, 2^{nd} orders and so on. In the above expression, $\mathrm{d}\mathbf{x}_{i_1} = \prod_{j=1}^{n} \mathrm{d}x_j$, $\forall\ j \neq i_1$ and $\mathrm{d}\mathbf{x}_{i_1 i_2} = \prod_{j=1}^{n} \mathrm{d}x_j$, $\forall\ j \neq i_1,\ i_2$. The component functions provide exclusive contribution to the output by subtracting all the lower hierarchial component terms associated with them. It continues till the n^{th} order where the final residual contribution is added to evaluate the output as specified above. Hence, it implies that the integral of any component function over the associated variables is zero [175]. This satisfies the orthogonality relationship between the different component functions in the HDMR.

The 0^{th} order component function (i.e. g_0) denotes the integral over the entire dimension which means that it

doesn't considers the influence of any random variable and can be evaluated by calculating the unconditional mean as

$$g_0 = \int_{N_n} g(\mathbf{x})\mathrm{d}\mathbf{x} \approx \frac{1}{n_s} \sum_{1 \le i \le n_s} g(\mathbf{x}^{(i)}) \tag{5.4}$$

over the input domain (i.e. $\mathbb{I}^n$). In case when $n_s \to \infty$ the estimation of g_0 becomes accurate, however an adequate sample size can also provide nearly accurate estimation of this component function for finite n_s. Further, to obtain the other component functions require freezing the associated random variables at fixed values. This direct estimation from averaging makes it impractical for efficient application. To address this issue, polynomial based expansion is often employed and thus, the second and third hierarchy of component functions can be determined by

$$g_{i_1}(x_{i_1}) \approx \sum_{1 \le j_1 \le p} \alpha_{j_1}^{i_1} \varphi_{j_1}(x_{i_1}) \tag{5.5a}$$

$$g_{i_1 i_2}(x_{i_1}, x_{i_2}) \approx \sum_{1 \le j_1, j_2 \le p} \alpha_{j_1 j_2}^{i_1 i_2} \varphi_{j_1}(x_{i_1}) \varphi_{j_2}(x_{i_2}) \tag{5.5b}$$

for different random variables and their combinations, respectively. In Eq. 5.5, $\varphi(\bullet)$ represents the polynomial basis utilized to approximate the component function and α is the unknown coefficient associated with the basis term which is evaluated by

$$\alpha_{j_1}^{i_1} \approx \frac{1}{n_s} \sum_{1 \le i \le n_s} g(\mathbf{x}^{(i)}) \varphi_{j_1}(x_{i_1}^{(i)}) \tag{5.6a}$$

$$\alpha_{j_1 j_2}^{i_1 i_2} \approx \frac{1}{n_s} \sum_{1 \le i \le n_s} g(\mathbf{x}^{(i)}) \varphi_{j_1}(x_{i_1}^{(i)}) \varphi_{j_2}(x_{i_2}^{(i)}) \tag{5.6b}$$

It can be noted that the determination of these coefficients require same support points for every order which makes it attractive for statistical applications.

5.2.2 Finite Difference-HDMR

In this form of dimension decomposition, performance function $g(\mathbf{x})$ in Eq. 5.2 is expanded with respect to a fixed reference point $\mathbf{c} = \{c_1, c_2, \ldots, c_n\}$ defined in the variable space. Thus, it is also known as cut-HDMR [112], Anchored Dimension Decomposition [114] or Anchored ANOVA-HDMR [127]. Use of this reference point helps to evaluate the component functions of different dimensions by cutting the function along a line, surface, sub-volume etc. Hence, $\hat{g}(\bullet)$ in the Eq. 5.2 denotes the value of $g(\bullet)$ at the reference point $\mathbf{c}$. Whereas, $\hat{g}(x_j)$ represents the function at the coordinates of the reference point except for the j^{th} variable which is replaced by x_j i.e. $g(c_1, c_2, \ldots, c_{j-1}, x_j, c_{j+1}, \ldots, c_n)$. Similar notation is followed for the multiple input variables such as $g(c_1, c_2, \ldots, c_{i_1-1}, x_{i_1}, c_{i_1+1}, \ldots, c_{i_2-1}, x_{i_2}, c_{i_2+1}, \ldots, c_n)$ for $\hat{g}(x_{i_1}, x_{i_2})$ and so on. This means the 0^{th} order term g_0 is the output function evaluated at the reference point i.e. $g(\mathbf{c})$. The 1^{st} order terms $g_{i_1}(x_{i_1})$ are evaluated along the variable x_{i_1} axis passing through the $\mathbf{c}$ after neglecting all higher order terms and by deducting 0^{th} order term from $g(\mathbf{x})$. Likewise, 2^{nd} order terms $g_{i_1 i_2}(x_{i_1}, x_{i_2})$ are evaluated along a bivariate grid formed by the variables x_{i_1} and x_{i_2}. To ensure the unique contribution of the bivariate, all the lower order terms are subtracted as given by

$$g_0 = \hat{g} \tag{5.7a}$$

$$g_{i_1}(x_{i_1}) = \hat{g}(x_{i_1}) - g_0 \tag{5.7b}$$

$$g_{i_1 i_2}(x_{i_1}, x_{i_2}) = \hat{g}(x_{i_1}, x_{i_2}) - g_{i_1}(x_{i_1}) - g_{i_2}(x_{i_2}) - g_0 \tag{5.7c}$$

Similarly, higher order terms ($o > 2$) can also be expressed, if required.

In this study, component functions up to the 1^{st} and 2^{nd} order terms are considered for the meta-modelling. Higher order terms (ϵ_1 and ϵ_2) in the expansion (i.e. Eq. 5.2) are denoted as the residual error for the 1^{st}

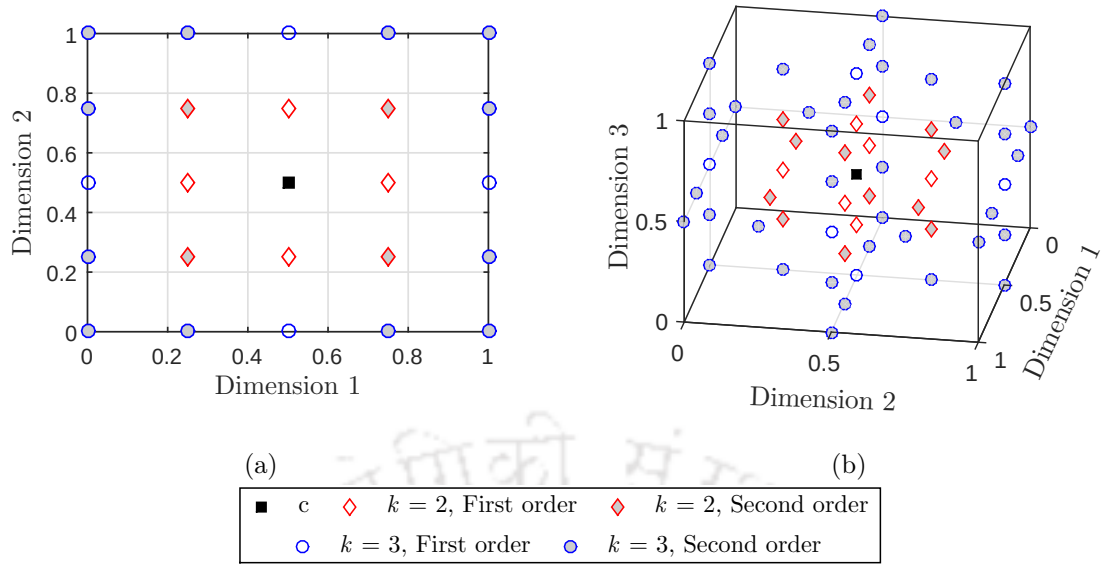

Figure 5.1: Schematic presentation of the support points generated in the conventional finite difference HDMR for (a) $n = 2$ and (b) $n = 3$

and 2nd order, respectively. Therefore, Eq. 5.2 is simplified up to the 1st order term as

$$g(\mathbf{x}) = g_0 + \sum_{i_1=1}^{n} g_{i_1}(x_{i_1}) + \epsilon_1 \tag{5.8}$$

and up to the 2nd order term as

$$g(\mathbf{x}) = g_0 + \sum_{i_1=1}^{n} g_{i_1}(x_{i_1}) + \sum_{i_1=1}^{n} \sum_{i_2 \geq i_1}^{n} g_{i_1 i_2}(x_{i_1}, x_{i_2}) + \epsilon_2 \tag{5.9}$$

Substituting Eqs. 5.7a and 5.7b in Eq. 5.8 yields

$$g(\mathbf{x}) = \sum_{i_1=1}^{n} g(c_1, c_2, \ldots, c_{i_1-1}, x_{i_1}, c_{i_1+1}, \ldots, c_n) - (n-1)g(\mathbf{c}) + \epsilon_1 \tag{5.10}$$

while substituting Eq. 5.7 up to 2nd order in Eq. 5.9 gives

$$\begin{aligned} g(\mathbf{x}) = & \sum_{i_1=1}^{n} \sum_{i_2 \geq i_1}^{n} g(c_1, c_2, \ldots, c_{i_1-1}, x_{i_1}, c_{i_1+1}, \ldots, c_{i_2-1}, x_{i_2}, c_{i_2+1}, \ldots, c_n) \\ & - (n-2) \sum_{i=1}^{n} g(c_1, c_2, \ldots, c_{i-1}, x_i, c_{i+1}, \ldots, c_n) + \frac{(n-2)(n-1)}{2} g(\mathbf{c}) + \epsilon_2 \end{aligned} \tag{5.11}$$

On neglecting the residual error terms (i.e. ϵ_1 and ϵ_2) in Eqs. 5.10 and 5.11, the approximation of the original function $g(\mathbf{x})$ is expressed as follows

$$\tilde{g}(\mathbf{x}) = \sum_{i=1}^{n} g(c_1, c_2, \ldots, c_{i-1}, x_i, c_{i+1}, \ldots, c_n) - (n-1)g(\mathbf{c}) \tag{5.12}$$

and

$$\tilde{g}(\mathbf{x}) = \sum_{i_1=1}^{n}\sum_{i_2\geq i_1}^{n} g(c_1, c_2, \ldots, c_{i_1-1}, x_{i_1}, c_{i_1+1}, \ldots, c_{i_2-1}, x_{i_2}, c_{i_2+1}, \ldots, c_n) - (n-2)\sum_{i=1}^{n} g(c_1, c_2, \ldots, c_{i-1}, x_i, c_{i+1}, \ldots, c_n) + \frac{(n-2)(n-1)}{2} g(\mathbf{c}) \tag{5.13}$$

It may be noted that the dimension decomposition based expansion is exact along the defined hyperplane cut through the reference point. However, interpolation is required to determine the output at any arbitrary point $\mathbf{x}$ in the variable space. This interpolation is guided by the functional values at the equally spaced sampling points (i.e. support points). Considering the contributions of the support points, the 1st order representation of the function $g(\mathbf{x})$ is

$$\tilde{g}(\mathbf{x}) = \sum_{i=1}^{n}\sum_{j=1}^{n_s} \varphi_j(x_i)\hat{g}(x_i^j) - (n-1)g_0 \tag{5.14}$$

while the 2nd order approximation is given by

$$\tilde{g}(\mathbf{x}) = \sum_{\substack{i_1,i_2=1\\ i_2\geq i_1}}^{n}\sum_{j_1,j_2=1}^{n_s} \varphi_{j_1 j_2}(x_{i_1}, x_{i_2})\hat{g}(x_{i_1}^{j_1}, x_{i_2}^{j_2}) - (n-2)\sum_{i=1}^{n}\sum_{j=1}^{n_s} \varphi_j(x_i)\hat{g}(x_i^j) + \frac{(n-2)(n-1)}{2} g_0 \tag{5.15}$$

In Eqs. 5.14 and 5.15, $\varphi_j(x_i)$ and $\varphi_{j_1 j_2}(x_{i_1}, x_{i_2})$ are the interpolation coefficients which can be determined by techniques like Lagrange interpolation [3,116,176], MLS [117,118] among many others. Also in the above equations, x_i^j denotes the coordinate of x_i for the j^{th} support point. These support points are generated along the sub-volumes using the reference point $\mathbf{c}$ based on the order of the component functions. It implies that the 0^{th} order component function is evaluated by generating the reference point $\mathbf{c}$. The axial points of the variables passing through the $\mathbf{c}$ are generated for the 1st order component functions. Following this sequence, points on the plane of the binary variables passing through the $\mathbf{c}$ are generated for the 2nd order component functions and so on. This can be clearly explained using a space $\mathbf{x} \in [0,1]$ where the reference point $\mathbf{c}$ is assumed at $[0.5, 0.5]$ or $[0.5, 0.5, 0.5]$ as shown in Figure 5.1 for 2D and 3D, respectively. As suggested by Chowdhury *et al.* [117,123] and others [3,116,118,121,122,124–126,176,177], these support points can be generated using the coordinates $c_i - (k-j_1)\sigma_i$, c_i and $c_i + (k-j_2)\sigma_i$. Here, σ_i is the standard deviation of x_i which is assumed to be 0.25 for all the variables in the Fig. 5.1 for demonstration when $j_1 = 1, 2, \ldots, k-1$ and $j_2 = k-1, \ldots, 2, 1$. In this formulation, the total number of support points is given by $n_s = \sum_{i=0}^{o} \frac{n!(n_a-1)^i}{(n-i)!i!}$ where, $n_a = 2k-1$ is the number of points on the axis passing through the $\mathbf{c}$. The factor k is a positive integer that signifies the level of the points required to populate the variable space.

It can be noted that a full grid demands functional evaluations at each combination of points making it computationally exhaustive. An efficient algorithm using the sparse grid scheme is described in the following section to reduce this computational burden.

5.3 Adaptive Finite Difference-HDMR

The present study aims to explore the benefits of multiple dimension decompositions coupled with MLS based fitting of orthogonal polynomials. The choice of the orthogonal polynomial is due to its faster convergence in L^2 sense where regular polynomial often suffers ill-conditioning and hence, fails to converge [17,58]. The formulation of the proposed method is presented below followed by the algorithm used for reliability analysis.

In the conventional dimension decomposition, unknown coefficients in Eqs. 5.14 and 5.15 are determined directly using original function values by Lagrange interpolation [3,116,176]. Usually, a single dimension decomposition of given order is employed to construct the response surface. However, researchers [126,176,177] have suggested multiple decompositions for limit states with more than one MPP. These methods use two

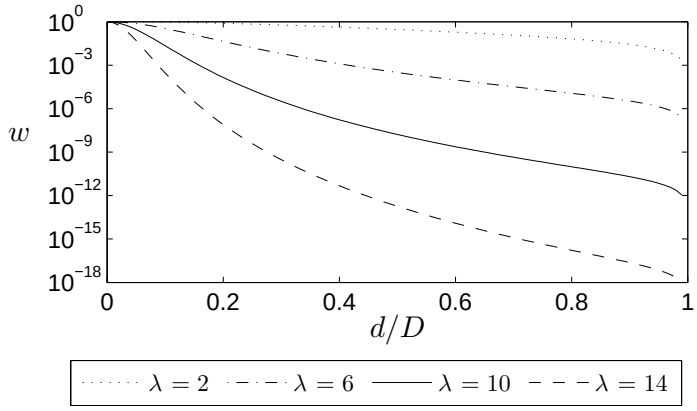

Figure 5.2: Weight function used in MLS

iterations to construct the response surface. The first step involved construction of the global response surface followed by locating the MPPs whereas the second iteration is dedicated to the local response surfaces with MPPs as the reference points. They try to replace the limit state using the union of multiple decompositions whereas the proposed method incorporates adaptive contributions of the multiple decompositions formed in successive iterations. This facilitates its application to more general problems (with or without multiple MPPs) and proves to be efficient than the single or multiple decomposition model (available in the literature). Also, the Lagrange interpolation is replaced by PCE with MLS to map the local variations in each component function.

The weight function w used in this chapter is defined as follows [178]

$$w(\delta_{\mathbf{x}}) = \begin{cases} \frac{\left\{1+\left(\lambda_w \frac{\delta_{\mathbf{x}}}{D}\right)^2\right\}^{-\frac{1+\lambda_w}{2}} - (1+\lambda_w^2)^{-\frac{1+\lambda_w}{2}}}{1-(1+\lambda_w^2)^{-\frac{1+\lambda_w}{2}}} & \text{if } \delta_{\mathbf{x}} \leq D_r \\ 0 & \text{elsewhere} \end{cases} \tag{5.16}$$

where, D_r is the influence radius and λ_w is a constant. The spatial distribution of the weight function in Eq. 5.16 along the distance $\delta_{\mathbf{x}}$ which is scaled to D_r is presented in Fig. 5.2. From this figure, it may be noted that an increase in λ_w results in the rapid decay of the weight function resulting in higher accuracy. However, steep decay may suffer singularity in matrix inversion (see Eq. 2.10) when working close to the precision of the computational system. Hence, an appropriate value of λ_w is chosen to determine the unknown coefficients.

This new coupled application of MLS-PCE based approximation for the component functions introduces polynomial basis in Eqs. 5.14 and 5.15. Hence, the modified version of the Eqs. 5.14 and 5.15 are given by

$$\tilde{g}_{\mathrm{I}}(\mathbf{z}) = \sum_{i=1}^{n}\sum_{j=0}^{p} \mathbf{b}_j|_{z_i} \boldsymbol{\Xi}_{\mathbf{j}}(\mathbf{z_i}) - (n-1)g_0 \tag{5.17}$$

and

$$\begin{aligned} \tilde{g}_{\mathrm{II}}(\mathbf{z}) = & \sum_{\substack{i_1,i_2=1 \\ i_2 \geq i_1}}^{n}\sum_{j=0}^{p} \mathbf{b}_j|_{z_{i_1},z_{i_2}} \boldsymbol{\Xi}_{\mathbf{j}}(\mathbf{z_{i_1}}, \mathbf{z_{i_2}}) \\ & - (n-2)\sum_{i=1}^{n}\sum_{j=0}^{p} \mathbf{b}_j|_{z_i} \boldsymbol{\Xi}_{\mathbf{j}}(\mathbf{z_i}) + \frac{(n-2)(n-1)}{2} g_0 \end{aligned} \tag{5.18}$$

Thus, making it a Polynomial Dimension Decomposition technique. In the above equations, $\mathbf{b}_j|_{z_{i_1}}$ and $\mathbf{b}_j|_{z_{i_1},z_{i_2}}$ denote the unknown coefficients associated with random variable z_{i_1} in Eq. 5.17 and the combination of random variables z_{i_1} and z_{i_2} in Eq. 5.18, respectively for the j^{th} degree of the polynomial. The framework of proposed method employs iterations of dimension decomposition with different reference points $\mathbf{c}$. Each iteration constructs a new decomposition model based on separate support points generated using

the reference point for that iteration. The contribution of these multiple decompositions on the final global response surface is summed up using the weight function as expressed in Eq. 5.16 which is given by

$$\tilde{g}(\mathbf{z}) = \frac{\sum_{i_1=1}^{it} w(|\mathbf{z}-\mathbf{z}^{*,i_1-1}|_2)\tilde{g}^{i_1}(\mathbf{z})}{\sum_{i_1=1}^{it} w(\underbrace{|\mathbf{z}-\mathbf{z}^{*,i_1-1}|_2}_{\delta_{\mathbf{z}}})} \tag{5.19}$$

where, $\tilde{g}^{i_1}(\bullet)$ represents the outcome from the individual decomposition. Hence, the mixed-order formulation is expressed as

$$\tilde{g}(\mathbf{z}) = \frac{\sum_{i_2=1}^{j} w(|\mathbf{z}-\mathbf{z}^{*,i_2-1}|_2)\tilde{g}_{\text{II}}^{i_2}(\mathbf{z}) + \sum_{i_1=j+1}^{it} w(|\mathbf{z}-\mathbf{z}^{*,i_1-1}|_2)\tilde{g}_{\text{I}}^{i_1}(\mathbf{z})}{\sum_{i_1=1}^{it} w(|\mathbf{z}-\mathbf{z}^{*,i_1-1}|_2)} \tag{5.20}$$

here, j and it denote iterations with order $o = 2$ and total number of iterations, respectively. Moreover, the influence radius D_r in Eq. 5.16 is also different for each iteration and is equal to the maximum distance between the support points and the reference point of that iteration. This means, if the location of $\mathbf{z}$ is outside the bounds of the support points in the i_1^{th} decomposition then its contribution is neglected for that point. It can be noted that the expression in Eq. 5.19 is extendable to any combination of order o.

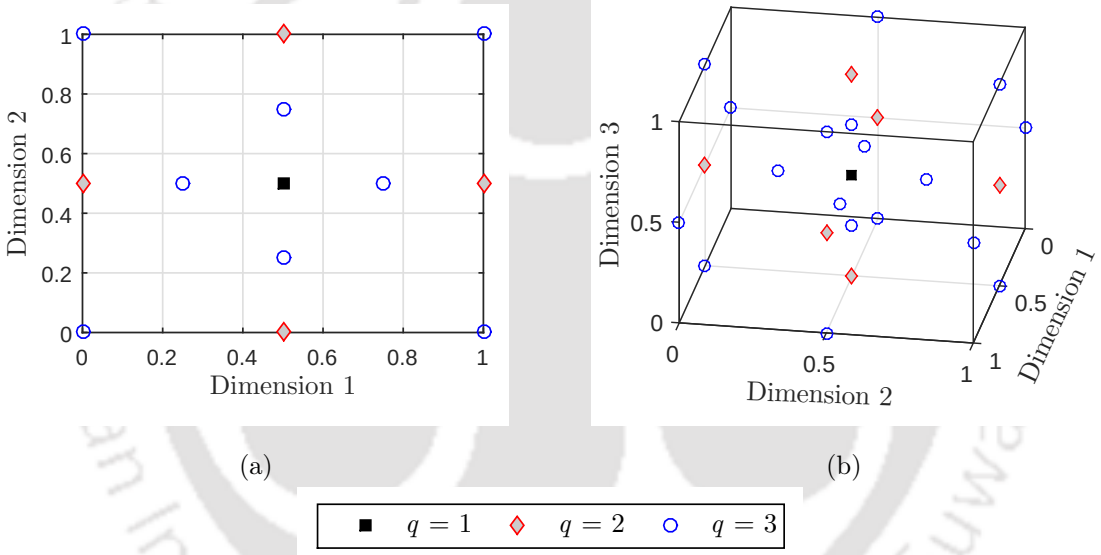

Figure 5.3: A schematic presentation of the Clenshaw-Curtis sparse grid for (a) $n = 2$ and (b) $n = 3$

Following this formulation, a judicious selection of the support points using sparse grid scheme is considered in this study to address the exponential rise in the support points with the increase of dimension in a full grid scheme. Based on $|\mathbf{i}|_1$, product grids are selected as per Eq. 4.22 and the resulting sparse grid for two and three dimensions are shown in the Fig. 5.3(a) and 5.3(b). It can be noticed that the sparse grid contains fewer nodes than the corresponding product grid. However, the novelty of this proposal is to generate these sparse grids sequentially in each successive iterations. The level of sparse grid q in Eq. 4.22 may or may not be varied in the successive iterations based on the convergence. Thus, present method lays no restriction on the choice of the level q but a tradeoff can be made by the designer to limit the total number of support points in different iterations. Coordinates of the sparse grid points, formed using Eq. 4.24, are given in unit space which requires transformation of these points to the original space where random variable $\mathbf{x}$ is defined. Recently, Chakraborty and Chowdhury [179] have proposed a distribution based support point generation scheme where uniform random sample from Sobol' sequence is transformed as per the given distribution of the random variable using CDF mapping. Similarly, the present study also employs the transformation of sparse grid coordinates to the original space. This step is required in order to be consistent with the equidistant generation of the points for $\mathbf{z}$. Therefore, the desired sub-volumes are cut to form the finite difference HDMR in the standard normal space. As suggested previously, Hermite polynomials scheme is adopted in the present study, however one can extend it for any other orthogonal polynomial scheme [51].

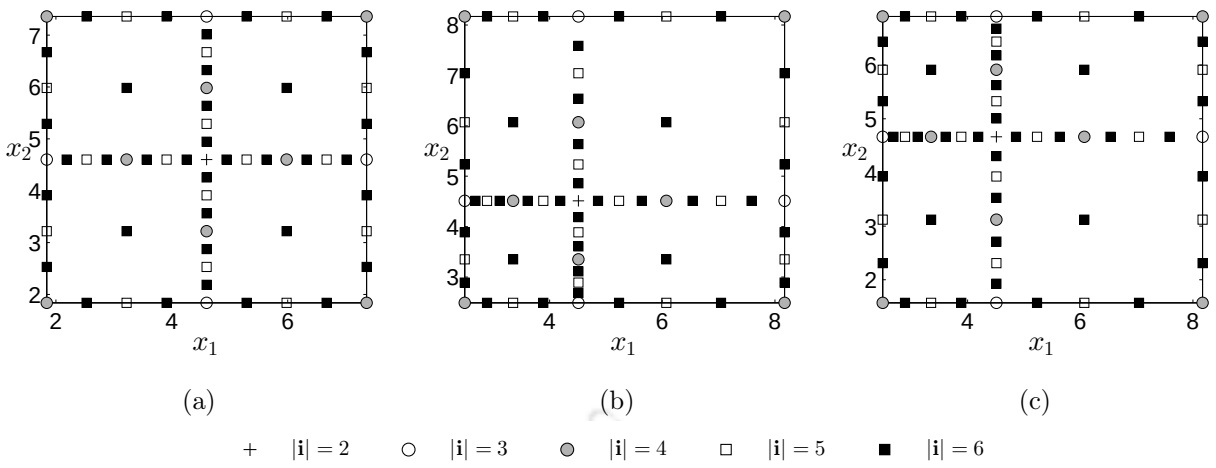

Figure 5.4: Support points generated by sparse grid for different probability distributions (a) Normal–Normal, (b) Lognormal–Lognormal and (c)Lognormal–Weibull

This will result in the development of generalized PCE (gPCE) under HDMR framework which is beyond the scope of the present thesis and hence, it is not discussed here. Once the locations in the standard normal space $\Omega_{\mathbf{z}}$ are evaluated, support points are transformed using CDF mapping as shown in Eq. 3.2. Following it, Fig. 5.4(a), 5.4(b) and 5.4(c) show transformed locations of the support points in the original space $\Omega_{\mathbf{x}}$ for different combination of the distributions e.g. Normal–Normal, Lognormal–Lognormal and Lognormal–Weibull with mean 4.60 and cov 20%. These figures also provide the hierarchial generation of the points as given in Eq. 4.22. This distribution adaptive sampling creates close locations, based on the distribution, which reflects the statistical importance of that region and aide in the stochastic computation. As discussed earlier, 1$^{\text{st}}$ and 2$^{\text{nd}}$ order HDMRs are employed in this study and their component functions $\hat{g}(\bullet)$ are obtained for combinations upto two random variables. Hence, the support points are formed through $\mathscr{H}_{q,n}$ for each component function.

The proposed method determines the unknown coefficients in each component function of all the decomposed levels. This requires multiple sparse grids for support points where the original function is evaluated. Usually, the computational effort associated with the meta-model is defined by the number of original function calls. However, the computation time in the construction of the meta-model (or the prediction of response by the meta-model) is often neglected. This computation cost is also important, particulary for MLS based interpolation as it is subjected to multiple matrix inversions. The interpolation is solved for each instance in the sampling schemes such as MCS or importance sampling. Thus, making the process computational exhaustive for large dimensional problems, especially when 2$^{\text{nd}}$ (or higher) order terms are used. This is due to the fact that the combinations of the random variables rises rapidly in the higher order decomposition. Hence, generation of full grids for multiple decompositions makes it expensive than the single decomposition model. Overall it limits their application to special limit states encountering more than one MPP.

Further, Fig. 5.5 demonstrates the number of support points n_s generated for different dimensions using the full grid and the sparse grid schemes. The difference between the two schemes grows with the dimension n which is more pronounced for the higher values. However, it may be noticed that the increase of q lead to more points than the other approach [117, 118, 121–126, 177]. To determine its value, n_s is calculated from the conventional grid scheme used in the MLS based finite difference-HDMR [117] for $o = 2$ (i.e. 2$^{\text{nd}}$ order). Fig. 5.5 illustrates the number of support points n_s generated from $k = 2$, 3 and 4. Similarly, n_s is evaluated for $q = 2$, 3 and 4 using the sparse grid scheme as per Eq. 4.22 as $2n + 1$, $2n^2 + 2n + 1$ and $(4n^3 + 6n^2 + 14n)/3 + 1$, respectively. In this comparison, $k = 1$ and $q = 1$ are not included because, for $n_s = 1$ both corresponds to the same reference point. For relatively low dimensional problem (say, $n < 10$), n_s from the sparse grid using $q = 2$, 3 and 4 are less than the conventional grid for 2$^{\text{nd}}$ order using $k = 2$, 3 and 4, respectively. However, n_s from $q = 4$ is more than the points generated by $k = 4$ for $n > 10$. Sparse grid generated for the high dimensional problem with $q > 3$ leads to relatively more number of points as compared to the conventional scheme whereas, for $q = 2$ and 3, Fig. 5.5 shows a significant reduction in n_s. Thus, in this study $q \leq 3$ is preferred to generate the sparse grid as it helps to reduce the computational cost significantly. The same can be said for the number of unknowns in HDMR formulation which will require

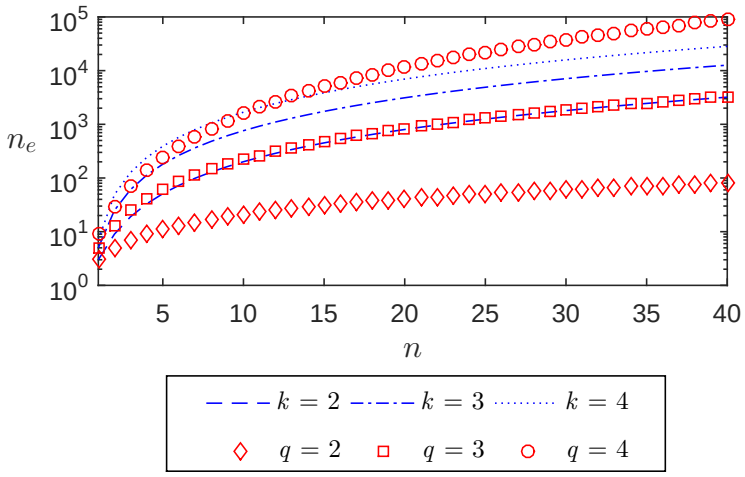

Figure 5.5: Comparison between the number of points generated using the full gird in conventional anchored dimension decomposition technique (represented by k) and the sparse grid scheme (represented by q)

more support points (i.e. higher q) as their number goes up. Hence, restricting their number will help in minimizing the computational cost. This will be further demonstrated in the numerical analysis.

It can be noted that the proposed method involves MLS based polynomial finite difference HDMR, mixed-order contribution of the decomposition models and multi-grid generation of the sparse grid points for efficient and accurate mapping of the limit state. Hence, it is termed as the *Adaptive Multiple Finite Difference HDMR* (AMFD-HDMR) technique. Using the above formulation, the step-wise procedure of the proposed AMFD-HDMR is explained in the Algorithm 5.1.

The present algorithm is developed for efficient reliability analysis however, it can be extended for other non-intrusive stochastic computation by adopting suitable objective functions. Numerical examples are solved in the following section to validate the efficiency of the proposed method.

5.4 Results and Discussion

In this section, performance of the proposed approach is demonstrated using numerical examples having different levels of complexities and the results are compared with other methods (e.g. MCS, gradient-based methods, MLS-HDMR as proposed by Chowdhury *et al.* [117] and AS-PCE by Hu and Youn [71]) to demonstrate its advantages. Different gradient-based methods employed in this study are based on the FORM [9] and SORM [10]. In this study, $o = 2$ is used for MLS-HDMR applications, unless otherwise specified. Benchmark examples and design problems illustrated here include non-algebraic function, non-differentiable function, nonlinear base isolation problem, portal frame with a large number of random variables and car crash problem with nonlinear correlation. Further, a design problem is solved that involves composite plate modelled in FE framework. Using these problems, the efficiency of the proposed reliability analysis is presented comparing different parameters like accuracy, number of function calls and computational time. Here, the accuracy is evaluated as the percentage of error i.e.

$$\epsilon_{\text{error}} = \frac{|p_f^{\text{exact}} - p_f^{\text{estimated}}|}{p_f^{\text{exact}}} \times 100 \tag{5.21}$$

In the above equation, subscripts 'estimated' and 'exact' denote the results from different methods and the actual solution, respectively. In general, MCS with adequate sample size is considered to be the exact solution. The software used for this numerical study is MATLAB® with a system configuration of Intel(R) Core(TM) i5-2430M processor of speed 2.40 GHz and 6.00 GB RAM and the CPU time consumed by different techniques are reported for comparison. However, it can be noted that the computational time may vary with the system. Results of these analyses are discussed in the forthcoming subsections.

Algorithm 5.1: AMFD-HDMR

1 **Initialize:** Assign the reference point (or initial design point) $\mathbf{c}^{it} = \mathbf{z}^{*,it-1} = \mu_{\mathbf{z}}$ for $it = 1$
2 Select a search domain $\Omega_{\mathbf{z}}$ and $\lambda_{\mathbf{z}} < 1$
3 Consider permissible errors $\mathscr{E}_1$ and $\mathscr{E}_2$, say 0.01
4 **while** $Criteria1 \longrightarrow |\mathbf{z}^{*,it-1} - \mathbf{z}^{*,it}| > \mathscr{E}_1$ and $Criteria2 \longrightarrow |\tilde{g}(\mathbf{z}^{*,it})| > \mathscr{E}_2$ **do**
5 Select q and generate support point $\mathscr{H}_{q,n}^{it}$ w.r.t. $\mathbf{c}^{it} = \mathbf{z}^{*,it-1}$
6 Support points are transformed into original space using the pdfs of $\mathbf{x}$
7 Evaluate $g(\mathbf{x})$
8 Determine polynomial basis matrix $\boldsymbol{\Xi}(\bullet)$ using Eq. 4.11 for all the component functions in Eq. 5.17, 5.18
9 Construct polynomial dimension decomposition $\tilde{g}^{it}(\bullet)$ from it^{th} iteration using $\mathscr{H}_{q,n}^{it}$ for order o
10 /* Form the adaptive mixed-order dimension decomposition */
11 Calculate $\tilde{g}(\bullet)$ $\longrightarrow$ Eq. 5.20
12 Perform optimization for region of interest $\longrightarrow$ Eq. 4.12
13 Determine the new reference point $\mathbf{z}^{*,it} \longrightarrow \mathbf{x}^{*,it} \longrightarrow \mathbf{c}^{it}$
14 Update $it \leftarrow it + 1$
15 **end**
16 /* Check for multiple regions of interest (i.e. failure region) */
17 **while** Eqs. 4.17 and 4.18 not satisfied **do**
18 Modify response surface to $\tilde{g}_m(\bullet)$ $\longrightarrow$ Eq. 4.15
19 Perform line 4–15 using $\tilde{g}_m(\bullet)$ and assign new failure point as $\mathbf{z}^{*,it+1}$
20 Update $it \leftarrow it + 1$
21 **end**
22 /* Perform population based simulations (say, importance sampling) over $\tilde{g}(\bullet)$ */
23 Estimate p_f $\longrightarrow$ Eq. 4.27

5.4.1 Benchmark Examples

In this section, different examples are studied to demonstrate the performance of the proposed AMFD-HDMR. Here, it is validated using a few benchmark examples with dimensions ranging from 2 to 10. The improvement in computational time and accuracy compared to other methods published in the literatures are presented and discussed in detail.

5.4.1.1 Example 1: Franke's Function

The details of this limit state and the associated random variables involved with this example are explained in Chapter 4. Using this limit state, reliability analysis is carried out by MCS with a sample size of 10^6. The probability of failure p_f obtained from this analysis is 0.02455 and is considered as the benchmark to check the results from other methods. MCS consumes nearly 15s for 10^6 original function evaluations which is an explicit mathematical expression in this example case. Results obtained from different methods are presented in the Table 5.1. FORM converges with large error if the initial point from an unfavourable domain e.g. $\{0.2, 0.2\}$. This leads to erroneous result if the initial guess for the starting point is inappropriate. However, it estimate p_f close to 0.02710 by considering an initial guess, say $\{0.3, 0.3\}$ that apparently lies in the favourable domain. It yields an error of $> 10\%$ using 36 function evaluations to estimate the gradients and subsequently, the MPP. The time consumption by FORM is nearly 1s which is least among the methods discussed in the Table 5.1. SORM improves this result (with error $< 3\%$) using the Hessian matrix at the MPP. MLS based HDMR as proposed by Chowdhury *et al.* [117] is then used for the reliability analysis where

Table 5.1: Results of the reliability assessment for the Franke's function

Methods	p_f	Function Calls	Error (%)	Time (s)
MCS	0.02455	10^6	-	15
FORM	0.02710	36	10.39	1
SORM	0.02386	56	2.81	1
MLS-HDMR [117]	0.02423	81	1.30	2803
Proposed Method	0.02468	41	0.53	23

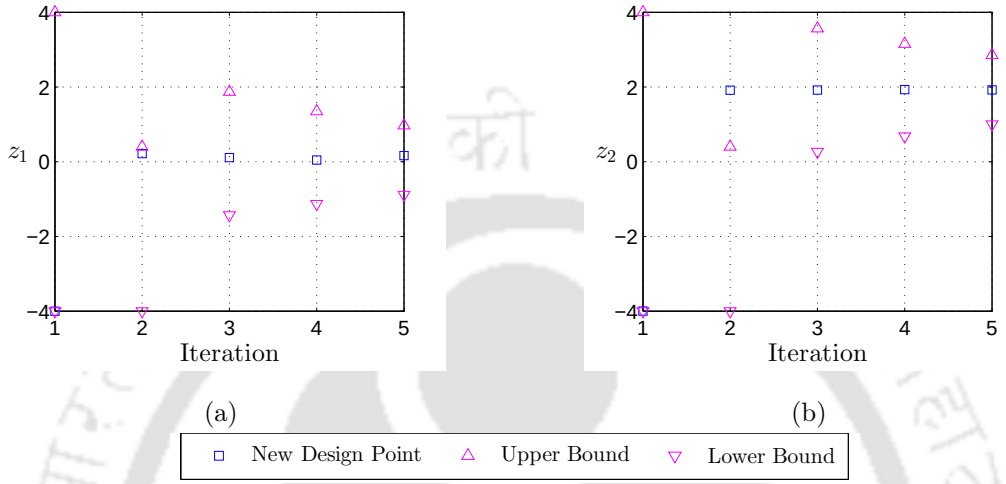

Figure 5.6: History of reference points and bounds over iterations for the Franke's function, (a) z_1 and (b) z_2

second order HDMR with complete quadratic polynomial bases for MLS is adopted. Here, $\mathbf{c} = \{0.4, 0.4\}$ (i.e. the mean $\mu_{\mathbf{x}}$) is taken as the reference point to generate the supports as prescribed in Chowdhury *et al.* [117] which are equidistant with $o = 2$. Coordinates of the individual variables are defined by $c_i - (k-1)\sigma_{x_i}$, $c_i-(k-2)\sigma_{x_i}, \ldots, c_i, \ldots, c_i+(k-2)\sigma_{x_i}$ and $c_i+(k-1)\sigma_{x_i}$. In this example, the value of k is considered to be 5 and thus, the number of function call for this analysis is 81. Using these support points, the p_f is estimated to be 0.02423 with an error of 1.30% using 2803s of CPU time. This result is also very close to the value reported by Chowdhury *et al.* [117] indicating exact replication of their method. It can be noticed that the CPU time consumption is higher for this case in spite of using 81 support points. This is due to the fact that MLS technique given in the Eq. 2.10 evaluates unknown coefficients $\mathbf{b}$ which vary according to the position of the point (i.e. $\mathbf{x}$). Hence, the solution of this equation involves matrix inversion separately for all the samples of MCS (i.e. 10^6) over the approximated surface. Also their HDMR formulation requires multiple MLS solutions for even a single point approximation depending on the number of individual variables and their combinations. Like in this case, there are two random variables which mean that the Eq. 2.10 is solved thrice (i.e. two times for the individual variables x_1, x_2 and once for their combination) for a single approximation. Moreover, if a problem has $n = 10$ then it will require $n + n(n-1)/2 = 10 + 45 = 55$ MLS solutions for one approximation. Here, it can be noticed that the major contribution is from the combination of the random variables which is higher in large dimension problems. Executing so many matrix inversions result in huge computational cost and eventually, make the process exhaustive and inefficient.

Finally, the proposed approach is used to estimate p_f following the algorithm presented in the previous section with the initial reference point $\mathbf{c}^1 = \{0.4, 0.4\}$. In the first iteration, adequate support points are generated to incorporate the failure region [i.e. $g(\mathbf{x}) \leq 0$] using $q = 3$ (i.e. the level of the sparse grid in Eq. 4.22) and decomposition order $o = 2$. This combination is used as the points generated in this level (i.e. $q = 3$) are based on the combination of random variables which is required to determine the component functions in the HDMR with order $o = 2$. Further an additional iteration is performed with $q = 3$ in view to capture the nonlinear profile of the surface. This results in adequate generation of the support points required to effectively map the desired 2^{nd} order contribution in the decomposition. With first two iterations using $q = 3$ and $o = 2$, 1^{st} order decomposition with $q = 2$ is adopted to find the MPP in the following iterations. The 1^{st} order decomposition model (i.e. $o = 1$) is selected for level $q = 2$ as it only considers axial

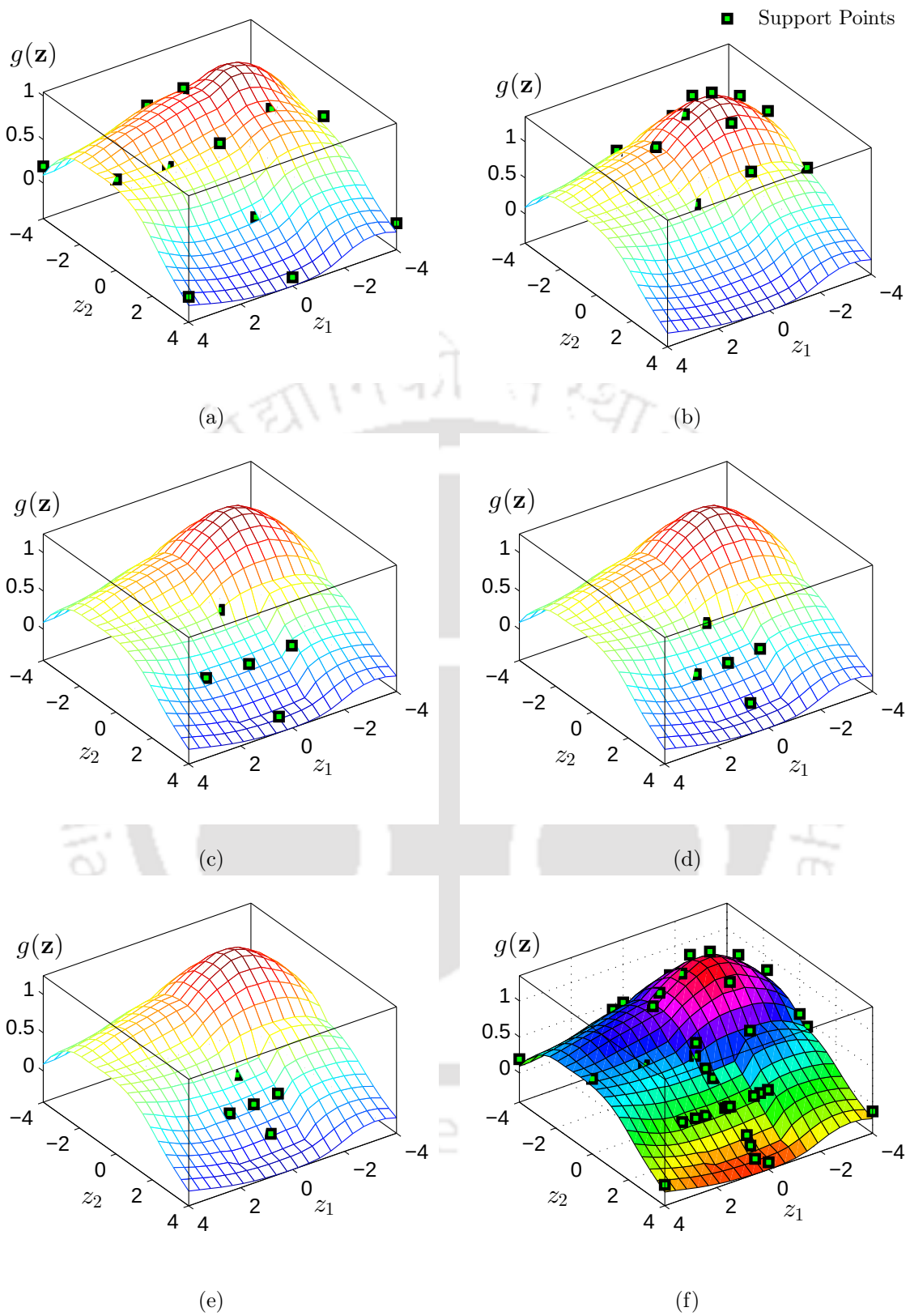

Figure 5.7: Approximation of Franke's function using the support points generated at iteration (a) 1, (b) 2, (c) 3, (d) 4, (e) 5 and (f) all

points. This strategy is followed here which is in agreement with the results demonstrated in the Chapter 4. Hence, it can be noted that here the dependence of the decomposition order o is based on the choice of the sparse grid level q. The convergence is achieved within 5 iterations using 41 support points. In the first

two iterations, support points are generated using $q = 3$ yields 13 points for each iteration. All successive iterations (i.e. 3 to 5) adopting $q = 2$ adds 5 new points per iteration. These multiple grids of different levels work in conjunction with the proposed mixed-order strategy. This tradeoff is effective as the desired number of points are limited and judiciously selected for accuracy.

Fig. 5.6 shows the convergence of the random variables x_1 and x_2 in their transformed standard normal space (i.e. z_1 and z_2, respectively). Higher and lower values of the coordinates of the new support points in each iteration (i.e. bounds) are also shown in the Fig. 5.6. It may be noted that the bounds in the successive iterations are reduced by 60%. This restricts the generation of support points closer to the reference point obtained from the previous iteration which, in turn, helps to map local variations accurately resulting in faster convergence to MPP. Although 60% reduction is used in this study, designer has the liberty to select this parameter that may vary from problem to problem. The localized adaptive response surface obtained after every iteration with support points generated in that iteration is shown in Fig. 5.7(a) to 5.7(e). Fig. 5.7(f) shows the final response surface obtained by merging all the individual surfaces. The limit state formed using the proposed method is compared with the other methods as shown in Fig. 5.8. FORM uses a first

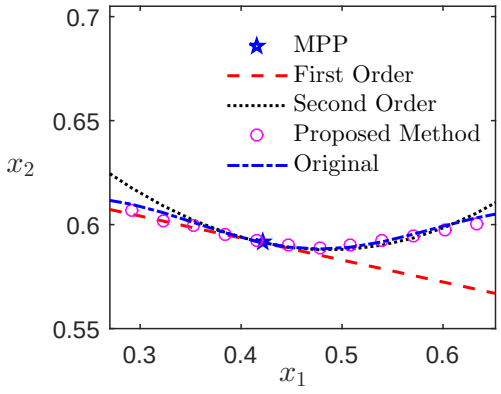

Figure 5.8: Approximation of limit state in the Franke's function using different methods

order approximation of Taylor's expansion which neglects the curvature of the limit state and results in over-estimation of failure. However, the second order approximation of Taylor's expansion (as in SORM) accommodates the curvature but overlooks the change in it. In this context, the contribution of multiple decompositions help to adaptively map the change in the curvature. This, indeed, improves the accuracy of the proposed method. Once the limit state is constructed, importance sampling with adequate sample size $n_c = 10^3$ is adopted for reliability assessment. The probability of failure p_f is estimated to be 0.02468 with an error of 0.53% which is in good agreement with the results reported by Chowdhury *et al.* [117] and MCS. However, the number of function evaluations are reduced by 49% in the proposed method. Moreover, use of multi-order dimension decomposition coupled with MLS based Hermite polynomial with importance sampling helps to reduce the number of time exhaustive matrix inversion compared to the other form of HDMR. This results in significant reduction of computational time which is 23s for this example. Although the time consumption is slightly more than MCS, FORM and SORM in this example, the advantage of the proposed method is obvious in reliability-based design optimization as it yields a significantly accurate result with minimum number of function calls.

5.4.1.2 Example 2: Non-differentiable Function

Further, the proposed AMFD-HDMR is tested with this piecewise continuous function for reliability analysis. The mathematical expression of this performance function and the statistical properties of the ten random variables associated with this example is defined in § 4.5.1.3. Using MCS with sample size 10^6, $p_f = 0.000396$ is estimated and is considered to be the benchmark. Although, the function is non-differentiable, an attempt has been made to solve this problem using FORM where differentiation is performed by the finite difference technique to calculate the direction cosines required for the estimation of the MPP and subsequently, the p_f. It consumes 115 function evaluations but yields significant error as shown in Table 5.2. However, SORM tries to improve this error which observes nearly 11% deviation from the MCS result. In this context, it may be

Table 5.2: Probability of failure of the non-differentiable function estimated from different methods

Methods	p_f	Function Calls	Error (%)	Time (s)
MCS	0.000396	10^6	-	17
FORM	0.000076	115	80.81	1
SORM	0.000353	295	10.94	1
MLS-HDMR [117]	0.000399	761	0.75	28718
Proposed Method	0.000407	610	2.78	146

noted that this numerical differentiation has no mathematical significance as the function is discontinuous and is used for demonstration purpose only. The p_f is estimated using a 2^{nd} order single-step HDMR [117] given in Table 5.2. Here, 5 equidistant support points (i.e. $k = 3$) are selected for each random variable separated by a distance equal to its standard deviation σ_{x_i}. The reference point is considered to be the mean (i.e. $\mathbf{c} = \mu_{\mathbf{x}}$) and altogether 761 function evaluations are performed to construct the 2^{nd} order HDMR. Using this method, the probability of failure is estimated to be 0.000399 as opposed to 0.000402 reported by Chowdhury *et al.* [117]. Finally, the proposed method is used with the same reference point $\mathbf{c}^1$ as the initial point and the response surface is generated where the solution converges after 10 iterations. The first two iterations generate 221 support points (i.e. $q = 3$) while the rest have 21 points in each as the q is reduced to 2. The $p_f = 0.000407$ is estimated by the proposed method which yields a marginal error of less than 3% as shown in Table 5.2. A total of 610 function calls are executed in the proposed method which reduces the number of support points n_s by nearly 20% from the other HDMR method. Moreover, the conventional HDMR using MCS for reliability evaluation consumes huge computational time as the coefficients are determined at each and every sample points in MCS. Besides the reduction in support points, the proposed algorithm is computationally less expensive as compared to another variant of HDMR (i.e. nearly 0.5%) due to the intelligent use of sequential support points and importance sampling for reliability evaluation.

5.4.1.3 Example 3: Ten-bar Truss

In this illustration, a ten-bar truss is considered whose performance is described by the serviceability based limit state given below [117, 180]

$$g(\mathbf{x}) = 18 + \delta_3(\mathbf{x}) \tag{5.22}$$

where, δ_3 denotes the deflection in the vertical direction at node 3 as shown in the Fig. 5.9. The truss is made

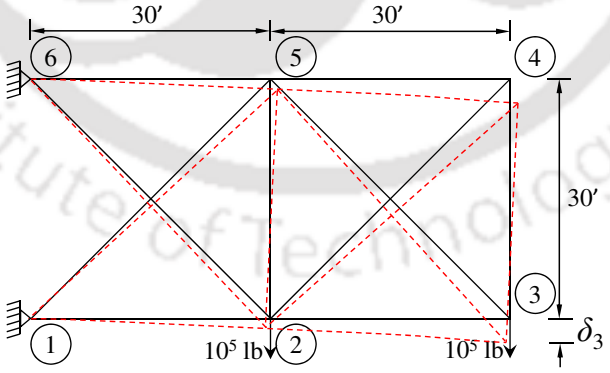

Figure 5.9: Ten-bar truss with applied loads and deformed shape

of 10 elastic bars with Young's modulus of 10^7psi. Two identical point loads of magnitude 10^5lb are applied as shown above. The truss is supported by the pinned attachments at node 1 and 6. The cross-sectional areas of the bars denoted by $x_i (i = 1, 2, \ldots, 10) \in \mathbf{x}$ are assumed to be independent normal random variables with mean 2.50in^2 and cov 0.20.

Using these properties of the random variables, five different techniques for reliability analysis are performed as described in the earlier examples and the results are listed in Table 5.3. MCS with one million samples provides a p_f of 0.1399 by consuming 227s while variants of gradient based method with 92 and 272 function

Table 5.3: Results from the reliability assessment of the ten-bar truss

Methods	p_f	Function Calls	Error (%)	Time (s)
MCS	0.1399	10^6	-	227
FORM	0.0863	92	38.31	1
SORM	0.0930	272	33.52	1
MLS-HDMR [117]	0.1429	761	2.14	28770
Proposed Method	0.1433	463	2.43	163

calls converge to 0.0863 (i.e. 38% error) and 0.0930 (i.e. 34% error), respectively. MLS-HDMR [117] with 761 function calls using 2^{nd} order model yields a $p_f = 0.1429$ with an error of 2%. However, as it employees MCS at each and every point, the computational time is exceptionally high. Finally, the proposed algorithm is used for its validation. As usual, $\mu_{\mathbf{x}}$ is considered as the reference point and first two iterations have sparse grid level $q = 3$ while each successive iteration has $q = 2$. Total function evaluations in this scheme is 463. Once the algorithm is converged, 10^3 samples are used for the importance sampling which gives a p_f of 0.1433 (i.e. error is 2%). Therefore, the proposed algorithm is capable to estimate the p_f with error $\ll 5\%$ at a significantly lower computational cost (i.e. 163s) as compared to the other similar method.

5.4.2 Reliability Assessment of Field Problems

Once the validation of the proposed AMFD-HDMR is established, it is further applied to reliability based design of engineering problems. Four such problems are picked from the literatures to prove the efficacy of the proposed algorithm for reliability analysis.

5.4.2.1 Problem 1: Five-storey Three-bay Portal Frame

In this problem, a five-storeyed three-bay portal frame subjected to static lateral loading (see § 4.5.2.1) is considered for validation. Fig. 4.14 shows the dimension of the frame and the element numbers. Altogether there are 21 random variables whose statistical properties are listed in Table 4.8. Static loads applied in this problem (i.e. P_i) follow Rayleigh distribution with correlation coefficient 0.5. All other random variables are normal with Young's moduli E_i having correlation coefficient equal to 0.90. The correlation coefficients among the variables A_i and I_i are 0.13 (i.e. $\rho_{A_iA_j} = \rho_{I_iI_j} = 0.13$) whereas the correlation between A_i and I_j is given by

$$\rho_{A_iI_j} = \begin{cases} 0.95 & : i = j \\ 0.13 & : i \neq j \end{cases} \tag{5.23}$$

These correlation coefficients between the random variables are tabulated in Table 5.4 below.

Based on the above description, the portal frame is analyzed for lateral displacement and the serviceability limit state function is defined based on the horizontal displacement of the top storey [i.e. $u(\mathbf{x})$] where the allowable deflection is 0.061m. Thus, the performance function of the portal frame is as follows [16,21,117,181]

$$g(\mathbf{x}) = 0.061 - u(\mathbf{x}) \tag{5.24}$$

Using the random variables described in Table 4.8, the probability of failure is estimated by different methods as explained in the previous problems and results are tabulated in Table 5.5.

As usual, MCS with 10^6 samples is carried out first which shows the p_f is 0.0003340 and is considered as exact to check the accuracy of other methods. It can be noticed from Table 5.5 that FORM fails to converge to the true MPP and ends up with an error of 70%. HDMR by Chowdhury *et al.* [117] yields an error of 6.4% after 7687 function calls while the proposed approach ends up with p_f having an error of 3.6% using 1979 function calls (i.e. 74.3% less function evaluation than Chowdhury *et al.* [117]). Moreover, the computational time required by the proposed method is much less compared to the other HDMR [117]. This clearly proves the advantage of the proposed sequential development of the multi-order adaptive dimension decomposition for the problem involving finite element models with large dimensions.

Table 5.4: Correlation coefficients between the random variables in the five-storeyed three-bay portal frame

	P_1	P_2	P_3	E_1	E_2	I_1	I_2	I_3	I_4	I_5	I_6	I_7	I_8	A_1	A_2	A_3	A_4	A_5	A_6	A_7	A_8
P_1	1																				
P_2	0.50	1																			
P_3	0.50	0.50	1																		
E_1	0	0	0	1																	
E_2	0	0	0	0.90	1																
I_1	0	0	0	0	0	1															
I_2	0	0	0	0	0	0.13	1														
I_3	0	0	0	0	0	0.13	0.13	1													
I_4	0	0	0	0	0	0.13	0.13	0.13	1												
I_5	0	0	0	0	0	0.13	0.13	0.13	0.13	1											
I_6	0	0	0	0	0	0.13	0.13	0.13	0.13	0.13	1										
I_7	0	0	0	0	0	0.13	0.13	0.13	0.13	0.13	0.13	1									
I_8	0	0	0	0	0	0.13	0.13	0.13	0.13	0.13	0.13	0.13	1								
A_1	0	0	0	0	0	0.95	0.13	0.13	0.13	0.13	0.13	0.13	0.13	1							
A_2	0	0	0	0	0	0.13	0.95	0.13	0.13	0.13	0.13	0.13	0.13	0.13	1						
A_3	0	0	0	0	0	0.13	0.13	0.95	0.13	0.13	0.13	0.13	0.13	0.13	0.13	1					
A_4	0	0	0	0	0	0.13	0.13	0.13	0.95	0.13	0.13	0.13	0.13	0.13	0.13	0.13	1				
A_5	0	0	0	0	0	0.13	0.13	0.13	0.13	0.95	0.13	0.13	0.13	0.13	0.13	0.13	0.13	1			
A_6	0	0	0	0	0	0.13	0.13	0.13	0.13	0.13	0.95	0.13	0.13	0.13	0.13	0.13	0.13	0.13	1		
A_7	0	0	0	0	0	0.13	0.13	0.13	0.13	0.13	0.13	0.95	0.13	0.13	0.13	0.13	0.13	0.13	0.13	1	
A_8	0	0	0	0	0	0.13	0.13	0.13	0.13	0.13	0.13	0.13	0.95	0.13	0.13	0.13	0.13	0.13	0.13	0.13	1

Table 5.5: Results for the reliability analysis of the five-storeyed three-bay portal frame

Methods	p_f	Function Calls	Error (%)	Time (s)
MCS	0.0003340	10^6	-	1.66×10^6
FORM	0.0001034	270	69.05	466
MLS-HDMR [117]	0.0003553	7687	6.38	220665
Proposed Method	0.0003220	1979	3.59	4195

5.4.2.2 Problem 2: Three-storey Base Isolated Building Excited by Dynamic Load

This numerical problem is also discussed in the previous chapter under the § 4.5.2.2 and the statistical parameters of the random variables are listed in Table 4.10. Reliability analysis is carried out using these

Table 5.6: Probability of failure p_f for the based isolated building estimated from different methods

Methods	p_f	Function Calls	Error (%)	Time (s)
MCS	0.19390	10^5	-	479774
FORM	0.22760	90	17.38	365
SORM	0.13838	202	28.63	903
MLS-HDMR [117]	0.19695	481	1.57	18437
Proposed Method	0.19492	307	0.53	1424

random variables by applying different methods described in the previous problems for validation and the results are listed in Table 5.6. The probability of failure estimated using MCS (i.e. 0.19390) with sample size 10^5 is considered as the benchmark result. FORM converges after 90 function calls offering $p_f = 0.22760$ with an error of 17% whereas SORM yields more error (i.e. 29%). HDMR, as proposed by Chowdhary *et al.* [117] needs 481 function calls and estimate a p_f of 0.19695 having error around 1.6%. However, due to MCS on top of the HDMR for reliability analysis, the computational time is relatively high. Finally, the proposed method is used that demands 307 function calls (i.e. 36% reduction from other HDMR). The p_f estimated by this technique using 10^3 samples in importance sampling is 0.19492 which has an error of 0.5%. Besides accuracy, sequential generation of the proposed meta-model consumes much less computational time (i.e. nearly 92%) as compared to other HDMR.

5.4.2.3 Problem 3: Car Crash Problem with Nonlinear Correlation

In this problem, an explicit expression of velocity during the side impact at the centre pillar of a passenger car front door (often known as B-pillar) [71] is studied for reliability analysis. The performance function is developed by setting the speed at 15.7mm/ms [71]

Table 5.7: Properties of the random variables in the car crash problem

Random Variables	Mean	Standard Deviation	*pdf*	Lower Limit	Upper Limit
x_1 (mm)	1.500	0.050	Beta	1.000	1.800
x_2 (mm)	1.000	0.087	Uniform	0.849	1.151
x_3 (mm)	0.849	0.087	Uniform	0.698	1.000
x_4 (mm)	1.000	0.087	Uniform	0.849	1.151
x_5 (GPa)	0.345	0.007	Triangular	0.327	0.363
x_6 (mm)	0.000	10.000	Normal	-	-
x_7 (mm)	0.000	10.000	Normal	-	-

$$g(\mathbf{x}) = 15.7 - (16.45 - 0.489x_1x_4 - 0.843x_2x_3 + 0.0432x_5x_6 - 0.0556x_5x_7 - 0.000786x_7^2) \tag{5.25}$$

Detailed description and statistical properties of the random variables are given in Table 5.7. Random variables x_1, x_2, ..., x_5 are uncorrelated whereas the correlation between x_6 and x_7 is considered to be nonlinear. Fig. 5.10(a) shows this bivariate correlation which is modelled using Clayton copula as explained in Hu and Youn [71]. The joint CDF for the correlated bivariate case is expressed as follows

$$C_\eta(h_1, h_2) = (h_1^{-\eta} + h_2^{-\eta} - 1)^{-1/\eta} \tag{5.26}$$

here, h_1, $h_2 \in [0, 1]$ represent the CDF of x_6 and x_7, respectively and $\eta \in [-1, \infty) \setminus \{0\}$ is the correlation parameter. These variables are mapped to independent standard normal space (i.e. z_6 and z_7) by employing Rosenblatt transformation [71]

$$z_6 = \Phi^{-1}[h_1] = \Phi^{-1}[F_{X_6}(x_6)] \tag{5.27a}$$

$$z_7 = \Phi^{-1}[C_\eta(h_2|h_1)] = \Phi^{-1}[C_\eta(F_{X_7}(x_7)|F_{X_6}(x_6))] \tag{5.27b}$$

In the above equation, $C_\eta(h_2|h_1)$ denotes the joint CDF with condition such that $\mathscr{P}(F_{X_7}(x_7) \leq h_2|F_{X_6}(x_6) = h_1)$ which can be evaluated using

$$C_\eta(h_2|h_1) = \frac{\partial C_\eta(h_1, h_2)}{\partial h_1} \Big/ \frac{\partial C_\eta(h_1)}{\partial h_1} \tag{5.28}$$

Substituting Eq. 5.28 into Eq. 5.27b yields the following expression

$$z_7 = \Phi^{-1}[h_1^{-(\eta+1)}\{h_1^{-\eta} + h_2^{-\eta} - 1\}^{-(1/\eta+1)}] \tag{5.29}$$

In this problem, Kendall correlation coefficient τ is used to define the nonlinear correlation which quantifies the copula correlation parameter as [182]

$$\eta = \frac{2\tau}{1 - \tau} \tag{5.30}$$

where, τ is assumed to be 0.75 and the results of the reliability analysis are summarized in Table 5.8. Besides other techniques used for reliability analysis in all the previous problems, the method proposed by Hu and Youn [71] (i.e. AS-PCE) is also used in this problem for comparison. Thus, five different techniques for reliability analysis are compared here. For validation purpose, MCS with sample size 10^6 (i.e. $p_f = 0.0568$) is checked and compared with the results mentioned in Hu and Youn [71] which gives 0.0563. This shows a close match between the two MCS results, one produced in this work and another reported by Hu and

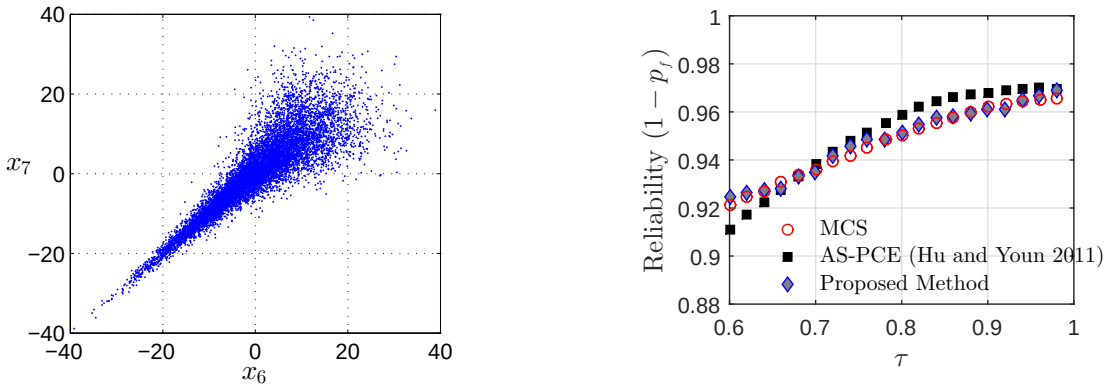

(a) (b)

Figure 5.10: (a) Scatter plot of nonlinear correlated random variables and (b) influence of Kendall correlation coefficient on reliability

Youn [71]. Gradient-based FORM does not converge to the MPP and subsequently, yields huge error in p_f estimation. Further, the problem is solved using MLS-HDMR [117] with $k = 2$ consuming 365 function calls in 1255s. The p_f estimated by this method is equal to 0.0748 which yields an error of 31.7%. Finally, the proposed approach is used where the time consumption is reduced to approximately 24s with 271 function calls. It took 5 iterations to converge with $q = 3$ for the first two iterations followed by $q = 2$ in subsequent iterations. The proposed method gives a better approximation of the probability of failure i.e. 0.0575 with an error of 1.2%. In this problem, another trial was executed with the $q = 3$ in the first iteration followed by $q = 2$ which also took 5 iterations. This reduced the number of function calls and computational time to 177 and 16s, respectively with p_f estimated as 0.0532 (i.e. 6.3% error). Both these cases produce errors less than that obtained from AS-PCE (i.e. 11.27%) [71].

Finally, the proposed method is employed to study the effect of nonlinear correlation coefficient τ on p_f. Fig. 5.10(b) shows the influence of Kendall coefficient τ which results in significant improvement of reliability (i.e. $1 - p_f$). With this benchmark problem, it can be concluded that the proposed method maintains consistent accuracy in p_f estimation with error well within 5% whereas the AS-PCE results shown in Hu and Youn [71] yields a relatively higher error (i.e. in the range of 20%). This proves the efficiency and accuracy of the proposed method for the problem involving non-normal random variables and/or nonlinear correlation.

5.4.2.4 Problem 4: Composite Plate

Once the benchmark problems are solved and the performance of the proposed method is established, a design problem is used to verify its efficiency in fragility analysis. For this purpose, a laminated composite plate is considered that consists of several layers of lamina stacked in a particular sequence with uniformly distributed load (UDL) over the span. Each layer of the laminates is assumed to have equal thickness and material properties. The plate is modelled using first order shear deformation theory (FSDT) where the rotation of normal to the mid-surface leads to the inclusion of transverse shear strains in the analysis. Thus,

Table 5.8: Results for the reliability analysis of the car crash problem

Methods	p_f	Function Calls	Error (%)	Time (s)
MCS	0.0568	10^6	-	15
FORM	0.1191	103	>100.00	1
AS-PCE [71]	0.0504	64	11.27	-
MLS-HDMR [117]	0.0748	365	31.69	1255
Proposed Method	0.0575	271	1.23	24

the displacement field of the plate based on FSDT is given by [170]

$$\begin{aligned} u(\hat{\mathbf{x}},\hat{\mathbf{y}},\hat{\mathbf{z}}) &= u_0(\hat{\mathbf{x}},\hat{\mathbf{y}}) + \hat{\mathbf{z}}\phi_{\hat{\mathbf{x}}}(\hat{\mathbf{x}},\hat{\mathbf{y}}) \\ v(\hat{\mathbf{x}},\hat{\mathbf{y}},\hat{\mathbf{z}}) &= v_0(\hat{\mathbf{x}},\hat{\mathbf{y}}) + \hat{\mathbf{z}}\phi_{\hat{\mathbf{y}}}(\hat{\mathbf{x}},\hat{\mathbf{y}}) \\ w(\hat{\mathbf{x}},\hat{\mathbf{y}},\hat{\mathbf{z}}) &= w_0(\hat{\mathbf{x}},\hat{\mathbf{y}}) \end{aligned} \tag{5.31}$$

where, u_0, v_0, w_0 are the midplane (i.e. $\hat{\mathbf{z}} = 0$) displacements in $\hat{\mathbf{x}}$, $\hat{\mathbf{y}}$ and $\hat{\mathbf{z}}$ directions, respectively. The components $\phi_{\hat{\mathbf{x}}}$ and $\phi_{\hat{\mathbf{y}}}$ are the rotations along the transverse normal about $\hat{\mathbf{y}}$-axis and $\hat{\mathbf{x}}$-axis, respectively. Following von-Karman assumptions for small strain and moderate rotations, the strain field associated with the above displacements are given by [170]

$$\varepsilon = \begin{Bmatrix} \varepsilon_{\hat{\mathbf{x}}\hat{\mathbf{x}}} \\ \varepsilon_{\hat{\mathbf{y}}\hat{\mathbf{y}}} \\ \gamma_{\hat{\mathbf{x}}\hat{\mathbf{y}}} \end{Bmatrix} = \begin{Bmatrix} \varepsilon^m_{\hat{\mathbf{x}}\hat{\mathbf{x}}} \\ \varepsilon^m_{\hat{\mathbf{y}}\hat{\mathbf{y}}} \\ \gamma^m_{\hat{\mathbf{x}}\hat{\mathbf{y}}} \end{Bmatrix} + \hat{\mathbf{z}} \begin{Bmatrix} \varepsilon^f_{\hat{\mathbf{x}}\hat{\mathbf{x}}} \\ \varepsilon^f_{\hat{\mathbf{y}}\hat{\mathbf{y}}} \\ \gamma^f_{\hat{\mathbf{x}}\hat{\mathbf{y}}} \end{Bmatrix} \tag{5.32}$$

where, the superscript m and f refer to the membrane and flexural components of the strain, respectively and $\gamma_{\hat{\mathbf{x}}\hat{\mathbf{z}}}$ and $\gamma_{\hat{\mathbf{y}}\hat{\mathbf{z}}}$ are the transverse shear strains.

Table 5.9: Properties of the random variables in the composite plate

RV	Units	Mean	cov	pdf
ν_{12}		0.281	0.075	Lognormal
E_1	GPa	154.900	0.059	Weibull
E_2	GPa	8.700	0.095	Weibull
G_{12}	GPa	4.500	0.088	Lognormal
X_t	GPa	2.409	0.067	Lognormal
X_c	GPa	1.148	0.181	Lognormal
Y_t	GPa	0.046	0.200	Weibull
Y_c	GPa	0.196	0.153	Weibull
T_{12}	GPa	0.083	0.050	Lognormal

The failure of the composite plate is modelled by modified Tsai-Hill criterion which is based on the distortion energy theory of von-Mises [75]

$$\mathfrak{F} = \left(\frac{\sigma_{11}}{X}\right)^2 + \left(\frac{\sigma_{22}}{Y}\right)^2 - \frac{\sigma_{11}\sigma_{22}}{X^2} + \left(\frac{\sigma_{12}}{T_{12}}\right)^2 \leq 1 \tag{5.33}$$

In Eq. 5.33, T_{12} is the shear strength and X and Y are the tensile and the compressive strengths depending upon the sign of σ_{11} and σ_{22}. Failure of the lamina is observed if the index exceeds unity [75] and thus, the limit state is given by

$$g(\mathbf{x}) = 1 - \mathfrak{F} \tag{5.34}$$

The material used in this problem is carbon-epoxy and the square composite plate is of size 1m and thickness 0.010m. The laminates are stacked in [0/90/0] sequence and the boundary condition is assumed to be simply supported on all sides. It is exposed to UDL over the entire area as shown in the Fig. B.1 where the load is considered to be constant with a magnitude of 25kN/m^2. An 8×8 mesh using a nine noded quadrilateral element is used for finite element model and the associated properties are given in Table 5.9. In addition to these properties of the random variables, out of plane shear moduli (i.e. G_{13} and G_{23}) are considered to be dependent on the in-plane shear modulus G_{12} by a factor of 1.0 and 0.8, respectively.

Using these parameters, MCS is conducted with a sample size of 10^6 which yields the probability of failure $p_f = 0.000570$ as shown in Table 5.10. As in the § 5.4.1.1, FORM has convergence issue and thus, a suitable starting point is chosen for further assessment. It suffers an error of 8% to estimate the probability of failure and consumes least number of function evaluations. SORM consumes more evaluations but fails to improve this error. Next, the MLS-HDMR [117] is executed with the reference point $\mathbf{c} = \mu_{\mathbf{x}}$. Second order HDMR is considered for this problem with the level of support points $k = 5$. A total of 2377 function evaluations

Table 5.10: Results for the reliability analysis of the simply supported composite plate subjected to UDL

Methods	p_f	Function Calls	Error (%)	Time (s)
MCS	0.000570	10^6	-	802260
FORM	0.000615	105	7.9	86
SORM	0.000619	249	8.6	207
MLS-HDMR [117]	0.001461	2377	156.3	87972
Proposed Method	0.000590	514	3.5	1042

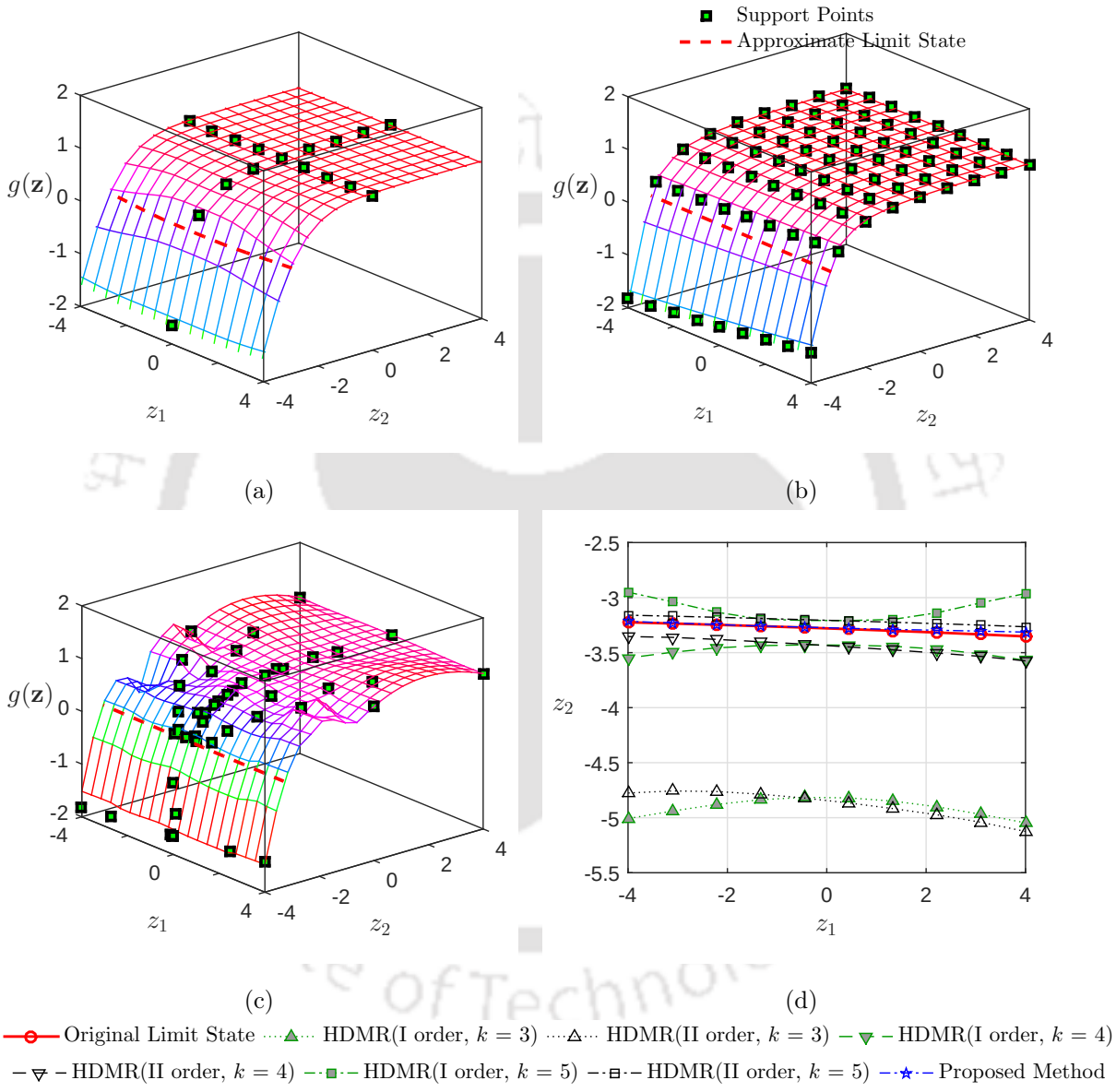

Figure 5.11: Response surface based on (a) first order HDMR ($k = 5$), (b) second order HDMR ($k = 5$), (c) proposed method and (d) the limit states using different approximation methods

are conducted and the estimated p_f is 0.001461. It may be noted that the MLS-HDMR overestimates the probability of failure which leads to erroneous results. The proposed method is then used where 514 function calls are utilized with a computational time of 1042s. It requires 10 iterations to converge with level $q = 3$ till the second iteration, followed by $q = 2$ for the rest. This method offers a p_f of 0.000590 with an error of 3.5%. Thus, it results in an efficient and speedy evaluation of p_f with 78% reduction in the number of function calls and a dramatic reduction in computational time as shown in Table 5.10. The error in MLS-HDMR is attributed to the nonlinear correlation between the random variables and the output function

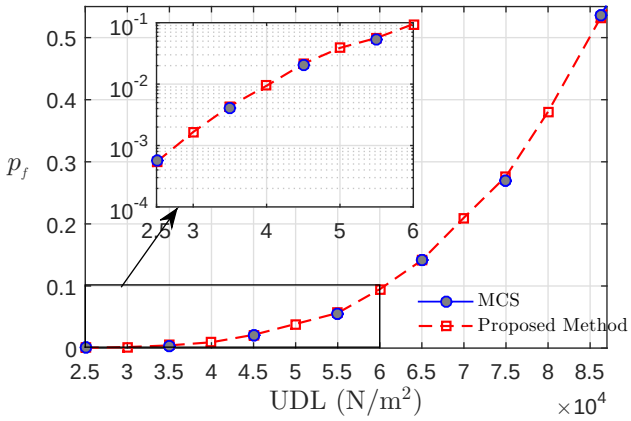

Figure 5.12: Fragility curve of [0/90/0] stacked laminate with respect to load

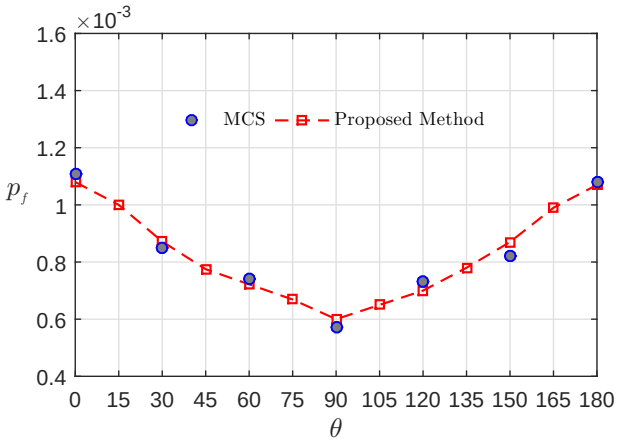

Figure 5.13: Fragility curve with respect to angle of orientation subjected to 25kN/m^2

$g(\bullet)$. This is further illustrated using the same example but by reducing the dimensions (i.e. the number of random variables n) of the problem to 2. For demonstration, G_{12} and Y_t are chosen as the random variables and the properties associated with them remain unchanged. All other random variables are frozen to their respective mean values. MLS-HDMR [117] with 1st and 2nd orders are solved to generate the approximate response surface to replace the original performance function and the limit state. Fig. 5.11(a) and 5.11(b) show the response surfaces with $k = 5$ for $o = 1$ and 2, respectively. Similarly, the response surface developed by solving the proposed algorithm is also shown in the Fig. 5.11(c). Although the MLS-HDMR develops a smooth response surface, the limit state approximation (i.e. $g(\mathbf{x}) = 0$) is not accurate as shown in Fig. 5.11(d). Different levels of k yield different approximations of the limit state whereas the proposed method yields a better approximation as compared to the 1st and 2nd order MLS-HDMR [117]. This helps the proposed method to accurately estimate probability of failure and subsequent reliability index.

Finally, fragility curves are developed for different load intensities and angle of orientation of the central laminate (i.e. $[0/\theta/0]$) using the proposed method. The fragility curves are presented in Fig. 5.12 and Fig. 5.13 for the load and θ, respectively. In both the cases, close match is observed between the MCS results and the proposed method. This, in turn, establishes the efficiency and accuracy of the proposed method for the actual design problems.

5.5 Summary

Development of adaptive mixed-order multi-grid dimension decomposition technique for efficient reliability analysis is the main theme of the work presented in this chapter. Here, multiple decompositions with equidistant support points are generated using Clenshaw-Curtis sparse grid scheme to replace the original limit state into the summands of lower order functions. Hermite polynomial with MLS technique is used for the interpolation between the support points that has inherent advantages over the other schemes. The proposed method is validated using different benchmark problems available in the literature. Finally, reliability-based design of a composite plate is demonstrated to prove the efficiency of the proposed approach. Based on the results obtained from the numerical analysis, following are the major conclusions made from this work -

- The proposed approach shows promising results for accurate reliability analysis of the problems involving large dimensions with different level of complexities (e.g. non-algebraic, non-differentiable, nonlinear performance functions, nonlinear correlation between random variables) using an adaptive combination of mixed-order (i.e. first and second order) approximation in an iterative manner. Besides accuracy, it also performs efficiently where other traditional methods (e.g. gradient-based optimization of FORM, SORM and/or other HDMR technique available in the literature) face difficulties to assess failure.
- Less evaluations of the original function are observed in this adaptive development of dimension decomposition as compared to other form of HDMR. This is due to the fact that generation of the support points are performed judiciously by coupling sparse grid scheme and the optimization process. In the study, objective function is selected to locate the MPP/failure region for limit state mapping. This information is updated in every iteration and subsequently, the support points are populated around the new reference point. Once the convergence is achieved, multiple grids of the support points are used to develop the final shape of the performance function.
- Apart from the evaluation counts, computational burden associated with the prediction of the limit state by the meta-model is usually neglected. Numerical results clearly demonstrate this unexplored issue due to numerous matrix inversion associated with the MLS technique in the HDMR framework. Proposed study suggests improvement by adopting importance sampling for reliability analysis on the final form of the response surface. This reduces the computational burden as compared to MCS used in the MLS-HDMR [117] or the other approaches proposed in the literature.
- The use of MLS with Hermite polynomial assists the interpolation of local variations in the decomposition model. Choice of Hermite polynomial transforms the problem into standard normal space that helps to solve the limit state without further transformation required for the estimation of reliability index. This also helps in avoiding any ill-conditioning of the matrices due to usage of small values in the weight function.

Overall, the proposed method proves to be efficient, especially for MLS-HDMR where it improves the accuracy, number of original FE evaluations and computational time required to estimate the probability of failure. With these in view, it may be concluded that the proposed adaptive mixed-order multi-grid dimension decomposition using Hermite polynomials in MLS framework can be used for the reliability based design of problems involving large number of random variables. Besides reliability analysis, this can also be extended to uncertainty quantification. However, an increase in dimension still requires a fair amount of computational effort in terms of FE solutions, if any. Hence, a dimension adaptive scheme can be developed using AMFD-HDMR to curtail some insignificant random variables in the performance function. This is studied in the next chapter where a dimension adaptive version is suggested.

Chapter 6

Dimension Adaptive HDMR

6.1 Introduction

The new numerical approaches described in the previous chapters clearly show the performance of the high-fidelity models that offer accuracy at the minimal computational cost. However, application of these methods to large dimensional problem is still a time-consuming task. In general, this leads to a huge demand for more support points in higher (say, 2^{nd}) order decomposition models which eventually reduces the efficiency of the proposed sequential generation. To address this issue, present study extends the design point based approximation by adding a dimension adaptive formulation in this chapter. The new approach introduces a sensitivity analysis based dimension reduction coupled with sequential and distribution adaptive generation of the support points. Moreover, the present proposal tries to address the limitation of the design point based approximation of limit state for large dimensions [11]. This novel technique is used to perform stochastic computation of high dimensional problem with random fields.

6.2 Proposed *d*AMFD-HDMR

As stated above, the present study proposes a different algorithm based on dimension decomposition technique with hierarchical selection of the sub-grid support points. Primary difference lies in the inclusion of case-specific dimension adaptiveness for efficiency and accuracy. In this algorithm, dimension of the problem is effectively decomposed using HDMR built over the support points generated based on the Smolyak's proposal [165]. Moreover, PCE is employed individually for each decomposition to interpolate response between the support points. Detailed explanation of this approach is presented below. is applied on The dimension-wise decomposition technique is presented here for a multivariate function, say $g(\mathbf{x})$ integrable in $\Omega^n \subset \mathbb{R}^n$. The projection of $g(\mathbf{x})$ is taken (i.e. $\mathbb{P}_i$) such that the dimension is reduced and it becomes independent of the variable x_i. The new function formed through the projection either assumes a constant value of x_i or keeps x_i out of the integral [168]. Hence, the projection operator can be mathematically defined as

$$\mathbb{P}_{\mathbf{w}} g(\mathbf{x}) = \int_{\Omega^{n-\overline{\overline{\mathbf{w}}}}} g(\mathbf{x})\, \mathrm{d}\mathbf{x}_{\mathbf{n}\setminus\mathbf{w}} \tag{6.1}$$

where, $\mathbf{n} = \{1, 2, \ldots, n\}$ denotes the index, $\mathbf{x} = \{x_1\, x_2\, \ldots\, x_n\}$ is the set of random variables and its subset with index $\mathbf{w} \subseteq \mathbf{n}$ which is presented by $\mathbf{x}_{\mathbf{w}} = \{x_i\}_{i\in\mathbf{w}}$. Similarly, the index in the projection expresses $\mathbb{P}_{\mathbf{w}} = \prod_{i\in\mathbf{w}} \mathbb{P}_i$ which suggests that $\mathbb{P}_{\emptyset} = \mathbb{I}$ and $\mathbb{P}_{\mathbf{w}_1}\mathbb{P}_{\mathbf{w}_2} = \mathbb{P}_{\mathbf{w}_1\cup\mathbf{w}_2}$, $\forall\, \mathbf{w}_1, \mathbf{w}_2 \subseteq \mathbf{n}$. Moreover, $\overline{\overline{\bullet}}$ represents cardinality of the set $\bullet$ and $\mathrm{d}\mathbf{x}_{\mathbf{n}\setminus\mathbf{w}} = \prod_{i\notin\mathbf{w}} \mathrm{d}x_i\ \forall\ i \in \mathbf{n}$. Applying this projection to decompose the function g leads to

$$g_{\mathbf{w}} = \left(\prod_{i\in\mathbf{w}} (\mathbb{I} - \mathbb{P}_i)\right) \mathbb{P}_{\mathbf{n}\setminus\mathbf{w}} g \tag{6.2}$$

Here, larger parentheses denotes highest common factor. For the classical ANOVA approach, the domain Ω is restricted to $[0,\ 1]$ and the resulting decomposition from Eq. 6.2 possesses orthogonal properties in $\mathcal{L}^2(\Omega)$ sense such that

$$\mathbb{I}(g_{\mathbf{w}_1} \cdot g_{\mathbf{w}_2}) = 0 \qquad \forall\ \mathbf{w}_1 \neq \mathbf{w}_2 \tag{6.3}$$

The above condition implies that the variance of the function $g(\mathbf{x})$ can also be decomposed as

$$\sigma^2(g) = \sum_{\mathbf{w}\subseteq\mathbf{n}} \sigma^2(g_{\mathbf{w}}) \qquad \forall\ \mathbf{w} \neq \emptyset \tag{6.4}$$

Using Eqs. 6.2 and 6.4 yield a finite decomposition of $g(\mathbf{x})$ as

$$g(\mathbf{x}) = \sum_{\mathbf{w}\subseteq\mathbf{n}} g_{\mathbf{w}}(\mathbf{x}_{\mathbf{w}}) \tag{6.5}$$

which can be expanded by a summand series of the form

$$g(x_1, x_2, \ldots, x_n) = g_0 + \sum_{i_1} g_{i_1}(x_{i_1}) + \sum_{i_1<i_2} g_{i_1 i_2}(x_{i_1}, x_{i_2}) + \cdots + g_{12\ldots n}(x_1, x_2, \ldots, x_n) \quad \forall\ i_1, i_2, \ldots \in \mathbf{n} \tag{6.6}$$

Further simplifying the decomposition process, a set of fixed reference point $\mathbf{c} = \{c_i\}_{i\in\mathbf{n}}$ is assumed along which the projections are formed. The decomposition in Eq. 6.6 forms a hierarchial setup which is often expressed by the order o given by $\overline{\overline{\mathbf{w}}}$. Now, the function $g(\bullet)$ can be decomposed as

$$\begin{aligned} g_0 &= g(\mathbf{c}), \qquad g_{i_1}(x_{i_1}) = g(\mathbf{x})|_{\mathbf{x}=\mathbf{c}\setminus x_{i_1}} - g_0, \\ g_{i_1 i_2}(x_{i_1}, x_{i_2}) &= g(\mathbf{x})|_{\mathbf{x}=\mathbf{c}\setminus x_{i_1}, x_{i_2}} - [g_{i_1}(x_{i_1}) + g_{i_2}(x_{i_2}) + g_0] \end{aligned} \tag{6.7}$$

for 0^{th}, 1^{st} and 2^{nd} orders, respectively with $g(\mathbf{x})|_{\mathbf{x}=\mathbf{c}\setminus x_i} = g(c_1, \ldots, c_{i-1}, x_i, c_{i+1}, \ldots, c_n)$. The component functions in Eq. 6.6 can be further extended to higher orders using the recursive sequence shown in the above equations. However, usually these component functions are truncated at either 1^{st} order

$$g(\mathbf{x}) = g_0 + \sum_{i_1=1}^{n} g_{i_1}(x_{i_1}) + \mathscr{R}_1 \tag{6.8}$$

or 2^{nd} order

$$g(\mathbf{x}) = g_0 + \sum_{i_1=1}^{n} g_{i_1}(x_{i_1}) + \sum_{\substack{i_1,i_2=1 \\ i_1<i_2}}^{n} g_{i_1 i_2}(x_{i_1}, x_{i_2}) + \mathscr{R}_2 \tag{6.9}$$

for computational tractability. Here, $\mathscr{R}_1$ and $\mathscr{R}_2$ represent the residual errors from the respective truncation of the decomposition. On applying the fixed point approach as per Eq. 6.7 and neglecting the residual terms $\mathscr{R}_1$ and $\mathscr{R}_2$, above equations are modified to form the approximate functions of order $o = 1$ and 2 as

$$\tilde{g}(\mathbf{x}) = \sum_{i_1=1}^{n} g(\mathbf{x})|_{\mathbf{x}=\mathbf{c}\setminus x_{i_1}} - \frac{n-1}{n}\binom{n}{1} g_0 \tag{6.10}$$

and

$$\tilde{g}(\mathbf{x}) = \sum_{\substack{i_1,i_2=1 \\ i_1<i_2}}^{n} g(\mathbf{x})|_{\mathbf{x}=\mathbf{c}\setminus x_{i_1}, x_{i_2}} - \binom{n-2}{1} \sum_{i_1=1}^{n} g(\mathbf{x})|_{\mathbf{x}=\mathbf{c}\setminus x_{i_1}} + \frac{n-2}{n}\binom{n}{2} g_0 \tag{6.11}$$

respectively. These expressions can be extended to determine the approximate response at any arbitrary point $\acute{\mathbf{x}} = \{\acute{x}_i\}_{i\in\mathbf{n}}$ through interpolation such as

$$\tilde{g}(\mathbf{x}) = \sum_{i_1=1}^{n} \hat{g}(\mathbf{x})|_{\mathbf{x}=\mathbf{c}\setminus \acute{x}_{i_1}} - \frac{n-1}{n}\binom{n}{1} g_0 \tag{6.12}$$

and

$$\tilde{g}(\mathbf{x}) = \sum_{\substack{i_1,i_2=1 \\ i_1<i_2}}^{n} \hat{g}(\mathbf{x})|_{\mathbf{x}=\mathbf{c}\setminus\acute{x}_{i_1},\acute{x}_{i_2}} - \binom{n-2}{1} \sum_{i_1=1}^{n} \hat{g}(\mathbf{x})|_{\mathbf{x}=\mathbf{c}\setminus\acute{x}_{i_1}} + \frac{n-2}{n}\binom{n}{2} g_0 \tag{6.13}$$

In Eq. 6.12, $\hat{g}(\bullet)$ is evaluated using

$$\hat{g}(\mathbf{x})|_{\mathbf{x}=\mathbf{c}\setminus\acute{x}_{i_1}} = \sum_{j_1=1}^{n_{s_1}} \varphi_{j_1}(\acute{x}_{i_1}) g(c_1, \ldots, c_{i_1-1}, x_{i_1}^{(j_1)}, c_{i_1+1}, \ldots, c_n) \tag{6.14}$$

and the shape function $\varphi_{j_1}(x_{i_1})$ is estimated by MLS based PCE technique. Here, n_{s_1} denotes the number of axial-points formed for random variable x_{i_1}. Substituting Eqs. 6.7 and 6.14 back into Eq. 6.10 gives the 1st order approximation as

$$\tilde{g}(\mathbf{x}) = \sum_{i_1=1}^{n} \sum_{j_1=1}^{n_{s_1}} \varphi_{j_1}(x_{i_1}) \hat{g}(\mathbf{x})|_{\mathbf{x}=\mathbf{c}\setminus x_{i_1}} - \frac{n-1}{n}\binom{n}{1} g(\mathbf{c}) \tag{6.15}$$

Similarly for the 2nd order, Eq. 6.14 is extended for $(\acute{x}_{i_1}, \acute{x}_{i_2})$ which results in

$$\hat{g}(\mathbf{x})|_{\mathbf{x}=\mathbf{c}\setminus\acute{x}_{i_1},\acute{x}_{i_2}} = \sum_{j_1,j_2=1}^{n_{s_2}} \varphi_{j_1 j_2}(\acute{x}_{i_1}, \acute{x}_{i_2}) g(c_1, \ldots, c_{i_1-1}, x_{i_1}^{(j_1)}, c_{i_1+1}, \ldots, c_{i_2-1}, x_{i_2}^{(j_2)}, c_{i_2+1}, \ldots, c_n) \tag{6.16}$$

where, n_{s_2} is the number of cross-point coordinates of x_{i_1} and x_{i_2}. Following the previous steps, Eqs. 6.7, 6.14 and 6.16 are substituted into Eq. 6.11 to obtain the 2nd order interpolation expression which is given by

$$\begin{aligned}\tilde{g}(\mathbf{x}) = &\sum_{\substack{i_1,i_2=1 \\ i_1<i_2}}^{n} \sum_{j_1,j_2=1}^{n_{s_2}} \varphi_{j_1 j_2}(x_{i_1}, x_{i_2}) \hat{g}(\mathbf{x})|_{\mathbf{x}=\mathbf{c}\setminus x_{i_1},x_{i_2}} \\ &- \binom{n-2}{1} \sum_{i_1=1}^{n} \sum_{j_1=1}^{n_{s_1}} \varphi_{j_1}(x_{i_1}) \hat{g}(\mathbf{x})|_{\mathbf{x}=\mathbf{c}\setminus x_{i_1}} + \frac{n-2}{n}\binom{n}{2} g(\mathbf{c})\end{aligned} \tag{6.17}$$

As stated in Chapter 5, procedure to determine the unknown shape function $\varphi_{j_1 j_2}(x_{i_1}, x_{i_2})$ in the above expression is similar to the AMFD-HDMR. The meta-model is formed by decomposing the dimension of the problem using HDMR formulation where its component functions are evaluated using MLS-PCE technique. Here, the support points are generated using multiple sparse grids following the optimization (refer Eq. 4.12) using the meta-model. This requires formation of separate HDMRs for each spare grid corresponding to every iteration, therefore the approximate function $\tilde{g}(\mathbf{x})$ is modified as

$$\tilde{g}(\mathbf{x})_{\text{MHDMR}} = \sum_{i=1}^{it} w_i^{\text{HDMR}} \tilde{g}_i(\mathbf{x}) \tag{6.18}$$

Here, w_i^{HDMR} represents the weight associated with i^{th} HDMR which should satisfy $\sum_{i=1}^{it} w_i^{\text{HDMR}} = 1$. It is determined using the Euclidean distance between $\mathbf{x}$ and the reference points within HDMRs (i.e. $\mathbf{c}^j = \{c_k^j\}_{k\in\mathbf{n}}$) which is given by [177]

$$w_i^{\text{HDMR}} = \frac{\prod_{j=1,\, j\neq i}^{it} \left[\sum_{k=1}^{n} (x_k - c_k^j)^2\right]^{\frac{1}{2}}}{\sum_{s=1}^{it} \prod_{l=1,\, l\neq s}^{it} \left[\sum_{k=1}^{n} (x_k - c_k^l)^2\right]^{\frac{1}{2}}} \tag{6.19}$$

This shows that Eq. 6.18 presents an adaptive contribution of multiple HDMRs that depends on the location of $\mathbf{x}$ to model the local variation, if any.

In addition to the above discussion for two steps i.e. generating the support points and constructing the meta-model, a third step based on the sensitivity analysis is included for dimension adaptiveness. Thus,

it is termed as *Dimension Adaptive Multiple Finite Difference HDMR* (dAMFD-HDMR). This requires modification in the HDMR formulations which is distinct from the curtailment of either polynomial basis terms in the PCE or the component functions in the HDMR where the associated coefficients are assigned to zero. To address this dimension curtailment, HDMR formulations are rewritten as

$$\tilde{g}(\mathbf{x}) = \sum_{k_1=1}^{n_r} \sum_{l_1=1}^{n_{s_1}} \varphi_{j_{l_1}}(x_{i_{k_1}}) \hat{g}(\mathbf{x})|_{\mathbf{x}=\mathbf{c}\setminus x_{i_{k_1}}} - \frac{n_r - 1}{n_r} \binom{n_r}{1} g(\mathbf{c}) \tag{6.20}$$

and

$$\begin{aligned} \tilde{g}(\mathbf{x}) = & \sum_{\substack{k_1,k_2=1 \\ k_1<k_2}}^{n_r} \sum_{l_1,l_2=1}^{n_{s_2}} \varphi_{j_{l_1} j_{l_2}}(x_{i_{k_1}}, x_{i_{k_2}}) \hat{g}(\mathbf{x})|_{\mathbf{x}=\mathbf{c}\setminus x_{i_{k_1}}, x_{i_{k_2}}} \\ & - \binom{n_r - 2}{1} \sum_{k_1=1}^{n_r} \sum_{l_1=1}^{n_{s_1}} \varphi_{j_{l_1}}(x_{i_{k_1}}) \hat{g}(\mathbf{x})|_{\mathbf{x}=\mathbf{c}\setminus x_{i_{k_1}}} + \frac{n_r - 2}{n_r} \binom{n_r}{2} g(\mathbf{c}) \end{aligned} \tag{6.21}$$

for 1st and 2nd order, respectively. In the above equations, n_r is the reduced dimension of the problem denoted by indices i_1, i_2, ..., i_{n_r}. Selection of these indices requires certain number of support points to indicate the significant dimension, if prior information is absent. This significance is observed based on the generation of support points which may lack adequate representation of near tail-end region. In this context, the above formulations of 1st and 2nd order HDMR will retain the variables, particularly sensitive in the neighbourhood of statistically favorable region e.g. area near mean. Hence, the support points populated based on some distribution and involved in determining the significant dimension can underestimate its influence. Consequently, this may yield large error in the estimation of probability of failure. To avoid this issue, the present study formulates an intermittent framework based on a tradeoff where the individual contributions (i.e. 1st order terms) are accepted but the collective contributions (i.e. 2nd order terms) are neglected. This is performed by limiting the cross-points as these terms soar high for large dimension in comparison to the axial-points, eventually making it computationally viable. HDMR of order $o = 1$ is evaluated using Eq. 6.15 as it only considers axial-points whereas 2nd order includes the cross-points, therefore the intermittent expression is given as

$$\begin{aligned} \tilde{g}(\mathbf{x}) = & \sum_{\substack{k_1,k_2=1 \\ k_1<k_2}}^{n_r} \sum_{l_1,l_2=1}^{n_{s_2}} \varphi_{j_{l_1} j_{l_2}}(x_{i_{k_1}}, x_{i_{k_2}}) \hat{g}(\mathbf{x})|_{\mathbf{x}=\mathbf{c}\setminus x_{i_{k_1}}, x_{i_{k_2}}} - \binom{n_r - 1}{1} \sum_{k_1=1}^{n_r} \sum_{l_1=1}^{n_{s_1}} \varphi_{j_{l_1}}(x_{i_{k_1}}) \hat{g}(\mathbf{x})|_{\mathbf{x}=\mathbf{c}\setminus x_{i_{k_1}}} \\ & + \sum_{i_1=1}^{n} \sum_{j_1=1}^{n_{s_1}} \varphi_{j_1}(x_{i_1}) \hat{g}(\mathbf{x})|_{\mathbf{x}=\mathbf{c}\setminus x_{i_1}} + \left\{ \binom{n_r}{2} - \frac{n-1}{n} \binom{n}{1} \right\} g(\mathbf{c}) \end{aligned} \tag{6.22}$$

Indices i_1, i_2, ..., i_{n_r} are determined using sensitivity analysis of the original responses at the support points. For random sampling based methods in HDMR framework, sensitivity analysis is performed using variance-based sensitivity indices. It requires the coefficients $\varphi_\bullet$ [119, 131] which in the present case have moving character as suggested by Eq. 4.9. Thus, an alternate method which is independent of the coefficients $\varphi_\bullet$ (e.g. Pearson correlation coefficient), is used here

$$\rho_{g x_i} = \frac{\mathbb{E}[(g - \mathbb{E}[g])(x_i - \mathbb{E}[x_i])]}{\sqrt{\mathbb{E}[(g - \mathbb{E}[g])^2] \;\; \mathbb{E}[(x_i - \mathbb{E}[x_i])^2]}} \qquad \forall\, i \in \mathbf{n} \tag{6.23}$$

Correlation coefficients are estimated for all the dimensions and those with significant value are screened as the reduced dimension for the problem. Multiple HDMRs are built by following 1st and/or 2nd (either from Eq. 6.17 or Eq. 6.22) order under the iterative scheme as suggested in AMFD-HDMR. Overall contribution of the HDMRs is evaluated using Eq. 6.18.

To calculate the unknown coefficients, present study employs distribution adaptive multi-sparse grid scheme as suggested in the previous chapter. It uses Smolyak's algorithm [165] and follows multiple HDMR decompositions to give efficient sparse generation of the support points. The application of Smolyak's algorithm results in curtailment of the full-grid interpolation, thus improving the computational tractability. In the

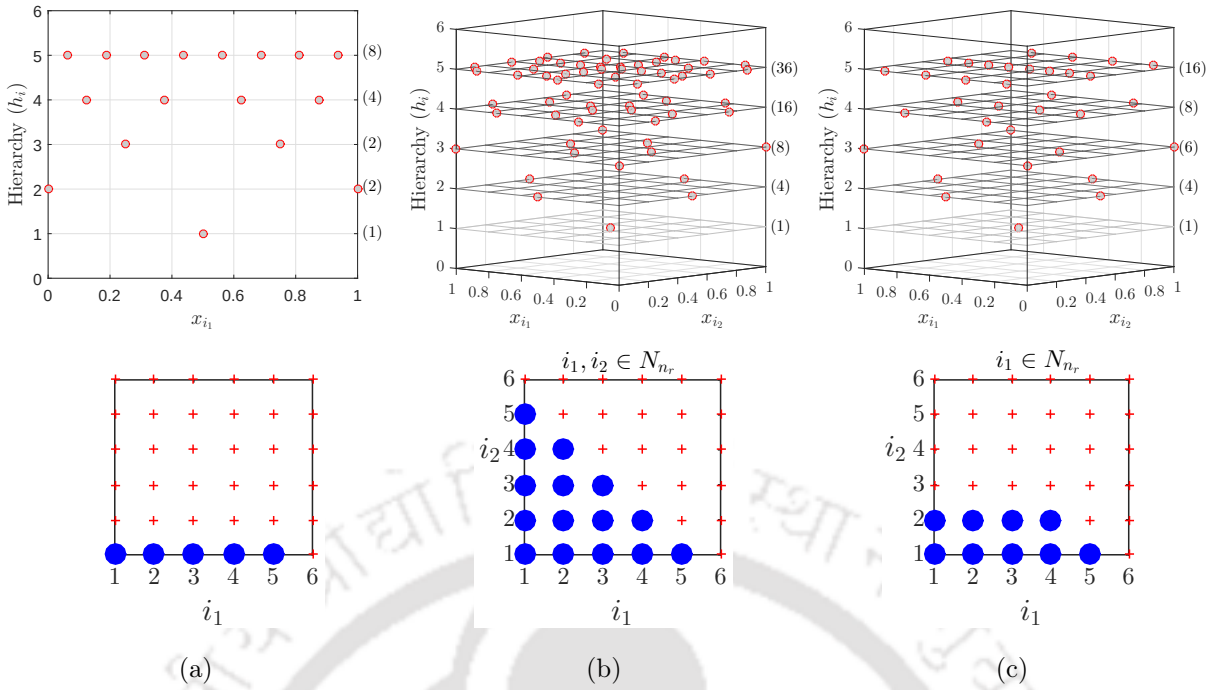

Figure 6.1: Hierarchal generation of sparse grids for different cases with (a) one random variable, (b) two random variables and (c) two random variables but only one is significant (i.e. x_{i_1}), here the number of points from each hierarchy is given in the brackets

present formulation, the generation of support points require a dimension-wise adaptive formulation which is given by

$$\Delta\mathscr{H}_{q,n} = \bigcup_{\substack{|\mathbf{i}|_1=q-n+1 \\ \sum i_j \leq q_{nr},\ \forall j \in N_n \setminus N_{n_r}}} (x_{1,\Delta}^{(i_1)} \otimes x_{2,\Delta}^{(i_2)} \otimes \ldots \otimes x_{n,\Delta}^{(i_n)}) \tag{6.24}$$

where, $x_{\bullet,\Delta}^{(i_l)} = x_{\bullet}^{(i_l)} \setminus x_{\bullet}^{(i_l-1)}$ with $x^{(0)} = \emptyset$, q is the level of sparse grid generation and q_{nr} is the level for insignificant random variables. Furthermore, in Eq. 6.24, $|\mathbf{i}|_1 = \sum_{k=1}^{n} i_k$ is the summation of hierarchies denoted by i_k for k^{th} random variable. $\Delta\mathscr{H}_{q,n}$ gives the locations of the support points generated exclusively at level q using tensor product. These locations are determined in a unit space (i.e. $\mathbb{I}^n$) by following Eq. 4.24 which can be linearly transformed to the original domain of the variable space $\Omega_{\mathbf{x}}$. The number of grid points $n_{s,i}$ in i^{th} hierarchial level is calculated by Eq. 4.23. This ultimately form a tree-like (or dendriform) structure as illustrated in Fig. 6.1(a) which starts with a centre point and fills the domain in successive levels like the branches of a tree. In the present study, the centre point reflects the reference point $\mathbf{c}$ in each iteration around which other points are placed. It may be noted that support points generated in the previous levels (i.e. $< q$) are considered in the i^{th} iterations i.e. $\mathscr{H}_{q,n} = \bigcup_{i \leq q} \Delta\mathscr{H}_{i,n}$. A 2D system with variables x_1 and x_2 is illustrated for visualization of the generation scheme adopted in the present study. Two cases are considered where the first case has both random variables as significant and in the other case, one random variable is insignificant. Fig. 6.1(b) and 6.1(c) gives the exclusive generation of supports points in each hierarchial level of sparse grid. Here, the individual hierarchal indices for x_1 and x_2 (i.e. i_1 and i_2, respectively) are assigned as 1, 2, ..., 5 for demonstration and the coordinates are evaluated using Eq. 4.24 in the unit space. In sparse grid, support points are selected based on the ℓ_1 norm of the hierarchal indices vector $\mathbf{i}$ and sparse grid q as in Eq. 6.24. Fig. 6.1(b) shows the selected indices based on its summation for different levels of q which are denoted by $\bullet$ in the plot. In the case of combination of significant and insignificant random variables, support points are generated based on additional constraint to limit the domain of the insignificant random variable. Thus, another ℓ_1 norm is introduced exclusively for the insignificant random variable. Here, the level q_{nr} is considered as 3 in this example. This results in equal generation of point for both the cases till the sparse grid level is 3. Thereon, only the hierarchal indices in the x_1 (i.e. significant random variable) direction are selected to generate the new locations. Subsequently, the number of support points generated in the case 2 are less than case 1 as shown in Fig. 6.1(c). Algorithm 6.1 shows these steps in dAMFD-HDMR for efficient stochastic computation which is given below.

Algorithm 6.1: dAMFD-HDMR with KLE

1 **Initialize:** Define the random fields and variables with $\mu_{\mathbf{x}}$, $\sigma_{\mathbf{x}}$ and $\rho_{\mathbf{x}}$. Assign $\mathbf{c}^1 \leftarrow \mu_{\mathbf{x}}$ and select a search domain $\Omega_{\mathbf{z}}$
2 Set *ind1* = true
3 $it = 1$
4 **while** *ind1* **do**
5 Assign q and o for iteration it
6 Generate $\mathscr{H}_{q,n}^{it}$ for $\binom{n}{o}$ combinations in $\Omega_{\mathbf{z}}$
7 Use KLE to discretize the random fields ⟶ Eq. A.5
8 Transform the coordinates to $\Omega_{\mathbf{x}}$ ⟶ Eq. 3.2
9 **if** $it > 1$ **then**
10 Squeeze the bounds by $\lambda_{it}^{\mathbf{x}}$
11 **end**
12 Obtain $g(\bullet)$ from the performance function
13 Perform sensitivity analysis ⟶ Eq. 6.23
14 Select n_r and screen respective indices $\mathbf{i}_d = \{i_1\, i_2\, \ldots\, i_{n_r}\}$ of the dimension
15 Generate more points using $\mathscr{H}_{q,n}^{it}$ ⟶ Eq. 6.24
16 Repeat line 6–12 but squeeze the bounds of points generated in previous line by $\lambda_{it}^{\mathbf{x}_{\mathbf{i}_d}}$
17 /* Check whether limit state is present in Ω_ξ */
18 **if** $g(\mathbf{z}) > 0$ and $\mathbf{z} \in \Omega_{\mathbf{z}}$ **then**
19 Extend $\Omega_{\mathbf{z}}$
20 **end**
21 Construct PCE for degree p ⟶ Eq. 4.11
22 Determine coefficients $\varphi_\bullet$ using MLS ⟶ Eq. 4.9
23 Build approximate response $\tilde{g}_{it}(\mathbf{x})$ for order o ⟶ Eqs. 6.15, 6.22
24 Evaluate $\tilde{g}(\mathbf{x})_{\text{MHDMR}}$ ⟶ Eq. 6.18
25 Optimization is performed over $\tilde{g}(\mathbf{x})_{\text{MHDMR}}$ to obtain $\mathbf{z}^{*,it}$ ⟶ Eq. 4.12
26 /* Convergence criteria is checked */
27 **if** $it > 1$ **then**
28 $criteria1 = |\mathbf{z}^{*,it} - \mathbf{z}^{*,it-1}|$
29 $criteria2 = |\tilde{g}(\mathbf{x}^{*,it})_{\text{MHDMR}} - \tilde{g}(\mathbf{x}^{*,it-1})_{\text{MHDMR}}|$
30 **if** $criteria1 \le \mathcal{E}_1$ and $criteria2 \le \mathcal{E}_2$ **then**
31 *ind1* = false
32 **else**
33 Update $it \leftarrow it + 1$
34 Assign new reference point $\mathbf{c}^{it} \leftarrow \mathbf{x}^{*,it} \leftarrow \mathbf{z}^{*,it}$
35 **end**
36 Increase $\lambda_{it}^{\mathbf{x}}$
37 **end**
38 Perform MCS over $\tilde{g}(\mathbf{x})_{\text{MHDMR}}$ to estimate moments and probability of failure

6.3 Numerical Results of Random Field Problem

In this section, the proposed multiple HDMR based stochastic computation is implemented for the analysis of composite plate whose parameters are modeled using random fields. Different methods such as direct

MCS and RS-HDMR [119] are also applied to prove the elegance of the proposed methods. Here, direct MCS is adopted as a benchmark to compare the accuracy of the results while RS-HMDR is a reference because of its analogous formulation to the proposed algorithm. Recently, RS-HDMR has been used for uncertainty quantification of composite plate with random variables [120]. The present study extends its application for random field problem where the discretization of the field is done using KLE as discussed in Appendix A. RS-HDMR used in this study involves 1st and 2nd order dimension decomposition as per Eq. 6.6 with modified Legendre polynomial scheme of the form [175]

$$\gamma_1 = \sqrt{3}(2x-1), \qquad \gamma_2 = \sqrt{5}(6x^2-6x+1), \qquad \gamma_3 = \sqrt{7}(20x^3-30x^2+12x-1) \tag{6.25}$$

and so on. It must be noted that the above equation is presented for one-dimension with $x \in [0\ 1]$ and can be extended for multi-dimension as well. The support points are generated using quasi-random sampling such as Sobol' sequence in the unit space. This requires linear transformation of the locations in the unit space to the original space of $\mathbf{x}$ such that all points lie within $\mu_{\mathbf{x}} \pm h_r \sigma_{\mathbf{x}}$, where h_r denotes the extent of support points in the original space. Moreover, component functions are adaptively selected using the variance-based sensitivity index with desired significance level [119]. The degree of orthogonal polynomials p is also determined adaptively by optimizing the error of the component functions. To avoid computational intractability, the maximum value of p is restricted to 5 for 1st and 2nd order RS-HDMR in this numerical study.

The value of p for AMFD-HDMR and its dimension adaptive version (i.e. dAMFD-HDMR) is selected based on the conclusions in Chapter 4 where orthogonal polynomial of degree 2 with MLS was found sufficiently adequate. Use of relatively lower polynomial degree allows a better control on the number of terms for which the coefficients $\mathbf{b}_\bullet$ are determined. Also, as discussed earlier, the sparse grid levels are selected judiciously to form computationally viable multiple grids. Consequently, the polynomial degree is preferred to be low as the number of support points are less due to the reduced sparse grid levels. This suggestion doesn't restricts the application of higher degree polynomials in the proposed work as one can extend it by using full PCE with adequate support points or by applying ad-hoc schemes for optimal selection of terms.

6.3.1 Validation Exercise

Firstly, the FE formulation of the linear composite plate as per Appendix B is examined by comparing with published results in Sasikumar *et al.* [75]. This validation exercise is conducted based on deterministic as well as stochastic analysis. The composite plate used here is square of size $b = 1$m as shown in Fig. B.1 with thickness $h = 0.010$m. Two different boundary conditions are examined with all sides are either simply supported or clamped which are represented by symbols 'S' and 'C', respectively. Three different laminate stacking sequences [0/90/0], [30/-30/30] and [0/30/60] are considered here which are denoted by numerals viz. '1', '2' and '3', respectively. Nomenclature presented here is same as in Sasikumar *et al.* [75]. For deterministic analysis, three different materials (i.e., HTS/M18, UMS/M18 and M55J/M18) are considered as given in Table 6.1. A 6×6 uniform mesh is used with nine noded quadrilateral element for FE modeling. It is subjected to constant UDL over the complete area which is shown by shaded region in Fig. B.1. The

Table 6.1: Properties of different composite plate materials in deterministic case

Material Property	Unit	HTS/M18	UMS/M18	M55J/M18
E_1	GPa	154.900	253.100	346.100
E_2	GPa	8.700	6.400	6.500
G_{12}	GPa	4.500	4.200	4.600
ν_{12}		0.281	0.250	0.310
X_t	GPa	2.409	2.103	1.891
X_c	GPa	1.148	8.269	0.587
Y_t	GPa	0.046	0.028	0.021
Y_c	GPa	0.196	0.174	0.106
T_{12}	GPa	0.083	0.060	0.054

magnitude of the load is determined corresponding to a desired failure index $\mathfrak{F}$ as per Eq. B.15. The failure index $\mathfrak{F} = 0.75$ is adopted here and the resulting UDL determined from the FE model is presented in Fig. 6.2. It is compared with the results from Sasikumar *et al.* [75] which shows a close match between them. Using

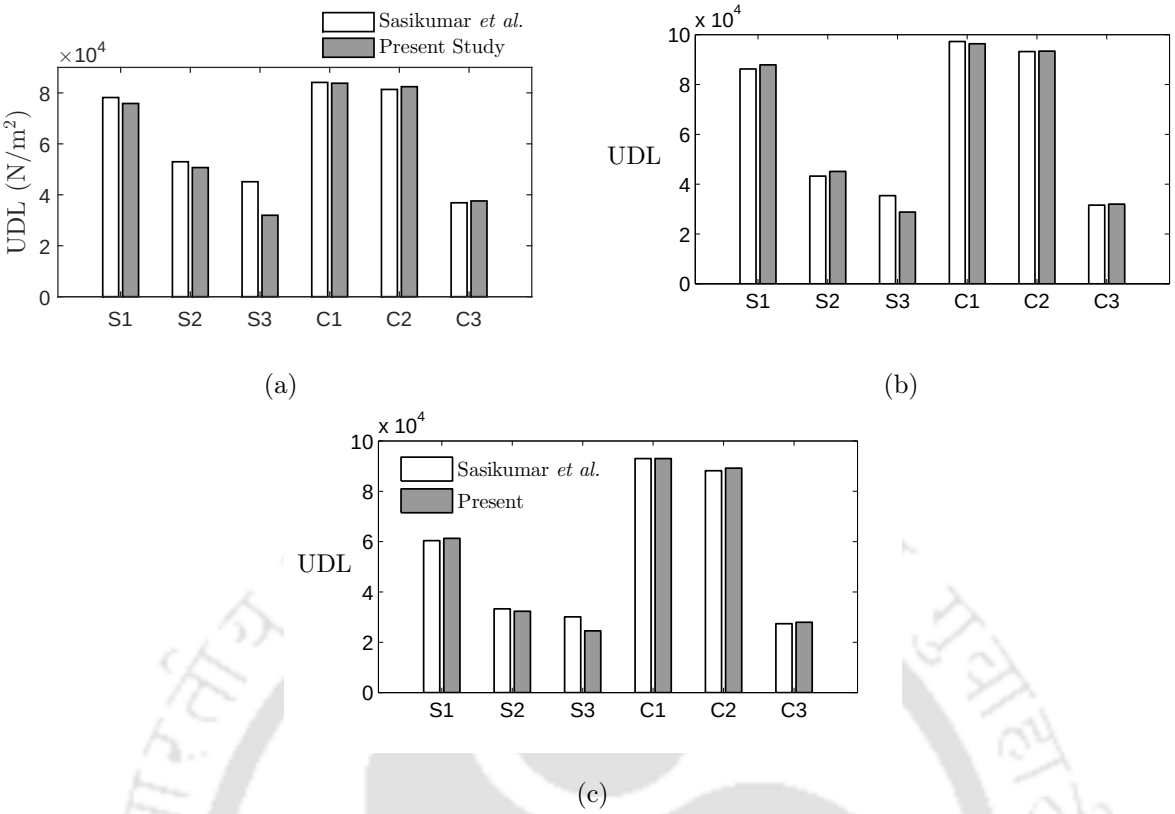

Figure 6.2: Uniformly distributed load for various cases of composite plate with material properties (a) HTS/M18, (b) UMS/M18 and (c) M55J/M18

Table 6.2: Probability of failure estimated for validation of the present FE model

Case	MCS done by [75]	Present Study	
		p_f	Error (%)
S1	0.2433	0.2382	2.10
S2	0.2110	0.2170	2.84
S3	0.3004	0.3005	0.03
C1	0.2234	0.2362	5.73
C2	0.2110	0.2172	2.94
C3	0.2234	0.2214	0.90

these loads, failure index is estimated with the random properties prescribed by Sasikumar *et al.* [75] (see Table 3.5). MCS is performed with a sample size of 5000 and the resulting *pdf* of the failure index is shown in Fig. 6.3 for different support conditions and sequences. Moreover, probability of failure p_f is estimated for the limit state defined at $\mathfrak{F} = 1$. Estimated p_f from the present study using MCS is given in Table 6.2 for validation with the published MCS data [75]. It can be observed that these estimates are also in close agreement with the published results.

6.3.2 Uncertainty Quantification and Reliability Analysis

Once the FE model is validated, stochastic analysis is performed using proposed models for AMFD-HDMR and dAMFD-HDMR. Here, the material parameters E_1, E_2 and G_{12} are modeled as random fields following non-Gaussian distribution with their statistical properties given in Table 3.5. The correlation function of spatial random field is defined as in Eq. A.2 with isometric correlation structure, $l_x = l_y = 0.40$. Remaining parameters in the table such as ν_{12}, X_t, X_c, Y_t, Y_c and T_{12} are considered to be random variables. The FE model of the composite plate is discretized by a 6×6 uniform mesh which results in 6×6×3 variables for the above mentioned random fields, thus this plate problem has a total of 114 (i.e. $6 \times 6 \times 3 + 6$)

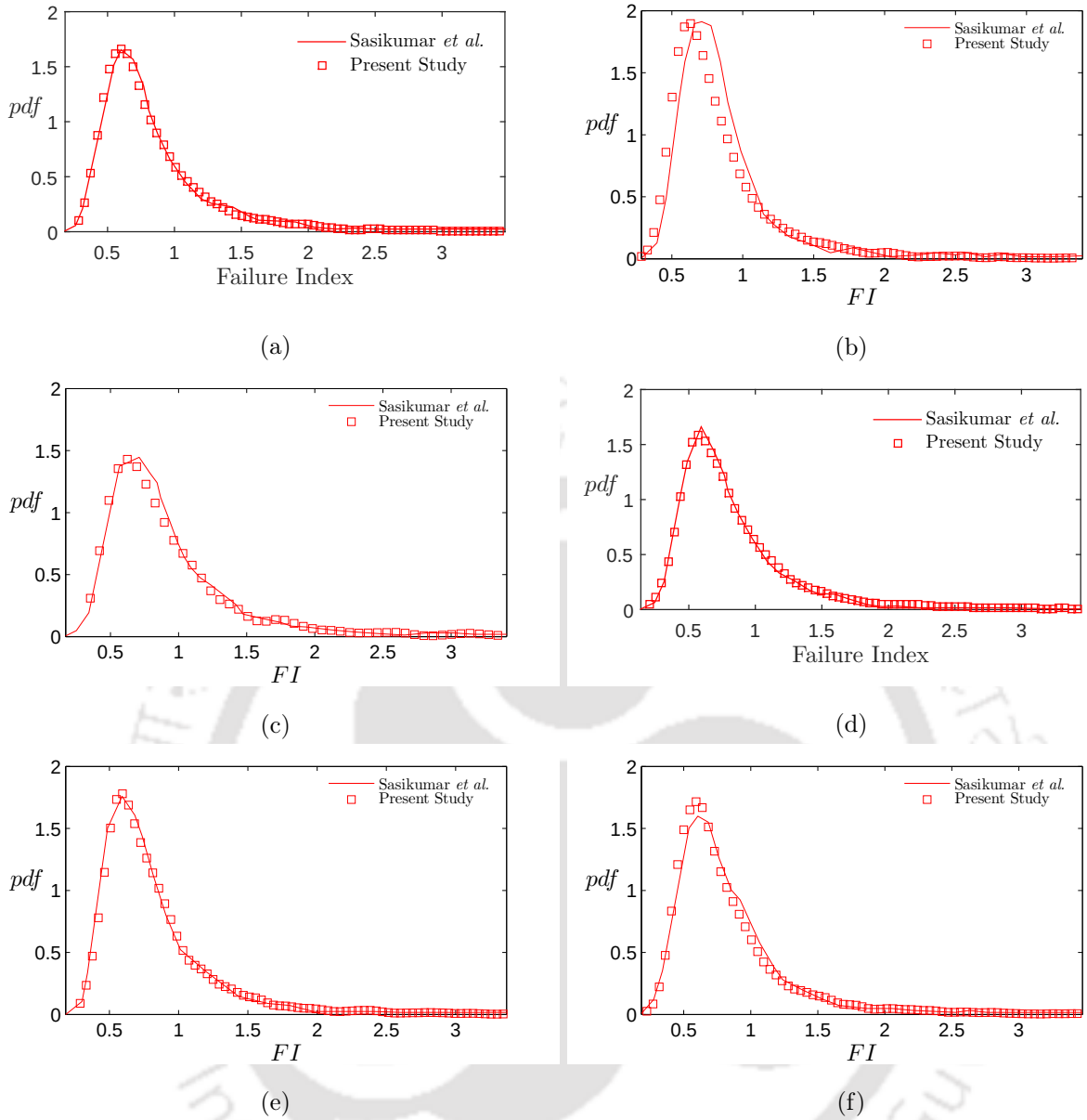

Figure 6.3: Comparison of *pdf* for various cases of composite plate; (a) S1, (b) S2, (c) S3, (d) C1, (e) C2 and (f) C3

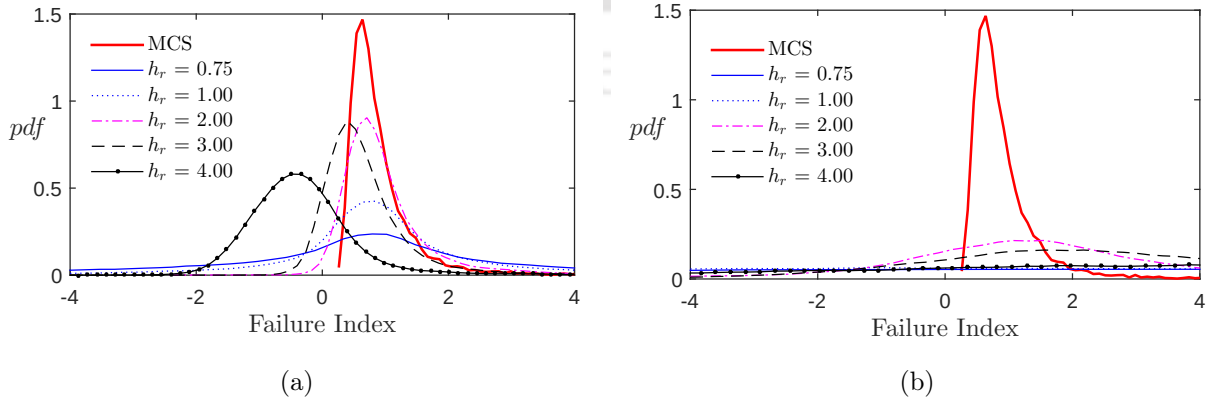

Figure 6.4: Probability distribution using different h_r values for (a) 1st order and (b) 2nd order RS-HDMR

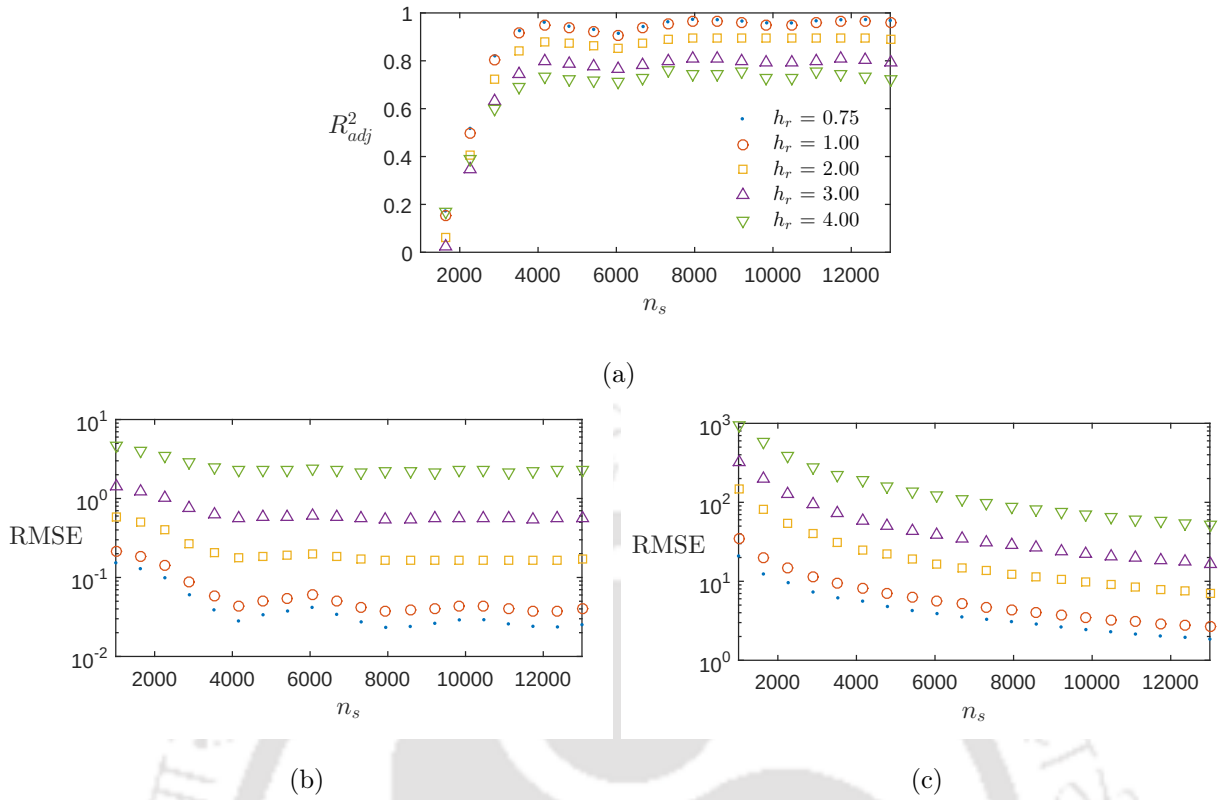

Figure 6.5: Effect on accuracy of RS-HDMR due to number of support points using (a) adjusted R^2, (b) RMSE for 1st order RS-HDMR and (c) RMSE for 2nd order RS-HDMR

random variables. For brevity, S1 composite plate is considered for further analysis in this study. Using the above information, spatially variable composite plate is solved for stochastic analysis using direct MCS with a sample size of 5000. The results are compared with RS-HDMR [119] where both 1st and 2nd orders are applied along with KLE. The support points required to construct the RS-HDMR are generated using Sobol' sequence with varying $h_r = 0.75$, 1.00, 2.00, 3.00 and 4.00. A maximum number of 114^2 (i.e. 12996) support points are populated for each case of h_r. Fig. 6.4 shows the *pdf* estimated using different h_r values for 1st and 2nd order RS-HDMR. It is observed that both orders yield significant error for all the cases of h_r in spite of using more original FE evaluations than direct MCS. Contrary to the usual notion, 2nd order RS-HDMR [see Fig. 6.4(b)] suffered more error which can be argued plausibly due to the contributions of spurious component functions. These is caused by collective effect of the insignificant variables in the 2nd order component functions. Quality of the fit is further investigated with varying support points using adjusted R^2 and root mean square error (RMSE). It may be noted that in RS-HDMR, additional test points are not generated but the same support points are used to estimate the modelling error. For 1st order approximation, Fig. 6.5(a) and 6.5(b) show improvement with the increase of support points till 8000 beyond which the change in quality remains marginal. Also, the improvement is noticed with decrease in h_r value as it confines the support points in a smaller domain. Similar observation is made in Fig. 6.5(c) for 2nd order RS-HDMR where the modelling error monotonically decreases with more support points. Moreover, as predicted from 6.4(b), large error is noticed for 2nd order RS-HDMR as compared to 1st order. These results infer that computational effort required is more for better fitting of RS-HDMR than direct MCS which makes it inefficient as well as inaccurate for large dimensional problem like the one illustrated here.

Next, the meta-model is developed using the proposed AMFD-HDMR algorithm with 1st order which consumes 2290 support points and take 10 iterations to converge. The extent of new sparse grids $\mathscr{H}^{it}_{2,n}$ are reduced by 60%–90% during successive iterations as suggested in Chapter 4 i.e. $\lambda^{\mathbf{x}}_{it} = 1 - 0.75^{(it-1)}$. The results obtained from the AMFD-HDMR are shown in Fig. 6.6 which illustrates adequate mapping of the *pdf* and CDF with direct MCS data. On extending it to 2nd order, support points require generation of $\mathscr{H}^{it}_{3,n}$ for $\binom{n}{2}$ combinations (i.e. a total of 26221 points). Hence, only $it = 1$ is considered with 2nd order HDMR followed by the successive iterations with order 1 to alleviate the computational expense. The 2nd

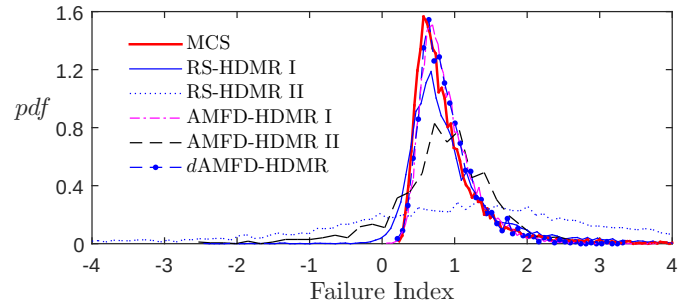

(a)

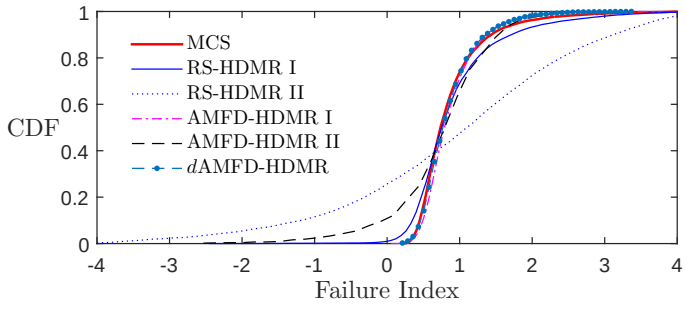

(b)

Figure 6.6: Probability distribution of failure index from composite plate with spatial correlation using different methods

Table 6.3: Results of the reliability assessment for linear composite with random field

Method	p_f	Error (%)	No. of Function Calls	Remark
MCS	0.2826	-	5000	-
	0.3379	19.57		$h_r = 0.75$
	0.1862	34.11		$h_r = 1.00$
RS-HDMR I	0.0082	97.10	12996	$h_r = 2.00$
	0.0576	79.62		$h_r = 3.00$
	0.7285	157.78		$h_r = 4.00$
	0.3682	30.29		$h_r = 0.75$
	0.3672	29.94		$h_r = 1.00$
RS-HDMR II	0.2393	15.32	12996	$h_r = 2.00$
	0.1992	29.51		$h_r = 3.00$
	0.2356	16.63		$h_r = 4.00$
AMFD-HDMR I	0.2842	0.57	2290	$it = 10$
AMFD-HDMR II	0.3620	28.10	26679	$it = 3$
dAMFD-HDMR	0.2828	0.08	2067	$it = 7$

order formulation also suffered inaccuracy as observed in RS-HDMR. To address this issue i.e. *curse of dimensionality* in 2[nd] order, dAMFD-HDMR is employed following Algorithm 6.1. The initial HDMR is constructed using $o = 1$ with $\mathscr{H}^1_{3,n}$ for all the random variables. Using the values of $g(\bullet)$ at these support points, correlation coefficients are determined with respect to each dimension. In general, threshold value of correlation coefficient can be selected between 0.2–0.5. The present study adopts it as 0.35 to curtail the dimension. From $it = 2$ onwards, intermittent HDMR formulation as suggested in Eq. 6.22 is utilized which provides better convergence with less support points (see Table 6.3). This observation strengthens the previous argument made on the erroneous mutual effect caused by the spurious terms which are eliminated in the dAMFD-HDMR algorithm. It can be noted that the sensitivity analysis only assumes axial-points

(i.e. $\mathscr{H}^{it}_{2,n}$) which overlooks the combined effect of variables. This limitation is overcome by the iterative scheme which incorporates different locations based on multiple reference points evaluated in the optimization process. Fig. 6.6(a) and 6.6(b) highlight the efficiency of the proposed method which commences with all available KLE terms but gradually screen them based on the sensitivity. This reduces the number of random variables in the discretized random fields while preserving their overall influence on the performance function. The probability of failure estimated using the above mentioned algorithm is also given in Table 6.3. A close match is observed between the MCS results, 1st order AMFD-HDMR and dAMFD-HDMR. In addition to the weight function employed in this formulation (i.e. [178]), effect of the different weight functions used in MLS technique are also studied here. Fig. 6.7 illustrates the performance of these weights within the present framework without the loss of generality and bias.

Using the proposed methods, fragility curves are generated for cases with non-Gaussian and Gaussian random fields as shown in Fig. 6.8. It is found that non-Gaussianity affects p_f especially in the low range (say 10^{-4}) where 60% difference is reported. However, this exercise clearly establishes the efficiency and accuracy of the proposed AMFD-HDMR and its dimension adaptive version that can estimate p_f even at a very low range. Furthermore, it can be noted that AMFD-HDMR II (i.e. with 2nd order) suffers large error as opposed to general notion that inclusion of 2nd order term improves the quality of meta-modeling. To address this issue, dAMFD-HDMR improvises with the 2nd order terms and truncates all unwanted terms based on the sensitivity analysis. As it employs a combination of all 1st order terms and selective 2nd order terms, the overall performance (i.e. accuracy and computational cost) is enhanced. In this context, it should be mentioned that a clear distinction is difficult to draw between the applications of these two methods. Both of them are found to produce excellent results for the same problem. As these numerical methods are improvised in two different ways for optimal performance, either of them may be adopted for real life problems.

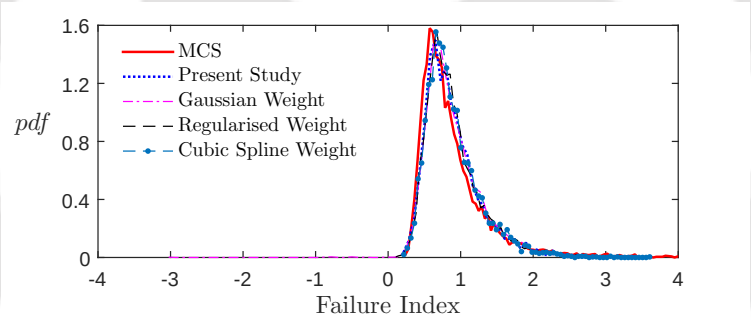

(a)

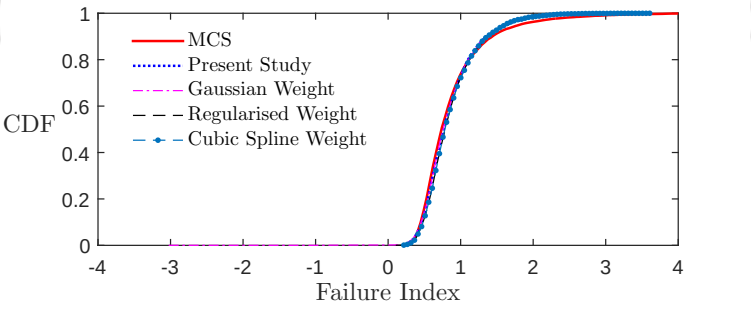

(b)

Figure 6.7: Probability distribution of failure index from composite plate with spatial correlation using different using different weight functions in the MLS technique

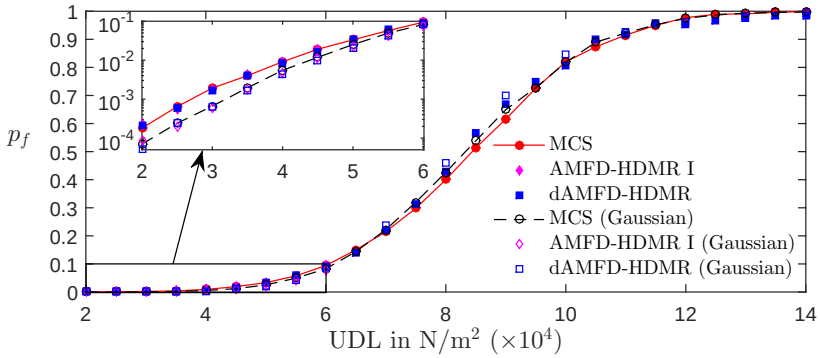

Figure 6.8: Fragility plot of composite plate having Gaussian and non-Gaussian random fields with varying UDL

6.4 Summary

In this chapter, a novel combination of adaptive dimension decomposition technique with hierarchical selection of the sub-grid support points is proposed. It uses finite difference HDMR which has not been studied much in the recent past for stochastic FE analysis as compared to random sampling based ANOVA decomposition. An adaptive algorithm (viz., dAMFD-HDMR) is proposed for efficient and accurate estimation of the uncertainty in structural problems with random fields discretized by KLE. The proposed approach provide an effective way to apply multiple HDMR based decomposition with sparse grids for stochastic computations of large dimension problems. Orthogonal polynomial bases are adopted to determine the interpolation of component functions in HDMR for better efficiency. The present study illustrates the application of Hermite polynomial scheme involving standard normal random variables. Adaptiveness of these interpolations are improved using MLS technique which also helps in limiting the number of unknown terms. The notable contributions of the work are summarized as follows

- Generation of multiple sparse grids based on the optimization to the find most probable failure point results in adequate population of the support points near the limit state. It has proved to be an efficient generation scheme for low sparse grid levels which produce enough support points close to the limit state.
- Moreover, distribution adaptive locations of support points are generated by incorporating the statistical properties of the respective variables. This helps in gaining points near statistically important regions (e.g. area near mean and tail ends), consequently aiding in uncertainty quantification.
- Application of MLS-PCE technique requires low polynomial degree to determine unknown coefficients of the component functions which, in turn, yields limited number of basis terms making the interpolation computationally attractive.
- Two different algorithms are proposed for anchored HDMR which outperform conventional RS-HDMR for stochastic finite element analysis. This argument do not refute the importance and effectiveness of the RS-HDMR which has other important applications but highlights its performance in large dimension problems where significant error is generated by the global random sampling.
- In stochastic analysis, dimension of random field discretization are often reduced by curtailing the KLE terms (typically upto 10). The proposed dimension adaptive approach (i.e. dAMFD-HDMR) addresses this limitation by evaluating sensitivity of the dimension with respect to the output. Therefore, screening the undesired dimension based on its significance instead of crude elimination. Furthermore, this exercise makes dAMFD-HDMR attractive for application with different random field expansion schemes (e.g. Neumann Expansion, Optimal Linear Expansion) which can be explored in future.
- Proposed approach provide an efficient way to evaluate design point based approximation for high dimensional problems (> 100) using meta-models.

Therefore, it can be summarized that the proposed approach show potential for problems with large dimension modeled using random fields with short correlation lengths. The evolving distribution adaptive

characteristics of the algorithms prove to be efficient for accurate estimation of uncertainty and/or reliability than its analogous methods (e.g. RS-HDMR) available in the literature.

Chapter 7

Hybrid Dimension Adaptive HDMR

7.1 Introduction

The previous chapters in this thesis have proposed considerable modifications of the basis, terms (i.e. component functions) and unknown coefficients of the meta-model formulation. These modifications include MLS technique which employs evolving coefficients to minimize the error at individual locations based on an assumed weight function. Hence, making the proposed formulation scalar in the sense that each realization needs to be solved independently. It, eventually, results in computation of multiple matrix inversions for uncertainty quantification and reliability analysis. This issue is addressed in this chapter where a new alternative formulation of the dAMFD-HDMR is proposed. Besides matrix inversion, the error term in this proposal is assumed to follow Gaussian distribution. This new adaptive sparse formulation of the HDMR is based on the significance of the dimension. Thus, the model presented in this chapter uses the apt combination of dimension adaptive (d-Adaptive) formulation with multiple generations of the HDMR. Here, the error is also modelled along with the adaptive sparse formulation of HDMR for local approximation of the response surface. This combination of multiple dimension decompositions with Gaussian error makes the proposal a hybrid meta-model. It is applied to solve different problems in stochastic computation which includes accurate estimation of the probability of failure by near exact representation of the limit state, especially near the failure region. It also improves the computational cost of a reliability based design problem with large number of random parameters for optimal solution. The application of the proposed method is studied for stochastic composite plates with different support conditions when exposed to spatial randomness in material properties. The mathematical framework of the proposed hybrid HDMR is discussed in the following section.

7.2 Development of Proposed Hybrid d-Adaptive HDMR

In the previous chapter, the basic formulation of d-Adaptive HDMR is presented to model the input–output relation of large dimensional problems. In general, this relation involves lower order influences of the input variables for a well-defined physical system [112]. The proposal uses this characteristic for hierarchical decomposition of the original function, thus making it robust for reliability analysis and uncertainty quantification.

Let a physical system or model which yields an output $g(\mathbf{x})$ is subjected to a n-dimensional vector of input variables represented by $\mathbf{x}$ where the performance function is expressed by Eq. 6.6. The number of component functions in the j^{th} order is given by $\binom{n}{j}$. On determining these component functions and substituting them back into Eq. 6.6 gives the simplified summand expansion of the original function $g(\mathbf{x})$. As suggested earlier, it is assumed that the higher order component functions in HDMR formulation are insignificant and hence, they are neglected for computational efficiency. Thus, only limited lower order terms are considered for accurate and efficient determination of the output. This truncation typically proves to be

adequate for practical problems, however, it doesn't undermines the significance of any higher order term in Eq. 6.6. The importance of a particular order is specific to the problem which can be determined based on the sensitivity analysis (e.g. Sobol' sensitivity indices). This, in turn, makes the formulation adaptive where only important terms are retained for the analysis. This procedure (i.e. sensitivity analysis) demand significant computational cost which in this chapter is alleviated by an efficient hybrid *d*-Adaptive approach as explained below.

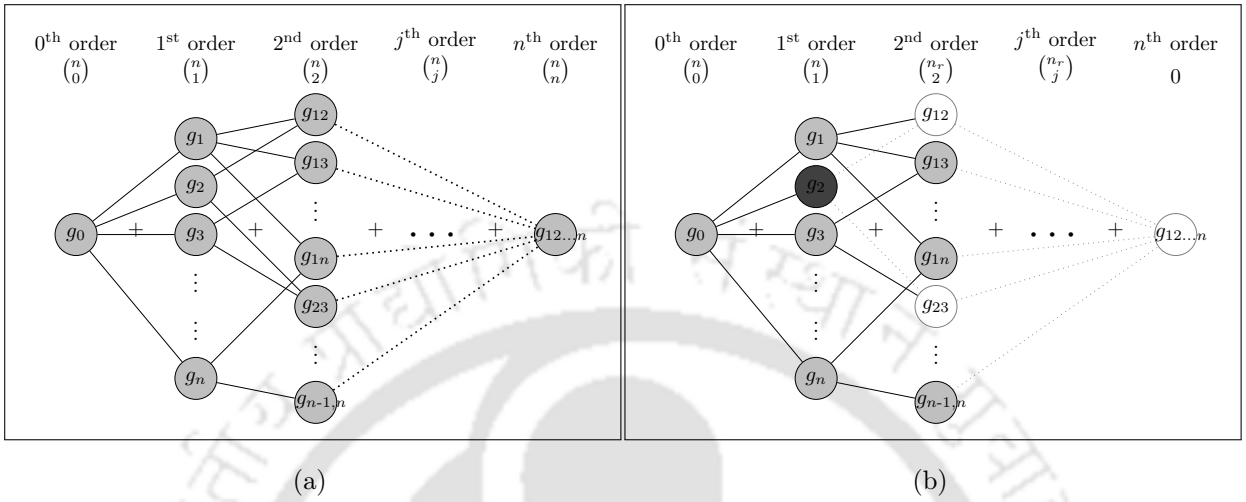

Figure 7.1: Schematic representation of hierarchy in HDMR in terms of component functions for (a) complete formulation with n variables and (b) sparse formulation as per d-Adaptive proposal where only variable x_2 is screened as insignificant such that $n_r = n - 1$ (highlighted by dark grey colour). The number of component function in each order is calculated by binomial operator as specified and for simplicity $g(x_i)$ is denoted by g_i.

Suppose, a few input variables in $\mathbf{x}$ are significant (*viz.* x_{i_1}, x_{i_2}, ..., $x_{i_{n_r}}$) to the output whose indices $\{i_1, i_2, \ldots, i_{n_r}\} \in N_{n_r}$ form a subset of $N_n = \{1, 2, \ldots, n\}$. The component functions associated with the insignificant variables (i.e. x_i, $\forall\, i \in N_n \setminus N_{n_r}$) constitute a residual term $\hat{\mathscr{R}}_{n_r}$. This residual is neglected in the HDMR formulation without loss of accuracy for all practical purpose. It leads to the curtailment of the expansion in Eq. 6.6 as shown in Fig. 7.1b where the insignificant variables are marginalized to save the computational cost. Hence, the basic dimension curtailed formulation of the HDMR is given by

$$g(\mathbf{x}) = g_0 + \sum_{i_1 \in N_{n_r}} g_{i_1}(x_{i_1}) + \sum_{\substack{i_1, i_2 \in N_{n_r} \\ i_1 < i_2}} g_{i_1 i_2}(x_{i_1}, x_{i_2}) + \cdots + \sum_{\substack{i_1, i_2, \ldots, i_j \in N_{n_r} \\ i_1 < i_2 < \cdots < i_j}} g_{i_1 i_2 \ldots i_j}(x_{i_1}, x_{i_2}, \ldots, x_{i_j}) + \cdots + g_{i_1 i_2 \ldots i_{n_r}}(x_{i_1}, x_{i_2}, \ldots, x_{n_r}) + \hat{\mathscr{R}}_{n_r} \tag{7.1}$$

In this study, finite difference HDMR is used with a reference point (or anchor point) through which hyperplanes are constructed. Let $\mathbf{c} = \{c_{i_1}\ c_{i_2}\ \cdots\ c_{n_r}\}$ be this point to construct the component functions. As a practical choice, the reference point is often set to the mean values $\mu_{\mathbf{x}}$ of the input variables. The component functions are determined by the formation of the hypothetical planes through $\mathbf{c}$ which cuts the function for an accurate representation. This results in a sequential evaluation of the component functions as

$$g_0 = g(\mathbf{c}), \quad g_{i_1}(x_{i_1}) = g(\mathbf{c}_{i_1}, x_{i_1}) - g_0, \quad g_{i_1 i_2}(x_{i_1}, x_{i_2}) = g(\mathbf{c}_{i_1 i_2}, x_{i_1}, x_{i_2}) - g_{i_1}(x_{i_1}) - g_{i_2}(x_{i_2}) - g_0 \tag{7.2}$$

and so on, where $g(\mathbf{c}_{i_1}, x_{i_1})$ and $g(\mathbf{c}_{i_1 i_2}, x_{i_1}, x_{i_2})$ denote the subfunctions $g(x_{i_1}, c_{i_2}, \ldots, c_{n_r})$ and $g(x_{i_1}, x_{i_2}, c_{i_2}, \ldots, c_{n_r})$, respectively. In the subfunctions, the coordinates of all the input variables are locked at the reference point except for the specific input variables which are mentioned in the brackets. Similarly, the notations can be extended for the other component functions of the HDMR expansion. These component functions are subtracted by the preceding orders (as in Eq. 7.2) to assure the exclusive contribution of that

order in the expansion. Substituting Eq. 7.2 till 1st order terms back in Eq. 7.1 leads to

$$g(\mathbf{x}) = \sum_{i_1 \in N_{n_r}} g(\mathbf{c}_{i_1}, x_{i_1}) + (n_r - 1) g(\mathbf{c}) + \hat{\mathscr{R}}_1 \tag{7.3}$$

where, $\hat{\mathscr{R}}_1$ is the residual contribution of all orders above 1. The bivariate contributions of the input variables are presented by the 2nd order component function $g_{i_1 i_2}(x_{i_1}, x_{i_2})$. These are determined by a surface cut through the variable space defined by x_{i_1} and x_{i_2} at a location $\mathbf{c}$. Hence, the 2nd order dimension curtailed HDMR expansion can be obtained following the similar process

$$g(\mathbf{x}) = \sum_{\substack{i_1, i_2 \in N_{n_r} \\ i_1 < i_2}} g(\mathbf{c}_{i_1 i_2}, x_{i_1}, x_{i_2}) - (n_r - 2) \sum_{i_1 \in N_{n_r}} g(\mathbf{c}_{i_1}, x_{i_1}) + \frac{(n_r - 1)(n_r - 2)}{2} g(\mathbf{c}) + \hat{\mathscr{R}}_2 \tag{7.4}$$

where, the notation $\hat{\mathscr{R}}_2$ represents the residual in 2nd order HDMR. The above expressions (i.e. Eqs. 7.3 and 7.4) explicitly eliminate the contributions of all the insignificant dimensions from the expansion. However, in the present study it is proposed to use 1st order with all the random variables and thereon, the dimensions are curtailed from 2nd order onward. This intermittency is recommended for practical purpose as it reduces the number of component functions which increases with order. Hence, the new dimension curtailed expansion is given as

$$\begin{aligned} g(\mathbf{x}) = & \sum_{\substack{i_1, i_2 \in N_{n_r} \\ i_1 < i_2}} g(\mathbf{c}_{i_1 i_2}, x_{i_1}, x_{i_2}) - (n_r - 1) \sum_{i_1 \in N_{n_r}} g(\mathbf{c}_{i_1}, x_{i_1}) \\ & + \sum_{i_1 \in N_n} g(\mathbf{c}_{i_1}, x_{i_1}) + \left\{ \frac{n_r(n_r - 1)}{2} - (n - 1) \right\} g(\mathbf{c}) + \acute{\mathscr{R}}_2 \end{aligned} \tag{7.5}$$

The residual in this expansion is represented by $\acute{\mathscr{R}}_2$. The above expansion can also be expressed in the compact for $g(\mathbf{x}) = \tilde{g}(\mathbf{x}) + \acute{\mathscr{R}}$, where $\tilde{g}(\mathbf{x})$ is the approximation without the residual influence. Also, this expression is subjected to evaluation of $g(\bullet)$ at only the reference point $\mathbf{c}$ and the support points around it. Hence, to determine the output at any arbitrary point $\mathbf{x}$, the expansion in Eq. 7.5 is modified as

$$\begin{aligned} \tilde{g}(\mathbf{x}) = & \sum_{\substack{i_1, i_2 \in N_{n_r} \\ i_1 < i_2}} y_{i_1 i_2}(\mathbf{c}_{i_1 i_2}, x_{i_1}, x_{i_2}) - (n_r - 1) \sum_{i_1 \in N_{n_r}} y_{i_1}(\mathbf{c}_{i_1}, x_{i_1}) \\ & + \sum_{i_1 \in N_n} y_{i_1}(\mathbf{c}_{i_1}, x_{i_1}) + \left\{ \frac{n_r(n_r - 1)}{2} - (n - 1) \right\} y_0 \end{aligned} \tag{7.6}$$

In this context, the sensitivity analyses to identify the important input variables are performed using Pearson correlation coefficient as given in Eq. 6.23 where the correlation coefficients $\rho_{g x_i}$ are evaluated to detect the importance of that particular variable.

Once the significant variables are selected, associated unknown terms are represented by the subfunctions of $g(\mathbf{x})$. In this chapter, these terms are expressed by truncated PCE for local approximation. This secondary representation of each component function is required to determine the response at any arbitrary point based on the values at the support points. Earlier, the coefficients associated with the PCE were used to address the local approximation using MLS technique as suggested in Chapter 6. Application of MLS incurred a scalar approach which leads to independent determination of the unknown coefficients at each realization. This issue is addressed by introducing additional nonparametric terms [i.e. $U(\bullet)$] in each cut made by the finite difference-HDMR under the proposed formulation. Hence, the secondary approximation in each component function is represented by

$$y_k(\bullet) = \alpha_0 \Gamma_0 + \sum_{i_1 \in k} \alpha_{i_1} \Gamma_1(z_{i_1}) + \sum_{i_1, i_2 \in k} \alpha_{i_1 i_2} \Gamma_2(z_{i_1}, z_{i_2}) + \cdots$$

$$+ \sum_{i_1,i_2,\ldots,i_p \in k} \alpha_{i_1 i_2 \ldots i_p} \Gamma_p(z_{i_1}, z_{i_2}, \ldots, z_{i_p}) + \underbrace{\sum_{1 \le j \le n_e} \beta_j R_k(\mathbf{z}, \mathbf{z}^j)}_{U_k(\bullet)} \tag{7.7}$$

Here, the notation k represents the associated indices i_1, i_2, …, i_{n_r}, $i_1 i_2$, …, $i_{n_r-1} i_{n_r}$ as per Eq. 7.6 in a set and p denotes the degree of orthogonal polynomial bases Γ_p. Previous literatures [51, 53, 162] suggest various orthogonal bases Γ as per Askey scheme which can be adopted in this formulation. However, Hermite polynomial bases are used in this study as given in Eq. 4.5. The unknown coefficients associated to theses bases in Eq. 7.7 are α_0, α_{i_1}, $\alpha_{i_1 i_2}$, …, $\alpha_{i_1 i_2 \ldots i_p}$ and the variable z is Gaussian with $\mathcal{N}(0,1)$. This discretization is also helpful as it can be directly adopted for random fields modelled by Karhunen-Loève transformation as both are in the standard normal space. Moreover, this formulation can be extended for different distributions using standard transformation techniques e.g. Rosenblatt transformation [4] or Nataf model [148].

Here, it may be noted that in this formulation, the component functions includes nonparametric terms $U_k(\bullet)$ in PCE framework. It helps to capture the influence of n_s support points based on the spatial correlation function $R_k(\mathbf{z}^I, \mathbf{z}^J)$ in the variable space. Different correlation functions exist in the literature for this purpose e.g. linear, cubic, spline, exponential, Gaussian etc. [103]. In this study, the nonparametric term $U_k(\bullet)$ is assumed to be Gaussian with zero mean and $\sigma_k^2 R_k(\mathbf{z}^I, \mathbf{z}^J)$ as the covariance, where σ_k is the standard deviation. On simplification, Eq. 7.7 can be rewritten as

$$y_k(\bullet) = \boldsymbol{\Gamma}_k(\bullet)^\mathsf{T} \boldsymbol{\alpha}_k^* + \mathbf{r}_k(\bullet)^\mathsf{T} \boldsymbol{\beta}_k^* \tag{7.8}$$

which is substituted back into Eq. 7.6 to get the proposed hybrid formulation of the d-Adaptive HDMR in the following format

$$\begin{aligned}\tilde{g}(\mathbf{x}) = &\underbrace{\sum_{\substack{i_1,i_2 \in N_{n_r} \\ i_1<i_2}} \boldsymbol{\Gamma}_{i_1 i_2}(x_{i_1}, x_{i_2})^\mathsf{T} \boldsymbol{\alpha}_{i_1 i_2}^* - (n_r - 1) \sum_{i_1 \in N_{n_r}} \boldsymbol{\Gamma}_{i_1}(x_{i_1})^\mathsf{T} \boldsymbol{\alpha}_{i_1}^* + \sum_{i_1 \in N_n} \boldsymbol{\Gamma}_{i_1}(x_{i_1})^\mathsf{T} \boldsymbol{\alpha}_{i_1}^*}_{\text{proposed } \textit{hybrid} \text{ formulation}} \\ &+ \underbrace{\sum_{\substack{i_1,i_2 \in N_{n_r} \\ i_1<i_2}} \mathbf{r}_{i_1 i_2}(x_{i_1}, x_{i_2})^\mathsf{T} \boldsymbol{\beta}_{i_1 i_2}^* - (n_r - 1) \sum_{i_1 \in N_{n_r}} \mathbf{r}_{i_1}(x_{i_1})^\mathsf{T} \boldsymbol{\beta}_{i_1}^* + \sum_{i_1 \in N_n} \mathbf{r}_{i_1}(x_{i_1})^\mathsf{T} \boldsymbol{\beta}_{i_1}^*}_{\text{proposed } \textit{hybrid} \text{ formulation}} \\ &+ \left\{ \frac{n_r(n_r-1)}{2} - (n-1) \right\} \boldsymbol{\Gamma}_0^\mathsf{T} \boldsymbol{\alpha}_0^*\end{aligned} \tag{7.9}$$

Expanding the above equation gives the complete expression for the proposed *hd*A-HDMR which takes the following form

$$\begin{aligned}\tilde{g}(\mathbf{x}) = &\sum_{j_1=1}^{n_r-1} \sum_{j_2>j_1}^{n_r} \left[\sum_{k_2=0}^{p} \left\{ \sum_{l_1=1}^{2} \cdots \sum_{l_{k_2}=1}^{l_{k_2-1}} \alpha_{i_{j_{l_1}} \ldots i_{j_{l_{k_2}}}} \Gamma_{k_2}(z_{i_{j_{l_1}}}, \ldots, z_{i_{j_{l_{k_2}}}}) \right\} \right] \\ &- (n_r - 1) \sum_{j_1=1}^{n_r} \left\{ \sum_{k_1=0}^{p} \alpha_{i_{j_1},k_1} \Gamma_{k_1}(z_{j_1}) \right\} + \sum_{j_1=1}^{n} \left\{ \sum_{k_1=0}^{p} \alpha_{i_{j_1},k_1} \Gamma_{k_1}(z_{j_1}) \right\} \\ &+ \sum_{j_1=1}^{n_r-1} \sum_{j_2>j_1}^{n_r} \left[\sum_{m_2=1}^{n_s} \beta_{m_2} R_{i_{j_1} i_{j_2}}(\mathbf{z}, \mathbf{z}^{m_2}) \right] - (n_r - 1) \sum_{j_1=1}^{n_r} \left[\sum_{m_1=1}^{n_s} \beta_{m_1} R_{i_{j_1}}(\mathbf{z}, \mathbf{z}^{m_1}) \right] \\ &+ \sum_{j_1=1}^{n} \left[\sum_{m_1=1}^{n_s} \beta_{m_1} R_{i_{j_1}}(\mathbf{z}, \mathbf{z}^{m_1}) \right] + \left\{ \frac{n_r(n_r-1)}{2} - (n-1) \right\} \alpha_0 \Gamma_0\end{aligned} \tag{7.10}$$

It can be noted that the above formulation in Eq. 7.10 is constructed for a single decomposition around the reference point. However, the proposal involves an iterative scheme for efficient support point generation around multiple reference points. In this regard, multiple HDMRs are constructed over these associated

reference points. The contribution of each HDMR is summarized as

$$\tilde{g}(\mathbf{x}) = \sum_{i=1}^{it} \gamma^{(i)}(\mathbf{x}, \mathbf{c}^{(i)}) \tilde{g}^{(i)}(\mathbf{x}) \tag{7.11}$$

where, it is the number of iterations. These multiple generations also provide flexibility by incorporating different polynomial degree p and order o for individual HDMR. A typical example of this can be explained using two different orders, say 1st and 2nd orders, in different iterations. Here, the first iteration utilizes 2nd order model whereas successive iterations use 1st order. This is applied to limit the number of support points and subsequently, the computational effort without loss of accuracy as suggested in Chapter 6. Thus, the *hd*A-HDMR formulation is expressed here by

$$\begin{aligned}
\tilde{g}(\mathbf{x}) = \gamma^{(1)}(\mathbf{x}, \mathbf{c}^{(1)}) \Bigg[& \sum_{j_1=1}^{n_r-1} \sum_{j_2>j_1}^{n_r} \left[\sum_{k_2=0}^{p^{(1)}} \left\{ \sum_{l_1=1}^{2} \cdots \sum_{l_{k_2}=1}^{l_{k_2-1}} \alpha^{(1)}_{i_{j_{l_1}} \cdots i_{j_{l_{k_2}}}} \Gamma^{(1)}_{k_2}(z_{i_{j_{l_1}}}, \ldots, z_{i_{j_{l_{k_2}}}}) \right\} \right] \\
& - (n_r - 1) \sum_{j_1=1}^{n_r} \left\{ \sum_{k_1=0}^{p^{(1)}} \alpha^{(1)}_{i_{j_1},k_1} \Gamma^{(1)}_{k_1}(z_{i_{j_1}}) \right\} + \sum_{j_1=1}^{n} \left\{ \sum_{k_1=0}^{p^{(1)}} \alpha^{(1)}_{i_{j_1},k_1} \Gamma^{(1)}_{k_1}(z_{i_{j_1}}) \right\} \\
& + \sum_{j_1=1}^{n_r-1} \sum_{j_2>j_1}^{n_r} \left[\sum_{m_2=1}^{n_s^{(1)}} \beta^{(1)}_{m_2} R^{(1)}_{i_{j_1} i_{j_2}}(\mathbf{z}, \mathbf{z}^{m_2}) \right] - (n_r - 1) \sum_{j_1=1}^{n_r} \left[\sum_{m_1=1}^{n_s^{(1)}} \beta^{(1)}_{m_1} R^{(1)}_{i_{j_1}}(\mathbf{z}, \mathbf{z}^{m_1}) \right] \\
& + \sum_{j_1=1}^{n} \left[\sum_{m_1=1}^{n_s^{(1)}} \beta^{(1)}_{m_1} R^{(1)}_{i_{j_1}}(\mathbf{z}, \mathbf{z}^{m_1}) \right] + \left\{ \frac{n_r(n_r-1)}{2} - (n-1) \right\} \alpha^{(1)}_0 \Gamma^{(1)}_0 \Bigg] \\
& + \sum_{i=2}^{it} \gamma^{(i)}(\mathbf{x}, \mathbf{c}^{(i)}) \left[\sum_{j_1=1}^{n_r} \left\{ \sum_{k_1=0}^{p^{(i)}} \alpha^{(i)}_{i_{j_1},k_1} \Gamma^{(i)}_{k_1}(z_{i_{j_1}}) \right\} + \sum_{j_1=1}^{n_r} \left[\sum_{m_1=1}^{n_s^{(i)}} \beta^{(i)}_{m_1} R^{(i)}_{i_{j_1}}(\mathbf{z}, \mathbf{z}^{m_1}) \right] + (n_r - 1) \alpha^{(i)}_0 \Gamma^{(i)}_0 \right]
\end{aligned} \tag{7.12}$$

Highlighted terms in the above equation constitute the proposed hybrid dimension decomposition formulation. The use of lower orders in this expression is not restricted and the influence of higher order HDMR can be incorporated extending the sequence shown in Eq. 7.2. The degree p of the orthogonal bases in PCE can be either chosen by the designer or selected based on the number of support points n_s available for its complete generation. The unknown coefficients, $\alpha^{(\bullet)}_{\bullet}$, $\beta^{(\bullet)}_{\bullet}$ and $\gamma^{(\bullet)}$, in the above equation are determined utilizing the support points which are discussed in the following section.

7.3 Determination of Unknown Coefficients

In this study, the unknown quantities in Eq. 7.12 are characterized in three categories based on their evaluation strategies. A steps-wise evaluation of these coefficients are given below –

Step 1: The unknown coefficients $\alpha^{(\bullet)}_{\bullet}$ associated to the orthogonal bases are evaluated using mean square error between the PCE and the original values. It is minimized using best linear unbiased prediction (BLUP) [84, 90, 183] as in Kriging which is similar to MLS technique (i.e. Eq. 2.9) for unbiased prediction. Using this optimization, the coefficients are determined as

$$\boldsymbol{\alpha}_{\bullet} = [\boldsymbol{\Gamma}^{\mathsf{T}}(\bullet)\mathbf{R}^{-1}\boldsymbol{\Gamma}(\bullet)]^{-1}\boldsymbol{\Gamma}^{\mathsf{T}}(\bullet)\mathbf{R}^{-1}\underline{\mathbf{g}}(\bullet) \tag{7.13}$$

where, $\underline{\mathbf{g}}_k = [\underline{g}_k(\mathbf{x}^1)\ \underline{g}_k(\mathbf{x}^2)\ \ldots\ \underline{g}_k(\mathbf{x}^{n_s})]^{\mathsf{T}} \in \mathbb{R}^{n_s \times 1}$ is the normalized output such that $\underline{g}_k(\bullet) =$

$[g_k(\bullet) - \mu_k^g]/\sigma_k^g$. The notations μ_k^g and σ_k^g are calculated as follows

$$\mu_k^g = \frac{1}{n_s}\sum_{i_1=1}^{n_s} g_k(\bullet^{i_1}) \tag{7.14a}$$

$$\sigma_k^g = \sqrt{\frac{1}{n_s}\sum_{i_1=1}^{n_s}(g_k(\bullet^{i_1}) - \mu_k^g)^2} \tag{7.14b}$$

Further, the polynomial bases in Eq. 7.13 are presented as $\mathbf{\Gamma}_k = [\Gamma_k(\mathbf{z}^1)\ \Gamma_k(\mathbf{z}^2)\ \ldots\ \Gamma_k(\mathbf{z}^{n_s})]^\mathsf{T} \in \mathbb{R}^{n_s \times n_b}$ and the correlation matrix $\mathbf{R}_k \in \mathbb{R}^{n\times p}$ is formed as $\mathbf{R}_k^{ij} = R_k(\mathbf{x}^i, \mathbf{x}^j)$, $i, j = 1, 2, \ldots, n$, where $\mathbf{r}_k(\mathbf{x}) = [R_k(\mathbf{x}, \mathbf{x}^1)\ R_k(\mathbf{x}, \mathbf{x}^2)\ \ldots\ R_k(\mathbf{x}, \mathbf{x}^n)]^\mathsf{T}$ and the kernels of the correlation structure are evaluated using Gaussian expression as follows

$$R_k(\mathbf{z}^I, \mathbf{z}^J) = \prod_{i=1}^{n_s} \exp[-\hat{\theta}_i(\mathbf{z}_i^I - \mathbf{z}_i^J)^2] \tag{7.15}$$

In this study, the value of $\hat{\theta}$ is adopted as 0.75 for all the variables in the upcoming numerical analysis. The selection of this value depends on the designer and it is not decided based on any prior sensitivity analysis. The authors envisage that such ad-hoc sensitivity analysis will not influence the proof of concept established here. However, the present study does not restrict its evaluation using the sensitivity of $\hat{\theta}$ on the output which can be performed as a separate study.

Step 2: Next, the coefficients $\beta_\bullet^{(\bullet)}$ associated with the nonparametric terms are determined utilizing the solution strategy involved in Step 1 as

$$\boldsymbol{\beta}_\bullet = \mathbf{R}^{-1}[\underline{\mathbf{g}}(\bullet) - \mathbf{\Gamma}(\bullet)\boldsymbol{\alpha}_\bullet] \tag{7.16}$$

Step 3: Since, all the unknown coefficients in $\alpha_\bullet^{(\bullet)}$ and $\beta_\bullet^{(\bullet)}$ are determined in the previous two steps, Eq. 7.10 is applied to construct the individual HDMRs. Finally, the individual contribution of these HDMRs are evaluated as

$$\gamma^{(i)} = \frac{\prod_{j=1,\, j\neq i}^{it} \sqrt{\sum_{k=1}^{n}(x_k - c_k^{(j)})^2}}{\sum_{o=1}^{it}\prod_{l=1,\, l\neq o}^{it}\left[\sum_{k=1}^{n}(x_k - c_k^{l})^2\right]^{\frac{1}{2}}} \tag{7.17}$$

where, $\sum_{i=1}^{it}\gamma^{(i)} = 1$. It can be noted that similar to the above two steps, $\gamma^{(\bullet)}$ also utilizes the location of the arbitrary point. That apart, the determination of this coefficient considers the reference point of the HDMR to ascertain its influence. It justifies the adaptive nature introduced by γ based on the proximity of HDMR with respect to the arbitrary point where the approximation is evaluated. It helps in a better fit, especially when mapping the local variations of the original function.

To calculate these coefficients, present study employs the distribution adaptive multi-sparse grid scheme as suggested in the Chapter 6.

7.4 Application to Stochastic Computation

In this section, the proposed *hd*A-HDMR is discussed for different applications in the stochastic field. As the method employs an iterative framework based on the adaptive contributions of the multiple HDMRs, it requires adequate selection of the component surfaces. In this regard, selection of the reference point(s) after the initial iteration is a critical task to achieve the desired objective. Hence, as a solution to this issue, the objective function is defined depending upon the problem statement which are illustrated as follows:

- **Uncertainty Quantification:** In uncertainty analysis, the response surface is required to map the statistically favourable regions, like area near mean, tail ends accurately to estimate the moments. Hence, the components of HDMR and support points are required to be generated in these regions of

interest. In this regard, without the loss of generality the reference point is preferably selected at the mean values of the random variables in the first iteration. The support points are generated following their respective probability distributions. This can be performed by mapping the CDF as

$$\mathbf{x} = F_{\mathbf{X}}^{-1}[\Phi(\mathbf{z})] \tag{7.18}$$

if the random variables are uncorrelated. In the above expression, notations $F_{\mathbf{X}}(\bullet)$ and $\Phi(\bullet)$ represent the CDFs of $\mathbf{x}$ and $\mathbf{z}$, respectively. Apart from the distribution based influence, multiple generations of the support points in iterative manner is performed by assuming same reference location such that $\mathbf{c}^{it} = \mathbf{c}^{it-1}$. However, the influence domain of the support point is reduced using the reduction factor $\lambda_{\mathbf{x}}$. This factor iteratively reduces the extent of $\Omega_{\mathbf{x}}$ in successive generations unless otherwise mentioned for the specific case. In this study, the reduction factor is assumed to be 0.75 for the uncertainty quantification. Once the global *hd*A-HDMR is constructed, population based sampling schemes (e.g. MCS) with adequate sample size is adopted for the uncertainty quantification.

- **Reliability Analysis:** The region of interest in the reliability analysis is the limit state (i.e. $g(\mathbf{x}) = 0$), especially near the failure point or MPP. Hence, in this study, a MPP based optimization is demonstrated using *hd*A-HDMR to determine the probability of failure. As explained earlier, use of Hermite polynomials makes the optimization straightforward as shown in Eq. 4.12. The solution of the optimization process gives the MPP as $\mathbf{z}^{*,it}$ and subsequently, $\mathbf{x}^{*,it}$ for that iteration which is followed by successive iterations to locate the actual MPP for the problem. Hence, additional points are added in these successive iterations to improve the quality of *hd*A-HDMR. These additional points are generated around the MPP evaluated in each iteration i.e. $\mathbf{c}^{(it+1)} = \mathbf{x}^{*,it}$. The convergence of this process is checked using permissible errors $\mathcal{E}_1$ and $\mathcal{E}_2$ for the change in the $\tilde{g}(\mathbf{x}^{*,\bullet})$ and $\mathbf{z}^{*,\bullet}$. Usually, the values of these permissible errors ranges within $10^{-2}\sim10^{-3}$. Once the global surface is ready, simulation techniques are adopted for failure estimation.

- **Reliability Based Design Optimization:** RBDO problem solves a constraint optimization to determine the design point $\mathbf{x}_d^{*,it}$ in the variable space $\Omega_{\mathbf{x}_d}$ which is given by

$$\begin{aligned} &\text{Maximize} && \mathbf{x}_d \\ &\text{Subjected to :} && \mathscr{P}\left[\tilde{g}(\mathbf{x},\mathbf{x}_d) \leq 0\right] = p_f^* \\ & && \mathbf{x}_d \in \Omega_{\mathbf{x}_d} \end{aligned} \tag{7.19}$$

where, $\mathscr{P}[\bullet]$ denotes the probability of occurrences defined in $[\bullet]$ and $\mathbf{x}_d$ is the design variable vector which can be random or deterministic in nature. To solve the above equation, response surface is built using both $\mathbf{x}$ and $\mathbf{x}_d$. The new reference points are defined using the optimized value of $\mathbf{x}_d$ and the mean values of $\mathbf{x}$ when the iterations are continued till the convergence is achieved satisfactorily. In this regard, permissible tolerance for the convergence of the $\mathbf{x}_d^{*,\bullet}$ is chosen as discussed in the above reliability analysis (i.e. $\mathcal{E}_1$ and $\mathcal{E}_2$).

Above applications bypass multiple evaluations of the original stochastic FE model required in the simulation and ease the computational burden. It can be noted that the nonlinear multidimensional optimization processes as in Eqs. 4.12 and 7.19 can be solved using any standard tool available in the literature [184]. The present study employs SQP technique available in the MATLAB® [96]. A flowchart summarizing the complete process for different applications is presented in Fig. 7.2. Following these steps, the numerical simulations are performed to justify the merits of the proposed hybrid *d*-Adaptive HDMR in the upcoming section.

7.5 Results and Discussion

In this section, the proposed *hd*A-HDMR is implemented for stochastic FE analysis of composite plates to determine the free vibration characteristic and failure index when subjected to transverse loading. The composite plate considered here is characterised by the two-dimensional homogeneous random field for the material properties that are modelled using KLE. The proposed method is used here for uncertainty quantification, reliability analysis and design optimization. The problem is solved using other similar methods

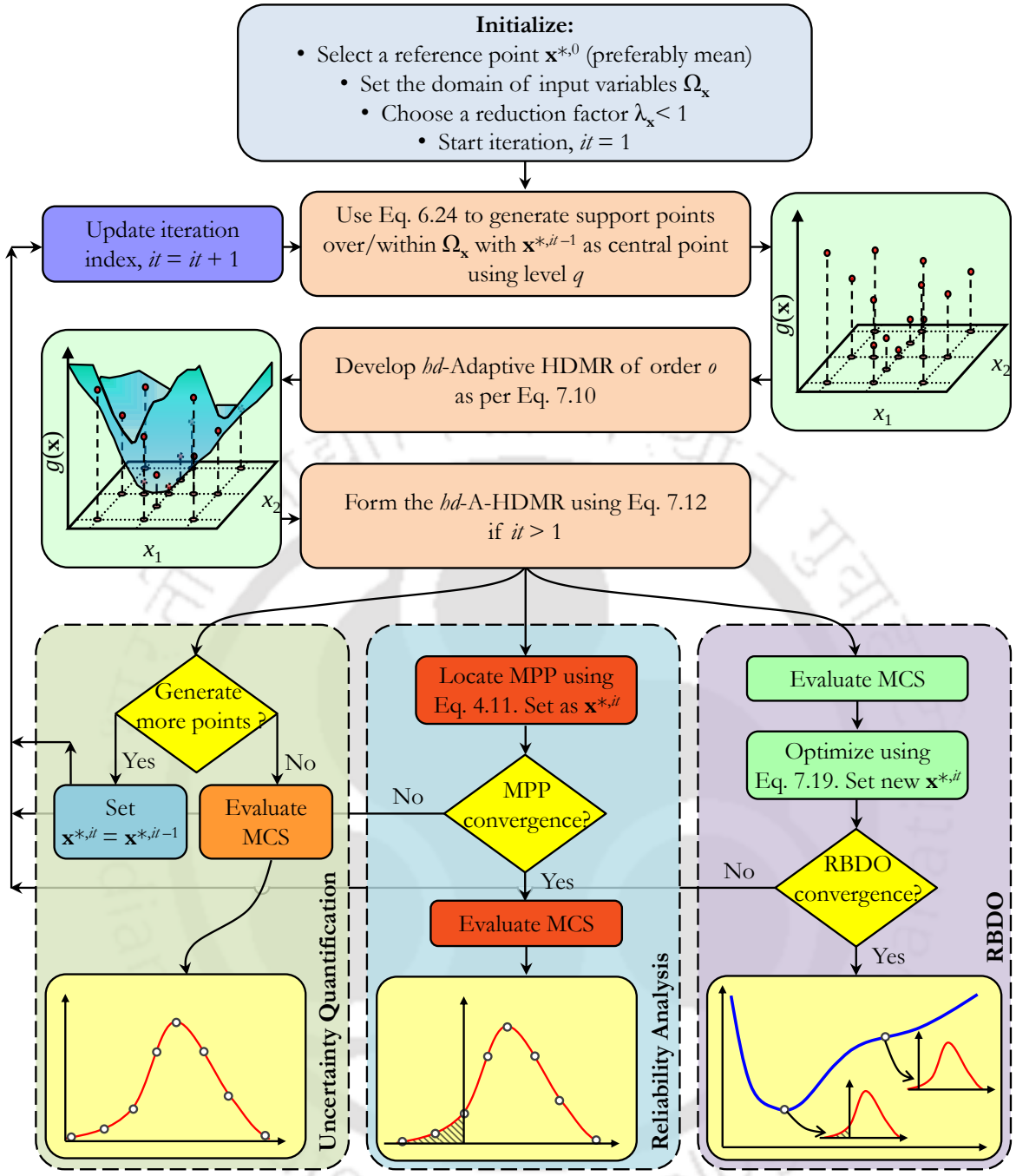

Figure 7.2: Flowchart of the proposed algorithms using *hd*A-HDMR for uncertainty quantification, reliability analysis and RBDO

like MLS-HDMR [117, 122, 123], RS-HDMR [119] and Kriging [97] for comparison. The MLS-HDMR [117, 122, 123] is a finite difference HDMR where the component functions are modelled by regular polynomial bases. It is formed using cartesian grid based support points with coordinates $c_i - (k-j)\sigma_{x_i}$, c_i and $c_i + (k-j)\sigma_{x_i}$, where σ_{x_i} represents the standard deviation of i^{th} variable, k is the level of support points and index $j = 1, 2, \ldots, k-1$. The coordinates of the reference point c_i are set at the mean μ_{x_i} of the random variables and the number of support points for order o is evaluated using $n_s = \sum_{i=0}^{o} \frac{n!(n_a-1)^i}{(n-i)!i!}$ with $n_a = 2k-1$. MLS technique is utilized to determine the coefficients associated with the regular polynomial bases i.e. $[1\ x_1\ x_2\ \ldots\ x_n\ x_1^2\ x_1x_2\ \ldots\ x_n^2]$ in the component functions. The weight function employed as suggested in Chowdhury *et al.* [117, 122, 123] to assist the MLS based calculations. RS-HDMR [119] involves quasi random sampling like Sobol' sequence to represent the component functions based on the orthogonal polynomials like modified Legendre polynomial as given by Dey *et al.* [120]. The degree of these polynomials

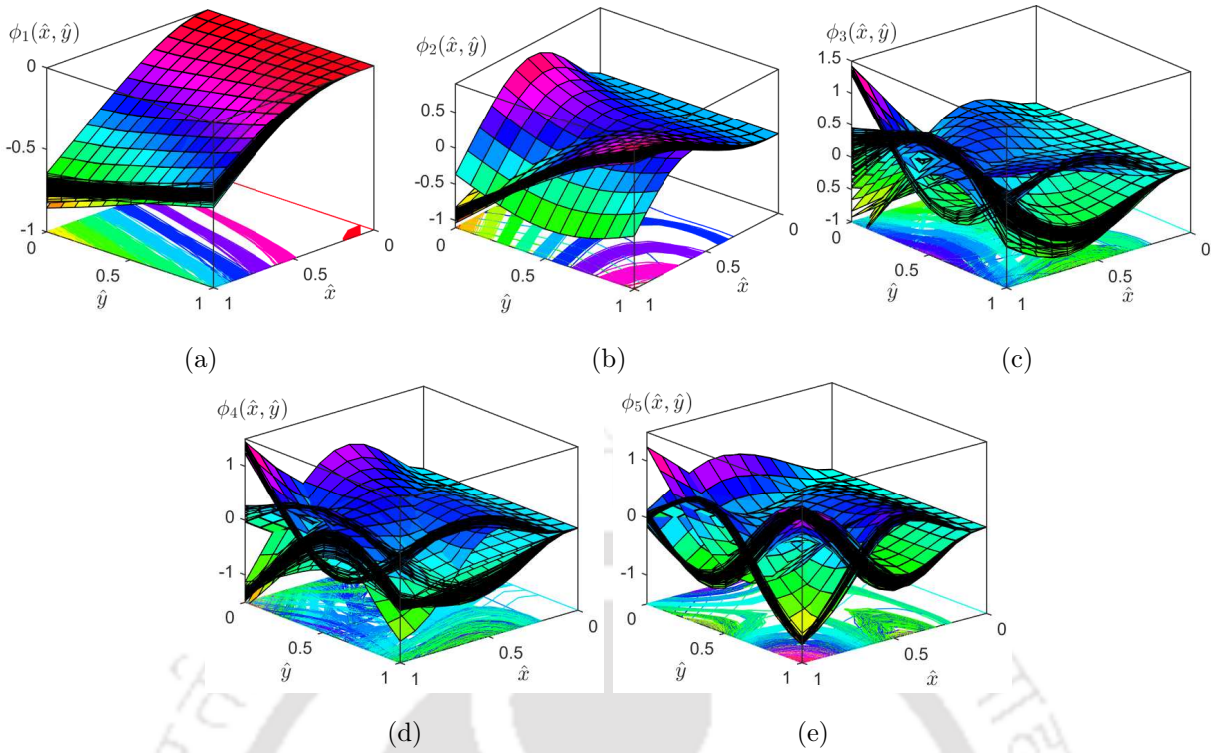

Figure 7.3: Mode shapes due to stochastic material properties where (a) mode 1, (b) mode 2, (c) mode 3, (d) mode 4 and (e) mode 5

are adaptive based on the Sobol' sensitivity index. Both these methods employ a single generation of the HDMR to construct the dimension decomposition based response surface. Third method considered in this study is Kriging using DACE Toolbox [97] which also uses regular polynomial bases. In addition to the bases, correlation functions are defined between the support points to form the meta-model. It uses random sampling scheme such as LHS to generate the support points. The efficacy of these methods are justified based on the computational effort involved in the simulation and the accuracy of the results. In this study, the accuracy of the aforementioned methods is determined using MCS with adequate sample size as benchmark. The computational cost is indicated based on the number of original FE analysis performed. This indicates the amount of CPU time consumed by the particular method for computation. The inference from the numerical analysis is presented in the following subsections.

7.5.1 Uncertainty Quantification

A square cantilever composite laminated plate is modelled here which is made of graphite-epoxy stacked in different angles. The stacking sequence of these plies are considered as random with mean at $[-45/+45/-45]$ (in degree) having 10% coefficient of variation (cov). The deterministic values of the material properties are as follows: $E_2 = 8.90$ GPa, $G_{12} = 7.10$ GPa, $G_{23} = 2.84$ GPa and $G_{13} = 7.10$ GPa [120]. The other material properties of the graphite-epoxy composite plate such as E_1 and ρ_c are considered as two-directional independent homogeneous Gaussian random fields with mean at 138.00 GPa and 3202.00 kg/m^3, respectively, where Poisson's ratio $\nu \sim \mathcal{N}(0.3000, 0.0009)$. The standard deviation $\sigma_{\mathbf{x}}$ of these fields are defined as 13.80 GPa and 320.20 kg/m^3, and the correlation lengths $l_{\hat{x}}$, $l_{\hat{y}}$ are 0.50. Using these statistical properties, the covariance function of the random fields are given by $\sigma_{\mathbf{x}}\,\rho(\hat{\mathbf{x}},\hat{\mathbf{x}}')$. The thickness of the laminas are equal and the thickness to length ratio (i.e. h_c/b) of the composite plate is 0.004. Stochastic FE analysis is performed using a 6×6 mesh with uniform size. Each element of the plate is modeled using nine-noded quadrilateral iso-parametric elements, hence a total of 155 nodes are formed in the FE model. The fields are discretized to form the vectors of random fields with respect to 36 elements using KLE as described in Appendix A.

In this study, free vibration analysis is carried out to determine the first five natural frequencies of the

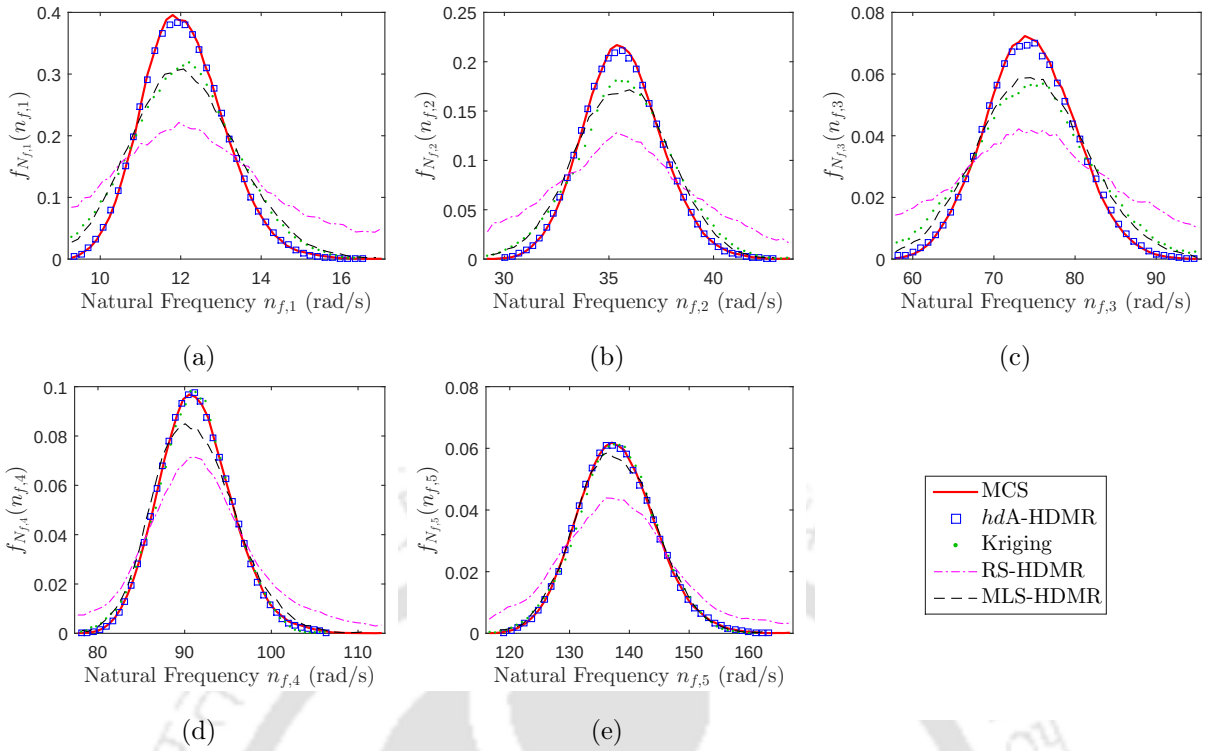

Figure 7.4: Comparison of *pdf* of modal responses from a spatially uncertain cantilever composite plate where (a) 1st, (b) 2nd, (c) 3rd, (d) 4th and (e) 5th natural frequencies

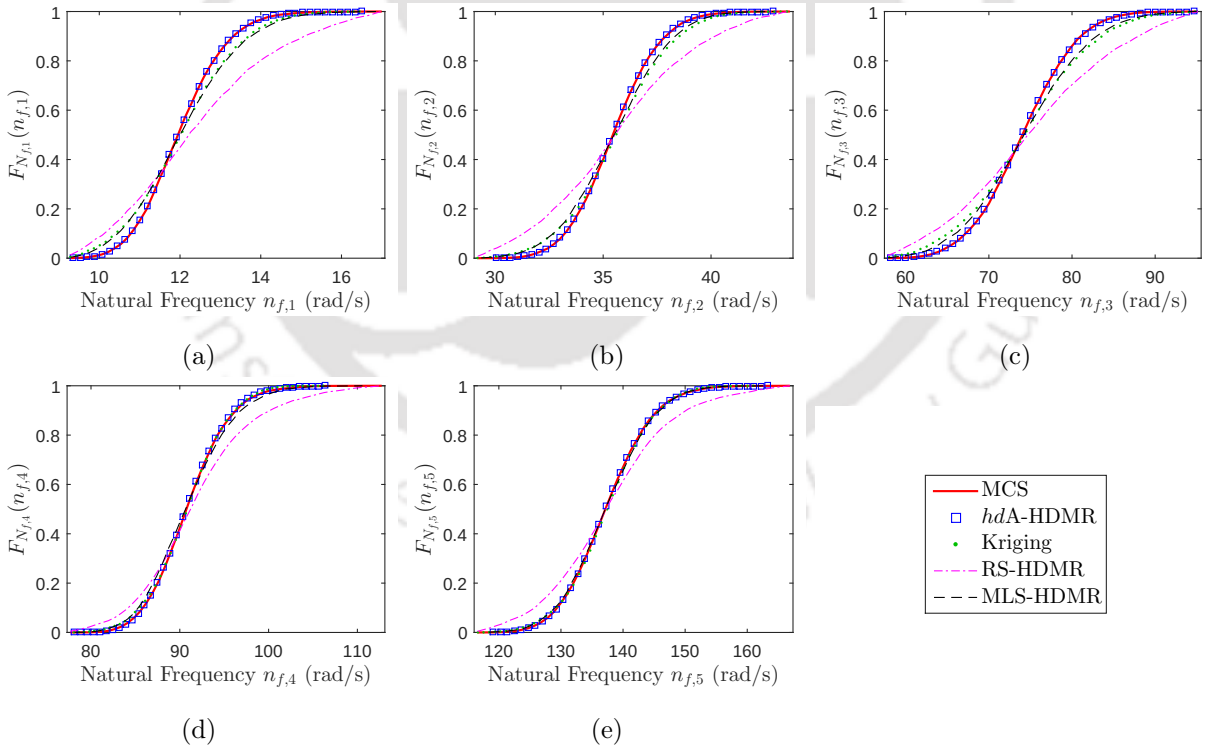

Figure 7.5: Comparison of CDF of modal responses from a spatially uncertain cantilever composite plate where (a) 1st, (b) 2nd, (c) 3rd, (d) 4th and (e) 5th natural frequencies

composite plate. These frequencies and the corresponding mode shapes are obtained using the above mentioned properties. Direct MCS is adopted to determine the frequencies using 10^4 realizations. The effect of uncertainties on the modal properties are presented in Fig. 7.3. The probability distribution functions of

Table 7.1: Statistical properties of the first five stochastic natural frequencies of a cantilever composite plate (units in rad/s)

Nat. Freq.	Method	Mean	Std. Dev.	Skewness	Kurtosis
	Direct MCS	12.090	1.001	0.388	3.325
	*hd*A-HDMR	12.085	0.998	0.318	3.137
1	Kriging	12.063	1.318	0.008	3.060
	MLS-HDMR	12.117	1.309	0.244	3.076
	RS-HDMR	10.712	36.167	-2.735	79.482
	Direct MCS	35.658	1.828	0.213	3.119
	*hd*A-HDMR	35.639	1.837	0.193	3.091
2	Kriging	35.761	2.257	-0.022	3.001
	MLS-HDMR	35.635	2.215	-0.039	2.965
	RS-HDMR	33.854	60.939	-3.267	100.820
	Direct MCS	74.504	5.366	0.096	2.878
	*hd*A-HDMR	74.508	5.500	0.109	3.078
3	Kriging	74.544	7.306	0.014	3.039
	MLS-HDMR	74.710	6.710	0.094	2.986
	RS-HDMR	68.492	181.320	-5.270	120.810
	Direct MCS	91.317	4.113	0.366	3.385
	*hd*A-HDMR	91.240	4.034	0.283	3.161
4	Kriging	91.099	4.150	-0.005	3.000
	MLS-HDMR	91.255	4.591	0.351	3.179
	RS-HDMR	90.467	118.290	-2.380	112.870
	Direct MCS	137.900	6.361	0.244	3.171
	*hd*A-HDMR	137.860	6.333	0.250	3.123
5	Kriging	137.900	6.471	-0.011	3.013
	MLS-HDMR	137.780	6.592	0.100	3.001
	RS-HDMR	137.570	134.220	-2.427	93.551

Note: The number of FE calls by MCS, *hd*A-HDMR, Kriging, MLS-HDMR and RS-HDMR are 10^4, 730, 3000, 609 and 3000, respectively.

these modal parameters obtained from MCS are plotted in Fig. 7.4 which are considered as the benchmark for further analysis. Apart from MCS, other meta-models are also used to quantify the uncertainties in the natural frequencies. It can be seen in Fig. 7.4 that the *pdf*s obtained from RS-HDMR have significant mismatch with MCS. This is due to unwanted effects of the spurious component functions. The number of FE solutions carried out to construct this model is 3000 with 2^{nd} order component functions. The lower and upper bounds of the support points are set to $\mu_{\mathbf{x}} \pm h_r \sigma_{\mathbf{x}}$, where $h_r = 1$ based on the sensitivity analysis shown in the previous chapter. The maximum degree of the orthogonal polynomial basis is fixed at 5. MLS based finite difference-HDMR is then employed which improves the results from the previous case i.e. RS-HDMR. However, it still yields significant error, especially for first four natural frequencies as shown in Fig. 7.4(a) to 7.4(d). In this case, the order o of the HDMR is reduced to 1 as the number of support points required to form the 2^{nd} response surface is high (> 3000). A total of 609 FE solutions are used for the level of grid points $k = 4$. The results explain that even if it considers till the 1^{st} order terms (i.e. no combined effects are used), the accuracy is inconsistent. Hence, the performance of the above two methods infer that an adaptive selection of the order should provide the desired results. However, before using the proposed algorithm, performance of the Kriging based meta-model is also verified in this study to quantify the uncertainties. Support points are generated using LHS with sample size of 3000 to construct this meta-model. The 4^{th} and 5^{th} natural frequencies observe a close match with the MCS results, however, the first three natural frequencies face error in estimation. Finally, the proposed *hd*A-HDMR is used which shows a close match with the MCS results and distinctly marks its accuracy with resect to other methods applied here. This dimension decomposition is built in two iterations with first iteration starting at mean $\mu_{\mathbf{x}}$ as the reference point (i.e. $\mathbf{c}^{*,0}$). In this uncertainty quantification, no objective function is defined, hence

the second iteration follow the same reference point but the bounds of the support points are reduced by 25% prior to populate with more points. Overall, the proposed method offers a better fit and can map the *pdf*s of the first five natural frequencies with insignificant error of estimation.

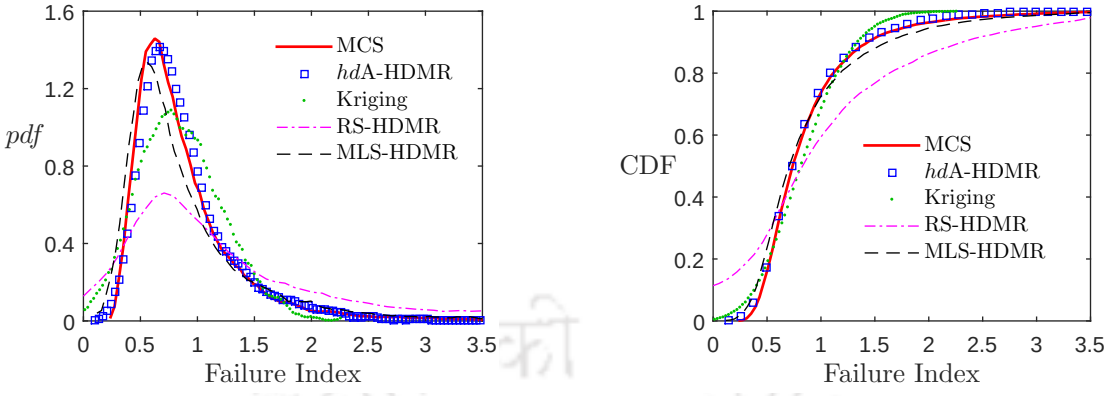

(a) (b)

Figure 7.6: Comparison of (a) *pdf* and (b) CDF based on failure index from a spatially uncertain simply supported composite plate using different methods

The CDF of the natural frequencies are also plotted in Fig. 7.5 which shows the accuracy of different methods when compared with the MCS data. A comparative study is performed based on the statistical moments (such as mean, standard deviation, skewness and kurtosis) of the first five fundamental frequencies as shown in Table 7.1. The tabulated results show adequate match in the estimation of the first moment (i.e. mean) among all the methods performed in this study except from RS-HDMR. Higher moments show better quality when the proposed *hd*A-HDMR is used as compared to the other methods. This proves the consistency of the proposed method as compared to the other models adopted here. As a general observation among all these methods, performance of the RS-HDMR is significantly erroneous for stochastic finite element analysis. In this context, a dimension adaptive version of the multiple finite difference-HDMR has proved to be accurate for stochastic computations.

The proposed *hd*A-HDMR is also adopted to solve a simply supported composite plate with non-normal random fields subjected to UDL as reported in the § 6.3.2. Fig. 7.6 shows the probability distribution of the failure index for this composite plate using MCS, *hd*A-HDMR, RS-HDMR, MLS-HDMR and Kriging. In this analysis, RS-HDMR, MLS-HDMR and Kriging call 3000, 685 and 3000 original function evaluations, respectively. The proposed *hd*A-HDMR requires 1380 function evaluations as opposed to 2067 FE calls (see Table 6.3) in *d*AMFD-HDMR. Fig. 7.6 demonstrates the accuracy in the *pdf* and CDF estimation of failure index obtained from different methods. These results show a close match between the probability distributions using the *hd*A-HDMR and MCS. MLS-HDMR with 1^{st} order also offers better results among the other methods illustrated here. However, the level of accuracies obtained from the proposed method is superior than the others.

7.5.2 Reliability Analysis

Using the same composite plate, probability of failure is estimated for different values of UDL to develop the fragility curve as shown in Fig. 7.7. For reliability analysis, a larger sample size of MCS (i.e. n_c = 5E5) is employed to estimate low p_f. The FE solutions made by different methods (i.e. RS-HDMR, MLS-HDMR and Kriging) for each load case remain same as mentioned in the above discussion. It is observed that the Kriging using DACE Toolbox [97] faces difficulty to deal with large dimensions. The issue is severe in the case of p_f estimation, especially for low p_f where sample size is inevitably large. The simulation technique adopted by the models require estimation of the correlation between the support points and the sampled realizations as per Eq. 7.15. In this case, both these values (i.e. number of support points n_s and sample size n_c) are relatively high, hence it faces difficulty to compute the correlation matrix $\mathbf{R}$ of the Gaussian process. Also, these calculations are performed simultaneously for all the coordinates of the support points as opposed to MLS technique which employs a scalar approach where these calculations are performed one-by-one. This computational issue makes the application of Kriging based meta-model very slow and eventually,

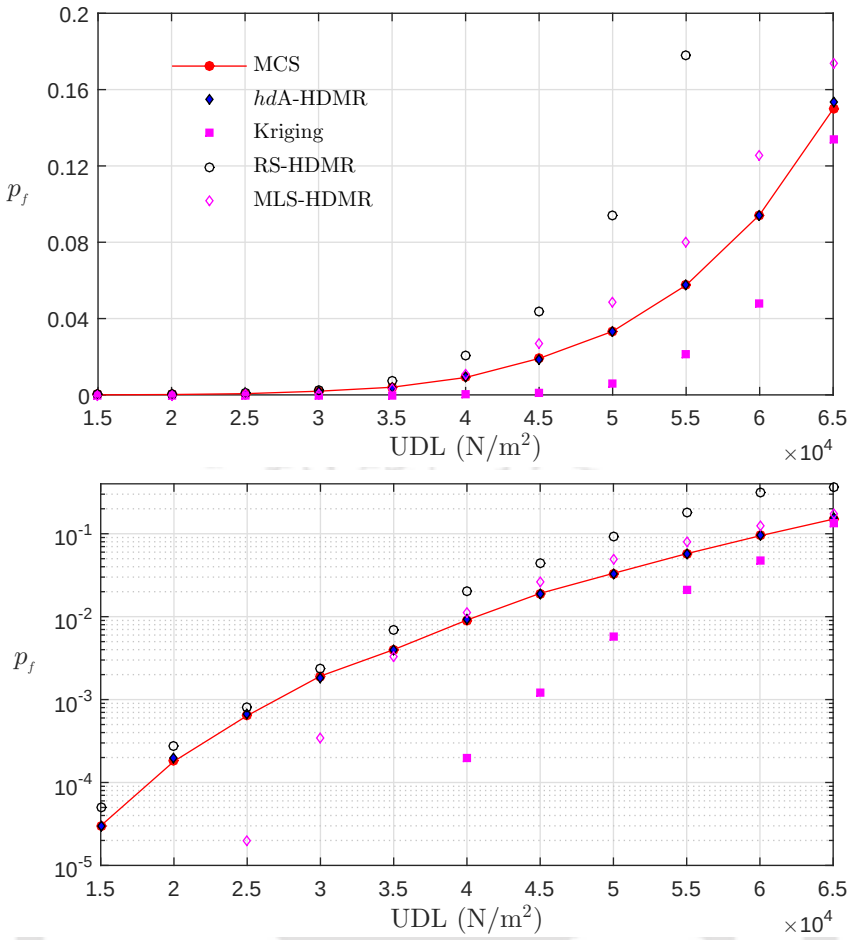

Figure 7.7: Reliability analysis of simply supported composite plate using different methods

time exhaustive. The aforementioned issue is addressed in this study by the proposed hybrid d-Adaptive HDMR formulation which breaks the complete polynomial basis into smaller sub-matrices. It reduces the computational burden associated with the simultaneous calculations of the support points by dividing it into various sub-matrices. Also, it can be noted that deterministic sampling offered by the sparse grid scheme helps to reduce the computational cost associated with the calculation of correlation structure. This can be explained for any component function where only limited number of variables are effective due to dimension decomposition. Accordingly, these effective locations of the random variables are only considered for the correlation calculations. However, this is not the case for random sampling based DoE where irrespective of the component functions, all coordinates are considered. This problem makes Kriging [97] with random sampling less preferable for reliability analysis as all the variables need to be considered for correlation calculation. In brief, it can be stated that this process is streamlined in the present proposal which helps to improve the efficiency. It ultimately yields at a much faster computation of the reliability analysis. In addition to this computational efficiency, the proposed method converges using 922 to 2067 support points for different load cases in the fragility curve. Fig. 7.7 shows the p_f estimated from this numerical exercise which are matching to the ones obtained from MCS. The figure also presents the fragility curve using a logarithm scale to emphasize the quality of results obtained in the lower tail end. The failure probabilities from the other methods illustrated in this study yield significant error, however, RS-HDMR performs relatively better in the low p_f range. Apart from the MLS-HDMR (with $k = 4$) shown in Fig. 7.7, $k = 3$ and 5 ($n_s = 457$ and 913, respectively) are also studied which yield significant inaccuracies in the end results. These results are not produced in this chapter to avoid repetition as they are inconsequential to the outcome of this study. In summary, this discussion comprehensively states the merit of the proposed method over the well-known similar tools for reliability analysis.

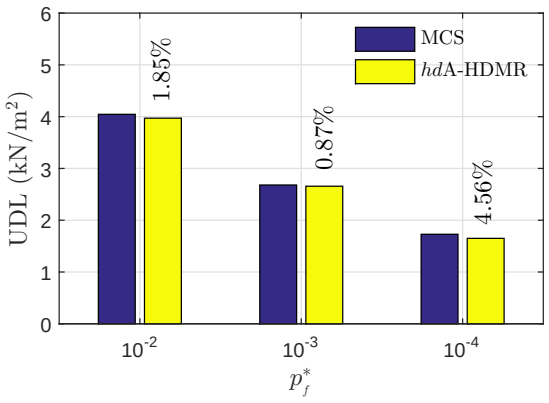

Figure 7.8: Design load estimated from RBDO using the proposed method and MCS for given threshold p_f^*

7.5.3 Reliability Based Design Optimization

Previous subsections clearly demonstrates the superiority of the proposed method in stochastic computations. Finally, it (i.e. *hd*A-HDMR) is applied to a RBDO problem using the same composite plate. Here, the design problem is solved by evaluating the maximum UDL in transverse direction for a desired reliability of the carbon-epoxy composite plate. The load is a deterministic variable in this problem of dimension decomposition using random variables as suggested in Eq. 7.19. The probability of failure is estimated using MCS with a sample size of 5E5. Three different values of desired p_f^* (i.e. 10^{-2}, 10^{-3} and 10^{-4}) are adopted to design the maximum load under the present condition. The UDLs corresponding to these reliabilities are optimized and the results are presented in Fig. 7.8. The maximum load is also obtained using MCS and it is observed that the results from *hd*A-HDMR are fairly accurate in load estimation. In total the RBDO for case 1 (i.e. $p_f^* = 10^{-2}$), case 2 (i.e. $p_f^* = 10^{-3}$) and case 3 (i.e. $p_f^* = 10^{-4}$) require 930, 930 and 1161 FE calls to convergence. The quality of end results obtained by the proposed method proves to be cost effective for reliability based design optimization.

The problems demonstrated above require multiple high-fidelity estimations of the p_f which face notable challenges such as inaccuracies, convergence and computational cost. Also, the results presented here clearly show that other methods discussed previously (e.g. RS-HDMR, MLS-HDMR and Kriging) either lack accuracy, efficiency or both and hence, may not be suitable for large dimensional problems.

7.6 Summary

The present chapter proposes an alternative hybrid formulation of the dimension adaptive HDMR. Here, the uncertainty propagation are modelled by multiple generations of the dimension decomposition at different anchored locations. In nutshell, the proposed *hd*A-HDMR performs satisfactorily for problems with large number of input variables. Different methods are used to demonstrate the advantages of the proposed *hd*A-HDMR. The major contributions in this study are as follows:

1. A novel dimension adaptive formulation is developed using finite difference HDMR, PCE and Gaussian model for error. The support points are judiciously selected in a dimension adaptive sparse grid framework for better accuracy at an optimal computational cost.

2. The error is modelled using a correlation function based on the distance between the support points. The associated unknown coefficients are quantified using best linear estimation predictor along with the PCE. Multiple error terms are defined for component functions in the HDMR using this modelling approach (i.e. hybrid formulation) which has proved to be significantly accurate for stochastic computations.

3. The proposed hybrid dimension adaptive modelling constitutes of mixed-order HDMRs which helps to model uncertainty propagation in case of large dimensional problems (> 100). Three strategies

are suggested using the proposed method for different applications such as uncertainty quantification, reliability analysis and RBDO. Overall, it proves to be very effective for high-fidelity modelling as justified by the numerical results, particularly in RBDO where multiple estimations of the probability of failure are required.

Chapter 8

Concluding Remarks

The work discussed in this thesis primarily contributes to the development of efficient meta-model schemes for time-invariant stochastic computation. Different algorithms are proposed in this study using polynomial chaos expansion and multi-level dimension decompositions which are tested using problems that offers different levels of challenges. Overall, the efficiency and accuracy of the proposed schemes are tested for reliability analysis and uncertainty propagation in non-intrusive framework. In particular, the work presented in this thesis explores its application in FE model updating, reliability analysis by orthogonal formulation with correlated non-normal random variables, RBDO of structural components when exposed to uncertain environment and design of laminated composite plates with non-Gaussian random fields. The major contributions of this research work along with their possible extension in the future are reported in the following sections.

8.1 Summary of the Contributions

In this thesis, different meta-modelling strategies are developed addressing the demerits of conventional RSM, SRSM and HDMR based approaches. These developments are sequentially presented from the element level to clearly justify the background of this study. Overall, it proposes five different adaptive algorithms using various meta-models such as RSM, SRSM, HDMR and Kriging. Each of these models are discussed to show the improvements while addressing the issues of curse of dimensionality, convergence, accuracy and computational difficulties particulary in the region of low failure problems. The following are the major conclusions and the salient contributions from the numerical study reported in this thesis:

1. First, different features of the RSM based optimization are studied and their performances are demonstrated using different example cases. These includes least square based RSM, MLS based RSM with exponential and regularized weight functions for linear and quadratic polynomial bases. Each RSM is formed iteratively with a specific DoE scheme to generate the support points. The optimization is performed in each iteration to determine the location of the centre point for the generation of new points as per the selected DoE. Four widely accepted deterministic DoE schemes are selected to study their relative performances in LS and MLS framework. Numerical results clearly prove that MLS based RSM with regularized weight function outperforms LS based RSM and provides fairly accurate results. Faster convergence is observed when central composite design is used with quadratic basis. Overall, MLS based RSM offers satisfactory results for practical problems as it has been demonstrated by the FE model updating of a bridge.

2. The meta-modelling is then applied to moderate dimensional problem subjected to uncertainty. A unique *two-step RSM* based algorithm is proposed to solve the governing differential equations with random coefficients. It is applied to tune a passive controller for RBDO where the primary structure and the excitations are random. The first level response surface is utilized for the optimization whereas the second level quantifies the statistical moments to determine the reliability. Both these steps construct separate response surfaces with different input variables. This approach offers con-

siderable accuracy to estimate the moments using limited evaluation of the original function. In the conventional approach, this process requires time exhaustive multiple evaluations which are bypassed in the proposed algorithm. In brief, the two-step response surface based stochastic design optimization has proved to be efficient and can be adopted for real-life design applications as demonstrated using the vibration control problem.

3. A general perception is that higher degree of the regular polynomial used in RSM yields better accuracy [31, 58]. However, contradicting to this notion, RSM often suffers ill-conditioning which yields significant error, especially for large dimensional problem [160]. To address this issue, orthogonal polynomials are used in the meta-modelling to form the SRSM. In this regard, a new method (i.e. *Sequential SRSM*) is suggested using MLS technique and PCE for reliability analysis. The PCE forms the orthogonal bases where the unknown coefficients are determined by MLS technique using regularized weight function. The moving characteristic of the MLS technique helps in better approximation. Moreover, this method sequentially generates the support points using the MPP(s) based optimization to approximate the global performance function for reliability analysis. As the reliability based optimization process is performed in the standard normal space, hence, the Hermite polynomial scheme is adopted in this study. However, the objective can be altered to locate minima and/or maxima based on the applications. Besides improving the accuracy of the SRSM based reliability analysis, the proposed Seq. SRSM outperforms other higher order SRSM techniques (e.g. HO-SRSM [58]) in terms of computational cost. The numerical results presented in this thesis elucidates these advantages of the Seq. SRSM for high dimensional problems.

4. Besides above improvements, orthogonal subfunctions (i.e. HDMR) are also utilized in this study for the replacement of the original performance function. These subfunctions are defined using the contribution of the random variables and their combinations where MLS based PCE is employed to approximate these subfunctions. Multiple generation of these subfunctions are adopted here for modelling the limit states having multiple design points. The philosophy behind this approximation is to dedicate individual subfunctions for different maxima or minima. However, the use of multiple subfunctions are not fully explored in the literature for high-fidelity representations of the limit state. With this in view, this study explores the advantages of the adaptive multiple HDMRs (i.e. *AMFD-HDMR*) for the reliability analysis. This is achieved in an iterative manner where the optimization in successive iterations help to identify the most suitable regions for the following iteration. The order of these subfunctions are adaptively controlled in the iteration process to optimize the computational cost. The overall contribution of each individual HDMR leads to an adaptive high-fidelity mixed-order approximation of the limit state for large dimensional problem. The probability of failure is estimated using importance sampling as the global MPP is known. It reduces the computational burden associated with the repetitive matrix inversion required in the MLS technique. The numerical exercise presented in this thesis clearly shows the significant improvement in accuracy and computational cost offered by AMFD-HDMR with respect to the other published techniques.

5. The application of AMFD-HDMR is further extended to determine the reliability and uncertainty propagation for problems with spatial randomness. Here, it is observed that the lower order HDMR formulation outperforms the higher order HDMR as it curtails the undesired contributions of the component functions (i.e. subfunctions) in the higher order approximation. An improvement is suggested based on a dimension adaptive proposal of the AMFD-HDMR. This results in a novel sparse HDMR formulation based on the significant dimensions which is termed as *dAMFD-HDMR* in this thesis. It provides a nearly accurate determination of the probability of failure and the uncertainty in stochastic FE analysis. Fragility curves are also developed for composite plate whose material properties are modelled by Gaussian and non-Gaussian random fields. The component functions in the *d*AMFD-HDMR are evaluated using the MLS technique where the basis is defined by Hermite polynomials. This proposal proves to be very accurate than other HDMR (e.g. RS-HDMR [119]).

6. The numerical results presented for both AMFD-HDMR and *d*AMFD-HDMR clearly establish the accuracy and efficiency of these algorithms compared to other versions of HDMR proposed in the literature. However, these algorithms need to invert matrix for each realization to solve the coefficients of the MLS based functional representation. This matrix inversion can offer serious challenges for the numerical implementation of these algorithms for problems with large dimensions. With this in view, an improved meta-modelling technique is proposed here. In this proposal, the Gaussian error is modelled within the HDMR framework using suitable interpolation function and hence, it is called hybrid dimension adaptive HDMR (*hdA-HDMR*). This hybrid version of dimension adaptive

HDMR has three sets of unknown coefficients corresponding to component functions, error and multiple HDMRs. The computational advantage of the proposed algorithm lies in its ability to determine these unknown coefficients from the same set of support points for a particular iteration. Hence, additional computation cost for matrix inversion becomes redundant. The proposed algorithm is generic as it can be tuned for uncertainty quantification, reliability analysis and RBDO. The performance of the proposed algorithm is demonstrated using non-Gaussian random field problem where the dimension is more than 100 and for low failure probability ($\sim 10^{-5}$).

7. Besides algorithmic development, generations of sparse grids are also studied and efficient schemes are proposed for smarter numerical implementation of the proposed meta-modelling techniques. The main objective of this investigation is to develop efficient support point generation so as to reduce the computational cost associated with the original function evaluation. For this purpose, Clenshaw-Curtis sparse grid is adopted to generate the support point using selective tensor product based on the hierarchy as advocated by Smolyak. It employs the same optimization process in tandem with the aforementioned meta-modelling techniques to adaptively generate more points in the region of interest. The variable space is judiciously filled by the sequential application of the sub-grids tensor products. Three key features of the proposed generation scheme of support point are as follows:

   – *Multi-level generation:* It is observed in the numerical analysis that higher level of sparse grid is susceptible to the curse of dimensionality. This, in turn, reduces the efficiency of the support point generation scheme. To address this issue, different levels of sparse grids are proposed in successive iterations to achieve a reasonable tradeoff between the number of support points and the accuracy of the end results.

   – *Distribution adaptiveness:* In this scheme, support points are generated following the statistical description of the input random variables. This is particularly helpful to generate points near the statistically important regions as opposed to uniform generation over the entire domain where many support points may fall beyond the region of influence.

   – *Dimension adaptiveness:* The support points in this scheme are generated under the framework of the *d*AMFD-HDMR and *hd*A-HDMR where a dimension adaptive approach is implemented. It introduces additional sparsity in the tensor product for judicious selection of the dimension and the associated level based on their sensitivity to the output.

Overall, the work is dedicated to the development of surrogate modelling for different deterministic and stochastic applications. These are achieved in different stages where efficient reliability analysis tools are developed for coefficient evaluations, smarter uses of terms/bases and accurate estimation of error. Each proposal is validated using different benchmark and design problems to prove their robustness. This, in turn, advocates the potential of the proposed meta-modelling techniques for stochastic computation involving actual field problems. Table 8.1 is presented to briefly summarize different traits of the proposed techniques. It also highlights the relative performance of these techniques with respect to the accuracy and computational difficulties addressed in this study.

8.2 Avenues of Future Research

The above section outlines major contributions of the research work reported in this thesis. It lays a promising proof-of-concept for high-fidelity modelling for stochastic computations in different fields of engineering. Although, different engineering applications are demonstrated in this thesis satisfactorily, the proposed algorithms have the scope for further developments. With this in view, the following avenues are identified for further research on this topic:

- The present study employs finite difference HDMR to construct the dimension decomposition model. It restricts the use of random sampling schemes and only grid based support point generations are adopted here. Hence, this study can be further extended to incorporate random sampling (pseudo or quasi) based HDMR for adaptive mixed-order application in efficient reliability analysis.
- The framework of the proposed study is developed for non-intrusive applications where the governing equation can be considered as black-box. In such problems, the path of uncertainty propagation is

Table 8.1: Summary of the various novel approaches proposed in this study

Proposed Techniques	Applications	DoE Scheme	Simulation Strategy	Dimension Adaptive-ness	Dimensions Handled	Modelling Fidelity	Comp. Efficiency		Remarks/ Limitations
							Function Calls	Comp. Time	
Dual-level ARSM	UQ, RBDO	CCD	MCS	No	< 10	Moderate	Low	Low	Number of support points rises exponentially with dimension
Seq. SRSM	RA	Sparse Grid	Importance Sampling	No	> 20	High	High	High	Considers orthogonal polynomials only
AMFD-HDMR	RA	Sparse Grid	Importance Sampling	No	> 20	High	High	High	Also, includes orthogonal subfunctions in the framework Effective when all the dimensions are significant
*d*AMFD-HDMR	RA, UQ	Sparse Grid	MCS	Yes	> 100	High	High	Moderate	Employs scalar approach to determine coefficients using MLS technique
*hd*A-HDMR	RA, UQ, RBDO	Sparse Grid	MCS	Yes	> 100	High	High	High	Improves the computational effort in determining the coefficients using vector approach as per Kriging technique

unknown and hence, uncontrollable. This may produce difficulty to the designer to check the quality control of the output. To address such issues, an intrusive formulation using the proposed approaches discussed in this thesis can be studied using techniques like Galerkin projections.

- The support point generation schemes developed in this thesis are based on the proposal of Clenshaw-Curtis which uses uniform generation. There are a few other ways to generate these coordinates as listed in the literatures [166, 185, 186] which can be applied to study any potential improvement in the present framework. The norm considered in the Smolyak's algorithm is linear which can be modified to limit the generation of non-axial locations in the sparse grid scheme. All these modifications can be studied for further improvements for high dimensional problems.

- The present study considers the support points which are free from any noise or perturbations in a grid based framework to provide nonlinear but smooth surface. However, these support points can be based on field data with inherent noise. To address such issues, robust stochastic or updated meta-model can be proposed using the aforementioned formulations.

- The polynomial basis considered in this study incorporates a full expansion of a given degree which might include some insignificant basis terms. It can be modified using either sparse expansion based on the significance of the terms [64, 65] or applying norm other than one to get the hyperbolic expansion as suggested in the literatures [67, 70, 99].

- In this thesis, Hermite scheme is adopted as the orthogonal basis which is defined in the standard normal space. Other schemes as per Gram-Schmidt orthogonalization can be also used to form a generalized PCE. This may enhance the convergence of the proposed methods as suggested by Xiu and Karniadakis [51].

- Numerical studies in this thesis include different limit states with very low probability of failures using MCS and importance sampling. It excludes designs subjected to extremely rare events of failure such as 6σ-design (i.e. $p_f < 10^{-9}$). Such problems can be solved using an ad-hoc application of advanced simulation techniques (e.g. subset simulation or its modified version) over the proposed meta-modelling approaches.

- In real-life problems, the performance function may have multiple limit states with different bounds as in Level 3 reliability analysis. These performance functions can be solved using the present proposals with minor modifications (e.g. penalty function) in the optimization process.

- Alternative to the MLS and Kriging techniques used in this study, other techniques e.g. ANN and SVR can be employed to train the dimension decomposition modelling (i.e. for interpolation). The pattern recognition feature in these techniques may help in mapping the highly nonlinear limit states with complex polynomial form. Their performance can be studied for high dimensional problems in structural reliability analysis.

Appendix A

KLE for Spatial Random Field

In general, a random field $\mathcal{H}(\mathbf{x},\theta)$ is a curve in the Hilbert space $\mathcal{L}^2(\Theta,\mathscr{F},\mathscr{P})$ formed by continuous collection of the random variables [187]. Here, $\theta \in \Theta$ represents the outcome in the probability space $(\Theta,\mathscr{F},\mathscr{P})$, $\mathbf{x} \in \Omega \subset \Re^n$ is the index for these random variables based on the system geometry and $\mathcal{L}^2(\Theta,\mathscr{F},\mathscr{P})$ implies finite second moments of the random variables. For a particular index $\mathbf{x}_0$, it implies that $\mathcal{H}(\mathbf{x}_0,\theta)$ represents a random variable whereas for outcome θ_0, $\mathcal{H}(\mathbf{x},\theta_0)$ gives a realization of the field. These fields are often considered to model the uncertainty in system properties with spatial variability which consequently makes the constituent equation as a function of $\mathbf{x}$ and θ. Using this concept, linear FE model can be expressed over the given spatial extent as

$$\mathbf{K}(\mathbf{x},\theta)\mathbf{u}(\mathbf{x},\theta) = \mathbf{f}(\mathbf{x},\theta) \tag{A.1}$$

where, $\mathbf{K}$, $\mathbf{u}$ and $\mathbf{f}$ follow classical notations of stiffness matrix, nodal displacement vector and force vector, respectively. A homogenous random field is defined by the constant mean $\mu(\mathbf{x},\theta_0)$ and variance $\sigma^2(\mathbf{x},\theta_0)$ with the correlation coefficient $\rho(\mathbf{x},\acute{\mathbf{x}})$. The correlation function is expressed by many forms in the literature, usually as a function of the distance between the locations of the random variable which are denoted by $\mathbf{x}_{(i)}$ and $\acute{\mathbf{x}}_{(i)}$ for the i^{th} spatial coordinate. Among various forms available in the literature, the present study uses the following form [75]

$$\rho(\mathbf{x},\acute{\mathbf{x}}) = \mathrm{e}^{-\left[\frac{|\mathbf{x}_{(1)}-\acute{\mathbf{x}}_{(1)}|}{l_x}+\frac{|\mathbf{x}_{(2)}-\acute{\mathbf{x}}_{(2)}|}{l_y}\right]} \tag{A.2}$$

where, l_x and l_y denote the correlation length along $\hat{x}$ and $\hat{y}$ directions, respectively, which reflect the influence of the correlation among the random variables. Hence, for a very large correlation length (i.e. $l_x,\ l_y \to \infty$) the random field approaches to random variable. Discretization of the random fields are classified into three categories: point-wise discretization, average-based discretization and series expansion-wise discretization [118, 187, 188]. The present study employs a series expansion method based on the assumption that the covariance structure of the input random field is known. In accordance with SSFEM, the input random field is discretized using KLE whereas the output response is presented through PCE.

KLE discretizes the random field $\mathcal{H}(\mathbf{x},\theta)$ based on the spectral decomposition of the autocovariance function $\mathcal{C}_{\mathcal{H}\mathcal{H}}[\mathbf{x},\acute{\mathbf{x}}]$. This technique is widely accepted due to its error minimization property in mean-square sense (i.e. $\mathcal{L}^2(\Omega)$). The random field is represented by a set of uncorrelated standard normal random variables ξ using KLE as follows [188]

$$\mathcal{H}(\mathbf{x},\theta) = \sum_{i=1}^{\infty} \sqrt{\lambda_i}\xi_i(\theta)\psi_i(\mathbf{x}) \tag{A.3}$$

In the above equation, λ_i and $\psi_i(\mathbf{x})$ are the eigen solutions of the autocovariance kernel which is of the form

$$\mathcal{C}_{\mathcal{H}\mathcal{H}}[\mathbf{x},\acute{\mathbf{x}}] = \mathbb{E}[\mathcal{H}(\mathbf{x},\theta)\mathcal{H}(\acute{\mathbf{x}},\theta)] = \sum_{i=1}^{\infty} \lambda_i\psi_i(\mathbf{x})\psi_i(\acute{\mathbf{x}}) \tag{A.4}$$

where, $\mathbb{E}[\bullet]$ and $\mathcal{C}_{\mathcal{H}\mathcal{H}}[\bullet,\bullet]$ denote the expectation operator and autocovariance matrix, respectively. The infinite series of KLE given in Eq. A.3 can be truncated till M^{th} terms for the practical purpose and can be

expressed as follows

$$\mathcal{H}(\mathbf{x},\theta) \approx \mu_{\mathcal{H}}(\mathbf{x}) + \sum_{i=1}^{M} \sqrt{\lambda_i}\xi_i(\theta)\psi_i(\mathbf{x}) \tag{A.5}$$

where, $\mu_{\mathcal{H}}(\mathbf{x})$ is the mean value of the random field. It can be noticed from Eq. A.5 that the accuracy of expansion depends on the choice of M. Hence, a tradeoff can be made for the desired level of accuracy with respect to the discretization scheme (i.e. the number of random variables).

Appendix B

Stochastic FE Formulation of Composite Plate

The present study considers an elastic multi-ply laminated composite plate as shown in Fig. B.1 with random fields. The geometric axes are presented by $\hat{x}$, $\hat{y}$ and $\hat{z}$ whereas deflections of the plate along these axes are denoted by u_0, v_0 and w_0, respectively. A square composite plate of size b having equal ply thickness $\frac{h}{n_m}$ is adopted, where n_m is the number of plies. The FE model of composite plate is formed adopting first order shear deformation theory (FSDT) which provides the following constitutive equation [170]

$$\begin{Bmatrix} \mathbf{N} \\ \mathbf{M} \\ \mathbf{V} \end{Bmatrix} = \begin{bmatrix} \mathbf{A} & \mathbf{B} & \mathbf{0} \\ \mathbf{B} & \mathbf{D} & \mathbf{0} \\ \mathbf{0} & \mathbf{0} & \mathbf{S} \end{bmatrix} \begin{Bmatrix} \boldsymbol{\epsilon}^f \\ \boldsymbol{\epsilon}^b \\ \boldsymbol{\epsilon}^s \end{Bmatrix} \tag{B.1}$$

In the above equation, $\mathbf{N}$, $\mathbf{M}$ and $\mathbf{V}$ are the vectors of in-plane force, bending moment and transverse force resultants, respectively which are measured per unit length. Strain vectors associated with the membrane $\boldsymbol{\epsilon}^f$, bending $\boldsymbol{\epsilon}^b$ and transverse $\boldsymbol{\epsilon}^s$ can be expressed in terms of the displacement field as

$$\boldsymbol{\epsilon}^f = \begin{Bmatrix} \epsilon^f_{\hat{x}\hat{x}} \\ \epsilon^f_{\hat{y}\hat{y}} \\ \gamma^f_{\hat{x}\hat{y}} \end{Bmatrix} = \begin{Bmatrix} \frac{\partial u_0}{\partial \hat{x}} \\ \frac{\partial v_0}{\partial \hat{y}} \\ \frac{\partial u_0}{\partial \hat{y}} + \frac{\partial v_0}{\partial \hat{x}} \end{Bmatrix}, \quad \boldsymbol{\epsilon}^b = \begin{Bmatrix} \epsilon^b_{\hat{x}\hat{x}} \\ \epsilon^b_{\hat{y}\hat{y}} \\ \gamma^b_{\hat{x}\hat{y}} \end{Bmatrix} = \begin{Bmatrix} \frac{\partial \varphi_{\hat{x}}}{\partial \hat{x}} \\ \frac{\partial \varphi_{\hat{y}}}{\partial \hat{y}} \\ \frac{\partial \varphi_{\hat{x}}}{\partial \hat{y}} + \frac{\partial \varphi_{\hat{y}}}{\partial \hat{x}} \end{Bmatrix}, \quad \boldsymbol{\epsilon}^s = \begin{Bmatrix} \gamma^s_{\hat{x}\hat{z}} \\ \gamma^s_{\hat{y}\hat{z}} \end{Bmatrix} = \begin{Bmatrix} \frac{\partial w_0}{\partial \hat{x}} - \varphi_{\hat{x}} \\ \frac{\partial w_0}{\partial \hat{y}} - \varphi_{\hat{y}} \end{Bmatrix} \tag{B.2}$$

where, $\varphi_{\hat{x}}$ and $\varphi_{\hat{y}}$ are the rotations of the transverse normal along $\hat{x}$ and $\hat{y}$ axes, respectively. The sub-matrices $\mathbf{A}$, $\mathbf{B}$, $\mathbf{D}$ and $\mathbf{S}$ represent the extensional, bending-extensional coupling, bending and shear stiff-

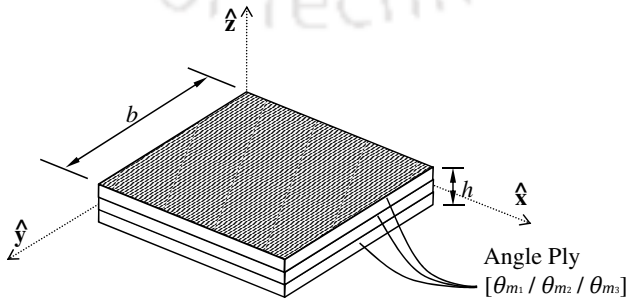

Figure B.1: Multi-ply laminated composite plate

nesses whose elements are evaluated by

$$A_{ij} = \int_{-\frac{h}{2}}^{\frac{h}{2}} \bar{Q}_{m_{ij}}\, \mathrm{d}\hat{z}, \quad B_{ij} = \int_{-\frac{h}{2}}^{\frac{h}{2}} \bar{Q}_{m_{ij}} \hat{z}\, \mathrm{d}\hat{z}, \qquad D_{ij} = \int_{-\frac{h}{2}}^{\frac{h}{2}} \bar{Q}_{m_{ij}} \hat{z}^2\, \mathrm{d}\hat{z}, \quad \forall\, i,j = 1,2,6$$
$$S_{kl} = \int_{-\frac{h}{2}}^{\frac{h}{2}} \bar{Q}_{m_{kl}}\, \mathrm{d}\hat{z}, \qquad \forall\, k,l = 4,5 \tag{B.3}$$

Here, $\bar{Q}_{m_{ij}}$ is an element of transformed constitutive matrix $\bar{\mathbf{Q}}_m$ for m^{th} ply and it is indexed as

$$\bar{\mathbf{Q}}_m = \begin{bmatrix} \bar{Q}_{m_{11}} & \bar{Q}_{m_{12}} & \bar{Q}_{m_{16}} & 0 & 0 \\ \bar{Q}_{m_{12}} & \bar{Q}_{m_{22}} & \bar{Q}_{m_{26}} & 0 & 0 \\ \bar{Q}_{m_{16}} & \bar{Q}_{m_{26}} & \bar{Q}_{m_{66}} & 0 & 0 \\ 0 & 0 & 0 & \bar{Q}_{m_{44}} & \bar{Q}_{m_{45}} \\ 0 & 0 & 0 & \bar{Q}_{m_{54}} & \bar{Q}_{m_{55}} \end{bmatrix} \tag{B.4}$$

Since $\bar{\mathbf{Q}}_m = \mathbf{T}_m^{\mathsf{T}} \mathbf{Q}_m \mathbf{T}_m$, it is determined from the constituent matrix $\mathbf{Q}_m$ and transformation matrix $\mathbf{T}_m$ which are

$$\mathbf{Q}_m = \begin{bmatrix} Q_{m_{11}} & Q_{m_{12}} & 0 & 0 & 0 \\ Q_{m_{12}} & Q_{m_{22}} & 0 & 0 & 0 \\ 0 & 0 & Q_{m_{66}} & 0 & 0 \\ 0 & 0 & 0 & Q_{m_{44}} & 0 \\ 0 & 0 & 0 & 0 & Q_{m_{55}} \end{bmatrix}, \quad \mathbf{T}_m = \begin{bmatrix} c^2 & s^2 & sc & 0 & 0 \\ s^2 & c^2 & -sc & 0 & 0 \\ -2sc & sc & c^2 - s^2 & 0 & 0 \\ 0 & 0 & 0 & c & -s \\ 0 & 0 & 0 & s & c \end{bmatrix} \tag{B.5}$$

The matrix $\mathbf{Q}_m$ depends on the material properties of the ply such as elastic modulus (E_1^m, E_2^m), Poisson's ratio (ν_{12}^m, ν_{21}^m) and shear modulus (G_{12}^m, G_{23}^m, G_{13}^m) whereas $\mathbf{T}_m$ is based on the angle θ_m between the direction cosines of the m^{th} ply axes with respect to the global axes. Moreover, their elements in Eq. B.5 are given as $Q_{m_{11}} = \frac{E_1^m}{1-\nu_{12}^m \nu_{21}^m}$, $Q_{m_{12}} = \frac{E_2^m \nu_{12}^m}{1-\nu_{12}^m \nu_{21}^m}$, $Q_{m_{22}} = \frac{E_2^m}{1-\nu_{12}^m \nu_{21}^m}$, $Q_{m_{66}} = G_{12}^m$, $Q_{m_{44}} = \kappa G_{23}^m$, $Q_{m_{55}} = \kappa G_{13}^m$, $s = \sin\theta_m$ and $c = \cos\theta_m$, where the factor κ is for shear correction.

Using constitutive equation, the total strain energy stored over the domain Ω_m^e of the composite plate for e^{th} element and m^{th} ply is obtained as [170]

$$\mathcal{U} = \sum_{e=1}^{n_e} \mathcal{U}^e = \frac{1}{2} \sum_{e=1}^{n_e} \left(\int_{\Omega_m^e} \mathbf{N}^{\mathsf{T}} \boldsymbol{\epsilon}^f \mathrm{d}\Omega_m^e + \int_{\Omega_m^e} \mathbf{M}^{\mathsf{T}} \boldsymbol{\epsilon}^b \mathrm{d}\Omega_m^e + \int_{\Omega_m^e} \mathbf{V}^{\mathsf{T}} \boldsymbol{\epsilon}^s \mathrm{d}\Omega_m^e \right) \tag{B.6}$$

$$= \frac{1}{2} \sum_{e=1}^{n_e} \mathbf{u}_e^{\mathsf{T}} \left(\sum_{m=1}^{n_m} \int_{\Omega_m^e} \mathbf{B}_m^{\mathsf{T}} \bar{\mathbf{Q}}_m \mathbf{B}_m \, \mathrm{d}\Omega_m^e \right) \mathbf{u}_e \tag{B.7}$$

where, $\mathbf{B}_m$ and n_e represent the strain-displacement transfer matrix and the number of mesh elements, respectively. The element-wise stiffness matrix $\mathbf{K}^e$ of the laminated composite plate is expressed as follows

$$\mathbf{K}^e = \sum_{m=1}^{n_m} \int_{\Omega_m^e} \mathbf{B}_m^T \bar{\mathbf{Q}}_m \mathbf{B}_m \, \mathrm{d}\Omega_m^e \tag{B.8}$$

Above expression of stiffness is deterministic as the material properties in the constitutive matrix $\bar{\mathbf{Q}}_m$ are assumed to be constant. Let the material properties such as elastic and shear modulli (i.e. E_1^m, E_2^m and G_{12}^m) are random. For simplicity, these properties are considered to be independent Gaussian random fields

which can be expressed by KLE following Eq. A.5 as

$$E_1^m(\mathbf{x},\theta) = \mu_1^m + \sum_{i=1}^{M} \sqrt{\lambda_{mi}^{(1)}}\xi_{mi}^{(1)}(\theta)\psi_{mi}^{(1)}(\mathbf{x}), \qquad E_2^m(\mathbf{x},\theta) = \mu_2^m + \sum_{i=1}^{M} \sqrt{\lambda_{mi}^{(2)}}\xi_{mi}^{(2)}(\theta)\psi_{mi}^{(2)}(\mathbf{x}),$$
$$G_{12}^m(\mathbf{x},\theta) = \mu_3^m + \sum_{i=1}^{M} \sqrt{\lambda_{mi}^{(3)}}\xi_{mi}^{(3)}(\theta)\psi_{mi}^{(3)}(\mathbf{x}) \tag{B.9}$$

with mean μ_1^m, μ_2^m, μ_3^m, eigenvalues $\lambda_{mi}^{(1)}$, $\lambda_{mi}^{(2)}$, $\lambda_{mi}^{(3)}$ and eigenfunctions $\psi_{mi}^{(1)}(\mathbf{x})$, $\psi_{mi}^{(2)}(\mathbf{x})$, $\psi_{mi}^{(3)}(\mathbf{x})$. As mentioned earlier, random variables $\xi_{mi}^{(1)}$, $\xi_{mi}^{(2)}$ and $\xi_{mi}^{(3)}$ are independent and follow $\mathcal{N}(0,1)$. It can be noticed that the remaining material properties are assumed as deterministic, unless stated otherwise. Incorporating the effect of theses random fields in the stochastic FE formulation by substituting Eq. B.9 back into Eq. B.8 leads to

$$\mathbf{K}^e(\mathbf{x},\theta) = \sum_{m=1}^{n_m}\left[\mathbf{K}_m^{e0} + \sum_{i=1}^{M}\mathbf{K}_{mi}^{e1}(\mathbf{x})\xi_{mi}^{(1)}(\theta) + \sum_{i=1}^{M}\mathbf{K}_{mi}^{e2}(\mathbf{x})\xi_{mi}^{(2)}(\theta) + \sum_{i=1}^{M}\mathbf{K}_{mi}^{e3}(\mathbf{x})\xi_{mi}^{(3)}(\theta)\right] \tag{B.10}$$

where, the individual sub-matrices of stiffness can be expressed as

$$\mathbf{K}_m^{e0} = \int_{\Omega_m^e}\mathbf{B}_m^{\mathsf{T}}\bar{\mathbf{Q}}_m^0\mathbf{B}_m\,\mathrm{d}\Omega_m^e, \qquad \mathbf{K}_{mi}^{e1}(\mathbf{x}) = \int_{\Omega_m^e}\sqrt{\lambda_{mi}^{(1)}}\psi_{mi}^{(1)}(\mathbf{x})\mathbf{B}_m^{\mathsf{T}}\bar{\mathbf{Q}}_m^1\mathbf{B}_m\,\mathrm{d}\Omega_m^e,$$
$$\mathbf{K}_{mi}^{e2}(\mathbf{x}) = \int_{\Omega_m^e}\sqrt{\lambda_{mi}^{(2)}}\psi_{mi}^{(2)}(\mathbf{x})\mathbf{B}_m^{\mathsf{T}}\bar{\mathbf{Q}}_m^2\mathbf{B}_m\,\mathrm{d}\Omega_m^e, \qquad \mathbf{K}_{mi}^{e3}(\mathbf{x}) = \int_{\Omega_m^e}\sqrt{\lambda_{mi}^{(3)}}\psi_{mi}^{(3)}(\mathbf{x})\mathbf{B}_m^{\mathsf{T}}\bar{\mathbf{Q}}_m^3\mathbf{B}_m\,\mathrm{d}\Omega_m^e \tag{B.11}$$

Here, the superscript ^{0} denotes the mean component and thus, $\mathbf{K}_m^{e0}$ gives the mean stiffness whereas $\mathbf{K}_{mi}^{ek}\ \forall k = 1,2,3$ represents the fluctuating stiffness components corresponding to the respective random fields. Eq. B.10 can be simplified further in the following form

$$\mathbf{K}^e(\mathbf{x},\theta) = \sum_{m=1}^{n_m}\mathbf{K}_m^{e0} + \sum_{j=1}^{n_m M}\mathbf{K}_j^{e1}(\mathbf{x})\xi_j^{(1)}(\theta) + \sum_{j=1}^{n_m M}\mathbf{K}_j^{e2}(\mathbf{x})\xi_j^{(2)}(\theta) + \sum_{j=1}^{n_m M}\mathbf{K}_j^{e3}(\mathbf{x})\xi_j^{(3)}(\theta) \tag{B.12}$$

Once the element-wise stiffness matrix $\mathbf{K}^e(\mathbf{x},\theta)$ for the entire mesh is obtained, global stiffness matrix $\mathbf{K}(\mathbf{x},\theta)$ is assembled using permutation matrix [189]. Similarly, the nodal displacements $\mathbf{u}$ can be determined using $\mathbf{u}_e$. It is obvious that the outcome of the nodal displacement $\mathbf{u}$ is uncertain irrespective of the applied force $\mathbf{f}$ since $\mathbf{K}$ is a function of θ. Hence, $\mathbf{u}$ can be represented in terms of PCE according to Eq. 4.3 which gives

$$\left[\sum_{m=1}^{n_m}\mathbf{K}_m^0 + \sum_{j=1}^{n_m M}\mathbf{K}_j^1(\mathbf{x})\xi_j^{(1)}(\theta) + \sum_{j=1}^{n_m M}\mathbf{K}_j^2(\mathbf{x})\xi_j^{(2)}(\theta) + \sum_{j=1}^{n_m M}\mathbf{K}_j^3(\mathbf{x})\xi_j^{(3)}(\theta)\right]\left[\sum_{i=0}^{p}\alpha_i\gamma_i(\theta)\right] = \mathbf{f} \tag{B.13}$$

Above expression is similar to the Eq. A.1 where $\mathbf{f}$ is also considered as random. Approximation for $\mathbf{u}$ can be determined from the mean square error minimization of Eq. B.13 [189]. However, as opposed to Eq. 4.3 in the present study $\mathbf{u}$ is solved directly from Eq. B.13 and consequently, the stress level at the output is approximated through PCE.

The stress $\boldsymbol{\sigma} = \{\sigma_1\ \sigma_2\ \tau_{12}\}$ generated in the ply are evaluated at Gauss quadrature points using

$$\boldsymbol{\sigma}_m = \left[\bar{\mathbf{Q}}_m(\mathbf{x},\theta)\right]_{1,2,6}\boldsymbol{\epsilon}_m \tag{B.14}$$

where, $\left[\bar{\mathbf{Q}}_m(\bullet)\right]_{1,2,6} = [\bar{Q}_{mij}]\ \forall i,j = 1,2,6$ and $\boldsymbol{\epsilon} = \{\epsilon_1\ \epsilon_2\ \gamma_{12}\}$ represents the strain. Based on these stresses, failure index $\mathfrak{F}$ is quantified for all the Gauss quadrature points according to the modified Tsai-Hill failure criterion [75] which is given as

$$\mathfrak{F} = \left(\frac{\sigma_1}{X}\right)^2 + \left(\frac{\sigma_2}{Y}\right)^2 + \left(\frac{\tau_{12}}{S}\right)^2 - \frac{\sigma_1\sigma_2}{X^2} \tag{B.15}$$

where, X, Y and S denote the longitudinal, transverse and shear strength, respectively. The present study considers $\mathfrak{F}$ for stochastic computation as it is a function of the variability induced due to random fields and thus, it is further referred as the performance function.

References

[1] R. Ranganathan, Structural Reliability Analysis and Design, Jaico Publishing House, 1999.

[2] S. K. Choi, R. V. Grandhi, R. A. Canfield (Eds.), Reliability-based Structural Design, 1st Edition, Springer-Verlag London Limited, 2007.

[3] S. Rahman, D. Wei, A univariate approximation at most probable point for higher-order reliability analysis, International Journal of Solids and Structures 43 (9) (2006) 2820–2839.

[4] O. Ditlevsen, H. O. Madsen, Structural Reliability Methods, John Wiley & Sons, Inc., Chichester, UK, 1996.

[5] R. Melchers, Importance sampling in structural systems, Structural Safety 6 (1) (1989) 3–10.

[6] A. Olsson, G. Sandberg, O. Dahlblom, On latin hypercube sampling for structural reliability analysis, Structural Safety 25 (1) (2003) 47–68.

[7] S. K. Au, J. L. Beck, Estimation of small failure probabilities in high dimensions by subset simulation, Probabilistic Engineering Mechanics 16 (4) (2001) 263–277.

[8] H. S. Li, Z. J. Cao, Matlab codes of subset simulation for reliability analysis and structural optimization, Structural and Multidisciplinary Optimization 54 (2) (2016) 391–410.

[9] Y. Zhang, A. Der Kiureghian, Two Improved Algorithms for Reliability Analysis, Springer US, Boston, MA, 1995, pp. 297–304.

[10] K. Breitung, 40 years FORM: Some new aspects?, Probabilistic Engineering Mechanics 42 (2015) 71–77.

[11] M. Valdebenito, H. Pradlwarter, G. Schuëller, The role of the design point for calculating failure probabilities in view of dimensionality and structural nonlinearities, Structural Safety 32 (2) (2010) 101–111.

[12] L. Faravelli, Response-surface approach for reliability analysis, Journal of Engineering Mechanics 115 (12) (1989) 2763–2781.

[13] S. S. Isukapalli, Uncertainty analysis of transport-transformation models, Ph.D. dissertation, Rutgers, The State University of New Jersey (1999).

[14] G. E. P. Box, K. B. Wilson, On the experimental attainment of optimum conditions, Journal of the Royal Statistical Society. Series B (Methodological) 13 (1) (1951) 1–45.

[15] R. H. Myers, A. I. Khuri, J. Carter, Walter H., Response surface methodology: 1966-1988, Technometrics 31 (2) (1989) 137–157.

[16] C. Bucher, U. Bourgund, A fast and efficient response surface approach for structural reliability problems, Structural Safety 7 (1) (1990) 57–66.

[17] M. R. Rajashekhar, B. R. Ellingwood, A new look at the response surface approach for reliability analysis, Structural Safety 12 (3) (1993) 205–220.

[18] Y. W. Liu, F. Moses, A sequential response surface method and its application in the reliability analysis of aircraft structural systems, Structural Safety 16 (1–2) (1994) 39–46.

[19] S. H. Kim, S. W. Na, Response surface method using vector projected sampling points, Structural Safety 19 (1) (1997) 3–19.

[20] P. Das, Y. Zheng, Cumulative formation of response surface and its use in reliability analysis, Probabilistic Engineering Mechanics 15 (4) (2000) 309–315.

[21] X. Guan, R. Melchers, Effect of response surface parameter variation on structural reliability estimates, Structural Safety 23 (4) (2001) 429–444.

[22] H. M. Gomes, A. M. Awruch, Comparison of response surface and neural network with other methods for structural reliability analysis, Structural Safety 26 (1) (2004) 49–67.

[23] J. E. Hurtado, An examination of methods for approximating implicit limit state functions from the viewpoint of statistical learning theory, Structural Safety 26 (3) (2004) 271–293.

[24] N. Gayton, J. Bourinet, M. Lemaire, CQ2RS: a new statistical approach to the response surface method for reliability analysis, Structural Safety 25 (1) (2003) 99–121.

[25] V. Romero, L. Swiler, A. Giunta, Construction of response surfaces based on progressive-lattice-sampling experimental designs with application to uncertainty propagation, Structural Safety 26 (2) (2004) 201–219.

[26] S. Gupta, C. Manohar, An improved response surface method for the determination of failure probability and importance measures, Structural Safety 26 (2) (2004) 123–139.

[27] I. Kaymaz, C. A. McMahon, A response surface method based on weighted regression for structural reliability analysis, Probabilistic Engineering Mechanics 20 (1) (2005) 11–17.

[28] X. S. Nguyen, A. Sellier, F. Duprat, G. Pons, Adaptive response surface method based on a double weighted regression technique, Probabilistic Engineering Mechanics 24 (2) (2009) 135–143.

[29] S. Wong, R. Hobbs, C. Onof, An adaptive response surface method for reliability analysis of structures with multiple loading sequences, Structural Safety 27 (4) (2005) 287–308.

[30] S. H. Lee, B. M. Kwak, Response surface augmented moment method for efficient reliability analysis, Structural Safety 28 (3) (2006) 261–272.

[31] D. Allaix, V. Carbone, An improvement of the response surface method, Structural Safety 33 (2) (2011) 165–172.

[32] S. C. Kang, H. M. Koh, J. F. Choo, An efficient response surface method using moving least squares approximation for structural reliability analysis, Probabilistic Engineering Mechanics 25 (4) (2010) 365–371.

[33] A. Taflanidis, S. Cheung, Stochastic sampling using moving least squares response surface approximations, Probabilistic Engineering Mechanics 28 (0) (2012) 216–224.

[34] T. Marwala, Finite-element-model updating using computional intelligence techniques, London: Springer, 2010.

[35] W. X. Ren, H. B. Chen, Finite element model updating in structural dynamics by using the response surface method, Engineering Structures 32 (8) (2010) 2455–2465.

[36] M. Brehm, V. Zabel, C. Bucher, An automatic mode pairing strategy using an enhanced modal assurance criterion based on modal strain energies, Journal of Sound and Vibration 329 (25) (2010) 5375–5392.

[37] S. Shahidi, S. Pakzad, Generalized response surface model updating using time domain data, Journal of Structural Engineering 140 (8).

[38] S. Chakraborty, A. Sen, Adaptive response surface based efficient finite element model updating, Finite Elements in Analysis and Design 80 (2014) 33–40.

[39] V. Tandjiria, C. I. Teh, B. K. Low, Reliability analysis of laterally loaded piles using response surface methods, Structural Safety 22 (4) (2000) 335–355.

[40] L. Deng, C. S. Cai, Bridge model updating using response surface method and genetic algorithm, Journal of Bridge Engineering 15 (5) (2010) 553–564.

[41] W. X. Ren, S. E. Fang, M. Y. Deng, Response surface–based finite-element-model updating using structural static responses, Journal of Engineering Mechanics 137 (4) (2011) 248–257.

[42] N. Buratti, B. Ferracuti, M. Savoia, Response surface with random factors for seismic fragility of reinforced concrete frames, Structural Safety 32 (1) (2010) 42–51.

[43] K. Lin, H. Qiu, L. Gao, Y. Sun, Comparison of stochastic response surface method and response surface method for structure reliability analysis, in: 2009 Second International Conference on Intelligent Computation Technology and Automation, Vol. 3, 2009, pp. 172–175.

[44] H. P. Gavin, A. Zaicenco, Performance and reliability of semi-active equipment isolation, Journal of Sound and Vibration 306 (1–2) (2007) 74–90.

[45] W. Shi, J. Guo, S. Zeng, J. Ma, A mechanism reliability analysis method based on polynomial chaos expansion, in: The Proceedings of 2011 9th International Conference on Reliability, Maintainability and Safety, 2011, pp. 110–115.

[46] N. Wiener, The homogeneous chaos, American Journal of Mathematics 60 (4) (1938) 897–936.

[47] R. H. Cameron, W. T. Martin, The orthogonal development of non-linear functionals in series of fourier-hermite functionals, Annals of Mathematics 48 (2) (1947) 385–392.

[48] M. A. Tatang, Direct incorporation of uncertainty in chemical and environmental engineering systems, Ph.D. thesis, Massachusetts Institute of Technology, Cambridge, MA, USA (February 1995).

[49] D. Wei, Z. Cui, J. Chen, Uncertainty quantification using polynomial chaos expansion with points of monomial cubature rules, Computers & Structures 86 (23–24) (2008) 2102–2108.

[50] B. Sudret, A. D. Kiureghian, Comparison of finite element reliability methods, Probabilistic Engineering Mechanics 17 (4) (2002) 337–348.

[51] D. Xiu, G. E. Karniadakis, Modeling uncertainty in flow simulations via generalized polynomial chaos, Journal of Computational Physics 187 (1) (2003) 137–167.

[52] S. K. Choi, R. V. Grandhi, R. A. Canfield, Structural reliability under non-Gaussian stochastic behavior, Computers & Structures 82 (13–14) (2004) 1113–1121.

[53] O. G. Ernst, A. Mugler, H.-J. Starkloff, E. Ullmann, On the convergence of generalized polynomial chaos expansions, ESAIM: M2AN 46 (2) (2012) 317–339.

[54] S. Huang, S. Mahadevan, R. Rebba, Collocation-based stochastic finite element analysis for random field problems, Probabilistic Engineering Mechanics 22 (2) (2007) 194–205.

[55] B. Liang, S. P. Huang, K. K. Phoon, An excel add-in implementation for collocation-based stochastic response surface method, in: ISGSR2007 First International Symposium on Geotechnical Safety & Risk, 2007, pp. 18–19.

[56] P. Bressolette, M. Fogli, C. Chauvière, A stochastic collocation method for large classes of mechanical problems with uncertain parameters, Probabilistic Engineering Mechanics 25 (2) (2010) 255–270.

[57] L. Ying, Application of stochastic response surface method in the structural reliability, Procedia Engineering 28 (2012) 661–664, 2012 International Conference on Modern Hydraulic Engineering.

[58] H. P. Gavin, S. C. Yau, High-order limit state functions in the response surface method for structural reliability analysis, Structural Safety 30 (2) (2008) 162–179.

[59] G. Hou, N. Borade, B. Florsheim, Reliability sensitivity analysis using polynomial chaos expansions, in: 3rd International ASRANet Colloquim, Glasgow, UK, 2006.

[60] G. Schuëller, H. Pradlwarter, Benchmark study on reliability estimation in higher dimensions of structural systems – an overview, Structural Safety 29 (3) (2007) 167–182.

[61] R. Ghanem, G. Saad, A. Doostan, Efficient solution of stochastic systems: Application to the embankment dam problem, Structural Safety 29 (3) (2007) 238–251.

[62] K. Maute, G. Weickum, M. Eldred, A reduced-order stochastic finite element approach for design optimization under uncertainty, Structural Safety 31 (6) (2009) 450–459.

[63] C. Proppe, Reliability computation with local polynomial chaos approximations, ZAMM - Journal of Applied Mathematics and Mechanics / Zeitschrift für Angewandte Mathematik und Mechanik 89 (1) (2009) 28–37.

[64] G. Blatman, B. Sudret, Sparse polynomial chaos expansions and adaptive stochastic finite elements using a regression approach, Comptes Rendus Mécanique 336 (6) (2008) 518–523.

[65] G. Blatman, B. Sudret, An adaptive algorithm to build up sparse polynomial chaos expansions for stochastic finite element analysis, Probabilistic Engineering Mechanics 25 (2) (2010) 183–197.

[66] G. Blatman, B. Sudret, Efficient computation of global sensitivity indices using sparse polynomial chaos expansions, Reliability Engineering & System Safety 95 (11) (2010) 1216–1229.

[67] G. Blatman, B. Sudret, Adaptive sparse polynomial chaos expansion based on least angle regression, Journal of Computational Physics 230 (6) (2011) 2345–2367.

[68] L. Hawchar, C. P. E. Soueidy, F. Schoefs, Principal component analysis and polynomial chaos expansion for time-variant reliability problems, Reliability Engineering & System Safety 167 (2017) 406–416.

[69] Q. Pan, D. Dias, Sliced inverse regression-based sparse polynomial chaos expansions for reliability analysis in high dimensions, Reliability Engineering & System Safety 167 (2017) 484–493.

[70] G. Blatman, B. Sudret, Reliability and Optimization of Structural Systems, CRC Press, 2010, Ch. Reliability analysis of a pressurized water reactor vessel using sparse polynomial chaos expansions, pp. 9–16.

[71] C. Hu, B. D. Youn, Adaptive-sparse polynomial chaos expansion for reliability analysis and design of complex engineering systems, Structural and Multidisciplinary Optimization 43 (3) (2011) 419–442.

[72] D. Li, Y. Chen, W. Lu, C. Zhou, Stochastic response surface method for reliability analysis of rock slopes involving correlated non-normal variables, Computers and Geotechnics 38 (2011) 58–68.

[73] G. Mollon, D. Dias, A. H. Soubra, Probabilistic analysis of pressurized tunnels against face stability using collocation-based stochastic response surface method, Journal of Geotechnical and Geoenvironmental Engineering 137 (4) (2011) 385–397.

[74] A. Ahmed, A. H. Soubra, Probabilistic analysis at the serviceability limit state of two neighboring strip footings resting on a spatially random soil, Structural Safety 49 (2014) 2–9.

[75] P. Sasikumar, R. Suresh, S. Gupta, Analysis of CFRP laminated plates with spatially varying non-Gaussian inhomogeneities using SFEM, Composite Structures 112 (0) (2014) 308–326.

[76] P. Sasikumar, R. Suresh, P. Vijayaghosh, S. Gupta, Experimental characterisation of random field models for CFRP composite panels, Composite Structures 120 (0) (2015) 451–471.

[77] P. Sasikumar, A. Venketeswaran, R. Suresh, S. Gupta, A data driven polynomial chaos based approach for stochastic analysis of CFRP laminated composite plates, Composite Structures 125 (0) (2015) 212–227.

[78] R. Tipireddy, R. Ghanem, Basis adaptation in homogeneous chaos spaces, Journal of Computational Physics 259 (2014) 304–317.

[79] P. Tsilifis, R. G. Ghanem, Reduced Wiener chaos representation of random fields via basis adaptation and projection, Journal of Computational Physics 341 (2017) 102–120.

[80] W. C. M. van Beers, J. P. C. Kleijnen, Kriging for interpolation in random simulation, The Journal of the Operational Research Society 54 (3) (2003) 255–262.

[81] D. G. Krige, A statistical approach to some basic mine valuation problems on the Witwatersrand, Journal of the Southern African Institute of Mining and Metallurgy 52 (6) (1951) 119–139.

[82] G. Matheron, Principles of geostatistics, Economic Geology 58 (8) (1963) 1246–1266.

[83] N. Cressie, The origins of kriging, Mathematical Geology 22 (3) (1990) 239–252.

[84] N. A. C. Cressie, Statistics for Spatial Data, Revised Edition, John Wiley & Sons, Ltd., New York, USA, 1993.

[85] J. P. Kleijnen, Kriging metamodeling in simulation: A review, European Journal of Operational Research 192 (3) (2009) 707–716.

[86] L. L. Gratiet, J. Garnier, Recursive co-kriging model for design of computer experiments with multiple levels of fidelity, International Journal for Uncertainty Quantification 4 (5) (2014) 365–386.

[87] S. Ulaganathan, I. Couckuyt, D. Deschrijver, E. Laermans, T. Dhaene, A matlab toolbox for kriging metamodelling, Procedia Computer Science 51 (2015) 2708–2713, International Conference on Computational Science, ICCS 2015.

[88] B. Kamiński, A method for the updating of stochastic kriging metamodels, European Journal of Operational Research 247 (3) (2015) 859–866.

[89] H. S. Ahmed, S. Sen, S. Ghosh, Prediction of the buckling strength of CFS members with local geometric imperfection using stochastic Kriging, in: C. Bucher, B. R. Ellingwood, D. M. Frangopol (Eds.), Safety, Reliability, Risk, Resilience and Sustainability of Structures and Infrastructure, Vienna, Austria, 2017, pp. 768–777, 12th International Conference on Structural Safety and Reliability.

[90] T. Mukhopadhyay, S. Chakraborty, S. Dey, S. Adhikari, R. Chowdhury, A critical assessment of Kriging model variants for high-fidelity uncertainty quantification in dynamics of composite shells, Archives of Computational Methods in Engineering 24 (3) (2017) 495–518.

[91] G. S. Watson, Trend-surface analysis, Journal of the International Association for Mathematical Geology 3 (3) (1971) 215–226.

[92] J. Sacks, S. B. Schiller, W. J. Welch, Designs for computer experiments, Technometrics 31 (1) (1989) 41–47.

[93] J. Sacks, W. J. Welch, T. J. Mitchell, H. P. Wynn, Design and analysis of computer experiments, Statistical Science 4 (4) (1989) 409–423.

[94] A. I. Forrester, A. J. Keane, Recent advances in surrogate-based optimization, Progress in Aerospace Sciences 45 (1) (2009) 50–79.

[95] I. Kaymaz, Application of kriging method to structural reliability problems, Structural Safety 27 (2) (2005) 133–151.

[96] MATLAB, version 7.13.0.564 (R2011b), The MathWorks Inc., Natick, Massachusetts, 2011.

[97] S. N. Lophaven, H. B. Nielsen, J. Søndergaard, DACE: A MATLAB kriging toolbox, version 2.0, Tech. Rep. IMM-TR-2002-12, Informatics and Mathematical Modelling (IMM), Technical University of Denmark (August 2002).

[98] J. P. Kleijnen, W. van Beers, I. van Nieuwenhuyse, Constrained optimization in expensive simulation: Novel approach, European Journal of Operational Research 202 (1) (2010) 164–174.

[99] R. Schobi, B. Sudret, J. Wiart, Polynomial-chaos-based Kriging, International Journal for Uncertainty Quantification 5 (2) (2015) 171–193.

[100] R. Schobi, B. Sudret, S. Marelli, Rare event estimation using polynomial-chaos kriging, ASCE-ASME Journal of Risk and Uncertainty in Engineering Systems, Part A: Civil Engineering 3 (2) (2017) D4016002.

[101] S. Dutta, S. Ghosh, M. M. Inamdar, Optimisation of tensile membrane structures under uncertain wind loads using PCE and kriging based metamodels, Structural and Multidisciplinary Optimization 57 (3) (2018) 1149–1161.

[102] P. Wang, Z. Lu, Z. Tang, An application of the kriging method in global sensitivity analysis with parameter uncertainty, Applied Mathematical Modelling 37 (9) (2013) 6543–6555.

[103] G. Jia, A. A. Taflanidis, Kriging metamodeling for approximation of high-dimensional wave and surge responses in real-time storm/hurricane risk assessment, Computer Methods in Applied Mechanics and Engineering 261–262 (2013) 24–38.

[104] B. Gaspar, A. Teixeira, C. G. Soares, Assessment of the efficiency of Kriging surrogate models for structural reliability analysis, Probabilistic Engineering Mechanics 37 (2014) 24–34.

[105] L. Zhang, Z. Lu, P. Wang, Efficient structural reliability analysis method based on advanced Kriging model, Applied Mathematical Modelling 39 (2) (2015) 781–793.

[106] A. Haeri, M. J. Fadaee, Efficient reliability analysis of laminated composites using advanced Kriging surrogate model, Composite Structures 149 (2016) 26–32.

[107] B. Echard, N. Gayton, M. Lemaire, AK-MCS: An active learning reliability method combining Kriging and Monte Carlo simulation, Structural Safety 33 (2) (2011) 145–154.

[108] Z. Wen, H. Pei, H. Liu, Z. Yue, A sequential kriging reliability analysis method with characteristics of adaptive sampling regions and parallelizability, Reliability Engineering & System Safety 153 (2016) 170–179.

[109] W. Jian, S. Zhili, Y. Qiang, L. Rui, Two accuracy measures of the kriging model for structural reliability analysis, Reliability Engineering & System Safety 167 (2017) 494–505.

[110] Z. Jiang, J. Li, High dimensional structural reliability with dimension reduction, Structural Safety 69 (2017) 35–46.

[111] J. P. Kleijnen, Regression and kriging metamodels with their experimental designs in simulation: A review, European Journal of Operational Research 256 (1) (2017) 1–16.

[112] H. Rabitz, Ö. F. Aliş, J. Shorter, K. Shim, Efficient input-output model representations, Computer Physics Communications 117 (1–2) (1999) 11–20.

[113] Ö. F. Aliş, H. Rabitz, Efficient implementation of high dimensional model representations, Journal of Mathematical Chemistry 29 (2) (2001) 127–142.

[114] I. Sobol', Theorems and examples on high dimensional model representation, Reliability Engineering & System Safety 79 (2) (2003) 187–193.

[115] S. Rahman, H. Xu, A univariate dimension-reduction method for multi-dimensional integration in stochastic mechanics, Probabilistic Engineering Mechanics 19 (4) (2004) 393–408.

[116] H. Xu, S. Rahman, Decomposition methods for structural reliability analysis, Probabilistic Engineering Mechanics 20 (3) (2005) 239–250.

[117] R. Chowdhury, B. N. Rao, A. M. Prasad, High-dimensional model representation for structural reliability analysis, Communications in Numerical Methods in Engineering 25 (4) (2009) 301–337.

[118] R. Chowdhury, S. Adhikari, High dimensional model representation for stochastic finite element analysis, Applied Mathematical Modelling 34 (12) (2010) 3917–3932.

[119] T. Ziehn, A. Tomlin, GUI-HDMR – a software tool for global sensitivity analysis of complex models, Environmental Modelling & Software 24 (7) (2009) 775–785.

[120] S. Dey, T. Mukhopadhyay, S. Adhikari, Stochastic free vibration analysis of angle-ply composite plates - A RS-HDMR approach, Composite Structures 122 (4) (2015) 526–536.

[121] B. N. Rao, R. Chowdhury, Probabilistic analysis using high dimensional model representation and fast Fourier transform, International Journal for Computational Methods in Engineering Science and Mechanics 9 (6) (2008) 342–357.

[122] B. N. Rao, R. Chowdhury, A. M. Prasad, High dimensional model representation for piece-wise continuous function approximation, Communications in Numerical Methods in Engineering 24 (12) (2008) 1587–1609.

[123] R. Chowdhury, B. Rao, A. Prasad, Stochastic sensitivity analysis using HDMR and score function, Sadhana 34 (6) (2009) 967–986.

[124] R. Chowdhury, B. Rao, Hybrid high dimensional model representation for reliability analysis, Computer Methods in Applied Mechanics and Engineering 198 (5–8) (2009) 753–765.

[125] R. Chowdhury, B. Rao, Assessment of high dimensional model representation techniques for reliability analysis, Probabilistic Engineering Mechanics 24 (1) (2009) 100–115.

[126] A. S. Balu, B. N. Rao, Multicut-high dimensional model representation for structural reliability bounds estimation under mixed uncertainties, Computer-Aided Civil and Infrastructure Engineering 27 (6) (2012) 419–438.

[127] X. Ma, N. Zabaras, An adaptive high-dimensional stochastic model representation technique for the solution of stochastic partial differential equations, Journal of Computational Physics 229 (10) (2010) 3884–3915.

[128] X. Luo, Z. Lu, X. Xu, Reproducing kernel technique for high dimensional model representations (HDMR), Computer Physics Communications 185 (12) (2014) 3099–3108.

[129] S. Chen, W. Chen, S. Lee, Level set based robust shape and topology optimization under random field uncertainties, Structural and Multidisciplinary Optimization 41 (4) (2010) 507–524.

[130] S. Chakraborty, R. Chowdhury, Assessment of polynomial correlated function expansion for high-fidelity structural reliability analysis, Structural Safety 59 (1) (2016) 9–19.

[131] S. Chakraborty, R. Chowdhury, Towards 'h-p adaptive' generalized ANOVA, Computer Methods in Applied Mechanics and Engineering 320 (2017) 558–581.

[132] A. I. J. Forrester, A. Sóbester, A. J. Keane, Engineering Design via Surrogate Modelling: A Practical Guide, John Wiley & Sons, Ltd, West Sussex, UK, 2008.

[133] M. Q. Chau, X. Han, Y. C. Bai, C. Jiang, A structural reliability analysis method based on radial basis function, Computers, Materials & Continua 27 (2) (2012) 128–142.

[134] A. Chojaczyk, A. Teixeira, L. Neves, J. Cardoso, C. G. Soares, Review and application of artificial neural networks models in reliability analysis of steel structures, Structural Safety 52 (2015) 78–89.

[135] S. Kameshwar, J. E. Padgett, Multi-hazard risk assessment of highway bridges subjected to earthquake and hurricane hazards, Engineering Structures 78 (2014) 154–166.

[136] W. Ma, J. P. Kruth, Nurbs curve and surface fitting for reverse engineering, The International Journal of Advanced Manufacturing Technology 14 (12) (1998) 918–927.

[137] G. G. Wang, S. Shan, Review of metamodeling techniques in support of engineering design optimization, Journal of Mechanical Design 129 (4) (2007) 370–380.

[138] H. Wang, L. Tang, G. Li, Adaptive MLS-HDMR metamodeling techniques for high dimensional problems, Expert Systems with Applications 38 (11) (2011) 14117–14126.

[139] S. Dey, T. Mukhopadhyay, S. Adhikari, Metamodel based high-fidelity stochastic analysis of composite laminates: A concise review with critical comparative assessment, Composite Structures 171 (2017) 227–250.

[140] R. H. Myers, D. C. Montgomery, C. M. Anderson-Cook, Response surface methodology: process and product optimization using designed experiments, John Wiley & Sons, Hoboken, New Jersey, USA, 2009.

[141] OptiSLang, The optimizing structural language, DYNARDO GmbH, Weimar, Luthergasse 1D, Germany, documentation version 3.2.1 Edition (July 2011).

[142] T. Most, C. Bucher, A moving least squares weighting function for the element-free Galerkin method which almost fulfills essential boundary conditions, Structural Engineering and Mechanics 21 (3) (2005) 315–332.

[143] R. S. Koshal, Application of the method of maximum likelihood to the improvement of curves fitted by the method of moments, Journal of the Royal Statistical Society 96 (2) (1933) 303–313.

[144] ANSYS, Structural analysis guide - Release 13.0, ANSYS, Inc. (2010).

[145] Indian Standard–456: 2000, Plain and Reinforced Concrete-Code of Practice, Bureau of Indian Standards, Manak Bhawan, New Delhi, India, 2000.

[146] N. E. Huang, Z. Shen, S. R. Long, M. C. Wu, H. H. Shih, Q. Zheng, N.-C. Yen, C. C. Tung, H. H. Liu, The empirical mode decomposition and the hilbert spectrum for nonlinear and non-stationary time series analysis, Proceedings of the Royal Society of London. Series A: Mathematical, Physical and Engineering Sciences 454 (1971) (1998) 903–995.

[147] S. Mahato, M. V. Teja, A. Chakraborty, Combined wavelet–hilbert transform based modal identification of road bridge using vehicular excitation, Journal of Civil Structural Health Monitoring 7 (1) (2017) 29–44.

[148] P. L. Liu, A. D. Kiureghian, Multivariate distribution models with prescribed marginals and covariances, Probabilistic Engineering Mechanics 1 (2) (1986) 105–112.

[149] T. Abdo, R. Rackwitz, A new beta-point algorithm for large time-invariant and time-variant reliability problems, in: A. Der Kiureghian, P. Thoft-Christensen (Eds.), Reliability and Optimization of Structural Systems '90, Springer, 1991, Ch. 1, pp. 1–12, lecture Notes in Engineering 61.

[150] A. Haldar, S. Mahadevan, Reliability assessment using stochastic finite element analysis, John Wiley & Sons, Inc., New York, USA, 2000.

[151] R. Fletcher, Practical Methods of Optimization, 2nd Edition, John Wiley & Sons, Ltd, 1987.

[152] K. Kiyoshi, Semi-empirical formula for the seismic characteristics of the ground, University of Tokyo Bulletin of the Earthquake Research Institute 35 (1957) 309–324.

[153] H. Tajimi, A statistical method of determining the maximum response of a building structure during an earthquake, in: Proceedings of the 2nd World Conference on Earthquake Engineering, Tokyo and Kyoto, Japan, July 11–18, 1960, pp. 781–798.

[154] N. C. Nigam, S. Narayanan, Applications of Random Vibrations, Narosa Punblishing House, New Delhi, 1994.

[155] G. Warburton, Optimum absorber parameters for minimizing vibration response, Earthquake Engineering & Structural Dynamics 9 (3) (1981) 251–262.

[156] G. B. Warburton, Optimum absorber parameters for various combinations of response and excitation parameters, Earthquake Engineering & Structural Dynamics 10 (3) (1982) 381–401.

[157] T. Asami, O. Nishihara, A. Baz, Analytical solutions to H_∞ and H_2 optimization of dynamic vibration absorbers attached to damped linear systems, Journal of Vibration and Acoustics 124 (2) (2002) 284–295.

[158] Y. Fujino, M. Abé, Design formulas for tuned mass dampers based on a perturbation technique, Earthquake Engineering & Structural Dynamics 22 (10) (1993) 833–854.

[159] M. B. Ozer, T. J. Royston, Extending Den Hartog's vibration absorber technique to multi-degree-of-freedom systems, Journal of Vibration and Acoustics 127 (4) (2004) 341–350.

[160] S. S. Sastry, Introductory Methods of Numerical Analysis, 5th Edition, PHI Learning Pvt. Ltd., New Delhi, India, 2012.

[161] R. G. Ghanem, P. D. Spanos, Stochastic finite elements: a spectral approach, 1st Edition, Springer-Verlag New York, 1991.

[162] F. Xiong, W. Chen, Y. Xiong, S. Yang, Weighted stochastic response surface method considering sample weights, Structural and Multidisciplinary Optimization 43 (6) (2011) 837–849.

[163] F. Xiong, Y. Liu, Y. Xiong, S. Yang, A double weighted stochastic response surface method for reliability analysis, Journal of Mechanical Science and Technology 26 (8) (2012) 2573–2580.

[164] A. D. Kiureghian, T. Dakessian, Multiple design points in first and second-order reliability, Structural Safety 20 (1) (1998) 37–49.

[165] A. Klimke, B. Wohlmuth, Computing expensive multivariate functions of fuzzy numbers using sparse grids, Fuzzy Sets and Systems 154 (3) (2005) 432–453.

[166] M. Holtz, Sparse Grid Quadrature in High Dimensions with Applications in Finance and Insurance, Springer Berlin Heidelberg, Berlin, Heidelberg, 2011, Ch. Sparse Grid Quadrature, pp. 51–76.

[167] X. Ma, N. Zabaras, An adaptive hierarchical sparse grid collocation algorithm for the solution of stochastic differential equations, Journal of Computational Physics 228 (8) (2009) 3084–3113.

[168] M. Griebel, M. Holtz, Dimension-wise integration of high-dimensional functions with applications to finance, Journal of Complexity 26 (5) (2010) 455–489.

[169] X. Huang, Y. Liu, Y. Zhang, X. Zhang, Reliability analysis of structures using stochastic response surface method and saddlepoint approximation, Structural and Multidisciplinary Optimization 55 (6) (2017) 2003–2012.

[170] J. N. Reddy, Mechanics of laminated composite plates and shells: theory and analysis, CRC Press, Boca Raton, Florida, USA, 2004.

[171] T. L. Anderson, Fracture Mechanics: Fundamentals and Applications, 3rd Edition, CRC Press, Boca Raton, Unite States, 2005.

[172] M. J. Pais, Variable amplitude fatigue analysis using surrogate models and exact XFEM reanalysis, Ph.d. dissertation, University of Florida, USA (2011).

[173] M. J. Pais, Matlab extended finite element (MXFEM) code v1.2, Tech. rep. (2011).

[174] H. Rabitz, Ö. F. Aliş, General foundations of high-dimensional model representations, Journal of Mathematical Chemistry 25 (2) (1999) 197–233.

[175] G. Li, S. W. Wang, H. Rabitz, Practical approaches to construct RS-HDMR component functions, The Journal of Physical Chemistry A 106 (37) (2002) 8721–8733.

[176] D. Wei, S. Rahman, A multi-point univariate decomposition method for structural reliability analysis, International Journal of Pressure Vessels and Piping 87 (5) (2010) 220–229.

[177] R. Chowdhury, B. Rao, Multicut high dimensional model representation for reliability analysis, Structural Engineering and Mechanics 38 (5) (2011) 651–674.

[178] B. N. Rao, S. Rahman, An efficient meshless method for fracture analysis of cracks, Computational Mechanics 26 (4) (2000) 398–408.

[179] S. Chakraborty, R. Chowdhury, Sequential experimental design based generalised ANOVA, Journal of Computational Physics 317 (Supplement C) (2016) 15–32.

[180] R. C. Penmetsa, R. V. Grandhi, Efficient estimation of structural reliability for problems with uncertain intervals, Computers & Structures 80 (12) (2002) 1103–1112.

[181] P. L. Liu, A. D. Kiureghian, Optimization algorithms for structural reliability, Structural Safety 9 (3) (1991) 161–177.

[182] R. B. Nelsen, An Introduction to Copulas (Springer Series in Statistics), 2nd Edition, Springer, New York, USA, 2006.

[183] G. Xue, H. Dai, H. Zhang, W. Wang, A new unbiased metamodel method for efficient reliability analysis, Structural Safety 67 (2017) 1–10.

[184] J. Nocedal, S. J. Wright, Numerical Optimization, 2nd Edition, Springer Series in Operations Research, Springer Verlag, New York, USA, 2006.

[185] A. Klimke, Sparse grid interpolation toolbox user's guide, Tech. Rep. V5.1, Universität Stuttgart, Germany (February 2008).

[186] G. T. Buzzard, Global sensitivity analysis using sparse grid interpolation and polynomial chaos, Reliability Engineering & System Safety 107 (2012) 82–89.

[187] B. Sudret, A. Der Kiureghian, Stochastic finite element methods and reliability: A state-of-the-art report, Tech. rep., University of California, Berkley, USA, report No. UCB/SEMM-2000/08 (November 2000).

[188] H. G. Matthies, C. E. Brenner, C. G. Bucher, C. G. Soares, Uncertainties in probabilistic numerical analysis of structures and solids-stochastic finite elements, Structural Safety 19 (3) (1997) 283–336.

[189] N. Z. Chen, C. G. Soares, Spectral stochastic finite element analysis for laminated composite plates, Computer Methods in Applied Mechanics and Engineering 197 (51–52) (2008) 4830–4839.